Exploiting the synergies from coupled electricity and heat distribution networks : modelling, simulation and optimization based on an extended energy hub approach

Getnet Tadesse Ayele

THESE DE DOCTORAT DE / DOCTORAL THESIS

L'ÉCOLE NATIONALE SUPERIEURE MINES-TELECOM ATLANTIQUE BRETAGNE PAYS DE LA LOIRE - IMT ATLANTIQUE
ECOLE DOCTORALE N° 602 : *Sciences pour l'Ingénieur*
Spécialité : Energétique, Thermique et Combustion

ET/AND

KTH ROYAL INSTITUTE OF TECHNOLOGY

Par/by **Getnet Tadesse AYELE**

Exploiting the Synergies from Coupled Electricity and Heat Distribution Networks

Modelling, simulation and optimization based on *an extended energy hub approach*

Thèse présentée et soutenue à / Defended in: Nantes, France le/on Dec 04, 2020
Unité de recherche : GEPEA UMR CNRS 6144
Thèse N° : 2020IMTA0215

JURY/ COMMITTEE

Rapporteurs / Reviewers:	**Bertrand RAISON**, Prof., Université Grenoble Alpes, France **Vittorio VERDA**, Prof., Politecnico di Torino, Italy
Président / President:	**Mohamed Tahar MABROUK**, Maître de conférences, IMT Atlantique, France
Examinateurs / Members:	**Bertrand RAISON**, Prof., Université Grenoble Alpes, France **Vittorio VERDA**, Prof., Politecnico di Torino, Italy **Louise ÖDLUND**, Prof., Linköping University, Sweden **Marianne BOIX**, Maître de conférences, Université de Toulouse INP-ENSIACET, France **Mikael AMELIN**, Assoc. Prof., KTH Royal Institute of Technology, Sweden
Opponent**:**	**Filip JOHNSSON**, Prof., Chalmers University of Technology, Sweden
Dir. de thèse / Supervisors:	**Bruno LACARRIÈRE**, Prof., IMT Atlantique, France **Björn LAUMERT**, Prof., KTH Royal Institute of Technology, Sweden
Encadrant / Co-supervisor:	**Pierrick HAURANT**, Maître de Assistant, IMT Atlantique, France

DOCTORAL THESIS IN ENERGY TECHNOLOGY

NANTES, FRANCE, 2020

Exploiting the Synergies from Coupled Electricity and Heat Distribution Networks

Modelling, simulation and optimisation based on *an extended energy hub approach*

Getnet Tadesse Ayele

IMT Atlantique
Sciences pour l'Ingénieur
Département SEE
UMR CNRS GEPEA 6144
44307 Nantes, France

KTH Royal Institute of Technology
Industrial Engineering and Management
Department of Energy Technology
Heat and Power Technology
SE-100 44 Stockholm, Sweden

TRITA-ITM-AVL 2020:43
Thèse N°: 2020IMTA0215
ISBN: 978-91-7873-679-9

Printed by: IMT Atlantique, 4 rue Alfred Kastler, 44307 Nantes cedex 3, France

To my beloved parents and siblings!

It could have been impossible to reach the level where I am now without your endless support and enormous encouragement.

Thanks a lot!

Abstract

Recent literature shows that there is a significant potential of decarbonisation and efficiency improvement that can be achieved through the synergy from multi-energy systems (MESs). Coupling technologies, such as co-generation plants, heat pumps and thermal storages are widely recommended as means of unlocking additional flexibility and increasing the penetration of renewables in the heating and electricity sectors. In view of that, the size and number of coupling technologies, such as combined heat and power plants and heat pumps (HPs), being installed in the heat distribution networks are increasing. As these technologies are exclusively managed by the district heating network operators, their operation sometimes becomes suboptimal from the electricity network point of view, and they (in particular large HPs) may cause overloading of the low voltage electricity distribution networks.

Integrated simulation and optimisation models are required to exploit the synergies effectively without compromising the constituent distribution networks of MES. Such models are not yet well developed. The conventional single-energy-carrier simulation tools are not capable of capturing key operating parameters of the multi-carrier distribution networks either.

A novel methodology for simulation and optimisation of MES is developed in this thesis based on an Extended Energy Hub (EEH) approach. The general framework is first developed in modular form so that it can be easily adapted for any type of multi-carrier energy networks. The framework is then used to develop the details of an integrated load flow model governing coupled heating and electricity distribution networks. Various load flow case studies with radial and meshed topologies are considered for demonstration and numerical validation of the proposed model.

The load flow model is further combined with a particle swarm optimisation algorithm in order to conduct integrated optimal power flow studies. Its contribution to the state of art is demonstrated by studying the optimal placement of coupling technologies, such as HPs and boilers in coupled heating and electricity distribution networks. The capacity of the model is further illustrated by exploiting the synergies using HPs together with thermal storage in the presence of intermittent renewables and variable electricity price signal.

It is shown that the EEH-based simulation and optimisation methodologies proposed in this thesis are very effective, flexible and easily scalable in capturing the key operating parameters of integrated electricity and district heating networks. The models can be used as a platform for further studies on integration of smart grids and smart thermal networks.

Keywords
District heating networks; Electricity distribution networks; Extended energy hub approach; Integrated load flow study; Integrated optimal power flow; Multi-carrier energy networks; Multi-energy system; Optimal placement; Thermal storage.

Résumé substantiel

Préface

Cette thèse est basée sur une recherche réalisée dans le cadre du programme conjoint de doctorat Erasmus Mundus SELECT + 'Environomical Pathways for Sustainable Energy Services' coordonné par KTH Royal Institute of Technology, Stockholm, Suède. La recherche faisait partie du projet « Analyse des opportunités du réseau électrique décentralisé et de l'interaction du réseau de chauffage urbain ». Il a été financé avec le soutien de l'Agence exécutive pour l'éducation, l'audiovisuel et la culture (EACEA) (FPA-2012-0034) de la Commission Européenne.

La recherche se concentre sur l'intégration optimale des réseaux d'électricité et de chauffage urbain. Elle a été réalisée au sein de deux instituts (d'origine et d'accueil). Le département des systèmes énergétiques et de l'environnement (DSEE) de IMT Atlantique, Nantes, France (qui fait partie de l'UMR CNRS 6144 GEPEA) a été l'institut d'origine où un peu plus de la moitié de la période de recherche a été réalisée. Le reste du temps s'est déroulé au sein de la division Heat and Power Division (EKV) du Department of Energy Technology (EGI), à la School of Industrial Engineering and Management (ITM) de KTH Royal Institute of Technology, Stockholm, Suède, qui a servi d'hôte institut.

En résumé des recherches menées, cette thèse présente de nouvelles approches de modélisation, simulation et optimisation qui peuvent être utilisées pour exploiter les synergies du couplage des réseaux de chauffage urbains et d'électricité sans compromettre les réseaux de distribution respectifs.

« Exploiter les synergies des réseaux couplés de distribution d'électricité et de chaleur : Modélisation, simulation et optimisation basées sur une approche étendue de hub énergétique »

Contexte

L'énergie est un apport indispensable pour gérer les activités humaines quotidiennes. Tous les secteurs, de l'agriculture à l'industrie, de l'éducation au système de santé, du résidentiel au commercial, ont besoin d'une ou plusieurs formes d'énergie pour fonctionner correctement. La quantité d'énergie consommée au niveau des ménages est également l'un des indicateurs importants pour estimer la qualité de vie d'un pays [1–3]. La consommation mondiale d'énergie continue de croître avec l'urbanisation et l'industrialisation. Il est rapporté que la consommation d'énergie dans le monde a augmenté de 2,3% en 2018, un taux qui est près du double du taux moyen depuis 2010 [4]. La croissance de l'économie mondiale n'est pas le seul facteur explicatifs de ce taux de croissance record. L'augmentation de la demande de chauffage et de refroidissement due au changement climatique, qui se manifeste par des températures moyennes d'hiver et d'été dépassant leurs records historiques dans certaines

régions, a également contribué à cette augmentation. Bien que la capacité installée d'énergies renouvelables ait doublé pour la même période, le taux d'EnR n'étant pas suffisant pour faire face au taux de croissance de la demande énergétique, une partie importante de l'augmentation de la demande a donc été couverte par l'utilisation accrue de combustibles fossiles. En conséquence, les émissions de CO_2 liées à l'énergie ont augmenté de 1,7%. Cette situation pourrait conduire à une boucle circulaire de cause à effet : plus d'émissions de CO_2 - conditions météorologiques pires - croissance de la demande d'énergie - plus d'émissions de CO_2.

Il est également signalé qu'en raison de l'augmentation de la demande mondiale d'énergie, d'une part, et de la rareté et des préoccupations environnementales des combustibles fossiles, d'autre part, l'énergie est devenue l'un des principaux défis auxquels l'humanité est confrontée au cours du siècle actuel [5]. Une transition énergétique vers un système énergétique plus renouvelable et durable est largement préconisée comme solution. Cette transition énergétique est une voie par laquelle le secteur mondial de l'énergie doit passer de « fossile » à « zéro carbone » d'ici la seconde moitié de ce siècle. On estime que jusqu'à 90% des objectifs de décarbonation peuvent être potentiellement couverts par l'application de mesures drastiques sur les énergies renouvelables et l'efficacité énergétique [6]. Les Nations Unies ont également défini « l'énergie abordable et propre » comme l'un de ses 17 objectifs de développement durable [7]. Il vise à accroître l'efficacité énergétique mondiale, la part des énergies renouvelables et à moderniser l'infrastructure énergétique afin que l'accès universel à des services énergétiques abordables, fiables et modernes puisse être assuré d'ici 2030.

Dans le cadre de l'effort mondial et en accord avec les objectifs de l'Accord de Paris [8], l'Union Européenne (UE) a récemment (2019) adopté un « Paquet Énergie propre pour tous les Européens » [9], initialement proposé en 2016. Avec la vision d'un système énergétique neutre en carbone d'ici 2050, le paquet fixe des objectifs intermédiaires pour l'année 2030 : une réduction de 40% des émissions de gaz à effet de serre (par rapport au niveau de 1990), une augmentation de 32% de la part des sources renouvelables dans le mix énergétique et une efficacité énergétique de 32,5% par rapport à un scénario de statu quo. Le cadre politique ainsi actualisé aide les États membres à renforcer leurs mécanismes de soutien conformément aux nouveaux objectifs. Les divers types de mécanismes de soutien qui ont été pratiqués à travers le continent comprennent les certificats d'électricité verte, les certificats d'économie d'énergie blanche, les prix variables de l'électricité à la fois dans le temps et l'emplacement géographique, les tarifs de rachat, les quotas, les incitations, le net-metering, le bonus-malus, la taxe carbone et ainsi que plusieurs autres leviers [4].

La Fig. 1-1 montre les progrès réalisés dans l'intégration des énergies renouvelables dans les secteurs de l'électricité, des transports et du chauffage et du froid dans les pays de l'UE28. Conformément aux tendances depuis 2015, les deux objectifs intermédiaires 2020 fixés pour la part des énergies renouvelables dans le secteur des transports et dans le système énergétique global pourraient ne pas être atteints. On peut voir qu'il y a une intégration relativement plus élevée des énergies renouvelables dans le secteur de l'électricité. L'un des facteurs contributifs est le progrès réalisé dans les technologies telles que l'hydroélectricité, l'éolien et le solaire. De plus, bien que les ressources géothermiques et solaires thermiques

soient couramment intégrées dans le secteur du chauffage, elles sont également installées dans le système électrique jusqu'à un certain niveau. En revanche, les technologies basées sur les biocarburants peuvent être intégrées dans les trois secteurs. L'électrification des transports et des secteurs du chauffage et du froid est une alternative pour utiliser tous les potentiels renouvelables afin que la transition énergétique puisse atteindre ses objectifs. Les véhicules électriques et les pompes à chaleur (PAC) sont des exemples de technologies pouvant être utilisées pour électrifier les secteurs du transport et du chauffage, respectivement.

Selon les données de l'Agence internationale de l'énergie, 56,55% de l'électricité et 34,1% de la chaleur consommée dans l'UE28 en 2017 ont été générés à partir de sources non fossiles, dont le nucléaire [4]. Cela montre que le secteur du chauffage et du froid est en retard sur le secteur de l'électricité en termes de décarbonation. De plus, le secteur du chauffage et du froid dans l'UE consomme environ 50% de l'énergie finale [11]. Le chauffage des locaux et l'eau chaude sanitaire représentent à eux seuls jusqu'à 79% de la consommation finale d'énergie des ménages de l'UE [12]. Cela implique que des potentiels plus élevés d'intégration et de décarbonation des énergies renouvelables sont disponibles dans le secteur du chauffage et du froid.

La Fig. 1-2 montre la part des énergies renouvelables sur le marché du chauffage et du froid dans les pays membres de l'UE28 en 2018. La Suède est le premier pays générant 65,4% de sa chaleur à partir d'énergies renouvelables, suivie de la Lettonie (55,9%) et de la Finlande (54,6%). Ces pays sont connus pour leur part de marché plus élevée dans le réseau de chauffage urbain (jusqu'à 90% en Suède) avec une part plus élevée de cogénération (jusqu'à 73% en Lettonie) [13, 14]. Les Pays-Bas, en revanche, affichent la fraction renouvelable la plus faible (6,1%) du fait que 93% de la demande de chaleur du pays est couverte par l'utilisation de chaudières à gaz [15]. La France, avec une part renouvelable de 21,8%, se situe au-dessus de la moyenne de l'UE28 (2018) et même au dessus de l'objectif de l'UE pour 2020 (qui est de 20%).

Le Fig. 1-3 compare la France et la Suède en termes de mix total d'approvisionnement en énergie primaire (TPES) par source pour l'année 2016. Avec un TPES non fossile de 72%, la Suède est l'un des principaux pays en termes de système énergétique durable [16]. Du fait de la part la plus élevée de l'énergie nucléaire, 52% du TPES en France est également non fossile [17]. Cependant, seuls 39% et 10% des TPES en Suède et en France, respectivement, proviennent des énergies renouvelables. Cela montre que la Suède est déjà en avance sur l'objectif d'énergies renouvelables 2030 fixé par l'UE tandis que la France doit faire plus d'efforts.

La France et la Suède figurent parmi les principaux pays à secteur électrique à faible émission de carbone. Comme le montre la Fig. 1-4, 92,3% et 98,6% de l'électricité produite en France et en Suède, respectivement, était produite à partir de technologies à faible émission de carbone en 2016. Le système électrique français est dominé par les centrales nucléaires (72,6% comme le montre la Fig. 1-4 (a)). La part de l'énergie nucléaire en Suède (40,4% comme le montre la Fig. 1-4(b)) est la deuxième plus élevée après la France. La Suède est au troisième rang après le Danemark et la Finlande en termes de carburants à base de biomasse

et de valorisation énergétique des déchets [16]. La part de l'éolien, de l'hydroélectricité, des déchets et des biocarburants dans le mix de production d'électricité suédois est supérieure aux valeurs correspondantes en France. En revanche, la part du gaz et du charbon dans le mix de production d'électricité est plus importante en France qu'en Suède.

La Fig. 1-5 montre les types de combustibles utilisés pour produire de la chaleur en France et en Suède. La Suède est bien connue pour son secteur du chauffage durable. En France, 54,5% seulement de la chaleur est produite à partir de sources non fossiles, comme le montre la Fig. 1-5(a). Le gaz naturel, couvre 36,9% du secteur français du chauffage. En revanche, 86,5% de la chaleur produite en Suède en 2016 provenait de sources sans fossiles (Fig. 1-5(b)). Les biocarburants représentent la part la plus élevée, environ 60,4%, dans le secteur du chauffage suédois.

Énoncé du problème

Idéalement, l'intégration de pompes à chaleur (PAC) à grande échelle et d'un stockage thermique pourrait aboutir à un système énergétique plus durable. Cela signifie que, plus d'énergies renouvelables peuvent être intégrées dans le système électrique sans aucune restriction, les demandes de chaleur de pointe peuvent être efficacement déplacées et, par conséquent, un système énergétique plus efficace, flexible et durable peut être établi. Les résultats basés sur des modèles simplifiés, tels que ceux utilisés dans EnergyPlan [31], RETScreen [32] et HOMER [33], confirment ce potentiel. Dans sa « stratégie de chauffage et de refroidissement », l'UE a également fortement recommandé l'utilisation de chaufferies et de production combinée de chaleur et d'électricité (cogénération) à base de biomasse afin de décarboner et d'augmenter l'efficacité de son secteur du chauffage et du froid [34, 35]. Les pays nordiques sont les premiers à suivre les lignes directrices de l'UE et à intégrer des PAC à grande échelle et des stockages thermiques, comme en témoignent la Suède [36 – 38], la Finlande [39] et le Danemark [40, 41].

Cependant, le fonctionnement des chaufferies est uniquement géré par des gestionnaires de réseaux de chaleur sans tenir pleinement compte du réseau de distribution d'électricité. Cela conduit à un fonctionnement sous-optimal du système global. Les gestionnaires de réseaux de distribution d'électricité, par exemple, estiment la demande d'électricité sur la base de ses propres données en considérant les PAC implicitement, généralement comme une demande fixe. Un opérateur de chauffage urbain, en revanche, considère le profil de demande de chaleur et toutes les sources de chaleur, y compris les PAC, et décide de la stratégie opérationnelle la plus économique de ces systèmes. Étant donné que les deux gestionnaires de réseaux de distribution agissent indépendamment, toute différence possible entre la stratégie opérationnelle supposée et réelle des PAC peut compromettre l'efficacité du système global [42]. De plus, l'insertion accrue des PAC a mis en pause un problème de sécurité car elle surcharge de plus en plus le réseau de distribution d'électricité basse tension [39, 43]. En outre, un placement optimal et une répartition économique des technologies de couplage telles que les cogénérations réalisées uniquement du point de vue du réseau de distribution de chaleur pourraient conduire à des solutions sous-optimales du point de vue du réseau de

distribution d'électricité. Cela montre à quel point il est difficile de capturer les détails des paramètres opérationnels du système multi-énergies (MES) à l'aide des outils classiques de modélisation et de simulation de mono vecteur énergétique car ils ne sont pas conçus pour de tels réseaux hybrides [44].

Des outils de modélisation et de simulation intégrés sont nécessaires pour quantifier cette synergie, évaluer la faisabilité technique et trouver les paramètres opérationnels optimaux d'un système multi-énergies. Les outils de simulation MES simplifiés, comme HOMER et EnergyPlan, n'ont pas cette capacité car ils ne prennent pas en compte les paramètres physiques et de fonctionnement des réseaux de distribution. Une revue de la littérature par Allegrini et al. [45] montre qu'il n'existe pas d'outils bien développés pouvant prendre en compte les paramètres physiques des réseaux de distribution MES. Les approches de modélisation sur mesure rapportées dans la littérature (voir l'état de l'art pour plus de détails), en revanche, manquent de généralité et de flexibilité pour répondre aux questions de recherche clés suivantes liées aux réseaux couplés de distribution d'électricité et de chaleur.

1. Comment intégrer les principaux paramètres de fonctionnement des deux réseaux de distribution, constitués de topologies maillées et de nœuds « conso-acteurs » (alternativement producteurs et consommateurs) ?

2. Comment gérer de manière optimale les technologies de couplage sans compromettre les réseaux deux de distribution ?

3. L'emplacement des technologies de couplage pourrait-il affecter les performances du système énergétique global ? Si oui, comment déterminer leur placement optimal ?

4. Quelle est l'importance du stockage thermique dans l'exploitation des synergies ? Comment la gérer de manière optimale en présence d'énergies renouvelables intermittentes et de signaux de prix variables tout en tenant compte de toutes les contraintes techniques ?

Cette thèse propose une nouvelle méthodologie de modélisation, simulation et optimisation des réseaux intégrés d'électricité et de chauffage basée sur une approche étendue de hub énergétiques (*An Extended Energy Hub - EEH)*. Des études de cas de démonstration sont considérées pour illustrer la capacité de l'outil à répondre aux questions de recherche ci-dessus en prenant des paramètres et des conditions aux limites très proches des systèmes réels.

Objectifs

L'objectif principal de cette thèse est de développer une modélisation, une simulation et une optimisation flexibles qui puissent intégrer les paramètres de fonctionnement des réseaux de distribution dans un système générique multi-énergie (MES), et démontrer son application dans un réseau intégré de chauffage et d'électricité. Il se décline en objectifs spécifiques, axés sur le développement :

- d'un modèle général et flexible de flux de charge capable de gérer des MES fortement couplés,
- de modèles détaillés de flux de charge intégré régissant les réseaux couplés de distribution d' électricité et de chaleur,
- d'un algorithme d'optimisation intégré au modèle de flux de charge MES,
- d'un sous - modèle de stockage thermique intégré au modèle MES
- d'un algorithme de contrôle prédictif du modèle (MPC) pour une gestion optimale du stockage thermique dans un MES.

Les objectifs applicatifs suivants sont également considérés pour démontrer la capacité de l'outil développé et sa nouveauté.

- Analyse statique et études des séries temporelles des flux des réseaux couplés d'électricité et de chauffage.
- Dispatch économique sur une heure, optimisation thermo-économique et placement optimal des technologies de couplage dans les réseaux intégrés de chauffage et d'électricité.
- Optimisation thermo-économique sur des séries temporelles.
- Démontrer la capacité de l'outil à exploiter la synergie des réseaux couplés d'électricité et de chauffage en présence de stockage thermique, d'énergies renouvelables intermittentes et d'un signal de prix de l'électricité variable.

Structure de la thèse

La Fig. 1-6 illustre comment la thèse est organisée en 8 chapitres en lien avec les publications (voir la section « Liste des publications » pour plus de détails) . Le premier chapitre couvre le contexte, l'énoncé du problème et les objectifs de la thèse. *Le chapitre 2* est consacré à l'état de l'art de la modélisation d'un MES. Dans ce chapitre, les compléments scientifiques nécessaires sont identifiées. Il est suivi des *chapitres 3* et 4 qui détaillent et discutent la méthodologie proposée dans cette thèse. *Le chapitre 3* décrit le cadre général appelé « *An Extended Energy Hub (EEH) »* pour la modélisation des MES. À l'aide de ce cadre, les détails d'un modèle de flux de charge intégré composé de réseaux de chauffage et d'électricité sont examinés au *chapitre 4*. La méthodologie est ensuite suivie par les *chapitres 5*, *6* et *7* qui présentent les résultats et les discussions sur les études de cas qui sont utilisées pour illustrer la nouveauté et la capacité de la méthodologie proposée. Des études de cas de flux de charge intégrés sont présentées au *chapitre 5* tandis qu'une étude de cas de flux de puissance optimale intégrée est discutée au *chapitre 6*. *Le chapitre 7* décrit comment le stockage thermique peut être intégré dans le modèle et présente l'application du MPC pour exploiter la synergie des réseaux couplés d'électricité et de chauffage. Bien que la principale

méthodologie utilisée pour modéliser le MES soit décrite dans les *chapitres 3* et *4*, des méthodologies supplémentaires spécifiques au flux de puissance optimal et au MPC sont incluses dans les *chapitres 6* et 7, respectivement. Les principales conclusions sont ensuite résumées au *chapitre 8*.

L'état de l'art

Dans la transition vers de futurs programmes d'énergie durable et renouvelable, le MES propose une nouvelle approche pour étudier les solutions possibles exploitant la synergie de différents secteurs de l'énergie, pour aller au-delà des limites de chacun des sous-secteurs individuels [25, 47]. Classiquement, les secteurs de l'énergie sont découplés du point de vue de la planification et de l'exploitation alors qu'en réalité, les deux doivent être abordés conjointement [47, 53]. Les véhicules électriques, la cogénération et les PAC sont des exemples de technologies énergétiques distribuées qui couplent les secteurs de l'électricité, du gaz, des transports, du chauffage et du froid. Lund et al. [24] ont également identifié que la capacité des réseaux thermiques à interagir avec les réseaux électriques intelligents est l'une des caractéristiques des futurs réseaux de chauffage urbain de 4ème génération. Dans cette optique, l'intégration des centrales de cogénération et des centrales thermiques dans le secteur du chauffage augmente dans les pays nordiques [36–41], qui sont des modèles pour des systèmes énergétiques de quartier durables. Une PAC utilise l'électricité pour élever une température basse à une température plus élevée, tandis qu'un cogénération produit à la fois de la chaleur et de l'électricité à partir de sources de carburant, telles que les déchets, la biomasse et le gaz naturel. Intégrer davantage ces technologies vise à renforcer le couplage et la synergie entre les réseaux.

Cependant, afin de quantifier cette synergie et de gérer efficacement les systèmes énergétiques de couplage, des outils de modélisation et de simulation appropriés sont nécessaires. Le fait d'avoir un certain nombre de dispositifs de conversion et de stockage d'énergie avec des caractéristiques différentes qui impliquent plusieurs vecteurs énergétiques et de nombreux paramètres rend le processus de modélisation et de simulation d'un MES très complexe et exigeant [42]. La prise en compte des paramètres de fonctionnement importants d'un MES à l'aide des outils conventionnels est lourde car ces outils ne sont pas conçus pour des systèmes de distribution d'énergie multi-vecteurs énergétiques [44]. Bien qu'il n'existe pas encore d'outil logiciel disponible sur le marché capable de capturer l'intégralité des paramètres physiques et de fonctionnement des réseaux de distribution multi-opérateurs [45, 49], des progrès ont été réalisés récemment au niveau de la recherche.

L'ensemble des travaux présentés dans la littérature peut être largement regroupé en deux grands groupes selon que les détails des paramètres du réseau de distribution sont pris en compte ou non (voir Fig. 2-1). Les travaux de littérature de la première catégorie ne prennent pas en compte le réseau de distribution. Ils se concentrent principalement sur l'évaluation de faisabilité d'un MES composé de différentes technologies énergétiques ou sur l'étude paramétrique détaillée d'une seule centrale électrique/bâtiment. Les pertes du réseau de distribution sont soit négligées, soit représentées en pourcentage fixe. Les paramètres de

fonctionnement et les contraintes du réseau de distribution ne sont pas étudiés. Ces approches de modélisation peuvent être classées en deux : d'un côté celles qui utilisent des progiciels existants et de l'autre celles qui utilisent leurs propres modèles mathématiques. Les études réalisées à l'aide de progiciels peuvent être regroupées en deux. Le premier sous-groupe se compose des études traitant des détails d'une centrale de co/polygénération et de bâtiments tandis que l'autre sous-groupe couvre la littérature se concentrent uniquement sur le bilan énergétique au niveau du bâtiment, de la ville ou du pays. Concernant les travaux basés sur des développements propres, on trouve des approches modulaires et non modulaires.

Les modèles de la deuxième grande catégorie prennent en compte les réseaux de distribution et abordent partiellement ou complètement leurs paramètres physiques et de fonctionnement. Ces modèles sont utilisés pour des études de flux de charge, de dispatch économique et des études de flux de puissance optimales. Un certain nombre de travaux ont proposé un environnement de co-simulation en utilisant les outils existants tandis que d'autres proposent leur propre modèle de réseaux de distribution multi-vecteurs.

Les progiciels de modélisation MES existants utilisent l'équilibre énergétique entre la demande agrégée et la source. Les réseaux de distribution ne sont pas correctement modélisés dans de tels outils. Il existe en revanche des outils de simulation et d'optimisation bien développés, capables de gérer un seul vecteur d'énergie. Très peu de travaux ont tenté de les combiner dans un environnement de co-simulation afin d'intégrer les paramètres de fonctionnement des réseaux de distribution. Il existe également travaux proposant des modèles et des algorithmes avec et sans prise en compte des paramètres de fonctionnement du réseau de distribution. La plupart d'entre eux sont spécifiques à chaque cas, suivant une approche modulaire ou non. Les modèles modulaires ont appliqué le concept de hub énergétique sur la base des flux de puissance du réseau. Cependant, l'hypothèse de flux unidirectionnels et de modèles hydrauliques isothermes limite leur champ d'application uniquement à un MES composé des seuls réseaux d'électricité et de gaz, sans aucun prosommateur (prosumer).

Le concept de hub énergétique doit être étendu (redéfini) pour ajouter une flexibilité de flux d'énergie bidirectionnels et une capacité à gérer les réseaux de distribution de chaleur. Par ailleurs, les modèles thermo-hydrauliques doivent être suffisamment généraux pour inclure des topologies maillées et suffisamment flexibles pour que tout changement dans la topologie ou la configuration du réseau de chauffage puisse être automatiquement détecté par l'algorithme. L'évolutivité et la modularité de la méthodologie pour intégrer tout vecteur d'énergie supplémentaire ou toute technologie de couplage additionnelle sont également cruciales.

Méthodologie

La structure de l'ensemble du modèle développé dans cette thèse est illustrée à la Fig. 3-1. Il comporte trois parties : *input data, core process* et *outputs*. La partie *input data* correspond aux informations fournies par l'utilisateur parmi lesquelles figurent les paramètres du MES. Les données concernant les réseaux de distribution incluent leurs schémas, les

paramètres physiques et les contraintes. Les profils de demande, les matrices de génération et de couplage locaux décrivant les technologies énergétiques installées dans chaque hub sont également intégrés dans le modèle par l'utilisateur. Des informations supplémentaires sur les valeurs de référence, les valeurs de base, les constantes, le coût des générations, etc. sont également fournies à ce niveau.

A partir de ces données d'entrée, la partie *core process* permet l'extraction automatique des informations requises pour formuler le problème de flux de charge. Les paramètres décrivant les différents vecteurs d'énergie sont convertis à l'aide d'un système unitaire commun (p.u.). Une distinction est alors faite entre les variables de référence (qui ont des valeurs fixes) et celles qui doivent être résolues. Ensuite, un système d'équations, également appelé problème de flux de charge intégré, est formulé et résolu pour ces variables inconnues. Si l'objectif opérationnel porte sur l'optimisation, le problème de flux de charge sera utilisé comme une contrainte d'égalité parmi d'autres contraintes d'inégalité. Comme le problème de flux de charge, la routine d'optimisation est également construite pour se configurer automatiquement avec très peu voire pas de changements de la partie *core process,* si l'utilisateur modifie les paramètres d'entrée, tels que la topologie du réseau et/ou l'emplacement et les types de technologies énergétiques impliquées. Une fois que l'optimisation ou le problème de flux de charge est résolu, les valeurs unitaires des variables sont reconverties à leurs valeurs réelles. Enfin, soit les solutions optimales ou des résultats de simulation flux de charge en fonction du mérite sont retournés à l'utilisateur (partie *outputs* de la méthodologie).

Dans la partie *core process* de la structure proposée à la Fig. 3-1, une nouvelle approche de modélisation du hub énergétique étendu (EEH) est utilisée pour définir le cadre général qui peut être appliqué à n'importe quel problème de flux de charge intégré régissant tout type de MES. La Fig. 3-2 illustre les trois parties composant un Hub Energétique dans sa définition étendue proposée dans ce travail: *le hub énergétique*, les *points d'interconnexion* et les *réseaux d'énergie*.

Le hub énergétique comprend différents types de puissances et de demandes locales générées localement ainsi qu'un système de couplage. Le *système de couplage* est associé à différents types de dispositifs de conversion d'énergie tels que les éoliennes, les panneaux photovoltaïques, les capteurs solaires, les échangeurs de chaleur, les transformateurs de puissance, les chaudières électriques, les chaudières à gaz, les radiateurs électriques, les centrales de cogénération, les PAC, les stockages de chaleur, les stockages de carburant, stockages d'électricité. Les matrices de couplage sont extraites en formulant la relation algébrique entre les demandes, les entrées de puissance nette dans le *système de couplage* et l'efficacité de ces dispositifs de couplage. L'équation (3-1) montre la représentation matricielle générale de la relation entre les demandes (*m* types), les entrées de puissance nette dans le système de couplage (*n* types) et le taux de transfert d'énergie dans les unités de stockage (*n* types) à un hub [59].

En se référant à la Fig. 3-2, on peut voir que chacune des puissances d' entrée nettes dans le système de couplage, (P_{γ_in}) termes de l'équation (3-1), est égale à la génération locale

correspondante ($P_{\gamma g}$) moins l'injection dans le réseau (P_{γ}) du vecteur d'énergie correspondant (voir équation (3-2)). En remplaçant l'équation (3-2) par l'équation (3-1), la version étendue de l'équation de couplage pour un réseau général de MCES peut être formulée comme indiqué dans l'équation (3-3). Comme les injections de puissance dans le réseau (qui font désormais partie de l'équation de couplage) sont des fonctions des paramètres du réseau à tous les hubs, elles décrivent le couplage entre les demandes et les productions au niveau de chaque hub.

Le *point d'interconnexion* est l'endroit où l'injection nette d'énergie (c'est-à-dire P_a, P_b, ..., P_n sur la Fig. 3-2 du hub dans le réseau a lieu pour différents vecteurs d'énergie. Il correspond au terme *bus* dans le réseau électrique et *nœud* dans le réseau de chauffage urbain. La distance entre le *système de couplage* et ce *point d'interconnexion* est supposée très courte par rapport à la longueur des branches reliant deux hubs différents. Cela permet de négliger les éventuelles chutes de tension, de pression et de température entre le *système de couplage* et le *point d'interconnexion.* Cependant, cela ne signifie pas qu'ils sont une seule et même chose. Par exemple, si des flux d'eau ayant des températures différentes se mélangent à un *point d'interconnexion donné* connecté à un hub de source de chaleur, les températures de l'eau sortante côté alimentation seront différentes de la température d'alimentation du concentrateur hub. Il est donc important de traiter séparément le hub énergétique et le point d'interconnexion afin de modéliser correctement les réseaux thermiques.

La partie *réseau d'énergie,* représente le reste du système global - le réseau de distribution multi-vecteur (voir Fig. 3-2). Si, pour un vecteur, il y a un excès de puissance à la quantité requise dans le hub, il sera injecté sur le réseau de ce vecteur et transporté vers les autres hubs du réseau où il y a un déficit. Si le hub présente plutôt un déficit d'un des vecteurs, il l'importera du réseau correspondant. Cependant, il convient de noter que le type et la quantité de vecteur d'énergie à fournir/importer vers/depuis le réseau dépendent non seulement des demandes et des générations locales, mais également des types de dispositifs de couplage disponibles sur un hub donné. En d'autres termes, selon les types de dispositifs de couplage disponibles dans le système de couplage, un type donné de demande locale peut être satisfait par une combinaison de puissance entrant dans le concentrateur à partir de différents vecteurs d'énergie. S'il y a une surproduction d'un vecteur d'énergie donné à l'intérieur du hub (en raison de la conversion entre différents porteurs d'énergie), il sera réinjecté dans le réseau.

Dans l'étude des flux de charge, seuls certains des paramètres de fonctionnement (variables) sont connus et les autres doivent être résolus. Tout calcul de l'injection de puissance basé sur des valeurs inexactes des variables inconnues s'écartera des injections de puissance exactes à chaque hub, calculées à l'aide de l'équation (3-3). La différence entre les deux est donnée par l'équation *de discordance (mismatch equation).* Les équations pour les injections de puissance à chaque *point d'interconnexion* (en fonction des paramètres de fonctionnement) sont combinées avec les équations de couplage (données par l'équation (3-3) pour définir toutes les équations de discordance à résoudre pour déterminer les variables inconnues. Cet ensemble d'équations de discordance est appelé le *problème de flux de charge* d'un MES donné. Des méthodes numériques, telles que la méthode de *Newton-Raphson*, sont utilisées pour réduire les amplitudes de non-concordance en modifiant (approximant) de façon itérative les valeurs des variables inconnues. La solution est dite convergente (c'est-à-dire

que les variables inconnues sont résolues) si et seulement si les amplitudes de tous les décalages sont inférieures à une tolérance acceptable.

Les réseaux couplés d'électricité et de chauffage sont représentés à l'aide de trois sous-modèles : les modèles électrique, hydraulique et thermique. Bien que la représentation rectangulaire de paramètres complexes, tels que la tension et l'impédance, puisse être utilisée pour la modélisation de réseaux électriques, la représentation hybride (profil de tension polaire et impédance rectangulaire) est la plus largement utilisée pour formuler les équations d'équilibre de puissance [99–101]. Les modèles hydrauliques basés sur *des équations d'écoulements en conduites* aboutissent à un modèle simple avec un taux de convergence aussi rapide (voire meilleur) que les équations nodales et en boucle [94]. Par conséquent, cette méthode est utilisée pour représenter la partie hydraulique du réseau de chauffage. Le modèle thermique est représenté à l'aide de trois groupes d'équations qui régissent l'injection d'énergie thermique, la chute de température le long d'une conduite du fait des pertes en ligne et la conservation de l'énergie lors du mélange de l'eau à chaque nœud.

Une fois que toutes les équations de couplage à chaque hub et les équations bilans pour chaque réseau de distribution sont formulées dans un système normalisé, le système d'équations (également appelé problème de flux de charge) est résolu comme un problème unique en utilisant la méthode itérative de *Newton-Raphson*. Les variables d'intérêt dans la solution de flux de charge sont l'amplitude de la tension, l'angle de tension, la température d'alimentation, la température de retour, la pression hydraulique et les débits massiques de chaque hub. À un hub donné, certaines des variables peuvent être connues tandis que les autres sont inconnues. L'étude de flux de charge a pour objectif de résoudre les variables inconnues à l'aide des variables connues. Selon les variables connues, les hubs peuvent être classés comme indiqué dans le Table 4-1. L'organigramme de l'algorithme développé pour résoudre toutes les variables inconnues du réseau d'électricité et de chauffage est représenté sur la Fig. 4-2. Tout le code est développé à l'aide de MATLAB [113].

Résultats et discussions sur l'intégration des études de flux de charge

Les études de cas de démonstration sont soigneusement conçues pour illustrer la capacité de l'outil développé à combler les lacunes scientifiques discutées précédemment. Tout d'abord, l'outil est utilisé pour mener une étude statique d'une heure sur le flux de charge sur les réseaux d'électricité et de chauffage couplés à plusieurs centrales de production combinée de chaleur et d'électricité (CHP). Quatre études de cas avec des topologies à la fois radiales et maillées sont considérées comme le montre la Fig. 5-2.

Un des cas (Case 5-A sur la Fig. 5-2a) est considéré pour comparaison avec les travaux antérieurs rapportés dans la littérature [95]. Les résultats de l'étude de cas comparative sont présentés dans le Table 5-1 to Table 5-4. Les résultats montrent que le modèle proposé dans cette thèse est plus précis.

La contribution de chaque hub et pour chaque vecteur en terme de production et de consommation globales des trois structures de réseaux considérées, est illustrée

graphiquement Fig. 5-3. Les résultats montrant pour chacun des nœuds des trois réseaux combinés d'électricité et de chauffage (amplitude de la tension, angle, générations de puissance active et réactive, demandes de puissance active et réactive, génération de puissance thermique, demande de puissance thermique, puissance de combustible générée, températures d'alimentation et de retour, tête hydraulique côté alimentation et côté retour du réseau) sont présentés dans le Table 5-7. Le Table 5-8, d'autre part, résume les évolutions des variables en différents le long des réseaux d'électricité et de chauffage (courant, puissance apparente transférée, perte de puissance active, perte de puissance réactive, débit massique dans chaque tuyau, températures au point final d'un tuyau côté alimentation et côté retour réseaux, chaleur transférée et perte de puissance calorifique). Les profils de température et de pression hydraulique après la solution de flux de charge sont représentés sur la Fig. 5-4, tandis que les profils de tension sont illustrés sur la Fig. 5-5.

Le potentiel de l'outil développé pour effectuer une simulation pseudo-dynamique est démontrée en considérant une étude de cas à six hubs (comme le montre la Fig. 5-6). L'année est représentée par huit jours, 6 février, 23 mars, 6 mai, 23 juin, 7 août, 23 septembre, 7 novembre et 23 décembre, donnant un total de 192 heures de simulation. Ces profils sont pris uniquement à titre d'illustration pour démontrer la capacité de l'outil proposé à gérer la simulation pseudo-dynamique d'un MES fortement couplé. Le Table 5-10 résume le profil de demande annuel pour chaque vecteur pour l'ensemble du réseau. L'énergie solaire photovoltaïque, l'incinération des déchets par cogénération, le gaz pour la chaudière et les PACs sont considérés pour satisfaire la demande de chaleur et d'électricité. La variation annuelle des paramètres opérationnels, notamment l'amplitude de la tension, l'angle de tension, le débit massique, les températures d'alimentation et de retour des hubs, les températures d'entrée et de sortie de l'eau dans les conduites aller et retour, les pertes de puissance sur les réseaux d'électricité et de chauffage, la consommation de combustible, la quantité d'énergie importée et exportée sont simulées en fonction du temps.

Les résultats de l'ensemble, une heure et plusieurs heures (pseudo-dynamique) simulation, ont démontré la flexibilité du modèle proposé. La capacité du modèle à capter tous les paramètres de fonctionnement importants des réseaux de distribution de chaleur et d'électricité est démontrée. Les inversions de débit sont automatiquement traitées par l'algorithme. Le modèle proposé considère également la variation du coefficient de transfert de chaleur global en conduite en fonction du débit massique et de la température du sol.

Son évolutivité par sa capacité à intégrer différentes technologies de générations et de couplage distribuées via les matrices de couplage est également illustrée.

Les simulations ont également été exécutées avec des conditions initiales différentes et ont convergé vers la même solution, mais avec un nombre différent d'itérations. Il est également démontré que le modèle proposé est plus précis et réaliste par rapport à ce qui a été précédemment rapporté dans la littérature.

Une comparaison entre les réseaux radiaux et maillés (pour des simulations horaires) a révélé la possibilité de pertes de distribution plus élevées dans le cas maillé. D'autre part, l'étude de cas de simulation pseudo-dynamique montre que la façon dont la cogénération et les PACs fonctionnent affecte aussi bien les réseaux d'électricité et de distribution de chaleur. Le dimensionnement des capacités de production des technologies de couplage en fonction d'un seul des deux types de profil de demande pourrait conduire à une capacité de production sous-dimensionnée ou surdimensionnée pour l'autre réseau. Ce travail présente également des pertes de distribution et le coût total d'exploitation qui varient en fonction de l'emplacement des pompes à chaleur. Cela montre que la prise en compte simultanée des deux réseaux est cruciale pour optimiser les technologies de couplage telles que les HP.

Résultats et discussions sur le flux de puissance optimal intégré

Une technique d'optimisation des essaims de particules (particle swarm optimisation – PSO) est intégrée au problème de flux de charge développé, et est appliquée pour trouver le placement optimal des technologies de couplage, telles que les HP et les chaudières. La fonction objective correspond à la minimisation du coût d'exploitation. Un algorithme PSO imbriqué (illustré à la Fig. 6-1) est ensuite appliqué à deux cas d'étude correspondants à deux tailles de structures de réseaux (Fig. 6-2 et Fig. 6-6, respectivement).

L'emplacement optimal et le dimensionnement des PACs et des chaudières pour les petites et les grandes études de cas sont résumés dans le Table 6-2 et le Table 6-4, respectivement. Le débit massique injecté dans le réseau à partir de chaque hub et les températures aller et retour correspondantes pour le cas de la petite structure de réseaux sont illustrés à la Fig. 6-3. Des résultats similaires pour l'étude de la structure de réseaux plus grande sont présentés sur la Fig. 6-7. Le débit massique dans chaque conduite et les tensions à chaque hub sont présentés sur les Fig. 6-4 et Fig. 6-5 (petite structure) et Fig. 6-8 et Fig. 6-10 (grande structure).

L'étude d'un cas supplémentaire (indiqué sur la Fig. 6-12) est considéré pour en vue d'une optimisation de la structure de distribution par identification des branches des réseaux les moins performantes. Une approche étape par étape est présentée dans ce sens Fig. 6-11 et la comparaison des pertes de distribution à différentes étapes est présentée sur la Fig. 6-14.

Les résultats montrent que l'optimisation de l'emplacement et de la taille des PAC uniquement du point de vue du réseau de chauffage pourrait réduire les pertes de chaleur, mais parfois elle pourrait surcharger et augmenter les pertes dans le réseau de distribution d'électricité, en particulier lorsque les HP sont installés sur des réseaux de distribution basse tension. Cela pourrait également conduire à des profils de tension inacceptables. D'autre part, une optimisation intégrée qui prend en compte les contraintes et les pertes de distribution dans les deux réseaux se traduit par un coût d'exploitation inférieur pour l'ensemble du système avec la possibilité d'un meilleur profil de tension dans le réseau de distribution d'électricité.

On constate que les pertes de charge par frottement sont tout aussi importantes que les pertes de charge aux postes consommateurs pour les réseaux plus importants. L'optimisation

thermo-économique a en outre révélé que l'abaissement de la température d'alimentation n'entraîne pas nécessairement une baisse des coûts d'exploitation. Le coût de pompage peut parfois contrebalancer les avantages de températures d'alimentation plus basses. Il convient donc de prendre en compte le coût total du pompage dans les optimisations thermo-économiques des grands réseaux. En revanche, l'abaissement de la température de retour des consommateurs (côté primaire) s'avère toujours économique.

Résultats et discussions sur l'intégration optimale du stockage thermique

Un modèle de réservoir d'eau de stockage thermique sensible stratifié est intégré au modèle d'optimisation. Un nouvel algorithme de contrôle prédictif basé sur un modèle PSO (MPC – illustré sur la Fig. 7-3a) est mis en œuvre pour analyser la synergie entre les réseaux d'électricité et de chauffage en présence d'énergies renouvelables intermittentes et d'un signal de prix de l'électricité variable. Une étude de cas illustrée à la Fig. 7-4 est utilisée avec les données d'entrée résumées aux Fig. 7-5 et Fig. 7-6.

La Fig. 7-7 montre le bilan énergétique de la chaleur, tandis que la Fig. 7-8 illustre l'état de charge et les paramètres de fonctionnement du stockage thermique. Les températures aller et de des hubs sélectionnés sont indiquées sur la Fig. 7-9. Tandis que les débits des conduites sont illustrés à la Fig. 7-10. De même, le bilan électrique actif, le bilan électrique réactif, les profils de tension et les courants de ligne sont représentés sur les Fig. 7-11, Fig. 7-12, Fig. 7-13 et Fig. 7-14, respectivement.

Le Table 7-2 compare le système avec et sans le stockage thermique en utilisant les paramètres clés du système énergétique global. Les deux systèmes ont utilisé une quantité importante de l'électricité excédentaire générée par la centrale éolienne.

En accord avec [28], la perte de distribution dans le réseau de chauffage avec stockage thermique est supérieure à celle du système sans stockage (voir Table 7-2). La raison en est l'exigence d'une température plus élevée pour charger le stockage. La consommation électrique plus élevée des pompes de circulation dans le système sans stockage indique également la présence d'un débit plus élevé dans les conduites en raison de températures d'alimentation plus basses. Cependant, il n'y a pas de différence significative sur les pertes de distribution d'électricité.

Le système avec le stockage thermique évitait totalement l'utilisation de la chaudière à gaz en déplaçant les demandes de chaleur de pointe dans les heures bon marché du signal de prix de l'électricité. Cela a réduit la consommation de gaz dans le système et le coût fonctionnel global.

Conclusions

Cette thèse présente une nouvelle approche en modélisation, simulation et optimisation de systèmes multi-énergies avec une prise en compte complète des paramètres de

fonctionnement des réseaux de distribution multi- vecteurs. Un cadre général de modélisation du problème de flux de charge en régime permanent des systèmes énergétiques multi-vecteurs est formulé sur la base du concept de hub énergétique étendu. L'approche de modélisation est ensuite illustrée en développant un outil qui peut être utilisé pour mener des études intégrées de flux de charge sur des réseaux d'électricité et de chauffage fortement couplés.

L'algorithme, développé sur MATLAB, se compose d'un modèle hydraulique plus flexible et d'un modèle thermique plus réaliste qui le rend suffisamment général pour que chaque fois qu'il est nécessaire de simuler différentes configurations de réseau, l'utilisateur n'a qu'à alimenter les données du réseau. Le système d'équations et la matrice Jacobienne nécessaire pour résoudre le problème de flux de charge intégré sont automatiquement configurés dans cet outil qui permet de surmonter les limites dans les modèles présentés dans la littérature. Une étude comparative a également montré que le modèle proposé dans cette thèse a une meilleure précision.

Tout changement possible de la direction du débit massique est automatiquement traité dans l'algorithme, comme le confirment les différentes études de cas. L'outil considère également la variation du coefficient de transfert de chaleur global d'un tuyau en fonction du débit massique, ce qui le rend plus réaliste. L'outil développé est également très flexible de telle sorte que différentes générations réparties peuvent être facilement intégrées en tant que générations locales.

La capacité de l'outil est également démontrée dans la gestion des flux d'énergie bidirectionnels à travers les branches et entre les concentrateurs et le réseau. Un hub énergétique donné peut être un « prosommateur » (producteur à certains instants et consommateur à d'autres) et non plus seulement consommateur. Différentes technologies de couplage peuvent également être intégrées dans l'outil via les matrices de couplage. Les cogénérations, les HPS, les chaudières, les centrales éoliennes, les stockages, les panneaux solaires photovoltaïques et thermiques sont pris en compte dans différentes études de cas en tenant pleinement compte des paramètres de fonctionnement des réseaux de chauffage et de distribution d'électricité.

L'outil a été testé pour différentes topologies de réseaux constituées de réseaux d'électricité et de chauffage fortement couplés. Les résultats trouvés sont cohérents avec la théorie. Les simulations ont également été effectuées dans des conditions initiales différentes et ont convergé vers la même solution, mais avec un nombre d'itérations différent. Les résultats de l'étude de flux de charge intégrée donnent les détails des paramètres du réseau tels que la tension, le débit massique, la température, la pression, les pertes thermiques, les pertes électriques, les générations aux nœuds d'équilibrage et la quantité de flux d'énergie à travers chaque conduite et ligne de transmission. Les études de cas présentées montrent que les pertes et les paramètres du réseau sont fortement affectés par la topologie des réseaux.

Des études de flux de charge sur plusieurs heures ont également été menées sous la forme d'une simulation pseudo-dynamique sur des réseaux électriques et de chauffage couplés

comprenant une cogénération, un solaire PV, une chaudière à gaz et des PACs. Il a été observé que le fonctionnement de la cogénération et des pompes à chaleur affecte les deux réseaux. En outre, le dimensionnement des technologies de production et de couplage sur la base d'un seul type de profil de demande pourrait conduire à une capacité de production sous-dimensionnée ou surdimensionnée pour l'autre réseau. Des études comparatives ont également montré que l'emplacement des HP affecte les pertes de distribution et les paramètres de fonctionnement dans les deux réseaux de distribution.

Pour une répartition économique des unités de production et des technologies de couplage, en tenant pleinement compte des paramètres des réseaux de distribution, un algorithme d'optimisation méta-heuristique a été développé sur la base de la technique PSO. Il est appliqué pour trouver l'emplacement et les tailles optimales des technologies de génération et de couplage distribuées. Une étude comparative est faite entre la gestion uniquement du point de vue du réseau de chauffage et la gestion en considérant les deux réseaux. Les résultats montrent que l'optimisation de l'emplacement et de la taille des HP uniquement du point de vue du réseau de chauffage pourrait réduire les pertes de chaleur. Mais, il est démontré qu'une telle stratégie de gestion peut entraîner une surcharge et davantage de pertes dans le réseau de distribution d'électricité. Cela pourrait également conduire à des profils de tension inacceptables. Le problème s'aggrave, en particulier lorsque de grandes PACs sont installées dans un réseau de distribution basse tension. D'autre part, une optimisation intégrée qui prend en compte les contraintes et les pertes de distribution dans les deux réseaux a entraîné une baisse des coûts d'exploitation pour l'ensemble du système et un meilleur profil de tension dans le réseau électrique.

Les pompes de circulation sont utilisées pour surmonter deux types de pertes de charge. Le premier correspond aux pertes par frottement dans les canalisations tandis que le second est lié à la différence de pression minimale requise aux postes (côté primaire). Leur ampleur relative dépend de la taille et de la stratégie d'exploitation du réseau de chauffage. On constate que la consommation électrique des pompes de circulation n'est généralement pas significative par rapport à la demande totale d'électricité, pour les réseaux étudiés. Cependant, comme le coût total du pompage de l'énergie peut concurrencer le coût de la perte de distribution, surtout s'il existe des sources de chaleur très bon marché, le coût du pompage doit être pris en compte dans les optimisations thermo-économiques.

Une approche étape par étape pour identifier et isoler les branches avec perte d'un réseau de chaleur maillé a été réalisée à l'aide d'un flux de puissance optimal intégré et de procédures d'optimisation thermo-économique. Une telle approche permet de faire fonctionner le réseau de chaleur efficacement en dehors des heures de pointe. Les résultats de l'optimisation thermo-économique ont en outre révélé que l'abaissement de la température d'alimentation n'entraîne pas nécessairement un coût d'exploitation inférieur. Le coût de pompage peut parfois contrebalancer les avantages de températures d'alimentation plus basses. Cependant, l'abaissement de la température de retour des consommateurs (côté primaire) s'avère toujours économique.

La synergie des réseaux de chauffage et d'électricité couplés peut être davantage exploitée à l'aide de réservoirs de stockage thermique. Les stockages thermiques peuvent augmenter la flexibilité du réseau de chaleur en réduisant les pics de demande. Ils augmentent également la pénétration des énergies renouvelables dans les réseaux de distribution d'électricité et de chaleur. Un système énergétique comprenant une cogénération, une PAC, une chaudière à gaz, une éolienne et un stockage thermique a été étudié. Un signal de prix variable pour l'électricité du réseau est également pris en compte. Un MPC basé sur PSO est mis en œuvre pour optimiser le système sur un horizon de 24 heures. Il est démontré qu'une part importante de la production éolienne peut être utilisée dans le système en couplant les réseaux d'électricité et de chauffage. Le système avec le stockage thermique évitait totalement l'utilisation de la chaudière à gaz en déplaçant les demandes de chaleur de pointe dans les heures bon marché du signal de prix de l'électricité. Cela a réduit la consommation de gaz dans le système et le coût fonctionnel global.

Il est démontré (à travers des études de cas) que les méthodologies de simulation et d'optimisation basées sur la notion de hubs énergétiques étendus, proposées dans cette thèse sont évolutives, flexibles et très efficaces pour considérer les paramètres de fonctionnement importants et quantifier la synergie qui peut être obtenue à partir des réseaux intégrés d'électricité et de chauffage. La flexibilité supplémentaire qui peut être obtenue en intégrant le stockage thermique est également explorée en tenant compte de toutes les contraintes techniques.

Mots clés :

Réseaux de chauffage urbain; Réseau de distribution d'électricité; Hub énergétique étendu; Étude intégrée du flux de charge; Flux de puissances intégrées optimaux; Réseaux énergétiques multi-vecteurs; Système multi-énergies; Placement optimal; Stockage thermique.

Sammanfattning

Ny litteratur visar att det finns en betydande potential för avkolning och effektivitetsförbättring som kan uppnås genom synergi från multi-energisystem (MES). Kopplingsteknik, såsom kraftvärmeanläggningar, värmepumpar och värmelager rekommenderas allmänt som medel för att låsa upp ytterligare flexibilitet och öka penetrationen av förnybara energikällor inom värme- och elsektorn. Mot bakgrund av detta ökar storleken och antalet kopplingstekniker, såsom kraftvärmeverk och värmepumpar (HP), som installeras i värmefördelningsnätet. Eftersom dessa tekniker uteslutande hanteras av fjärrvärmenätoperatörerna blir deras drift ibland suboptimal ur elnätets synvinkel, och de (särskilt stora HP) kan orsaka överbelastning av distributionsnätet för lågspänning.

Integrerade simulerings- och optimeringsmodeller krävs för att effektivt utnyttja synergierna utan att kompromissa med MES: s ingående distributionsnät. Sådana modeller är ännu inte väl utvecklade. De konventionella simuleringsverktygen för enenergibärare kan inte heller fånga viktiga driftsparametrar i distributionsnätet med flera bärare.

En ny metod för simulering och optimering av MES har utvecklats i denna avhandling baserad på ett EEH-synsätt (Extended Energy Hub). Det allmänna ramverket utvecklas först i modulär form så att det enkelt kan anpassas för alla typer av multibärare energinät. Ramverket används sedan för att utveckla detaljerna i en integrerad belastningsflödesmodell som styr kopplade värme- och eldistributionsnät. Olika fallflödesstudier med radiella och meshade topologier övervägs för demonstration och numerisk validering av den föreslagna modellen.

Lastflödesmodellen kombineras vidare med en algoritm för optimering av partikelvärm för att genomföra integrerade optimala effektflödesstudier. Dess bidrag till teknikens ståndpunkt demonstreras genom att studera den optimala placeringen av kopplingstekniker, såsom HP och pannor i kopplade värme- och eldistributionsnät. Modellens kapacitet illustreras ytterligare genom att utnyttja synergierna med hjälp av HP tillsammans med termisk lagring i närvaro av intermittenta förnybara energikällor och variabel elprissignal.

Det visas att de EEH-baserade simulerings- och optimeringsmetoderna som föreslås i denna avhandling är mycket effektiva, flexibla och lätt skalbara för att fånga de viktigaste driftsparametrarna för integrerade el- och fjärrvärmenät. Modellerna kan användas som en plattform för vidare studier om integration av smarta nät och smarta termiska nätverk.

Nyckelord
Fjärrvärmenät; Elektricitetsdistributionsnät; Utökad strategi för energihub; Integrerad belastningsstudie; Integrerat optimalt effektflöde; Energinät med flera bärare; Multi-energisystem; Optimal placering; Termisk lagring.

Preface

This thesis is based on a research performed within the framework of Erasmus Mundus Joint Doctorate SELECT+ program 'Environomical Pathways for Sustainable Energy Services' coordinated by the KTH Royal Institute of Technology, Stockholm, Sweden. The research was part of the intake project 'Opportunity Analysis of Decentralized Electricity Grid and District Heating Interaction'. It was funded with the support from the Education, Audiovisual and Cultural Executive Agency (EACEA) (FPA-2012-0034) of the European Commission.

The research focuses on optimal integration of electricity and heating networks. It was conducted in two (home and host) institutes. The Department of Energy Systems and Environment (DSEE) at IMT Atlantique, Nantes, France (which is part of the UMR CNRS 6144 GEPEA) served as a home institute, and it is where slightly more than half of the research period was spent. The remaining time was used at the host institute in the Division of Heat and Power (EKV), Department of Energy Technology (EGI), School of Industrial Engineering and Management (ITM), KTH Royal Institute of Technology, Stockholm, Sweden.

As a wrap-up to the research conducted, this thesis presents new modelling, simulation and optimisation approaches that can be used to exploit the synergies from coupled heating and electricity networks without compromising the respective distribution networks.

Nantes, France (Dec. 2020)
Getnet Tadesse Ayele

Acknowledgements

I am so grateful to the SELECT+ consortium for giving me a chance to pursue my PhD. I would also like to thank the European Commission, Audiovisual and Cultural Executive Agency (EACEA) for partly funding my study. I truly appreciate all the staffs in the DSEE at IMT Atlantique and in the EKV/EGI at KTH who made my stay at the two institutes comfortable and fruitful. Special thanks to *Chamindie Senaratne*, for facilitating all the SELECT+ administrative issues and for all the support during my stay at KTH.

I would like to express my sincere gratitude to my principal supervisors *Prof. Bruno Lacarrière* at IMT Atlantique and *Prof. Björn Laumert* at KTH, and also to my co-supervisor *Assoc. Prof. Pierrick Haurant* at IMT Atlantique. I am deeply grateful for their immense support, persistent guidance, encouragement and for the trust they put on me throughout the course of this PhD.

I want to express my greatest appreciation to *Assoc. Prof. Francesco Fuso Nerini*, from EGI/KTH, for evaluating the final seminar and giving valuable feedback on the draft thesis that helped me to improve its quality. I am also thankful to *Assoc. Prof. Anders Malmquist* from EGI/KTH and *Fabian Levihn* from Stockholm Exergi for their constructive feedbacks on the progresses of this research.

I am grateful to all the jury members for their time in reviewing this thesis and also for their participation in the PhD defence. Many thanks to *Prof. Vittorio Verda* (Politecnico di Torino), *Prof. Bertrand Raison* (Université Grenoble Alpes), *Prof. Louise Ödlund* (Linköping University), *Prof. Filip Johnsson* (Chalmers University of Technology), *Assoc. Prof. Marianne Boix* (Université de Toulouse INP-ENSIACET) and *Assoc. Prof. Mikael Amelin* (KTH Royal Institute of Technology).

I take this chance to thank *Assoc. Prof. Mohamed Tahar Mabrouk* (DSEE/IMT Atlantique) for the discussions and inputs as a co-author in most of the publications made out of this study. Also to *Prof Massimo Santarelli* (Politecnico di Torino), I am grateful for his feedback and contribution as a co-author in two of the publications. I am also thankful to *Monica Arnaudo* and *Johan Dalgren* from EGI/KTH for the fruitful discussions we had.

I want to show my appreciation to my colleagues and friends who contributed to my study and personal life in one way or the other. Thanks to *Imtisal-e- Noor*, *Manuel Betancourt, Mexitli Eva*, *Moritz Wegener*, *Mahrokh Samavati, José Fiacro* and all of those who are affiliated to the SELECT+ PhD programme who shared me their experiences. I owe my deepest gratitude to *Sylvestre Yaovi* and *Getenet Tesega* who encouraged me throughout the journey of this PhD. My special thanks go to *Daniel Minilu* and *Tigist Fetene* for their kind hospitability.

Nantes, France (Dec. 2020)
Getnet Tadesse Ayele

List of publications

Six peer-reviewed scientific publications are made during the course of this PhD program. All of them are original research papers. Four of them are either published on or submitted to international journals while the other two are presented at international conferences.

Journal papers

[Paper 1] **G. T. Ayele**, P. Haurant, B. Laumert, and B. Lacarrière, 'An extended energy hub approach for load flow analysis of highly coupled district energy networks: Illustration with electricity and heating', *Appl. Energy*, vol. 212, pp. 850–867, Feb. 2018, doi: 10.1016/j.apenergy.2017.12.090.

[Paper 2] **G. T. Ayele**, M. T. Mabrouk, P. Haurant, B. Laumert, and B. Lacarrière, 'Optimal placement and sizing of heat pumps and heat only boilers in coupled electricity and heating networks', *Energy*, vol. 182, pp. 122–134, Sep. 2019, doi: 10.1016/j.energy.2019.06.018.

[Paper 3] **G. T. Ayele**, M. T. Mabrouk, P. Haurant, B. Laumert, B. Lacarrière, M. Santarelli, 'Electrified district heating network: a thermo-economic optimisation based on exergy and energy analyses', *Int. J. Exergy,* vol. 34, No. 2, 2021 *(article in press).*

[Paper 4] **G. T. Ayele**, M. T. Mabrouk, P. Haurant, B. Laumert, and B. Lacarrière, 'Optimal heat and electric power flows in the presence of intermittent renewable source, heat storage and variable grid electricity tariff', *(submitted).*

Peer reviewed conference papers

[Paper 5] **G. T. Ayele**, M. T. Mabrouk, P. Haurant, B. Laumert, and B. Lacarrière, 'Pseudo-dynamic simulation on a district energy system made of coupling technologies', in *ECOS 2018 – 31st International Conference on Efficiency, Cost, Optimisation, Simulation and Environmental Impact of Energy Systems*, Guimaraes, Portugal, Jun. 2018.

[Paper 6] **G. T. Ayele**, M. Mabrouk, P. Haurant, B. Laumert, B. Lacarrière, and M. Santarelli, 'Exergy analysis and thermo-economic optimisation of a district heating network with solar- photovoltaic and heat pumps', in *ECOS 2019 – 32nd International Conference on Efficiency, Cost, Optimisation, Simulation and Environmental Impact of Energy Systems*, Wroclaw, Poland, Jun. 2019.

Author's contributions

This dissertation is basically based on the contents of the four journal papers, ([Paper 1], [Paper 2], [Paper 3] and [Paper 4]). Though not directly referred, the extended and revised versions of [Paper 5] and [Paper 6] are also used to complement the thesis. The contribution of the authors in the six papers is presented as follows.

[Paper 1] presents the general framework of MES load flow model based on an extended energy hub (EEH) approach. It also discusses the details of an integrated load flow model governing coupled heating and electricity distribution networks. The proposed model is tested and analytically validated by considering radial and meshed topologies of electricity and heating network topologies coupled using multiple combined heat and power (CHP) plants. Also, a comparison is made with a case study from literature. In this paper, the author of this dissertation contributed by designing the conceptual framework of the research, going through the literature review, developing the models, running the simulations, interpreting the results, drawing the conclusions, writing the original draft manuscript, and in the revision and editing process of the manuscript. The research was conducted under the supervision of Prof. Bruno Lacarrière, Assoc. Prof. Pierrick Haurant and Prof. Björn Laumert who participated in the discussions, and reviewed the draft manuscript.

The methodology proposed in [Paper 1] is further expanded in [Paper 5] to take hourly variations of demand and generations into account. Pseudo-dynamic simulations on integrated heating and electricity distribution networks consisting of CHPs, heat pumps (HPs) and heat-only-boiler (HOB) are investigated.

[Paper 2] demonstrates how the EEH approach can be integrated with optimisation techniques, such as Particle Swarm Optimisation (PSO), in order to conduct an integrated optimal power flow in coupled heating and electricity distribution networks. It shows how the model can overcome the challenge of having "automatically configurable" model that is crucial in finding the optimal placement of coupling technologies.

[Paper 4] further demonstrates the capacity of the proposed modelling and optimisation tool in exploiting the synergy, quantifying the flexibility and capturing key operating parameters of coupled heating and electricity distribution networks in the presence of intermittent renewables and variable price signals. It incorporates a detailed stratified thermal storage model and a PSO-based model predictive control algorithm.

In [Paper 2], [Paper 4] and [Paper 5], the author of this thesis contributed by designing the conceptual framework of the research, going through the literature reviews, developing the models, running the simulations, interpreting the results, drawing the conclusions, writing the original draft manuscripts, and in the revision and editing process of the manuscripts. Prof. Bruno Lacarrière, Assoc. Prof. Pierrick Haurant, Prof. Björn Laumert, and Assoc. Prof. Mohamed Tahar Mabrouk participated in the discussions, and reviewed the draft manuscripts.

[Paper 3] introduces exergy and energy analysis as a means of identifying and isolating lossy branches in an electrified district heating network. It also highlights the application of thermo-economic

optimisation in minimizing the operational cost of coupled heating and electricity networks. It is an invited paper based on its previous version, which was presented at ECOS 2019 international conference, [Paper 6]. In both versions, the author of this dissertation contributed by designing the conceptual framework of the research, going through the literature reviews, developing the models, running the simulations, interpreting the results, drawing the conclusions, writing the original draft manuscripts, and in the revision and editing process of the manuscripts. The work was done under the guidance of Prof Massimo Santarelli who, together with Prof. Bruno Lacarrière, Assoc. Prof. Pierrick Haurant, Assoc. Prof. Mohamed Tahar Mabrouk and Prof. Björn Laumert, participated in the discussions, and reviewed the draft manuscripts.

Nomenclature

Abbreviations and acronyms

AC	Alternating current
CHP	Combined heat and power
COP	Coefficient of performance of a heat pump
DC	Direct current
DG	Distributed generation
DHN	District heating network
DSO	Distribution system operator
EEH	Extended energy hub
EU	European Union
EU28	European Union member countries (including United Kingdom)
HP	Heat pump
MES	Multi-energy system
MPC	Model predictive control
PAC	Pompes à chaleur
PQ hub	A hub where active and reactive power generations are known
PSO	Particle swarm optimisation
PV hub	A hub where active power and voltage magnitude are known
pu	Per-unit
Solar PV	Solar photovoltaic
temp_return hub	A hub that imports heat from the network, its return temperature is known
temp_supply hub	A hub that injects heat into the network, its supply temperature is known
TPES	Total primary energy supply

Latin symbols

a	Transformer tap setting
A_{Rs}	Cylindrical surface area around a pipe at a radius R (m^2)
B	Susceptance of transmission line (S)
$Boiler_{Phg}$	Heat produced by a boiler (W)
$\boldsymbol{C}$	Coupling matrix
$C_{\delta\gamma}$	An element in a coupling matrix showing how much of the input power of type γ is converted into the local demand type of δ
CHP_{Pepg}	Active power produced by a combined heat and power plant (W)
CHP_{Peqg}	Reactive power produced by a combined heat and power plant (var)
CHP_{Phg}	Heat produced by a combined heat and power plant (W)
C_{loc}	A fraction to take the local pressure losses due to valves and junctions into account
C_p	Specific heat capacity of water ($J.kg^{-1}.K^{-1}$)
C_{Pelg}	Cost of electricity locally generated (€/h)
$C_{Pel(1)}$	Cost of imported/exported electricity through the slack hub (€/h)
C_{Pfg}	Cost of fuel used in the system (€/h)

C_{Phg}	Cost of heat locally generated (€/h)
$C_{Ph(1)}$	Cost of imported/exported heat through the slack hub (€/h)
c_1	Personal acceleration factor in the PSO algorithm
c_2	Global acceleration factor in the PSO algorithm
D	Internal diameter of a carrier pipe (m)
dl	Infinitesimal length of a pipe (m)
dQ	Infinitesimal heat loss across an infinitesimal length of a pipe (W)
dT_w	Infinitesimal change of water temperature (K)
e	Internal surface roughness of a pipe (m)
$\dot{E}_h$	A rate of change of stored thermal energy in a hot water storage tank (W)
$\dot{E}_\gamma$	Power from a storage (rate of change of stored energy) (W)
f	friction factor
$\mathcal{F}$	Objective function of an optimization
g	Gravitational acceleration (m.s^{-2})
$\boldsymbol{F}$	A multivariable system of equations
H	Hydraulic head (m)
$\boldsymbol{H}$	A vector of unknown hydraulic heads (pu)
H_{base}	Base value for hydraulic head (m)
HP_{Lep}	Active power consumed by a heat pump (W)
HP_{Leq}	Reactive power consumed by a heat pump (var)
HP_{Phg}	Heat produced by a heat pump (W)
h_w	Convective heat transfer coefficient of water (W.m^{-2}.K^{-1})
I	Current flow (A)
I_{base}	Base value for current flow (A)
I_{max}	Ampacity of a transmission line (A)
$\boldsymbol{J}$	Jacobian matrix
k_{ij}	Pressure resistance coefficient for the pipe flow connecting nodes i and j (m.s^2.kg^{-2})
k_2	Thermal conductivity of the carrier pipe (W.m^{-1}.K^{-1})
k_3	Thermal conductivity of the insulating material of the pipe (W.m^{-1}.K^{-1})
k_4	Thermal conductivity of the outer jacket of the pipe (W.m^{-1}.K^{-1})
k_s	Thermal conductivity of the soil (W.m^{-1}.K^{-1})
k_w	Thermal conductivity of the water (W.m^{-1}.K^{-1})
L	Length of a branch (transmission line or pipe) (m)
$\boldsymbol{L}$	Load vector
L_{base}	Base value for pipe length (m)
L_{ep}	Active electric power demand (W)
L_{eq}	Reactive electric power demand (var)
L_h	Heat power demand (W)
L_δ	Demand of energy carrier type δ (W, var)
$\dot{m}$	Mass flow rate from a hub to a node (kg.s^{-1})
$\boldsymbol{\dot{m}_{pipe}}$	A vector of unknown pipe mass flow rates (pu)
$\dot{m}_{base}$	Base value for mass flow rate (kg.s^{-1})
$\lvert\dot{m}_c\rvert$	Magnitude of mass flow rate on the primary side of the substation (kg.s^{-1})
$\dot{m}_{ij}$	Pipe mass flow rate from node i to j (kg.s^{-1})

$\dot{m}_{max}$	Maximum acceptable pipe flows (kg.s^{-1})
N_u	Nusselt number
$P_{el(pumping)}$	Active electricity consumed by a circulation pump (W)
P_{ep}	Electrical active power injected into the network (W)
P_{epg}	Electrical active power generated (W)
P_{ep-in}	Electrical active power flowing into the coupling system (W)
P_{eq}	Electrical reactive power injected into the network (var)
P_{eqg}	Electrical reactive power generated (var)
P_{eq-in}	Electrical reactive power flowing into the coupling system (var)
$\boldsymbol{P_{in}}$	Input power vector flowing into the coupling system
P_f	Fuel power injected into the network (W)
pf_{CHP}	Power factor of a combined heat and power plant
P_{fg}	Fuel power generated (W)
P_{f-in}	Fuel power flowing into the coupling system (W)
pf_{HP}	Power factor of a heat pump
P_h	Heat power injected into the network (W)
P_{hg}	Heat power generated (W)
P_{h-in}	Heat power flowing into the coupling system (W)
$P_{h(base)}$	Base value for heat power (W)
P_γ	Power of type γ injected from the hub into the network (W, var)
P_{γ_in}	Input power of type γ into a coupling system (W, var)
P_r	Prandtl number
R	Resistance of a transmission line (Ω)
R_e	Reynolds number
R_s	Radius of a cylindrical surface (m)
R_{tot}	Total thermal resistance (K.W^{-1})
r_1, r_2	Random numbers in the PSO algorithm
R_1, R_2	Internal and outer radius of a carrier pipe (m)
R_3	Outer radius of an insulation of a pipe in a district heating network (m)
R_4	Outer radius of an outer jacket of a pipe in a district heating network (m)
R'	Thermal resistance per unit length (K.m.W^{-1})
S	Shape factor
S_{base}	Base value of apparent power (VA)
S_e	Electrical apparent power injected into the network (VA)
T	Temperature (K)
$\boldsymbol{T_r}$	A vector of unknown return temperatures at temp_supply hubs (pu)
T_{ref1}	Lower reference temperature (K)
T_{ref2}	Upper reference temperature (K)
$T_{r(max)}$	Maximum return temperature limits at heat-sink hubs (K)
$T_{r(min)}$	Minimum return temperature limits at heat-sink hubs (K)
$\boldsymbol{T_s}$	A vector of unknown supply temperatures at temp_return hubs (pu)
$T_{s(max)}$	Maximum supply temperature limits at heat-source hubs (K)
$T_{s(min)}$	Minimum supply temperature limits at heat-source hubs (K)
T_{w_end}	Outlet water temperature (K)

T_{w_start}	Inlet water temperature (K)
U	Overall heat transfer coefficient ($W.m^{-2}.K^{-1}$)
U_{Rs}	Overall heat transfer coefficient of a cylindrical surface of radius R_s around a pipe ($W.m^{-2}.K^{-1}$)
V	Voltage (V)
$\|\boldsymbol{V}\|$	A vector of unknown voltage magnitudes (pu)
V_{base}	Base value for voltage (V)
v_{i-new}	New velocity of particle i in the PSO algorithm
v_{io}	Current velocity of particle i in the PSO algorithm
V_{min}, V_{max}	Minimum and maximum nodal voltage magnitude limits (pu)
X	Reactance of a transmission line (Ω)
$\boldsymbol{X}$	A vector of unknown variables to be solved from a system of equations
x_i	Current position of particle i in the PSO algorithm
x_{i-new}	New position of particle i in the PSO algorithm
x_{i-best}	Best position of particle i in the PSO algorithm
x_{g-best}	Global best position
Y_{ij}	An element in the admittance matrix of the electricity network
y_{ij}	Admittance of the line between buses i and j including a transformer (S)
y_{ii}	Susceptance at bus i (S)
Z	Depth of a buried pipe measured from the surface of earth (m)
Z_{base}	Base value for impedance (Ω)
$Z_{\delta\gamma}$	An element of the coupling matrix indicating how much of the power from a storage type γ is contributing to meet the local demand of type δ
$Z_{h(h)}$	Charging/discharging efficiency of a thermal storage

Greek symbols

β	An exponential constant in the pressure drop equation
$\Delta\boldsymbol{E_r}$	A vector of thermal energy mismatches at nodes connected to *temp_supply* hubs, in the supply pipe network side (pu)
$\Delta\boldsymbol{E_s}$	A vector of thermal energy mismatches at nodes connected to *temp_return* hubs, in the return pipe network side (pu)
$\Delta\boldsymbol{H_{pipe}}$	A vector of hydraulic head mismatches across a pipe (pu)
ΔH_p	Frictional head loss across a pipe p (m)
ΔH_c	Hydraulic head difference at the consumer substation (m)
$\Delta\boldsymbol{P_{ep}}$	A vector of mismatches in active power injections into the network (pu)
$\Delta\boldsymbol{P_{eq}}$	A vector of mismatches in the reactive power injections into the network (pu)
$\Delta\boldsymbol{P_h}$	A vector of mismatches in the heat power injections into the network (pu)
ΔT	Temperature difference (K)
ε	Surface roughness of a pipe (m)
η	Efficiency of a circulation pump
η_b	Thermal efficiency of a heat-only-boiler
η_{el}	Electrical efficiency of a combined heat and power plant
η_{th}	Thermal efficiency of a combined heat and power plant

θ	Voltage angle (rad)
$\boldsymbol{\theta}$	A vector of unknown voltage angles (rad)
θ_{ij}	Voltage angle difference between nodes i and j (rad)
μ	Dynamic viscosity of water (kg. $m^{-1}.s^{-1}$)
ρ	Density of water ($kg.m^{-3}$)
ω	Inertia factor in the PSO algorithm

Subscripts

a	Ambient
c	Consumer (heat) substation
ep	Active power
eq	Reactive power
f	Fuel power
g	Locally generated
i, j, k	Numbers identifying hubs, nodes, buses, particles in a PSO
p	Pipe
r	Return pipe of a DHN
s	Supply pipe of a DHN
w	Water

Table of Contents

List of Tables

List of Figures

1. Introduction

This chapter presents the research background, the motivation and the main research questions. It also briefly describes the set of objectives formulated to answer those questions. The chapter concludes by outlining the thesis structure.

1.1. Background

Energy is an indispensable input to run day-to-day human activities. Sectors ranging from agriculture to industry, from residential to commercial and from education to health care system, all of them need some sort of energy to function properly. The amount of energy consumed at household-level is also one of the important indicators in estimating the life quality of a given country [1–3]. The global energy consumption continues to grow with urbanization and industrialization. It is reported that energy consumption worldwide grew by 2.3% in 2018, a rate which is nearly twice of the average rate since 2010 [4]. The growth in the global economy was not the only factor for this record high growth rate. The increase in heating and cooling demands because of climate change, manifested by the average winter and summer temperatures exceeding their historical records in some regions, also contributed its part. Although the renewables installed capacity was doubled for the same period, the rate was not enough to cope up with the energy demand growth rate. Significant part of the increase in the demand was covered by using more fossil fuels. As a result, the energy-related CO_2 emission increased by 1.7%. This could lead into a circular cause and effect loop: more CO_2 emission – worse weather conditions – growth in energy demand – more CO_2 emission.

It is also reported that due to the increasing global energy demand, on one hand, and the scarcity and environmental concerns of fossil fuels, on the other hand, energy has become one of the main challenges faced by humanity in the current century [5]. An energy transition towards a more renewable and sustainable energy system is widely advocated as a solution. This energy transition is a pathway through which the global energy sector is transformed from fossil-based to zero-carbon by the second half of this century. It is believed that up to 90% the decarbonisation goals can be potentially covered by applying drastic measures on renewable energy and energy efficiency [6]. United Nation also set “affordable and clean energy” as one of its 17 sustainable development goals [7]. It aims at increasing the global energy efficiency, the share of renewables and upgrade the energy infrastructure so that universal access to affordable, reliable and modern energy services can be ensured by 2030.

1.1.1. Transitions of heat and electricity sectors in Europe

As part of the global effort and in commitment with the goals of The Paris Agreement [8], the European Union (EU) recently (2019) adopted a 'Clean Energy for all Europeans Packages' [9] which was initially proposed in 2016. With the vision of carbon neutral energy system by 2050, the package sets intermediate targets for the year 2030: a 40% cut in greenhouse gas emission (from 1990's level), a 32% increase in the share of renewable sources in the energy mix and a 32.5% energy efficiency relative to the 'business as usual' scenario. The updated policy framework helps Member States to strengthen their support mechanisms in compliance with the new targets. Varieties of support mechanisms that has been practised across the continent include green electricity certificates, white energy saving certificates, variable electricity prices both in time and geographical location, feed-in tariffs, quota, incentives, net-metring, bonus-malus, CO_2 tax and so on [4].

Fig. 1-1 shows the progress made in the integration of renewables in the electricity, transport, heating and cooling sectors in EU member (EU28) countries. Following the trends since 2015, both of the 2020's intermediate targets set for the share of renewables in the transport sector and in the overall energy system might be missed slightly. It can be seen that there is a relatively higher penetration of renewables in the electricity sector than the others. One of the contributing factors is the advancement made in the technologies such as hydro, wind and solar photovoltaics (solar PVs) which makes it relatively easier to integrate them in the electricity sector. In addition, though geothermal and solar thermal resources are commonly integrated in the heating sector, they are also being installed in the electricity system up to certain level. Technologies based on biofuels, on the other hand, can be integrated in all of the three sectors. Electrification of the transport, heating and cooling sectors is one alternative to use all the potential renewables so that the energy transition could hit its targets. Electric vehicles and heat pumps (HPs) are examples of technologies that can be used to electrify the transport and the heating sectors, respectively.

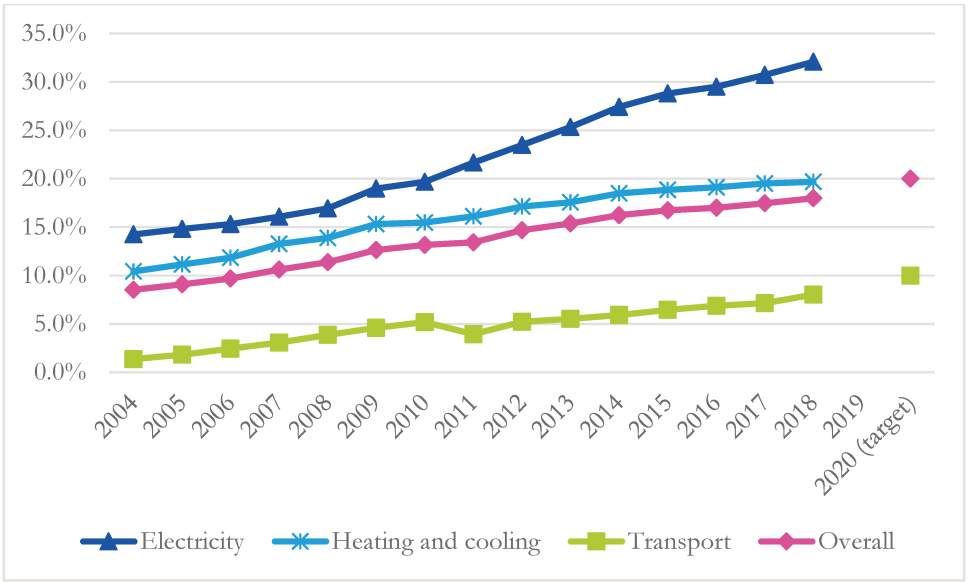

Fig. 1-1. Trends in the share of renewables in the EU28 energy mix (data taken from [10]).

According to the data from International Energy Agency, 56.55% of the electricity and 34.1% of the heat consumed in EU28 in 2017 was generated from fossil-free sources, including nuclear [4]. This shows that the heating and cooling sector is lagging behind the electricity sector in terms of decarbonisation. Moreover, the heating and cooling sector in EU consumes about 50% of the final energy [11]. Space heating and domestic hot water alone accounts up to 79% of the final energy consumption in EU households [12]. This implies that higher potentials of renewable integration and decarbonisation are available in the heating and cooling sector.

Fig. 1-2 shows the share of renewables in the heating and cooling market in EU28 member countries in 2018. Sweden is the leading country generating 65.4% of its heat from renewables followed by Latvia (55.9%) and Finland (54.6%). These countries are known for their higher market share of district heating network (DHN) (up to 90% in Sweden) with a higher share of combined heat and power (CHP) plants (up to 73% in Latvia) [13, 14]. Netherlands, on the other hand, shows the lowest renewable fraction (6.1%) due to the fact that 93% of the heat demand in the country being covered by using gas boilers [15]. France, with a 21.8% renewable share, lies above the EU28 average (2018) and even higher than the EU target for 2020 (which is 20%).

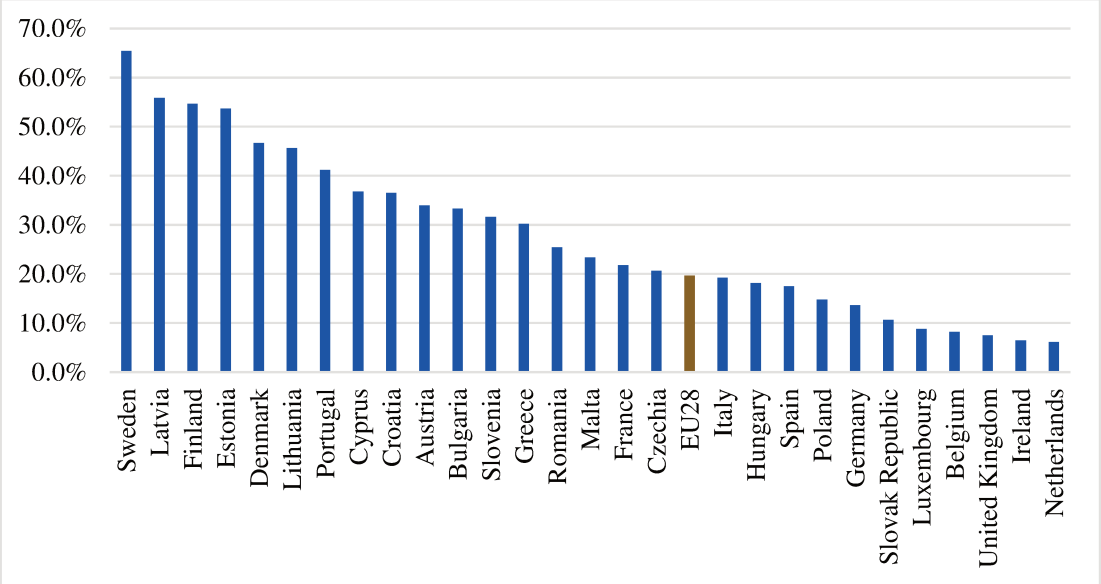

Fig. 1-2. Share of renewables in the heating and cooling sector in EU28 by 2018 (data taken from [10]).

1.1.2. The French and Swedish energy sectors at a glance

Fig. 1-3 compares France and Sweden in terms of total primary energy supply (TPES) mix by source for the year 2016. Having a 72% fossil-free TPES, Sweden is one of the leading countries in terms of sustainable energy system [16]. Because of the highest share of nuclear energy, 52% the TPES in France is also fossil-free [17]. However, only 39% and 10% of the TPES in Sweden and France, respectively, are coming from renewables. This shows that Sweden is already ahead of the 2030 renewables target set by EU while France has to put more effort.

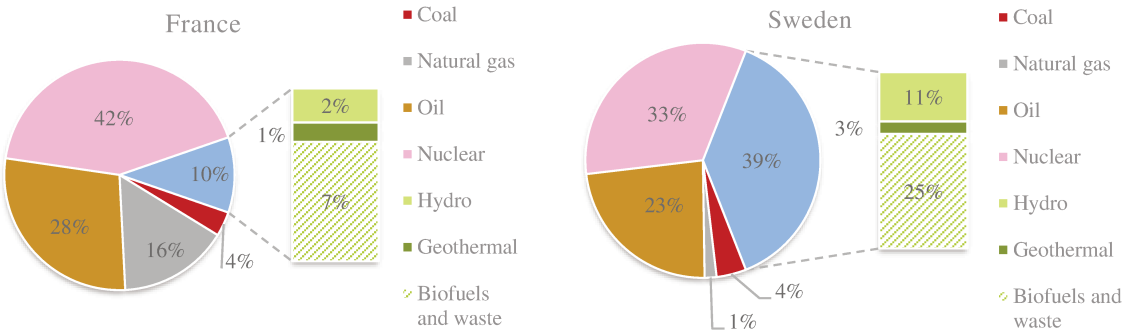

Fig. 1-3. Primary energy supply mix in France and Sweden by 2016 (data taken from [18, 19]).

Both France and Sweden are among the leading countries with low carbon electricity sector. As shown in Fig. 1-4, 92.3% and 98.6% of electricity produced in France and Sweden, respectively, was generated from low carbon technologies in 2016. The French electricity system is dominated by nuclear power plants (72.6% as shown in Fig. 1-4(a)). The share of nuclear power in Sweden (40.4% as shown in Fig. 1-4 (b)) is the second highest after France. Sweden is the third highest after Denmark and Finland in terms of biomass-based fuels and waste-to-energy [16]. The share of wind, hydro, waste and biofuels in Swedish electricity generation mix are higher than the corresponding values in France. On the other hand, the share of gas and coal in the electricity generation mix are more significant in France than in Sweden.

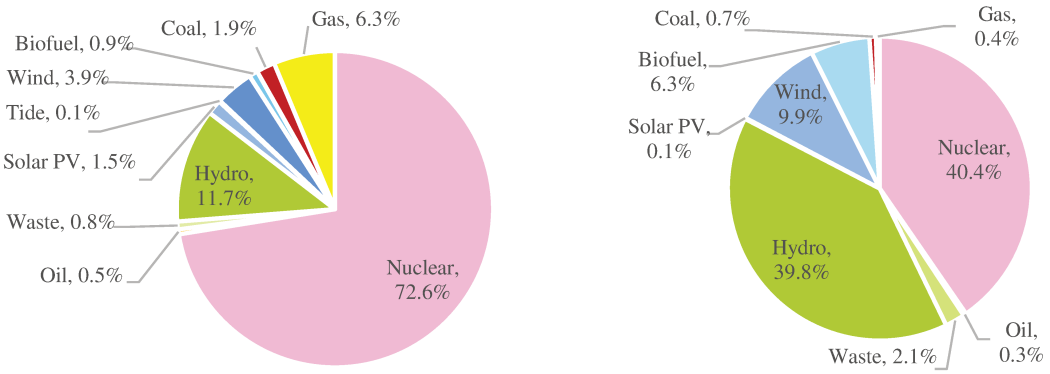

(a) (b)

Fig. 1-4. Electricity generation mix in terms of fuel sources by 2016: (a) France and (b) Sweden (data taken from [20]).

Fig. 1-5 shows the types of fuels used to generate heat in France and Sweden. Sweden is well known for its sustainable heating sector in which 86.5% of the heat generated in 2016 came from fossil-free sources (Fig. 1-5(b)). Biofuels cover the 60.4% of the heat generation. On the other hand, only 54.5% of the heat in France is generated from fossil-free sources, as shown in Fig. 1-5(a). Natural gas, covering 36.9%, takes the highest share.

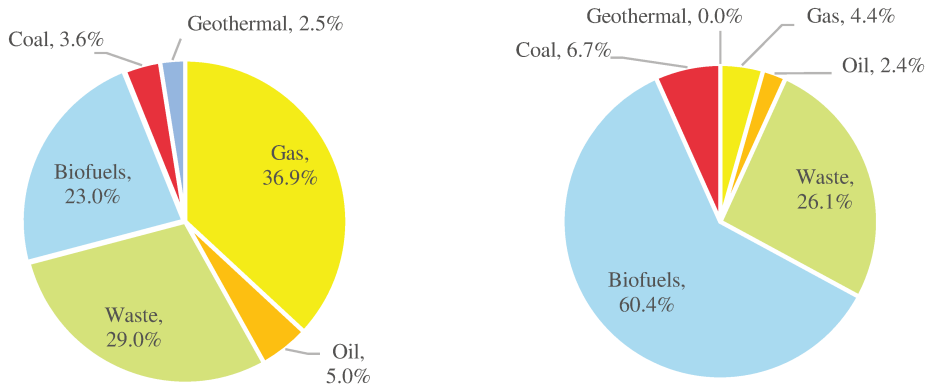

(a) (b)

Fig. 1-5. Heat generation mix in terms of fuel sources by 2016: (a) France (b) Sweden (data taken from [20]).

1.1.3. Synergy from coupled electricity and heating energy systems

The centralized conventional electricity grid has limitations in coping up with the increasing energy demand due to its poor efficiency, old infrastructure (which is very expensive to expand and renovate), and new types of loads (such as electric vehicles) [21]. Smart grid, which consists of distributed generations, energy storage, demand side management and smart meters together with information and communication technologies, are believed to overcome those limitations [22]. Distributed generation, as part of a smart grid, plays an important role in reducing carbon emission, improving power quality, decreasing power loss in the network and improving system reliability [23].

In a similar way, a smart thermal network (also referred to as 4th generation DHN) is supposed to replace the current 3rd generation DHN in the near future. Its key features include flexible distribution pipes, low temperatures, smart meters, distributed generations, thermal storages and, more importantly, its capability to be integrated with smart grids [24]. Smart thermal networks together with smart grids, smart gas networks and other energy carriers are collectively referred to as smart energy systems [25]. The corresponding distribution networks need to be managed in an integrated way to exploit their synergy, which is impossible otherwise within their independent domains.

Distributed generations are one of the common features in both smart grids and smart thermal networks. Combined Heat and Power (CHP) is one of such distributed generation options in which useful heat is generated, in addition to the electricity, by recovering the waste heat from conventional thermal power plants. Varieties of fuel types such as gas, biomass, waste and geothermal can be used as sources for CHPs to produce both heat and electricity. Furthermore, the heat recovered from such plants can easily be fed into the local heat distribution networks.

A compression heat pump (referred in this thesis as HP*) can also be considered as a distributed generation for the heating network. It uses electricity to transport heat from the colder to the hotter region. Hence, it acts as a distributed load from the electrical network point of view.

Renewables, such as wind and solar PV, are yet the other types of distributed generations that can be installed in the smart grids. The main challenge associated with them is their intermittent nature. In an off-grid application or in a grid-connected system where there are no sufficient incentives (like feed-in tariffs), integration of electrical storage is one alternative to increase the penetration of renewables. However, electrical storage systems, such as batteries and power-to-gas technologies, are 50 to 100 times more expensive than sensible thermal storage tanks [26]. On the other hand, electricity is much cheaper to transport than heat because of higher distribution losses in the latter case [25]. HPs, in combination with sensible thermal storage tanks, are better options in that case to effectively use the surplus electricity generated from renewables [22, 27]. In addition to the thermal storage tanks, thermal inertia of buildings and heat distribution network can also play a role in increasing flexibility in both electricity and heating energy systems [28–30].

As discussed above, integrating the heating and electricity energy systems using coupling technologies, such as HPs, CHPs and thermal storages, enables to exploit the synergy in terms of flexibility, efficiency and decarbonisation.

1.2. Problem statement

Ideally, integrating large scale HPs and thermal storage could result in a more sustainable energy system. It means that more renewables can be integrated in the electricity system without any curtailment, the peak heat demands can be effectively shifted, and, consequently, a more efficient, flexible and sustainable energy system can be established. Results based on simplified models, such as those used in EnergyPlan [31], RETScreen [32] and HOMER [33], also support the ideal premise. In its “Heating and Cooling Strategy”, EU also strongly recommended the use of HPs and biomass-based CHP plants in order to decarbonise and increase the efficiency of its heating and cooling sector [34, 35]. Nordic countries are the leaders in following the EU’s guideline and in integrating large scale HPs and thermal storages as it can be witnessed in Sweden [36–38], Finland [39] and Denmark [40, 41].

However, the HPs are solely managed by the heat distribution companies without the full consideration of the electricity distribution network. This leads to a suboptimal operation of the overall system. The electricity distribution company, for example, estimates the electricity demand based on its own data considering the HPs usually as a fixed demand. A district heating operator, on the other hand, considers the heat demand profile and all the heat sources, including the HPs, and decides on the most economical operational strategy of the HPs. As the two distribution system operators act independently, any possible difference

* Although the focus of this thesis is on the electrical heat pumps, absorption types can also be included like any other coupling technology.

between the assumed and actual operational strategy of the HPs may compromise the efficiency of the overall system [42]. Moreover, the increased penetration of HPs has paused a security issue as it is increasingly overloading the low voltage electricity distribution grid [39, 43]. Besides that, an optimal placement and economical dispatch of coupling technologies like CHPs made exclusively from the heating network perspective, could lead to suboptimal solutions from the electricity network point of view. This shows the limitation on the use of conventional single-energy carrier modelling and simulation tools in capturing the operating parameters of multi-carrier distribution grids [44].

Integrated modelling and simulation tools are required in order to quantify the synergy, assess the technical feasibility and find the optimum operational parameters of a multi-energy system (MES). The simplified MES simulation tools, like HOMER and EnergyPlan, lacks that capacity as they do not consider the distribution networks' physical and operating parameters. A literature review by Allegrini et al. [45] shows that there are no well-developed tools that can take the MES distribution networks' physical parameters into account. Tailor-made modelling approaches reported in literature (see *Chapter 2* for more details), on the other hand, lacks generality and flexibility in answering the following key research questions related to coupled electricity and heat distribution networks.

1. How can we capture the key operating parameters of both distribution networks consisting of meshed topologies with prosumers (nodes that act as producers and consumers alternatively)?

2. Could the location of coupling technologies affect the performance of the overall energy system?

3. If so, how can their optimal placement be determined and how can they be dispatched optimally without compromising the constituent distribution networks?

4. What is the significance of a thermal storage in exploiting the synergies? How can it be optimally managed in the presence of intermittent renewables and variable price signals while considering all the technical constraints?

This thesis proposes a novel methodology in modelling, simulation and optimisation of integrated electricity and heating networks based on an extended energy hub (EEH) approach. As a proof of concept, the capacity of the tool in answering the above research questions is demonstrated by considering case studies with parameters and boundary conditions that are very close to real systems.

1.3. Objectives

The main objective of this thesis is to develop a flexible modelling, simulation and optimisation tool that can capture the operating parameters of distribution networks in a multi-energy system (MES) in general, and demonstrate its application in an integrated heating and electricity networks. It consists of specific objectives, focussing on developing:

- a general and flexible load flow modelling framework capable of handling highly coupled MESs;
- the details of an integrated load flow model governing coupled electricity and heat distribution networks;
- an optimisation algorithm and its integration with the MES load flow model;
- a submodule for integration of thermal storage tank with the MES load flow model;
- a model predictive control (MPC) algorithm that can be used for optimal management of a thermal storage in a MES.

In addition, the following application-oriented specific objectives are also considered to demonstrate the capacity of the developed tool and its novelty.

- Conduct a single time step and time-series load flow studies on coupled electricity and heating networks.
- Conduct a single-hour economic dispatch, techno-economic optimisation and optimal placement of coupling technologies in the integrated heating and electricity networks.
- Illustrate the capacity of the tool in handling thermo-economic optimisation in time-series.
- Demonstrate the capacity of the tool in exploiting the synergy from coupled electricity and heating networks in the presence of thermal storage, intermittent renewables and variable electricity price signal.

1.4. Structure of the thesis

Figure 1-6 illustrates how the thesis is organized into 8 chapters and where the four journal papers are referred. As discussed in the previous sections, the first chapter covers the background, problem statement and objectives of the thesis.

Chapter 2 is dedicated for the state of the art in modelling a MES. It highlights the main scientific gaps that this thesis aims to address. *Chapters 3* and *4* presents the methodology followed in this thesis. *Chapter 3* describes the general framework called "*An Extended Energy Hub (EEH)"* approach for modelling MESs. Using this framework, the details of an integrated load flow model consisting of heating and electricity networks are discussed in *Chapter 4*.

The methodology is then followed by *Chapters 5*, *6* and *7* that illustrate the capacity of the proposed methodology in answering the research questions listed in *Section 1.2.* A proof of concept through theoretical validation is presented in *Chapter 5* by considering integrated load flow case studies. The optimal placement and economic dispatch of coupling

technologies are then discussed in *Chapter 6*. *Chapter 7* illustrates how the tool can be further applied in exploiting the synergy from coupled electricity and heating networks in the presence of intermittent renewables and variable price signals. In addition to the main methodology, which is covered in *Chapters 3* and *4*, specific methodologies on the optimal placement of coupling technologies and application of MPC are included in *Chapters 6* and *7*, respectively. The main findings, recommendations for improvement and research outlooks are then summarised in *Chapter 8*.

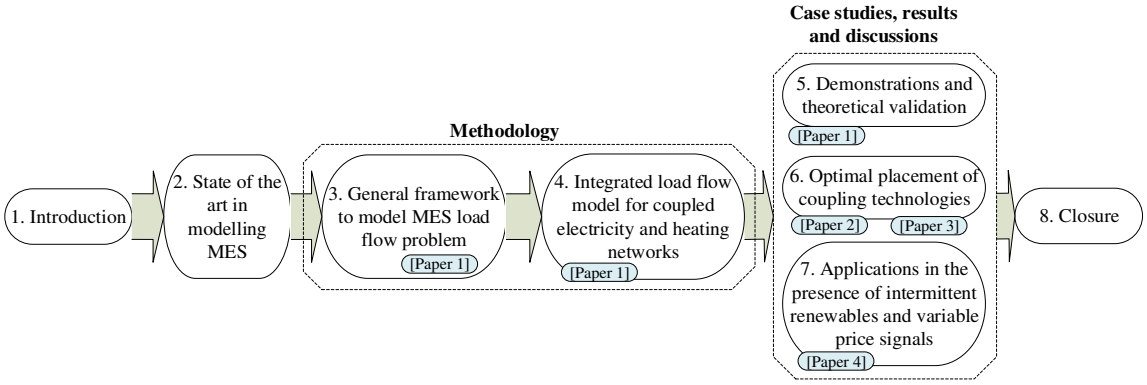

Fig. 1-6. Organization of the thesis.

2. State of the Art in Modelling Multi-Energy Systems

In this chapter, a survey of recent literature related to the modelling, simulation and optimisation of multi-energy systems (MESs) is presented. It ranges from those tools that are used for feasibility and pre-feasibility studies (at planning phase) up to those modelling approaches and tools that are used to study steady state and dynamic operating parameters of an energy system. As multi-energy system is a very wide multidisciplinary subject area, this chapter starts by defining the context of MES which is emphasised under the scope of this dissertation.

2.1. Context

Keirstead et al. [46] defined an urban energy system as a combined processes of acquiring and using energy to satisfy the energy service demands of a given urban area. An energy system can have four perspectives depending on the level of details and parameters of interest: *spatial*, *multi-service*, *multi-fuel* and *multi-network* perspectives [47]. The *spatial* perspective refers to the geographical domain ranging from a single building up to districts, cities, regions and countries. The *multi-service* perspective indicates the varieties of energy demands such as electricity, heat, cooling and chemicals. The sources of energy including gas, waste, biomass, electricity, renewables (e.g. wind, solar), and hydrogen are categorized into the *multi-fuel* category. The last, yet important, is the *multi-network* perspective that represents the distribution networks that are used to transport different energy carriers. Examples are the electricity and heat distribution networks. An energy system where a number of energy carriers interact at different levels is referred to as *multi-energy system (MES)* [42, 47–52]. Terms like "*integrated energy system*" [29, 30, 53–56] and "*multi-carrier energy networks*" [44, 57–63] are also used interchangeably. *Smart energy systems* [25] and *smart multi-energy grids* [64] are used to take into account the smart meters and information communication facilities. In this thesis, the term *multi-energy system (MES)* is used in the *multi-network* perspective to describe the overall energy system under consideration with the *spatial* scope ranging from few buildings up to few districts. The term "*integrated*" is used to indicate an all-inclusive simulation process of the MES under consideration.

2.2. Modelling MES

In the transition towards a future sustainable and renewable energy schemes, MES provides a new approach to find out the best feasible solution by exploiting the synergy from different energy sectors, which could be otherwise impossible within the limits of the individual sub-sectors [25, 47]. Conventionally, energy sectors are decoupled from the planning and operational viewpoint while, in reality, their interaction and coupling is very tight and increasing [47, 53]. Electric vehicles, CHPs and HPs are examples of distributed energy

technologies that couple the electricity, gas, transport, heating and cooling sectors. Lund et al. [24] also identified that the capability of thermal networks to interact with smart electricity grids is one of the characteristics of the future 4th generation DHNs. In line with that, the penetration of CHPs and HPs in the heating sector is increasing in Nordic countries [36–41], which are role models for having sustainable district energy systems.

In order to quantify the synergy and manage the coupled energy systems efficiently, however, suitable modelling and simulation tools are required. Having a number of energy conversion and storage devices with different characteristics that involve multiple energy carriers and lots of parameters makes the modelling and simulation process of a MES to be very complex and demanding [42]. Capturing the important operating parameters of a MES using the conventional single-carrier tools is cumbersome as such tools are not designed for such multi-carrier energy distribution systems [44]. Though there is no off-the-shelf software tool yet that can capture the full physical and operating parameters of multi-carrier distribution networks [45, 49], progress has been made recently at research level.

The body of work presented in literature can be broadly grouped into two major groups depending on whether the details of the distribution networks' parameters are considered or not (see Fig. 2-1). Those researches that did not consider the distribution network can be further classified into two: those using existing software packages on one side and those which used their own mathematical models on the other side. Studies made using existing software packages can be further grouped into two. The first group consists of those studies dealing with the details of a co/polygeneration plant while the other group cover the literature focussing only on the energy balance at building, city or national levels. Tailor-made approaches, on the other hand, can be divided as modular and non-modular.

In the second major category, which considers the distribution networks, there are also two group: those that use existing software packages in the co-simulation environment and those that use tailor-made models. Depending on how flexible they are, the tailor-made models are further classified as modular and non-modular.

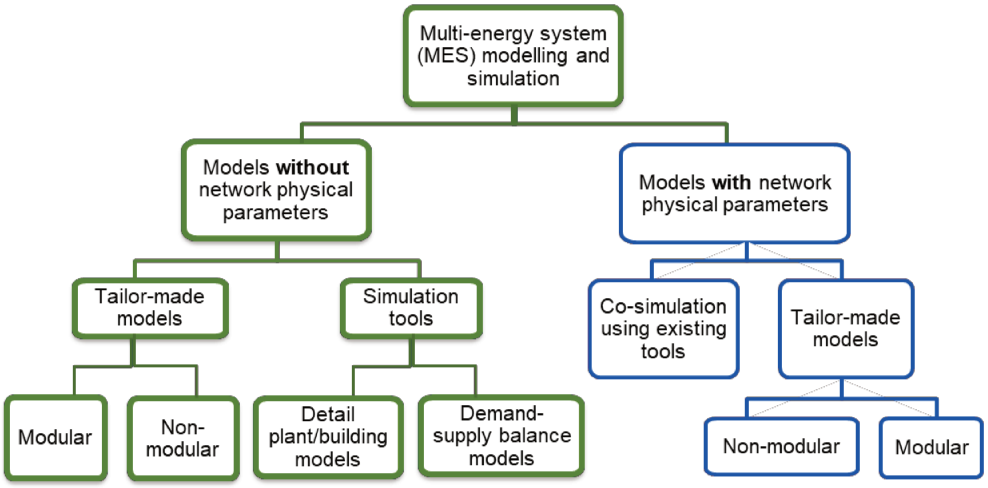

Fig. 2-1. Categories of MES modelling approaches reported in literature.

Most of the literature work dealing with MES to date falls into the first category. The second category is relatively new and there are only limited number of studies. In the following sections, the approaches followed in each of the above categories are discussed briefly.

2.3. MES models without the consideration of distribution networks

The literature work in this category mainly focuses on either the feasibility assessment of a MES that consists of different energy technologies or deals with the detailed parametric study of a single power plant/building. The losses in the distribution network are either neglected or represented in a fixed percentage. Operating parameters and constraints of the distribution network are not studied. Some of the available software tools and tailor-made models that fall in this category are discussed below.

2.3.1. Examples of available tools

A review on existing software tools that are used for district-scale energy systems is presented in [45]. It is reported that none of them are capable of modelling multi-carrier distribution networks. Some of the tools dealing with MES are discussed below.

2.3.1.1. TRNSYS

TRNSYS is a transient system simulation program developed by the University of Wisconsin Madison, USA [65]. It is a commercial tool. Examples of its application include detailed modelling and simulation of HPs [66], a thermal storage [67], a solar heating plant [68], building energy demand [69] and systems with CHP, gas boiler and thermal storage [54, 56]. It helps to study the performance of thermal storages, HPs and CHPs as a function flow rates and temperatures in time series. Its library consists of modules which can take electricity and gas carriers as an input or output. However, interconnecting pipes and transmission lines are assumed very short and lossless. Hence, this tool is not suitable for modelling larger systems where distribution losses are not negligible.

2.3.1.2. EnergyPLAN

EnergyPLAN is a free software tool, developed by the Sustainable Energy Planning Research group at Aalborg University, Denmark. It is used to simulate the operation of national or regional energy systems on an hourly basis, including the electricity, heating, cooling, industry and transport sectors [31]. It helps to conduct techno-economic analysis of an energy system consisting of thermal plants, renewables and storages. The components of the system are aggregated without the consideration of distribution networks and the simulation is run for one year in steps of one hour. As example, EnergyPLAN is used for studies on decarbonisation plan for large city's heating system using HPs [70], socioeconomic potential of introducing large-scale HPs in district heating system [41] and a 100% renewable energy

system [71]. As the distribution networks are totally neglected, this tool cannot be used for operational studies of MES distribution networks.

2.3.1.3. energyPRO

Another software tool that is used for techno-economic optimisation of energy systems that supply electricity and thermal energy is the energyPRO [72]. It is a commercial tool developed by EMD International, Denmark. The tool can be used to simulate cogeneration plants, such as CHP supported by renewables, HPs, and electrical and thermal storage technologies. Operational optimisations up to a minute step are possible. Variable price structures, such as grid electricity signals, can be taken into account. The outputs include detailed financial report for the entire project lifetime. The tool is also capable of comparative studies among alternative projects. The energy sources and demands can be either aggregated or interconnected with transport links with capacity constraints. The detail of the distribution network parameters, however, are not covered by this tool. Examples of its application include energy systems such as pumped-hydro with wind power plant, cogeneration plant, HPs and thermal storage in high-day and low-night electricity tariffs, participation of tri-generation and thermal storage in day-ahead market, and solar PV and battery [73].

2.3.1.4. RETScreen

RETScreen is a free clean energy management software, developed by Ministry of Natural Resource, Canada, for energy efficiency, renewable energy and cogeneration project feasibility analysis [32]. It is based on a comparative analysis of a “proposed case” energy investment with the “base case”. The output reports contain information regarding how much the “proposed case” is attractive in terms of economic and environmental savings made over the life span of the project. Having a climate data base makes it easy to analyse renewables, such as solar and wind projects. It has also cost and product databases for various energy technologies. RETScreen runs on a monthly time scale and it has no optimisation routine [74]. Like the previous tools, RETScreen does not have libraries for modelling distribution networks. Hence, it is used only at planning phase. Examples of its application include studies on energy systems with a CHP plant combined with renewables [75] and a ground source HP assisted with a solar PV [76]. Its combination with external optimiser to determine the sizes of renewable sources is also presented in [74].

2.3.1.5. HOMER

HOMER (Hybrid Optimisation of Multiple Energy Resources) is a commercial software tool, originally developed at the National Renewable Energy Laboratory, USA [33]. Using either of its HOMER Pro or HOMER Grid versions, it enables to study the financial and economic feasibility of an off-grid or grid-tied energy system projects. It has online database for monthly average wind speed, solar radiation and daily electrical and thermal load profiles. It has also incorporated algorithms which estimate the hourly wind and solar radiation profiles based on the monthly average values. Furthermore, it contains a list of commercial and

generic components such as wind turbines, battery storages, solar panels, power convertors and diesel generators together with their performance curves.

HOMER can be used to simulate, optimise and conduct sensitivity analysis on energy systems consisting of solar, wind, hydro, battery, CHP, diesel generator, electrical load, electric heater and thermal loads. However, both of the energy sources and demands are aggregated without the consideration of the distribution grids. Neither are the thermal components as detail as the electrical components. That limits its application only to MES at planning phase. In literature, HOMER is used to assess the feasibility of a small hydro/solar PV/wind hybrid off-grid system [77], a biomass gasification plant [78], a biomass-based, combined cooling, heating and power plant [79] and a hybrid renewable polygeneration system with membrane distillation [80].

2.3.2. Tailor-made models

The above mentioned software packages are being updated from time to time and more modules are being incorporated into their libraries in order to expand their application scope. However, they are not yet complete due to advances in new energy technologies and progress in their applications. Some researchers overcome such limitations by using a combination of two or more of available software tools while others designed and solved mathematical models governing all the components included in the MES (tailor-made). TRNSYS and EnergyPlus are, for instance, used in co-simulation to study the potential played by a building inertia in the demand side management of a heating system [56]. A combination of EnergyPlus with an *energy hub concept* (discussed in *Section 2.3.2.2*) is used to optimise geometry, size and operation of MES at a building [81–83]. The tailor-made numerical models, on the other hand, can be either modular or non-modular depending on their flexibility and easiness for scalability.

2.3.2.1. Non-modular approaches

Literature in this category devised case-specific mathematical models. For example, a thermo-economic optimisation of a combined heating, cooling and power system with compressed air storage is presented in [84]. Also a systematic approach to determine the optimal component sizes of a polygeneration plant fuelled by natural gas, biomass and solar energy is discussed in [85]. Similarly, techno-economic benefits of an energy system consisting of wind turbines, a CHP, an electrical heater, a thermal boiler, electrical batteries and a thermal storage is studied in [22]. In all of the three papers, mathematical models governing the operation of each component in the respective systems are solved altogether using numerical methods or optimisation algorithms. Energy balance equations are used in [51] to model a MES consisting of electricity, heat, natural gas and hydrogen energy carriers. A similar approach is used to study a MES involving electricity, natural gas, heating and cooling energy carriers [86]. A comprehensive mathematical models of devices in a residential MES, such as fridge, freezer, dishwasher, washer and dryer, stove, water heater, hot tub and pool pumps are formulated in [87]. A different approach of modelling a MES as

a multi-prosumer node is proposed in [50]. The dynamics of the components in the energy system are captured using their state space models while the interaction between different energy carriers are represented using power balances.

All the methodologies presented in this category show how mathematical details of components in a MES can be taken into account in the modelling and optimisation process. However, they do not say much about how a new energy carrier can be introduced in the model. Neither do they give hints on the scalability of the models for energy system applications with larger distribution networks.

2.3.2.2. A modular approach: the energy hub concept

The more general and modular tailor-made modelling approach of MESs is the energy hub concept. Geidl et al. [59] defined the energy hub as an interface where input/output, conversion, transformation and storage between multiple energy carriers take place. Accordingly, the energy hub has two ports to interact with its surrounding: the input and output ports. Unidirectional power flows coming from different energy carriers are assumed to go into the input port, pass through the conversion and storage devices and finally leave at the output port to supply the energy demands of various types (see the example in Fig. 2-2). The power converting devices include co-generation plants, polygeneration technologies, transformers, heat exchangers, power-to-heat systems, waste-to-energy technologies, boilers, electronic power converters and so on. Storage technologies include electrical batteries, pumped hydro, thermal storage technologies, compressed air, hydrogen tank etc. The converting devices and storage technologies altogether are referred to as coupling technologies.

The conversion efficiencies of the technologies are used to formulate the coupling matrix ($\boldsymbol{C}$) that relates the input power vector ($\boldsymbol{P_{in}}$) and output demand vector ($\boldsymbol{L}$) of an energy hub, as shown in equation (2-1). The required amount of input power to supply a given demand vector can be simply found by multiplying the load vector with the inverse of the coupling matrix. This makes the energy hub approach to be modular and easily adaptable.

$$[\boldsymbol{L}] = [\boldsymbol{C}][\boldsymbol{P_{in}}] \tag{2-1}$$

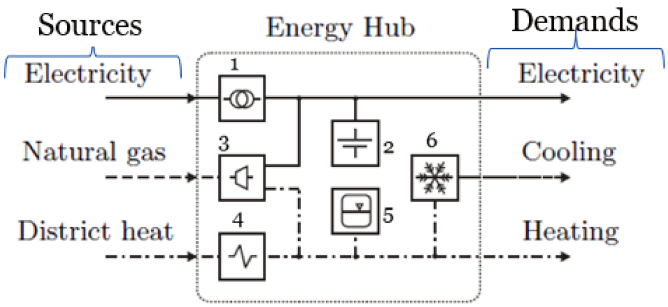

Fig. 2-2. Example of an energy hub where electricity, natural gas and district heat are interacting (adapted from [59]). The coupling devices are (1) transformer, (2) electrical battery, (3) CHP, (4) heat exchanger, (5) thermal storage and (6) absorption chiller.

Application areas of energy hub modelling approach range from a single cogeneration plant up to large industries, commercial buildings, islanded power supply systems, districts and even regions as far as the parameters of the internal distribution networks are less important.

In Fig. 2-2, the alternatives for supplying a given demand is increased due to the presence of various coupling devices. The electricity demand can be, for example, supplied using the electricity either generated from the CHP or from the one coming through the transformer or from the electrical battery or a combination of them. Similarly, the heat demand can be met using heat coming from the district heating, or from the CHP or by discharging the thermal storage. The cooling demand, on the other hand, is met using absorption chiller that converts heat into cold.

Economical dispatch of coupling technologies can be determined by combining the coupling matrix with optimisation algorithms. Deterministic approaches are reported in [59] while a gravitational search algorithm is proposed in [88]. The energy hub concept can also be used to study the effect of elastic demands in determining the price of energy generation in a MES [48].

The main limitation of representing the energy hub as described above lies on the unidirectional power flow assumption. Optimal dispatch of the coupling technologies is made only to meet the demands (in the output) and to charge the storages if there is any surplus. That is applicable only to islanded energy systems where there is no external grid. Many systems, like the one shown in Fig. 2-2, are connected to distribution networks. In that case, there could be prosumers which can use the coupling technologies to produce surplus of power that can be injected back into the distribution networks. For example, the CHP in Fig. 2-2 can be used to produce surplus of electricity and heat, which can be injected into the respective distribution networks. The unidirectional power flow model of the energy hub lacks that important feature. Furthermore, it is not clearly defined how local generations including renewables can be integrated in the model.

J. Wasilewski [89] proposed a modified energy hub concept that can overcome the above limitations. A graph and network theories are applied to model the interaction of coupling technologies inside the hub. In addition, local generations, such as solar PV, are connected using solar panels as energy conversion devices. The methodology is used to study steady state energy balances. Its complexity, however, makes it challenging to develop an algorithm suitable to determine optimal dispatch of the coupling technologies.

2.4. MES models with the consideration of distribution networks

The models in this category consider the distribution networks and address their physical and operating parameters partially/fully. Such models are used for load flow studies, economical dispatch and optimal power flow studies.

2.4.1. Co-simulation using existing tools

There are well-developed simulation and optimisation tools for single-energy-carrier distribution networks. Recently, quite few research papers highlighted the possibility of running multiple single-energy-carrier tools in a co-simulation environment. Widl et al. [44] used DIgSILENT for electricity and Modelica for DHNs, both running in a co-simulation environment. An electric boiler is the only coupling device used. Arnaudo et al., [43] used Panda Power, Modelica and python based models running in co-simulation to study the flexibility that can be gained from distributed HPs. The electricity distribution network is simulated using Panda Power and the residential buildings are modelled on Modelica. HPs, thermal storage and controllers are implemented on python. A similar study that includes DHN model is presented in [90]. Sequential coupling is implemented by first running the thermo-hydraulic model of the DHN followed by the steady state simulation of the electrical distribution network. Use of a well-established simulation tools in a co-simulation environment enables to capture all the relevant information including the dynamics of components at very small simulation time-steps. However, the sequential coupling approach, which is efficient for load flow studies and scenario based comparative studies, has limitation in handling optimisation problems that involve coupling technologies. A CHP is a good example for this. The optimal dispatch of a CHP found by simulating the DHN will rarely be in agreement with what would be found from running the electricity distribution network optimisation. This could result into a diverging solution.

2.4.2. Tailor-made models

Similar to the non-modular approaches that assumed aggregated source and demand, discussed in *Section 2.3.2*, there are also tailor-made models and algorithms that take the distribution network parameters into account. Putting all the governing equations together and solving them numerically helps to overcome the challenges of co-simulation approach. Some of the algorithms are non-modular and less flexible as they need reformulation of the governing equations whenever the configuration/layout of the application case study is changed. Others are modular with wider scope of application, and more importantly, they need little or no changes when the configuration of the MES is changed. They also follow modular approaches which enables easy integration of any coupling technology or even any additional energy carrier and its distribution network.

2.4.2.1. Non-modular approaches

Bracco et al. [91] studied a MES consisting of CHPs, solar PV, solar thermal, absorption chillers, electrical and thermal storages to supply residential demands and electric vehicles. The demands and the energy technologies are interconnected using the electricity distribution network which is modelled using direct current (DC) power flow approximations. The heat distribution network is not modelled at all. Renewable integration planning in urban multi-carrier energy distribution grids is discussed in [62]. The heat and electricity distribution networks are modelled using power flow balances with approximate loss functions. Such

approximations are acceptable only if the distribution network is small or if the reactive power flow in the system is not significant.

Li et al. [92] studied the electricity and heating networks that are coupled with a HP. AC power flow model is applied for electricity network while mass balance and temperature drops are used to model the heating network. The possibility of meshed heating network topologies is not considered. Also, a single coupling device is assumed. Awad et al. [55] and Liu et al. [93] followed a similar approach, but node-loop equations with pseudo-dynamic temperature drop equations are used to model the heating network considering meshed loops. However, the overall heat transfer coefficient is assumed to be constant for all mass flows, which is not true in reality. Furthermore, the node-loop equations used in the hydraulic models need pseudo-loop paths (the number of which depends on the network topology) in addition to the physical loops in order to have equal number of equations as the number of unknowns. As identification of pseudo-loops is not straight forward, it is difficult to develop a general algorithm for the models that are based on node-loop equations [94]. In their case study, Liu et al. [93] considered heating and electricity networks that are coupled through three CHP plants. All electrical demands and all CHP plants are assumed to be at unity power factor which is not always the case. There is also a requirement of reactive power to keep the voltage magnitude at the slack and PV hubs to a specified magnitude. However, no reactive power generation is considered in their case study [93].

Liu and Mancarella [57] and Shabanpour-Haghighi and Seifi [95] extended the load flow model presented in [93] into an energy system consisting of gas, electricity and DHN. The application of such models to study network congestion and uncertainties are presented in [52] and [61], respectively. Both active and reactive power flows are considered in their case studies. However, lack of generality on the hydraulic models remained unsolved due to the use of the node-loop equations. They also assumed constant value of the overall heat transfer coefficients in their thermal models.

In a load flow study of a MES, there are a number of equations for each network to be solved iteratively. Due to the coupling devices, some of the equations in one type of energy network are coupled with some of the equations in the other type of energy network. To handle this coupling issue, two types of iterative strategies are reported in literature: a decomposed approach and an integrated approach. In the first method, the overall system is decomposed into independent network models and one network model is solved at a time based on the previous values of the parameters in the other networks [96, 97]. The integrated approach, on the other hand, considers the coupling between different networks explicitly and solves the overall system of equations as a single load flow problem as described in [95, 98]. A comparative study of the two approaches presented in reference [93] shows that the integrated load flow approach is faster than the decomposed approach and the difference in computational time becomes significant as the network size gets larger.

2.4.2.2. Modular approaches

M. Geidl and G. Andersson [60] took the modularity advantage of the energy hub concept to represent a multi-carrier energy distribution network as an interconnection of energy hubs. Fig. 2-3 shows how such MES looks like. The vector $[P_{ag} \dots P_{ng}]$ represent n energy carriers solely generated at each hub while the vector $[L_a \dots L_m]$ denotes m types of loads connected at each hub. There are different types of coupling devices at each hub. All hubs are interconnected through n types of independent networks.

In the work of M. Geidl and G. Andersson [60], electricity, heat and gas energy carriers are considered. Alternating current (AC) power flow equations are used to model the electricity network while hydraulic equations are assumed to represent any isothermal pipe flow networks. A similar approach that includes thermal storage is discussed in [58]. In both papers, unidirectional power flows into the hubs are assumed, which implicitly limits the energy hubs to be consumers all the time. This is not always true as there could be more production of a given energy carrier inside a hub than is required by the hub itself. The hub shall have a flexibility to inject the excess power back to the network. In addition, some of the local generation, including renewables, are connected to the network directly while others are fed into the energy hub. Furthermore, heating networks are not considered in their analysis and all the thermal demands are assumed to be met locally at each hub.

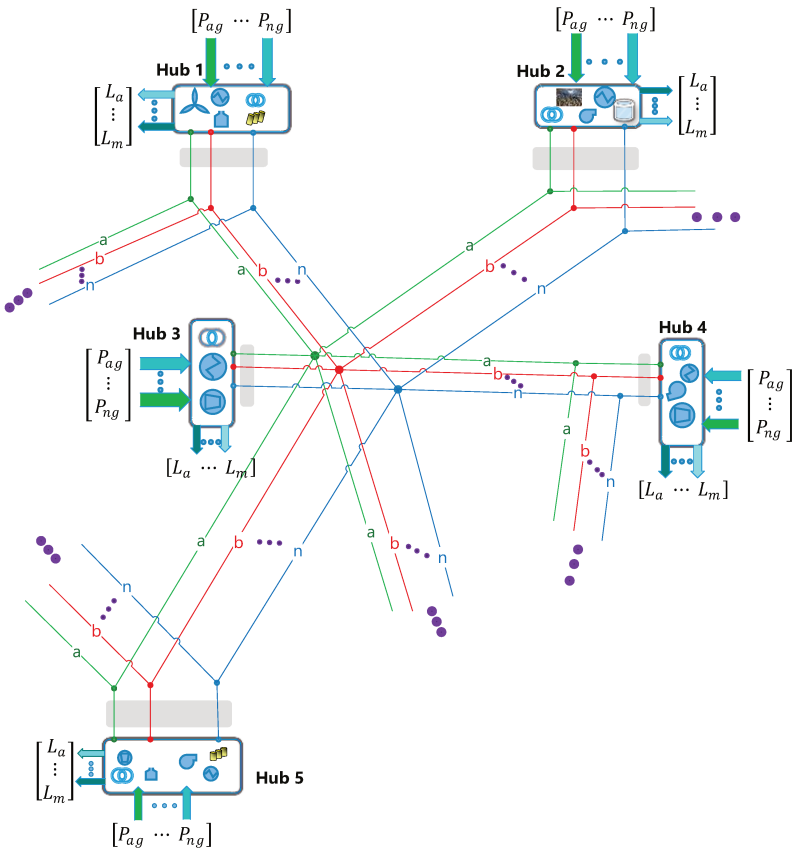

Fig. 2-3. General scheme of a highly coupled MES.

Moreover, the proposed hydraulic equations are not sufficient enough to model thermal networks as the temperature of water in the heating pipe network is not in the isothermal state. Besides to that, the inlet and outlet temperatures of water at a given node (where the energy hub is connected) are generally different due to the mixing of water at different temperatures. This requires treatment of the energy hub and the point of interconnection (node) separately, which needs a modified representation of the energy hub.

2.5. Summary

In this chapter, the state of the art in modelling and simulation of MES is discussed. Table 2-1 compares the features of the various modelling approaches with respect to the extended energy hub approach proposed in this thesis. The existing MES modelling software packages use energy balance between aggregated demand and source. Simulations and optimisations based on such tools are suitable for feasibility studies. Their application for operational optimisation is, however, limited as the distribution networks' parameters are ignored.

Table 2-1: Summary of MES modelling approaches.

Modelling approaches	**References**	**Features**					
		Modularity	**Power balance between generation and demand**	**Heat and electricity distribution networks**			
				Load flow simulations	**Meshed topologies**	**Flexibility to handle prosumers**	**Optimal dispatch of coupling technologies**
Existing tools (e.g. HOMER, RETScreen, TRNSYS, EnergyPLAN and energyPRO)	[54, 56, 65–80]	√	√	x	x	x	x
Tailor-made Type I	[22, 50, 51, 84–87]	x	√	x	x	x	x
Energy hub concept (Tailor-made Type II)	[48, 58, 59, 60, 89]	√	√	x	x	x	x
Co-simulation using existing tools	[43, 44, 90]	√	√	√	√	√	x
Tailor-made Type III	[52, 55, 57, 61, 91–98]	x	√	√	√	x	√ (lightly coupled)
Tailor-made Type IV ***(An extended energy hub approach)***		√	√	√	√	√	√

There are well-developed simulation and optimisation tools, on the other hand, capable of handling only one energy carrier. Quite few researchers combined two and more of them in a co-simulation environment so that distribution networks' operating parameters can be investigated. Their application for integrated optimisation is yet to be discovered.

Various tailor-made MES models are reported in literature with and without the consideration of distribution networks. Most of them are case-specific while quite a few followed a modular approach. The modular tailor-made models applied the energy hub concept together with network power flows. However, the unidirectional power flow assumption at the energy hubs and isothermal hydraulic models limits their application scope to a MES consisting of only electricity and gas networks. The models cannot handle prosumers either.

The energy hub concept shall, therefore, be extended (redefined) to add a bidirectional power flow flexibility and increase its capacity to handle heat distribution networks. Also, the thermo-hydraulic models discussed in the tailor-made approaches need to be general enough to include meshed topologies. In addition, the models are preferred to be more flexible so that any change in the topology or configuration of the heating network can be automatically detected in the computer-based algorithm. Furthermore, the modelling approach should treat the MES as a single problem so that multi-carrier power flows can be simulated simultaneously. This, in turn, makes it easier to apply an optimisation technique for the whole system. The scalability and modularity of the methodology to encompass any additional energy carrier or coupling technology is also crucial. The following chapter introduces a novel modelling framework that can address all these issues.

3. General Modelling Framework for Multi-Energy System's Load Flow Problem

This chapter presents the general framework of the novel MES modelling approach which is proposed to address the scientific gaps discussed in the previous chapter. MESs cover a wide range of disciplines, and most of the users rarely have that level of expertise to understand all the technical details of multi-carrier energy distribution networks. As it is crucial for the model to be able to capture the key operating parameters of the distribution networks, it is also equally important for it to be general and flexible so that it can be scaled up or configured easily by most of its users including those who are not experts. This feature is lacking in the non-modular modelling approaches reported in literature. Those models can be used only by experts as the system of equations governing the multi-carrier distribution networks need to be manually reconfigured whenever there is a change in the network topology and/or in the constituent coupling technologies. Those few articles which followed the modular approach based on the energy hub concept, on the other hand, were limited in application due to the drawbacks of the way the energy hub is formulated.

This dissertation proposes a general and flexible approach for modelling a MES by redefining the energy hub so that its modularity can be kept while allowing bidirectional interactions within a multi-carrier distribution network. In addition, the methodology proposed in this dissertation also configures the system of equations automatically. This avoids the tedious and manual process of formulating the governing equations whenever the case study is modified. It means that the users, even without modelling expertise, can easily modify the network topology and change constituent technologies. Its modular nature allows integration of additional energy technologies and distribution networks, including a thermal network (which was one of the limitations identified in the state of the art). The generic structure of the MES model which is used in this dissertation is discussed in the following section. It is then followed by a discussion on how an *Extended Energy Hub (EEH)* approach is used to define the general framework of a MES load flow problem.

3.1. Structure of the proposed modelling framework

The structure of the whole model developed in this PhD is shown in Fig. 3-1. It has three parts: the *data inputs*, the *core process* and the *output*. The *data inputs* part is where the user provides the parameters of the MES. The data regarding the distribution networks includes their layouts, physical parameters and constraints. The demand profiles, any local generation and coupling matrices describing the energy technologies installed at each hub are also fed into the model by the user. Additional information about the reference values, base values, constants, cost of generations and so on are also provided.

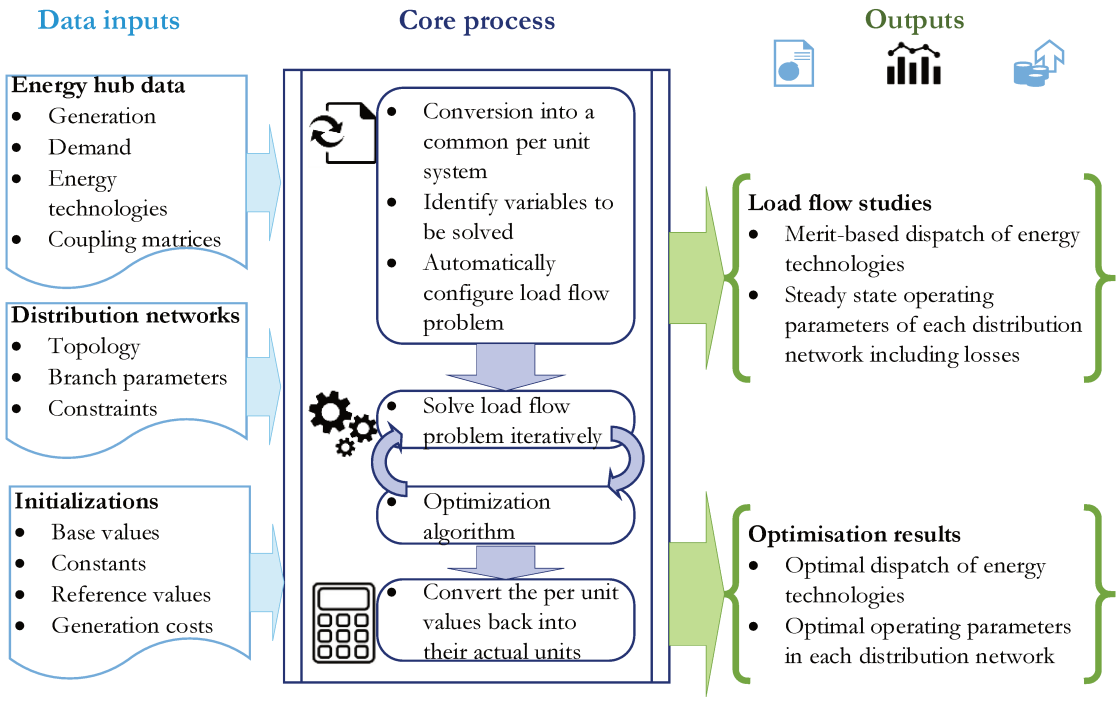

Fig. 3-1. Structure of a general and flexible MES simulation and optimisation model.

The *core process* is where the relevant information required to formulate an integrated load flow problem is automatically extracted from the input data. Parameters describing different energy carriers are converted using a common per-unit system. Distinction is then made between reference variables (which have fixed values) and those that need to be solved. Then, a system of equations, also called an integrated load flow problem, is formulated and solved for those unknown variables.

If the interest is on optimisation, instead, the load flow problem will be used as an equality constraint together with other inequality constraints. Like the load flow problem, the optimisation routine is also made to configure itself automatically with very little/no changes in the *core process* for any change in the input parameters, such as network topology and/or location and types of energy technologies. Once, either of the optimisation or the load flow problem is solved, the per-unit values of the variables are converted back to their actual values. Accordingly, either the optimal solutions or merit-based load flow simulation results are returned back to the user in the *outputs* part.

As part of the *core process* in the structure defined in Fig. 3-1, the EEH modelling approach is used to define the general framework that can be applied to derive the integrated load flow problem governing any MES.

3.2. The extended energy hub (EEH) modelling approach

An energy hub is an interface where transformations, conversion, storage and consumption take place between different energy carriers [60]. This concept is extended by taking local

generations at each energy hub into account. Coupling matrices are also combined with power injection equations to mathematically formulate the load flow problem. Moreover, the energy hub is treated separately from the interconnection point as this is important in dealing with thermal networks.

Fig. 3-2 illustrates how an extended energy hub representation of a MES is used to group different components into three sections: *energy hub*, *point of interconnection* and *multi-carrier energy network*.

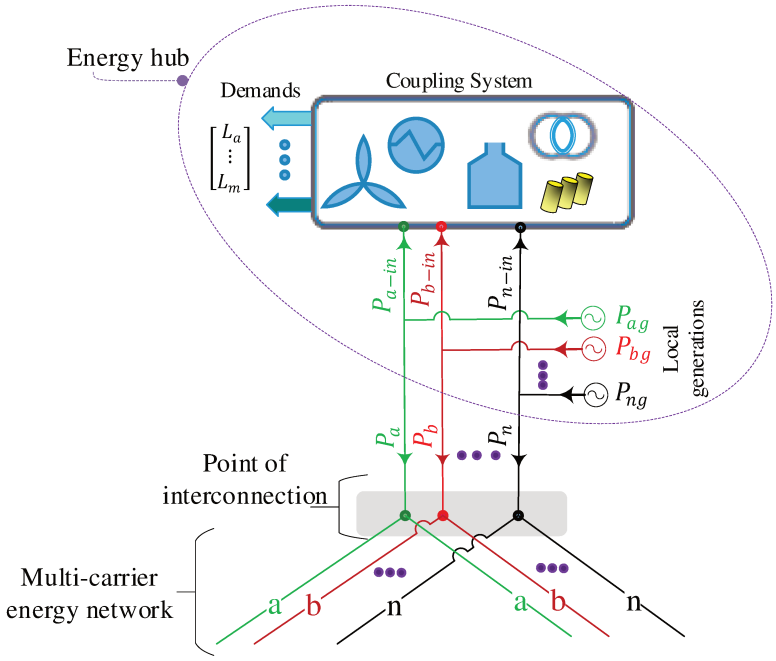

Fig. 3-2. Different parts of an extended energy hub

3.2.1. The energy hub

The *energy hub* section includes n types of locally generated powers (P_{ag} to P_{ng}), m types of local demands (L_a to L_m) and a *coupling system*. The *coupling system* consists of different types of energy conversion devices such as wind turbines, PV panels, solar collectors, heat exchangers, power transformers, electric boilers, gas boilers, electric heaters, CHP plants, HPs, heat storages, fuel storages, electricity storages and so on.

The solar panel can be part of the coupling system if solar radiation is considered as an energy carrier. The same is true for the wind turbine. However, if the energy conversion process of such devices is not a point of interest, only the output electricity can be taken as a locally produced power. Local generations include all those sources of power that produce only one type of energy carrier. Coupling matrices are extracted at each hub by formulating the algebraic relationship between the demands, the net power inputs into the *coupling system* and the efficiency of the coupling devices. In this dissertation, more emphasis is given to the relationship between those coupling matrices, demands, local generations and overall network parameters from the point of load flow studies. Equation (3-1) shows the general

matrix representation of the relationship between the demands (m types), the net power inputs into the coupling system (n types) and the rate of change of energy in the storage units (n types) [59].

$$\begin{bmatrix} L_a \\ \vdots \\ L_\delta \\ \vdots \\ L_m \end{bmatrix} = \begin{bmatrix} C_{aa} & \cdots & C_{a\gamma} & \cdots & C_{an} & Z_{aa} & \cdots & Z_{a\gamma} & \cdots & Z_{an} \\ \vdots & \vdots & \vdots & \vdots & \vdots & \vdots & \vdots & \vdots & \vdots & \vdots \\ C_{\delta a} & \cdots & C_{\delta\gamma} & \cdots & C_{\delta m} & Z_{\delta a} & \cdots & Z_{\delta\gamma} & \cdots & Z_{\delta n} \\ \vdots & \vdots & \vdots & \vdots & \vdots & \vdots & \vdots & \vdots & \vdots & \vdots \\ C_{ma} & \cdots & C_{m\gamma} & \cdots & C_{mm} & Z_{ma} & \cdots & Z_{m\gamma} & \cdots & Z_{mn} \end{bmatrix} \begin{bmatrix} P_{a\_in} \\ \vdots \\ P_{\gamma\_in} \\ \vdots \\ P_{n\_in} \\ \dot{E}_a \\ \vdots \\ \dot{E}_\gamma \\ \vdots \\ \dot{E}_n \end{bmatrix} \tag{3-1}$$

where L_δ is the local demand of type δ; P_{γ_in} is the net power input into the *coupling system* of type γ energy carrier; $\dot{E}_\gamma$ is the time rate of change of stored energy of type γ; $C_{\delta\gamma}$ is an element in the coupling matrix showing how much of the input power to the coupling system of type γ is converted into the local demand type of δ; $Z_{\delta\gamma}$ is an element of the coupling matrix indicating how much of the power from a storage type γ is contributing to meet the local demand of type δ; δ ranges from a to m while γ ranges from a to n.

By referring Fig. 3-2, it can be seen that each of the net input powers into the coupling system, (P_{γ_in}) terms in equation (3-1), is equal to the corresponding local generation ($P_{\gamma g}$) minus the injection into the network (P_γ) of the corresponding energy carrier (see equation (3-2)). By substituting equation (3-2) into equation (3-1), the extended version of the coupling equation for a general network of MES can be formulated as shown in equation (3-3). As the power injections into the network (which are now part of the coupling equation) are functions of the network parameters at all hubs, they act as a link between the demands and generations at different hubs.

$$P_{\gamma\_in} = P_{\gamma g} - P_\gamma \tag{3-2}$$

$$\begin{bmatrix} L_a \\ \vdots \\ L_\delta \\ \vdots \\ L_m \end{bmatrix} = \begin{bmatrix} C_{aa} & \cdots & C_{a\gamma} & \cdots & C_{an} & Z_{aa} & \cdots & Z_{a\gamma} & \cdots & Z_{an} \\ \vdots & \vdots & \vdots & \vdots & \vdots & \vdots & \vdots & \vdots & \vdots & \vdots \\ C_{\delta a} & \cdots & C_{\delta\gamma} & \cdots & C_{\delta m} & Z_{\delta a} & \cdots & Z_{\delta\gamma} & \cdots & Z_{\delta n} \\ \vdots & \vdots & \vdots & \vdots & \vdots & \vdots & \vdots & \vdots & \vdots & \vdots \\ C_{ma} & \cdots & C_{m\gamma} & \cdots & C_{mm} & Z_{ma} & \cdots & Z_{m\gamma} & \cdots & Z_{mn} \end{bmatrix} \begin{bmatrix} P_{ag} - P_a \\ \vdots \\ P_{\gamma g} - P_\gamma \\ \vdots \\ P_{ng} - P_n \\ \dot{E}_a \\ \vdots \\ \dot{E}_\gamma \\ \vdots \\ \dot{E}_n \end{bmatrix} \tag{3-3}$$

3.2.2. The point of interconnection

The *point of interconnection* is where the net injection of power (i.e. P_a to P_n in Fig. 3-2) from the hub into the network takes place for different energy carriers. It corresponds to the term *bus* in the electricity network and *node* in the DHN. The distance from the *coupling system* to this *point of interconnection* is assumed to be very short as compared to the length of branches connecting two different hubs. This enables to neglect the possible voltage, pressure and temperature drops between the *coupling system* and the *point of interconnection*. However, it does not mean that they are one and the same. For example, if water flows having different temperatures are mixing at a given *point of interconnection* connected to a heat-source hub, the temperatures of the outgoing water on the supply side will be different from the supply temperature of the corresponding hub. Hence, it is important to treat the energy hub and the point of interconnection separately in order to model thermal networks properly.

Whenever the distance between the *coupling system* and the *point of interconnection* becomes significant, it would rather be more convenient to define additional *point of interconnection* near the *coupling system.* It is also possible to define a *hub* with no generation and no load. In that case, the hub acts mainly as a *point of interconnection*.

3.2.3. The multi-carrier energy network

The *multi-carrier energy network* section, on the other hand, represents the remaining part of the overall system that interconnects all the hubs (see Fig. 3-2). If there is production of power for any carrier more than what is required in the hub itself, the excess will be transported to the other hubs where there is deficit. If the hub, instead, is in shortage of a given carrier type, it will import it from the network. However, it should be noted that the type and amount of energy carrier to be supplied/imported to/from the network depends not only on the demands and local generations, but also on the types of coupling devices available at a given hub. In other words, depending on the types of devices available in the coupling system, a given type of local demand can be met as a combination of power coming into the hub from different energy carriers. If there is an overproduction of a given energy carrier inside the hub (due to conversion between different energy carriers), then it will be injected back to the network.

3.3. MES load flow problem

As depicted in Fig. 2-3, the hubs in a multi-carrier distribution network are interconnected by multiple, but independent, transmission networks each of which is dedicated only for a single energy carrier. The values of the network parameters for each energy carrier depends on the net power injections of the same energy carrier from all the hubs. In other words, the injection of power into the network at each hub for each energy carrier can be defined as a function of each network's parameters. The electricity power injection at a given hub, for instance, is defined as a function of electricity network parameters such as voltage magnitudes, voltage angles and network admittance matrix (see Appendix A). These power

injections are then related to the local generations and demands at each hub using the coupling matrices.

In the load flow study, only some of the operating parameters (variables) are known and the others are to be solved. Any calculation of the power injection based on inaccurate values of the unknown variables will deviate from the exact power injections at each hub calculated using equation (3-3). The difference between the two, in an equation form, is called *mismatch equation*. Equations for power injections at each *point of interconnection* (as a function of operating parameters) are combined with the coupling equations (given by equation (3-3)) to define all the mismatch equations that are necessary to solve the unknown variables. This set of mismatch equations is called the *load flow problem* of a given MES. Iterative numerical methods, such as Newton-Raphson, are used to reduce the mismatch magnitudes by iteratively changing (approximating) the values of the unknown variables. The solution is said to be converged (i.e. the unknown variables are solved) if and only if the magnitudes of all the mismatches are below an acceptable tolerance.

3.4. Summary

In this chapter, the general structure of the tool developed in this thesis is presented. It is followed by the description of the EEH representation. Then the procedures that are used to formulate and solve the constituent mismatch equations of a MES load flow problem are discussed. The following chapter elaborates the procedures by considering coupled heating and electricity distribution networks in more details.

4. An Integrated Load Flow Model for Coupled Electricity and Heating Networks

In this chapter, the details of the mismatch equations are derived by applying the general framework of MES load flow model, discussed in the previous chapter, on a highly coupled electricity and heating networks. In the derivation, each hub is assumed to be equipped with local generations of fuel, heat and electricity. Electricity and heat demands are considered at all hubs. No fuel demand is considered in this study and hence no fuel network. The electricity energy carrier is split into active (subscript ep) and reactive (subscript eq) powers although both of them are transmitted through the same transmission line. The heat and fuel energy carriers are designated using subscripts h and f, respectively. Local generations for each carrier are indicated by attaching additional subscript g. Each hub is assumed to have different energy technologies that couple the fuel, heat and electricity. In the following sections, the details of equations that are used to model the electricity and heating networks together with the solution procedures are discussed.

4.1. The electricity model

The AC power flow in the electricity network is governed by Kirchhoff's current and voltage laws. The apparent power injection at each hub, which is a function of the network admittance and nodal voltages, is a complex quantity which is usually expressed in phasor representation. Although rectangular representation of complex parameters, such as voltage and impedance, can be used for electricity network modelling, the hybrid (polar voltage profile and rectangular impedance) representation is most widely used to formulate the power balance equations [99–101]. For an N bus electricity network, the per-unit (see *Section 4.4*) active (P_{ep}) and reactive (P_{eq}) power injections at any bus i are given by equations (4-1) and (4-2), respectively [102]. The derivations of these equations are included in Appendix A.

$$P_{ep(i)} = \sum_{j=1}^{N} |V_i|\,|V_j|\left(G_{ij}cos\theta_{ij} + B_{ij}sin\theta_{ij}\right) \qquad i,j = 1,2,3,\dots N \tag{4-1}$$

$$P_{eq(i)} = \sum_{j=1}^{N} |V_i|\,|V_j|\left(G_{ij}sin\theta_{ij} - B_{ij}cos\theta_{ij}\right) \qquad i,j = 1,2,3,\dots N \tag{4-2}$$

where $G_{ij} + jB_{ij} = Y_{ij}$ is an element of the network admittance matrix of size N by N and θ_{ij} is the voltage angle difference between nodes i and j (i.e. $\theta_i - \theta_j$).

The off-diagonal elements of the admitance matrix are formulated using equation (4-3) while the diagonal elements are calculated using equation (4-4).

$$Y_{ij} = -y_{ij} \tag{4-3}$$

$$Y_{ii} = \sum_{j=1}^{N} y_{ij} \tag{4-4}$$

where y_{ij} is the admittance of the line between buses i and j including a transformer (if any) while y_{ii} is the susceptance at bus i.

Equation (4-2) holds true only for a network without tap changing transformers. Transformer tap changing adjustments are usually represented by their π-equivalent models [103]. For a tap changing transformer connected between buses i and j having a per-unit tap setting ratio *a:1* in the specified order, the admittance matrix is formulated using equations (4-5) to (4-7) [103] (see Appendix A for the details).

$$Y_{ij} = -\frac{y_{ij}}{a} \tag{4-5 }$$

$$Y_{ii} = y_{ii} + \sum_{j=1, j\neq i}^{N} \frac{y_{ij}}{a^2} \tag{4-6}$$

$$Y_{jj} = y_{jj} + \sum_{i=1, j\neq i}^{N} y_{ij} \tag{4-7}$$

4.2. Hydraulic model

The parameters of interest that should be solved by the hydraulic model are the mass flow rate in each pipe and the pressure profile* at each node of the heating network. The heating network can be regarded as two separate hydraulic pipe networks: supply and return pipe networks. The supply pipe network delivers the hot water from the sources to the consumers while the return pipe network brings the colder water back to the source after the heat is delivered to the consumer. Both networks are coupled together with the mass flow rate in each pipe. That means if the mass flow rate in one pipe in the supply pipe network is known, the same amount of water flows in the corresponding return pipe. However, the pressure profile has to be solved separately for both supply and return pipe networks.

* The pressure profile in this dissertation is limited only to show the relative pressure difference that should be maintained to guaranty the mass flows in each pipe. If all the hydraulic heads at all nodes (point of interconnection) are shifted up or down by the same amount, the solution still remains valid. To determine the optimal hydraulic head (which is beyond the scope of this PhD), it requires to know the coordination of circulation pumps and valves, the pressure drop at the heat exchangers and altitudes of each node.

The different numerical methods that can be used to solve hydraulic head and mass flow rates in water supply networks are presented in [94, 104], while their applications in DHNs are discussed in [105]. The methods range from a classical Hardy-Cross loop-correction method to a computer based Newton-Raphson method. In any of the methods, continuity of flow (conservation of mass at each node) and conservation of energy (pressure drop equations) are the principles that should be guaranteed [106]. Boulos et al. [94] discussed four types of methods that can be used to combine and solve the two principles. These are *loop equations*, *node-loop equations*, *node equations* and *pipe equations*.

The *loop equations* are formulated using a non-linear relationship between pressure drop and mass flow rate across a closed loop. Although this method could give the least possible number of equations, it requires initial values that satisfy the conservation of mass throughout the network. Moreover, additional *pseudo-loops* (the number of which depends on the topology) are usually needed to balance the number of equations and the number of unknowns, which makes it difficult to use them on computer-based algorithms.

The *node-loop equations* method, on the other hand, uses mass conservation equations at each node and *loop equations* for closed loops. Additional *pseudo-loops* are defined, depending on the topology. This method doesn't need precise initial guess of mass flow rates, but the necessity of *pseudo-loops* is still a drawback. Due to this inflexibility, the *node-loop equations* are used to model only specific case studies of DHN as presented in [55, 57, 93, 95, 96, 105, 107].

In contrast to the previous two methods, in which every equation is expressed as a function of pipe mass flow rate, the *node equations* method defines the conservation of mass at each node as a function of nodal pressures. Hence, it requires only a number of equations equal to the number of nodes. This is analogous to the electricity network equations which are based on nodal voltage profiles. However, since the mass flow rates are the coupling parameters between the hydraulic and thermal models, expressing them as a highly non-linear function of pressure head makes the overall system highly complex and difficult to handle.

Unlike the other three methods, the *pipe equation* uses conservation of mass at each node and pressure drop equations for each pipe. Hence, both parameters (pressure and mass flow rate) are involved in this method with the cost of additional equations. However, the equations involved are relatively easier to compute. As a result, hydraulic models based on *pipe equations* result in a simple to handle model with equal (even better) convergence rate when compared to the other methods [94]. Hence, this method is used to represent the hydraulic part of the heating network.

Assuming incompressible and constant water properties throughout the network, the conservation of mass and pressure drop equations can be written as shown in equations (4-8) and (4-9) respectively. These equations are valid for both supply and return pipe networks of the heating network. It is assumed that each of the pipes in the network are circular and straight with uniform cross-section throughout their length. It is reported that the Darcy-Weisbach equation for the pressure resistance coefficient, k_{ij}, is applicable for a wide range

of mass flow rate [104]. Accordingly, β (the exponential constant) is taken to be *2* and k_{ij} is given by equation (4-10).

$$\sum(all\ mass\ flows\ into\ the\ node) = \sum(all\ mass\ flows\ leaving\ the\ node) \tag{4-8}$$

$$H_j - H_i = (sign)k_{ij}\left|\dot{m}_{ji}\right|^{\beta} = k_{ij}\dot{m}_{ji}\left|\dot{m}_{ji}\right|^{\beta-1} \tag{4-9}$$

$$k_{ij} = \frac{8Lf}{gD^5\rho^2\pi^2} \tag{4-10}$$

where H_j and H_i are the hydraulic heads (due to pressure and elevation) at nodes j and i respectively while $\dot{m}_{ji}$ is the mass flow rate flowing from node *j* to node i; L is the length of the pipe with internal diameter D while ρ is the density of water and *f* is the friction factor.

Equation (4-11) can be used to find the value of the friction factor (f) for laminar flow as a function of Reynolds number (R_e), absolute surface roughness (ε) and pipe diameter (D). For turbulent flow ($R_e > 4000$), the exact value of the friction factor is determined using the Colebrook equation as indicated in equation (4-12)[104]. The Reynolds number, as a function of the water flow rate ($\dot{m}$) and its dynamic viscosity (μ), is defined as shown in equation (4-13).

$$f = \frac{64}{R_e} \qquad (for\ 0 < R_e < 2300) \tag{4-11}$$

$$\frac{1}{\sqrt{f}} = -2log\left(\frac{\varepsilon}{3.7D} + \frac{2.51}{R_e\sqrt{f}}\right) \qquad (for\ R_e > 4000) \tag{4-12}$$

$$R_e = \frac{4\dot{m}}{\pi D\mu} \tag{4-13}$$

Due to the transcendental nature of the Colebrook equation (4-12), it is not convenient to use it directly in computer programs. Winning and Coole [108] made a comparative study on the accuracy and computational efficiency of different formulae used to approximate the Colebrook equation and concluded that the Buzzelli equation given by equation (4-14) is the most accurate one. Hence, this equation is used to determine the friction factor for the turbulent and transition intervals (i.e. for R_e>2300).

$$f = \left[B_1 - \frac{B_1 + 2log\frac{B_2}{R_e}}{1 + \frac{2.18}{B_2}}\right]^{-2} \qquad (for\ R_e > 2300) \tag{4-14}$$

where $B_1 = \frac{0.774\ln(R_e) - 1.41}{1 + 1.32\sqrt{\frac{\varepsilon}{D}}}$ and $B_2 = \frac{\varepsilon}{3.7D}R_e + 2.51B_1$

4.3. Thermal model

Dynamic models of thermal networks are usually applied at a device or heat exchanger level as described in [109, 110]. However, as such detailed dynamics of a thermal network is not required to study the load flow and optimisation problems, a rather pseudo-dynamic physical model is found to be preferable as far as the time step is long enough to reach steady state [57, 107]. In the pseudo-dynamic approach, the thermal model is represented using three groups of equations that govern the heat power injection, the temperature drop across a pipe and the conservation of energy during mixing of water at each node.

In the first group, the heat power supplied to/from a given hub i is given by

$$P_{h(i)} = C_p \dot{m}_{(i)} \left(T_{s(i)} - T_{r(i)}\right) \tag{4-15}$$

where $P_{h(i)}$ is the heat power (positive for source and negative for load), $\dot{m}_{(i)}$ is the mass flow rate flowing from the hub to the supply pipe network of the heating network (positive for source and negative for load); $T_{s(i)}$ and $T_{r(i)}$ are supply and return temperatures at hub i respectively; C_p is the specific heat capacity of water.

The temperature-drop equations (second group), on the other hand, are derived from the heat loss equations. As the hot water circulates throughout the network, part of the heat is lost to the surrounding causing the water temperature to drop along the pipe. Fig. 4-1 shows the layout of the supply and return pipes buried in the soil and their cross-section. The insulation level and the distance between the pipes is assumed to be wide enough to neglect the temperature interaction. The heat transfer with the surrounding is also assumed to be only in the radial direction.

In all case studies in this dissertation, the water in the pipes is assumed to be incompressible with constant density (982.6 kg/m^3), constant specific heat capacity (4.185 kJ/kgK), constant viscosity (485 µNS/m^2) and constant conductivity (0.6516 W/mk).

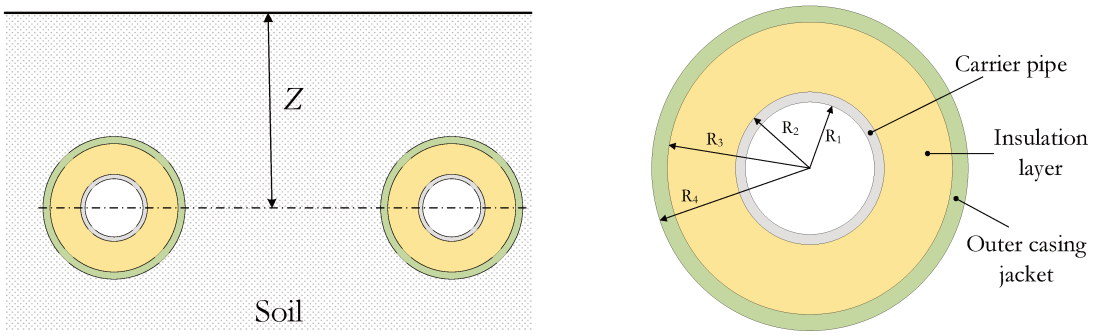

(a) (b)

Fig. 4-1. Buried heating network pipes (a) Layout of supply and return pipes, (b) cross-section of each pipe.

Neglecting the conductive heat transfer within the water, the thermal resistance between the water and the surface per unit length of the pipe (R') is given by equation (4-16) [111]. The last term corresponds to the thermal resistance of the soil, and it is expressed in terms of

conductive shape factor (S). For very long (relative to the diameter) underground pipes, the conductive shape factor per unit length is given by equation (4-17) [112]. If the soil temperature around the pipe is known, then equation (4-18) can be used to calculate the thermal resistance between the water inside the pipe and the outer surface of the casing jacket. As both of them are approximations of the heat transfer between a pipe and a semi-infinite sphere (earth), they have their own strength and limitation. Equation (4-16) is more accurate with the assumption of constant surface temperature, but does not take the earth's internal heat source into account. Equation (4-18), on the other hand, is better in taking the effect of the earth's internal heat into consideration. However, it is not perfect as it assumes a uniform temperature distribution around the pipe outer surface for its entire length.

$$R' = \frac{1}{2\pi R_1 h_w} + \frac{ln\left|\frac{R_2}{R_1}\right|}{2\pi k_2} + \frac{ln\left|\frac{R_3}{R_2}\right|}{2\pi k_3} + \frac{ln\left|\frac{R_4}{R_3}\right|}{2\pi k_4} + \frac{1}{Sk_s} \tag{4-16}$$

$$S = \frac{2\pi}{cosh^{-1}\left(\frac{Z}{R_4}\right)} \tag{4-17}$$

$$R' = \frac{1}{2\pi R_1 h_w} + \frac{ln\left|\frac{R_2}{R_1}\right|}{2\pi k_2} + \frac{ln\left|\frac{R_3}{R_2}\right|}{2\pi k_3} + \frac{ln\left|\frac{R_4}{R_3}\right|}{2\pi k_4} \tag{4-18}$$

where h_w represents the convective heat transfer coefficient of water, while k_2, k_3, k_4 and k_s denote the thermal conductivities of the carrier pipe, the insulating material, the outer jacket and the soil, respectively.

The convective coefficient of water is calculated using the Nusselt number (N_u) and its thermal conductivity (k_w) as shown in equation (4-19). The Nusselt number, by itself, is a function of the Prandtl number (P_r) and the Reynolds number (R_e), as defined in equations (4-20) and (4-21). The Prandtl number is determined using equation (4-22) while the Reynolds number is defined previously in equation (4-13) [112].

$$h_w = \frac{k_w N_u}{D} \tag{4-19}$$

$$N_u = 4.36 \quad (for\ 0 < R_e < 2300) \tag{4-20}$$

$$N_u = 0.023 R_e^{0.8} P_r^{0.3} \ \ (for\ R_e > 2300) \tag{4-21}$$

$$P_r = \frac{\mu C_p}{k_w} \tag{4-22}$$

Considering a small fraction of the pipe length dl, the rate of heat loss (dQ) from the water at temperature T_w to the ambient at temperature T_a can be expressed using equation (4-23). It should be noted that, depending on where the ambient temperature is taken, either of equations (4-16) or (4-18) is used to calculate the value of the thermal resistance (R').

$$dQ = \frac{(T_w - T_a)}{R'} dl \tag{4-23}$$

This heat loss will in effect reduce the temperature of water in the direction of its flow and it can be rewritten as a function of mass flow rate ($\dot{m}$) and temperature difference (dT_w).

$$dQ = -C_p \dot{m}\, dT_w \tag{4-24}$$

Equation (4-25) can be then obtained by equating equations (4-23) and (4-24) and rearranging the terms. Then it is solved for temperatures at the ends of the pipe as shown in equation (4-26).

$$\int_{T_{w\_start}}^{T_{w\_end}} \left(-\frac{dT}{(T_w - T_a)}\right) = \int_0^L \left(\frac{dl}{C_p \dot{m} R'}\right) \tag{4-25}$$

$$T_{w\_end} = T_a + (T_{w\_start} - T_a) exp\left(-\frac{L}{C_p \dot{m} R'}\right) \tag{4-26}$$

The term (R'/L) in equation (4-26) corresponds to the total thermal resistance of the pipe which is related to the overall heat transfer coefficient (U) as shown in equation (4-27) [112]. Putting (4-27) into (4-26) gives another form of temperature drop equation as given by (4-28).

$$\frac{L}{R'} = \frac{1}{R_{tot}} = U_{Rs} A_{Rs} = U_4 2\pi R_4 L = U_z 2\pi Z L \tag{4-27}$$

$$T_{w\_end} = T_a + (T_{w\_start} - T_a) exp\left(-\frac{U_{Rs} A_{Rs}}{C_p \dot{m}}\right) \tag{4-28}$$

where U_{Rs} is the overall heat transfer coefficient between the water in the pipe and the surrounding cylindrical surface area, A_{Rs}, with known temperature profile (either at R_4 or at Z in Fig. 4-1).

Either of equations (4-26) or (4-28) are reported in literature [57, 93, 95, 105, 107], but assuming a constant thermal resistance (overall heat transfer coefficient). Such assumptions neglect the variation in the convective coefficient of water as a function of its mass flow rates (which is defined in equations (4-19)). In this dissertation, the overall heat transfer coefficient is considered as a variable quantity that depends on the mass flow rate. In some case studies, the temperature at the surface of the earth is taken together with equation (4-16) while in the others the soil temperature at the outer most surface of the pipe is considered in combination with equation (4-18).

The last group of equations in the thermal model are those that relate the inlet and outlet temperatures at nodes where pipe flows at different temperatures are mixing. They are

derived from energy conservation, which can be expressed using equation (4-29). Complete mixing of water is assumed at each node.

$$\sum_{pipe\_in} \left(T_{j\_pipe\_in}\dot{m}_{j\_pipe\_in}\right) = T_{j\_out} \sum_{pipe\_out} \dot{m}_{j\_pipe\_out} \tag{4-29}$$

where $\dot{m}_{j\_pipe\_out}$ and T_{j_out} indicate the outgoing mass flow rates from a given node *j* and their temperatures while $\dot{m}_{j_pipe_in}$and $T_{j\_pipe\_in}$ denote the incoming mass flow rates and their corresponding temperatures.

4.4. Common per-unit (pu) system

The load flow analysis of the electricity network is usually computed in pu values using one-line diagram instead of three or four wire diagrams. The pu values are calculated by dividing each quantity by its base value. Although any arbitrary base value can be defined, the usual way is to take the highest MVA rating of the three-phase system (S_{base}). The rated line-to-line voltage at each side of a transformer is then taken as V_{base} for the corresponding circuit. The current and impedance base values, I_{base} and Z_{base}, are then calculated using equations (4-30) – (4-32) [102].

$$I_{base} = \frac{S_{base}}{V_{base}\sqrt{3}} \tag{4-30}$$

$$V_{base\,(phase)} = \frac{V_{base}}{\sqrt{3}} \tag{4-31}$$

$$Z_{base} = \frac{V_{base\,(phase)}}{I_{base}} = \frac{V_{base}}{I_{base}\sqrt{3}} = \frac{(V_{base})^2}{S_{base}} \tag{4-32}$$

Although the impedance base value is different at the two sides of a transformer, the pu of a given impedance remains the same when it is referred to either side of the transformer. This simplifies a three-phase network consisting of many transformers into a single one-line diagram.

As the equations governing the heating network are part of the integrated load flow problem, they should be expressed in pu so that the analysis could have consistency with the electricity quantities. The heat power is expressed in pu using the same base value as the electric power (equation (4-33)). In addition, the base value of either the temperature or the flow rate shall be defined. The other one is then determined from the heat power equation. The pu of temperature values are defined based on two reference values (as shown in equation (4-34)). These two references are T_{ref1} and T_{ref2} which correspond to the lower and higher temperature references, respectively. Accordingly, the pu equivalent of a temperature difference can be computed using equation (4-35) while the heat equation in pu and base values is given by equation (4-36).

$$P_{h(base)} = S_{base} \tag{4-33}$$

$$T_{i(pu)} = \frac{T_{i(actual)} - T_{ref1}}{T_{ref2} - T_{ref1}} \tag{4-34}$$

$$\Delta T_{i(pu)} = \frac{\Delta T_{i(actual)}}{T_{ref2} - T_{ref1}} \tag{4-35}$$

$$P_{h(pu)} P_{h(base)} = C_p \dot{m}_{(pu)} \dot{m}_{(base)} \Delta T_{(pu)} (T_{ref2} - T_{ref1}) \tag{4-36}$$

By defining the heat equation in pu as shown in equation (4-37), the relationship between base mass flow rate and temperature references is derived as shown in equation (4-38).

$$P_{h(pu)} = \dot{m}_{(pu)} \Delta T_{(pu)} \tag{4-37}$$

$$\dot{m}_{(base)} = \frac{P_{h(base)}}{C_p (T_{ref2} - T_{ref1})} \tag{4-38}$$

It is worth noting that the power injection equations for both electricity and heat expressed in actual units may not necessarily be in the same form as those expressed in pu.

In analogous to the electrical transmission line parameters, the base values for pipe parameters in the heating network need to be defined as they are part of the temperature drop equations. Let ΔT_{w_start} and ΔT_{w_end} be the temperature differences of the inlet and outlet water flows of a pipe relative to the ambient (surface at radius R_s) respectively. The pipe is defined with length L and flow rate $\dot{m}$. Recalling equation (4-28), ΔT_{w_start} and ΔT_{w_end} can be related by (4-39). Equation (4-40) expresses equation (4-39) in pu. If the base value of the pipe length is selected to be numerically equal to the base value of the mass flow rate (both in SI units) as shown in equation (4-41), then the temperature drop equation in pu can be expressed using equation (4-42) which has the same form as (4-39).

$$\Delta T_{w\_end} = \Delta T_{w\_start}\, exp\left(-\frac{U_{Rs}\, A_{Rs}}{C_p \dot{m}}\right) = \Delta T_{w\_start}\, exp\left(-\frac{U_{Rs}\, 2\pi R_s L}{C_p \dot{m}}\right) \tag{4-39}$$

$$(T_{ref2} - T_{ref1}) \Delta T_{w\_end(pu)} = (T_{ref2} - T_{ref1}) \Delta T_{w\_start(pu)} exp\left(-\frac{U_{Rs} 2\pi R_s L_{pu} L_{base}}{C_p \dot{m}_{pu} \dot{m}_{base}}\right) \tag{4-40}$$

$$Let, \qquad L_{base} = \dot{m}_{base} \tag{4-41}$$

$$\Delta T_{w\_end(pu)} = \Delta T_{w\_start(pu)} exp\left(-\frac{U_{Rs} 2\pi R_s L_{pu}}{C_p \dot{m}_{pu}}\right) \tag{4-42}$$

Another equation which needs a pu conversion is the pressure drop equation, which can be defined as shown in equation (4-43). Then, the base value of the hydraulic head can be derived to be equal to the square of the base mass flow rate as shown in equation (4-44).

$$\left(H_j - H_i\right)_{pu} = k_{ij}\left(\dot{m}_{ji}\left|\dot{m}_{ji}\right|\right)_{pu} \tag{4-43}$$

$$\frac{H_j - H_i}{H_{base}} = \frac{k_{ij}\dot{m}_{ji}\left|\dot{m}_{ji}\right|}{{\dot{m}_{base}}^2} \quad \Longrightarrow \quad H_{base} = {\dot{m}_{base}}^2 \tag{4-44}$$

4.5. Solving the integrated load flow problem

The overall load flow problem is solved as a single problem using the *Newton-Raphson* iterative method. The variables of interest in the load flow solution are voltage magnitude, voltage angle, supply temperature, return temperature, hydraulic head and mass flow rates to/from each hub. At a given hub, some of the variables might be known while the others are unknown. The objective of the load flow study is to solve for the unknown variables using the known variables. Depending on the variables that are known, hubs can be categorized as shown in Table 4-1.

A *slack* hub is usually a hub where there is maximum generation capacity of heat and electricity. Unless the electricity and heat generations are decoupled, in which case it is possible to have a separate slack hub for the heating and electricity networks, there will always be only one slack hub for both networks. This hub is responsible to supply all the power deficit and losses in both networks. At this hub, the references for voltage magnitude, voltage angle, hydraulic head (for both supply and return pipe networks) and the supply temperature are defined.

From the electricity network point of view, a hub (other than the slack hub) where there is reactive power generation reserved for voltage control is called *PV* hub. The remaining hubs are called *PQ* hubs.

From the heating network point of view, on the other hand, it is assumed that only either of the supply temperature or the return temperature is known at each hub and the other is to be solved from the load flow. Those hubs with known supply temperatures are referred to as *temp_supply* hubs while those with known return temperatures are referred to as *temp_return* hubs. The *temp_supply* hubs refer to those that are injecting heat power into the network while *temp_return* hubs are those that import heat power from the network.

Table 4-1: Types of hubs and the associated known and unknown variables.

Type of Hub	Network	Known variables	Unknown variables
Slack	Both	$\|V\|$, θ, T_s, H_s, H_r, L_{ep}, L_{eq}, L_h	P_{epg}, P_{eqg}, P_{hg}, P_{fg}, ṁ, T_r
PV	Electricity	$\|V\|$, P_{epg}, P_{fg}, L_{ep}, L_{eq}	θ, P_{eqg}
PQ	Electricity	P_{epg}, P_{eqg}, L_{ep}, L_{eq}, P_{fg}	$\|V\|$, θ
Temp_supply	Heating	T_s, P_{hg}, P_{fg}, L_h	T_r, H_s, H_r, ṁ
Temp_return	Heating	T_r, P_{hg}, P_{fg}, L_h	T_s, H_s, H_r, ṁ

In summary, the unknown variables for the electricity network are the voltage magnitudes and voltage angles at the *PQ* hubs, voltage angles and reactive electric power generations at

the *PV* hubs, and active and reactive electric power generations at the *slack* hub. For the heating network, on the other hand, the unknown variables are: the values of heat power generation at the slack hub; return temperatures at all *temp_supply* hubs; supply temperatures at all *temp_return* hubs; mass flow rates to/from each hub (to be solved from the mass flow rates inside each pipe); and the hydraulic heads at all non-slack hubs (both on the supply and return pipe networks of the heating network).

The flow chart of the algorithm that is used to solve all the unknown variables of integrated electricity and heating networks is depicted in Fig. 4-2. The algorithms for all the constituent submodules are developed using MATLAB® [113]. The description of each of the submodules follows below.

Network Data: This section is where the data for all the networks is fed by the user. Generations, loads, coupling matrices, network parameters and initial values for the load flow problem are defined here.

Initialization: The data fed by the user is extracted into matrices so that they can be easily manipulated in MATLAB®.

Maximum iteration: The maximum iteration (500 in this work) is the limit in which the solution has to converge with a predefined tolerance. If the solution is not converging within this maximum iteration, it means that either more iterations are required or the known parameters are technically impossible. In any case, the program quits displaying a warning message, the maximum absolute value of the error and the iteration number.

Electricity subroutine: In this subroutine, the electrical mismatches and the Jacobians that are specific to the electricity network are calculated using the latest values obtained from the Newton-Raphson subroutine.

Hydraulic subroutine: In this section, the pressure resistance coefficient and the overall heat transfer coefficient for each pipe are updated. In addition, the heat power and hydraulic head mismatches are computed using the latest values obtained from the Newton-Raphson subroutine.

Thermal subroutine: The new values of supply and return temperatures at each hub, together with the new values of pipe flow rates are used to update the inlet and outlet temperatures of each pipe. These end-point temperatures are then used to calculate the outgoing temperature at each node. The differences between these recalculated outgoing temperatures and their corresponding values returned from the Newton-Raphson subroutine give the temperature mismatch values. The values of two types of mismatch equations are calculated here: supply temperature mismatches at *temp_return* hubs and return temperature mismatches at *temp_supply* hubs.

Newton-Raphson subroutine: Here, the unknown variables are numerically solved from the system of nonlinear mismatch equations. Newton-Raphson iterative method is popular for its quadratic convergence rate and wider application area that encompasses meshed and highly

coupled topologies (see *Section 4.5.2* for the details). At each iteration, the correction values for the unknown variables are calculated by multiplying the mismatch vector with the inverse of the Jacobian matrix. If it is not yet converging, the Jacobian matrix is updated and the iteration continues. However, depending on the problem at hand, Quasi-Newton methods can also be used to approximate the Jacobian matrix. Even more simplified methods (like the forward and backward sweep electricity load flow analysis) can be implemented in the case of radial distribution networks.

Convergence: Compares the absolute values of all mismatches with the predefined convergence tolerance value (10^{-5} pu is used in this dissertation).

Pressure profile calculation on the return pipe network. The mass flow rates on the supply and return pipes of a given branch are equal implying equal pressure drop, but opposite in direction. Hence, the hydraulic heads in the return pipe network can be calculated node by node starting from a reference hub or using a separate Newton-Raphson iterative method.

Display results: This subroutine converts the pu values of the variables into their actual values and displays the load flow results.

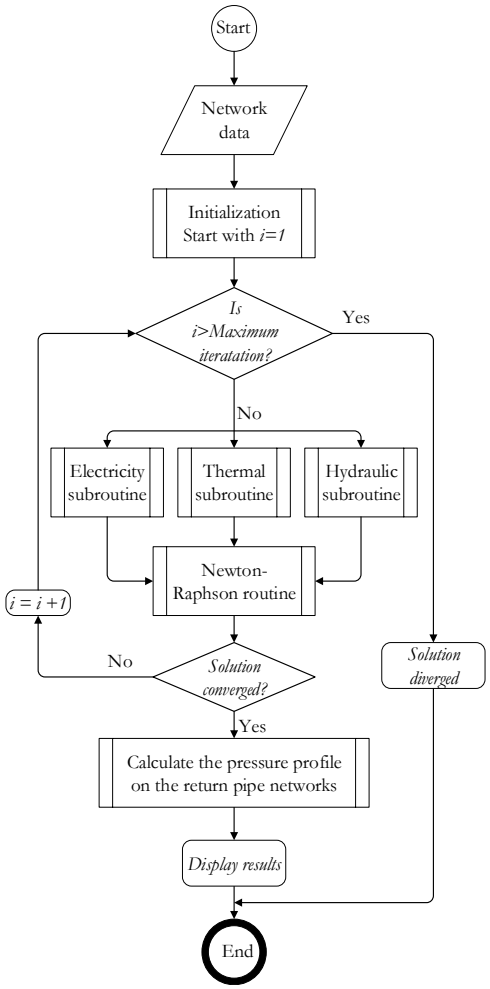

Fig. 4-2. Flow chart of integrated load flow analysis for coupled electricity and heating networks.

4.5.1. Formulation of mismatch equations

The coupling relationship at each hub in an integrated heat and electricity distribution networks (without a storage) can be derived from equation (3-3) as shown in equation (4-45). A load flow model that considers storage technologies is presented in *Chapter 7*.

$$0 = \begin{bmatrix} L_{ep} \\ L_{eq} \\ L_h \end{bmatrix} - \begin{bmatrix} C_{ep(ep)} & C_{ep(eq)} & C_{ep(h)} & C_{ep(f)} \\ C_{eq(ep)} & C_{eq(eq)} & C_{eq(h)} & C_{eq(f)} \\ C_{h(ep)} & C_{h(eq)} & C_{h(h)} & C_{h(f)} \end{bmatrix} \begin{bmatrix} P_{epg} - P_{ep} \\ P_{eqg} - P_{eq} \\ P_{hg} - P_h \\ P_{fg} - P_f \end{bmatrix} = \begin{bmatrix} \Delta P_{ep} \\ \Delta P_{eq} \\ \Delta P_h \end{bmatrix} \tag{4-45}$$

where L and P are the loads and powers (generation or injection) expressed in pu, respectively, while C represent the elements of the coupling matrix respectively; the subscripts ep, eq, h, and f indicate the active*, reactive, heat and fuel powers, respectively; ΔP_{ep}, ΔP_{eq} and ΔP_h represent the active, reactive and heat power mismatches at a given hub, respectively.

Equation (4-45) is applied to all hubs except the slack hub to formulate the system of equations to be solved using the *Newton-Raphson* iterative method. In addition to these coupled equations, there are additional mismatch equations for the hydraulic head and temperature variables as shown in equations (4-46) to (4-48).

$$\Delta H_{pipe(ij)} = 0 = \left(H_j - H_i - k_{ij}\dot{m}_{ji}\left|\dot{m}_{ji}\right|\right)_{pu} \tag{4-46}$$

$$\Delta E_{s(i)} = 0 = \left(\sum_{j \in in} T_{s\_ji}\dot{m}_{ji} - T_{s(i)}\sum_{j \in in}\dot{m}_{ji}\right)_{pu} \tag{4-47}$$

$$\Delta E_{r(k)} = 0 = \left(\sum_{j \in in} T_{r\_jk}\dot{m}_{jk} - T_{r(k)}\sum_{j \in in}\dot{m}_{jk}\right)_{pu} \tag{4-48}$$

where $\Delta H_{pipe(ij)}$ is the hydraulic head mismatch corresponding to the pipe connecting hub i (with hydraulic head H_i) and hub j (with hydraulic head H_j). $\Delta E_{s(i)}$ is the thermal energy mismatch at a node connected to a *temp_return* hub i. $\Delta E_{r(k)}$ is the thermal energy mismatch at a node connected to a *temp_supply* hub k. $\dot{m}_{ji}$ and $\dot{m}_{jk}$ are mass flow rates flowing from node j to node i and from node j to node k, respectively (they include mass flows from hubs i and k as well if the flows are from the hubs into the corresponding nodes). s and r indicate the supply and return pipe networks of the heating network. T_{s_ji} is the temperature of the water flowing from node j to node i as measured at node i on the supply pipe network while T_{r_jk} is the temperature of water flowing from node j to node k, as measured at node k on the return pipe network. $T_{s(i)}$ and $T_{r(k)}$ are the supply temperature at hub i and the return temperature at hub k, respectively.

* The terms 'active' and 'reactive' are used in this thesis to refer the active electric power and the reactive electric power, respectively.

For a system with N hubs, there will be $N-1$ mismatch equations for the active power. The number of reactive power mismatch equations will be equal to the number of PQ hubs. In addition, there will be $N-1$ mismatches for nodal heat power injection. The number of hydraulic head mismatches will be equal to the number of pipes in the heating network. The number of supply and return temperature mismatch equations will be equal to the number of *temp_return* hubs and *temp_supply* hubs, respectively.

4.5.2. The Newton-Raphson iterative method

The *Newton-Raphson* iterative method, which is used to solve for $\boldsymbol{X}$ in a multivariable system of equations (defined by $\boldsymbol{F(X)=0}$), can be defined by equation (4-49). In this equation, $\Delta\boldsymbol{F}$ represents the mismatches while $\boldsymbol{J}$ stands for the Jacobian matrix. The elements of $\boldsymbol{J}$ are found by computing the partial derivatives of each equation with respect to each variable. The corrections $\Delta\boldsymbol{X}$ are computed at each iteration by multiplying the mismatch vector with the inverse of the Jacobian matrix. The mismatches are then computed using the new values of $\boldsymbol{X}$. If any of the mismatches is outside the predefined tolerance, then the Jacobian matrix is updated, new corrections $\Delta\boldsymbol{X}$ are computed and the iteration continues.

In a similar way, combining the mismatches and unknown variables discussed in the previous sections and putting them in matrix form gives equation (4-50) which is then solved iteratively. Equations that are used to calculate the elements of the Jacobian matrix are listed in Appendix B.

$$-\Delta\boldsymbol{F}=\boldsymbol{J}\,\Delta\boldsymbol{X} \tag{4-49}$$

$$-\begin{bmatrix}\Delta\boldsymbol{P}_{ep}\\ \Delta\boldsymbol{P}_{eq}\\ \Delta\boldsymbol{P}_{h}\\ \Delta\boldsymbol{H}_{pipe}\\ \Delta\boldsymbol{E}_{s}\\ \Delta\boldsymbol{E}_{r}\end{bmatrix}=\begin{bmatrix}\frac{\partial(\Delta\boldsymbol{P}_{ep})}{\partial\boldsymbol{\theta}} & \frac{\partial(\Delta\boldsymbol{P}_{ep})}{\partial|\boldsymbol{V}|} & \frac{\partial(\Delta\boldsymbol{P}_{ep})}{\partial\dot{\boldsymbol{m}}_{pipe}} & \frac{\partial(\Delta\boldsymbol{P}_{ep})}{\partial\boldsymbol{H}} & \frac{\partial(\Delta\boldsymbol{P}_{ep})}{\partial\boldsymbol{T}_{s}} & \frac{\partial(\Delta\boldsymbol{P}_{ep})}{\partial\boldsymbol{T}_{r}}\\ \frac{\partial(\Delta\boldsymbol{P}_{eq})}{\partial\boldsymbol{\theta}} & \frac{\partial(\Delta\boldsymbol{P}_{eq})}{\partial|\boldsymbol{V}|} & \frac{\partial(\Delta\boldsymbol{P}_{eq})}{\partial\dot{\boldsymbol{m}}_{pipe}} & \frac{\partial(\Delta\boldsymbol{P}_{eq})}{\partial\boldsymbol{H}} & \frac{\partial(\Delta\boldsymbol{P}_{eq})}{\partial\boldsymbol{T}_{s}} & \frac{\partial(\Delta\boldsymbol{P}_{eq})}{\partial\boldsymbol{T}_{r}}\\ \frac{\partial(\Delta\boldsymbol{P}_{h})}{\partial\boldsymbol{\theta}} & \frac{\partial(\Delta\boldsymbol{P}_{h})}{\partial|\boldsymbol{V}|} & \frac{\partial(\Delta\boldsymbol{P}_{h})}{\partial\dot{\boldsymbol{m}}_{pipe}} & \frac{\partial(\Delta\boldsymbol{P}_{h})}{\partial\boldsymbol{H}} & \frac{\partial(\Delta\boldsymbol{P}_{h})}{\partial\boldsymbol{T}_{s}} & \frac{\partial(\Delta\boldsymbol{P}_{h})}{\partial\boldsymbol{T}_{r}}\\ \frac{\partial(\Delta\boldsymbol{H}_{pipe})}{\partial\boldsymbol{\theta}} & \frac{\partial(\Delta\boldsymbol{H}_{pipe})}{\partial|\boldsymbol{V}|} & \frac{\partial(\Delta\boldsymbol{H}_{pipe})}{\partial\dot{\boldsymbol{m}}_{pipe}} & \frac{\partial(\Delta\boldsymbol{H}_{pipe})}{\partial\boldsymbol{H}} & \frac{\partial(\Delta\boldsymbol{H}_{pipe})}{\partial\boldsymbol{T}_{s}} & \frac{\partial(\Delta\boldsymbol{H}_{pipe})}{\partial\boldsymbol{T}_{r}}\\ \frac{\partial(\Delta\boldsymbol{E}_{s})}{\partial\boldsymbol{\theta}} & \frac{\partial(\Delta\boldsymbol{E}_{s})}{\partial|\boldsymbol{V}|} & \frac{\partial(\Delta\boldsymbol{E}_{s})}{\partial\dot{\boldsymbol{m}}_{pipe}} & \frac{\partial(\Delta\boldsymbol{E}_{s})}{\partial\boldsymbol{H}} & \frac{\partial(\Delta\boldsymbol{E}_{s})}{\partial\boldsymbol{T}_{s}} & \frac{\partial(\Delta\boldsymbol{E}_{s})}{\partial\boldsymbol{T}_{r}}\\ \frac{\partial(\Delta\boldsymbol{E}_{r})}{\partial\boldsymbol{\theta}} & \frac{\partial(\Delta\boldsymbol{E}_{r})}{\partial|\boldsymbol{V}|} & \frac{\partial(\Delta\boldsymbol{E}_{r})}{\partial\dot{\boldsymbol{m}}_{pipe}} & \frac{\partial(\Delta\boldsymbol{E}_{r})}{\partial\boldsymbol{H}} & \frac{\partial(\Delta\boldsymbol{E}_{r})}{\partial\boldsymbol{T}_{s}} & \frac{\partial(\Delta\boldsymbol{E}_{r})}{\partial\boldsymbol{T}_{r}}\end{bmatrix}\begin{bmatrix}\Delta\boldsymbol{\theta}\\ \Delta|\boldsymbol{V}|\\ \Delta\dot{\boldsymbol{m}}_{pipe}\\ \Delta\boldsymbol{H}\\ \Delta\boldsymbol{T}_{s}\\ \Delta\boldsymbol{T}_{r}\end{bmatrix} \tag{4-50}$$

4.5.3. Additional considerations

It should be noted that the Jacobian matrix is an invertible square matrix. The number of unknown variables should be equal to the number of mismatch equations. To that end, equations listed in Appendix B need to be carefully implemented.

The pressure profiles on the return pipe network of a heating network are solved separately after the load flow problem, defined by equation (4-50), is solved. Newton-Raphson iteration is applied on a system of pipe equations (similar to those in the fourth row of equation (4-50)).

In that case, the number of equations will be equal to the number of unknown hydraulic head variables in the return pipe network. Hence, only return pipes that add new information about the hydraulic head variables should be included to avoid redundancy.

In addition, there are technical constraints that need to be considered in the solution process. The first is the limit on the reactive power capacity of the *PV* hubs in the electricity network. If the reactive power generation at a given *PV* hub falls outside the limit, then it needs to be fixed to its nearby limit. The corresponding bus is then treated as a *PQ* hub. Another constraint is the limit on the temperature profiles of the heating network. The supply temperature at a given hub is supposed to be higher or equal to the corresponding return temperature. In addition, some heating systems may apply a minimum temperature level and mass flow rates in the pipes.

Furthermore, the equations describing the thermo-hydraulic models (in Appendix B) need to be implemented in a flexible way so that they can be reconfigured automatically by detecting any change in the water flow direction from the hubs and through each pipe. All the above technical issues are addressed in the tool developed and used in this dissertation.

4.6. Summary

In this chapter, the extended energy hub approach is elaborated by taking an integrated heating and electricity distribution networks. The constituent equations are derived in such a way that the algorithm can automatically detect and configure them on the bases of the data input from the user. The Newton-Raphson iterative algorithm, which is commonly used to solve load flow problems of electricity distribution networks, is adapted to solve the load flow problems of both the electricity and heating networks simultaneously. Additional cautions while solving the integrated load flow problem are also highlighted. In the next chapter, examples of integrated load flow studies are discussed taking different case studies, including one from literature.

5. Demonstration and Theoretical Validation through Integrated Load Flow Case Studies

In this chapter, the integrated load flow model, developed in the previous chapter, is applied on various case studies to demonstrate its capacity in capturing the steady state operating parameters of both heat and electricity distribution networks. As a proof of concept, the model is theoretically validated by inspecting whether the results comply with the governing laws of Physics or not. Two groups of case studies are considered. The first group deals with only single-time-step (1 hour) simulations while the second group demonstrates a pseudo-dynamic simulation for a year.

5.1. Energy technologies considered

The energy technologies considered in the case studies include gas boiler, cogeneration plant, heat pump and renewables (such as wind and solar). Local generations like the wind, solar and geothermal plants are represented by their output power. The technologies such as heat pumps, boilers and cogeneration plants, on the other hand, are described by their conversion efficiencies. As the focus of this thesis is on the distribution networks, the technologies are assumed to have constant conversion efficiencies. However, the modularity of the model allows to integrate detailed models of the technologies operating at variable efficiencies. This is illustrated in *Chapter 7* with a thermal storage integration.

5.1.1. Heat-only-boiler (HOB)

The HOB uses fuel, such as coal, oil, natural gas, biogas, biomass and municipal waste to produce heat using water as a medium. Its performance is expressed by its thermal efficiency η_b. HOBs are usually used as a peak-load heat supply units where there is a DHN (e.g. in Sweden [37]). But, they can be also used as distributed heat supply units in countries having large reserve of natural gas (e.g. in the Netherlands [15]).

5.1.2. Combined heat and power (CHP) plant

CHP plants, unlike to the conventional thermal power plants, recover the waste heat which would otherwise be released into the environment. Like the HOBs, they can take a range of fuel types as input, but they produce electricity in addition to heat. The performance of a CHP plant is expressed by its electrical (η_{el}) and thermal (η_{th}) efficiencies. Depending on whether it is running at lagging or leading power factor (pf_{CHP}), the CHP plant either consumes or

produces reactive power. The efficiency of a CHP plant may vary depending on its size and the type of fuel used. For example, a gas fired CHP plant with an intake capacity of 538 kW has thermal and electrical efficiencies of 49% and 37%, respectively [54]. A waste-to-energy CHP plant (with an internal combustion engine), on the other hand, can have a thermal efficiency of 57% and an electrical efficiency of 31% [114].

5.1.3. Heat pump (HP)

The HP (compression type), uses electricity to transfer heat from a colder region to a hotter region. It can also be used to increase the temperature of water that is initially available so that it can be used for higher temperature application. The source of heat can be sewage, seawater, geothermal, waste heat or ambient air. Its efficiency is expressed using a coefficient of performance (COP) which is the ratio of the heat power transported to the amount of active electric power consumed. Apart from the COP, the power factor, pf_{HP}, is used to calculate the reactive power consumption of the HP.

Although the COP depends on the type of refrigerant, sink temperature, source temperature and compressor speed control, it can be assumed constant in certain operation conditions. For a 10 $^{\circ}$C source temperature, a HP operating in a DHN can have an average COP of 5.0 [115]. Levihn [37], on the other hand, concluded that a COP of 3.5 for a seawater based large scale HP operating in a temperature output range of 65 -115 $^{\circ}$C is practically achievable. The effect of COP variation due to partial loading and operating temperatures of a DHN at the distribution level is negligible [116]. Although series connection of a HP with a HOB or with a CHP can be used to increase the output temperature level at transmission level (i.e. at sources far from the consumers) [117], parallel connections are preferable to have higher and stable COP at distribution level (i.e. near to the consumers) of the DHN [116]. All the HPs considered in this study are assumed to have a COP of 4.0.

5.1.4. Renewables (Solar and Wind)

Renewable generations, such as wind, solar PV and solar thermal are also considered in some of the case studies. The electricity or heat produced from such technologies is considered as a locally generated electric or heat power, respectively. For single-hour simulation case studies, arbitrary generation outputs are considered. But, for those involving simulations in time-series, the generations from such renewables are forecasted using HOMER [33] based on the monthly average solar radiation and wind speed data available online.

5.2. Coupling equations

The EEH representation of the interaction between heat, electricity and fuel carriers that takes place in an energy hub having the above mentioned energy technologies are shown in Fig. 5-1. The corresponding coupling equations can be derived from the energy balance governing the corresponding coupling system as shown in equations (5-1) – (5-3). In the same way, the

coupling equation governing an energy hub without any coupling technology is given by equation (5-4).

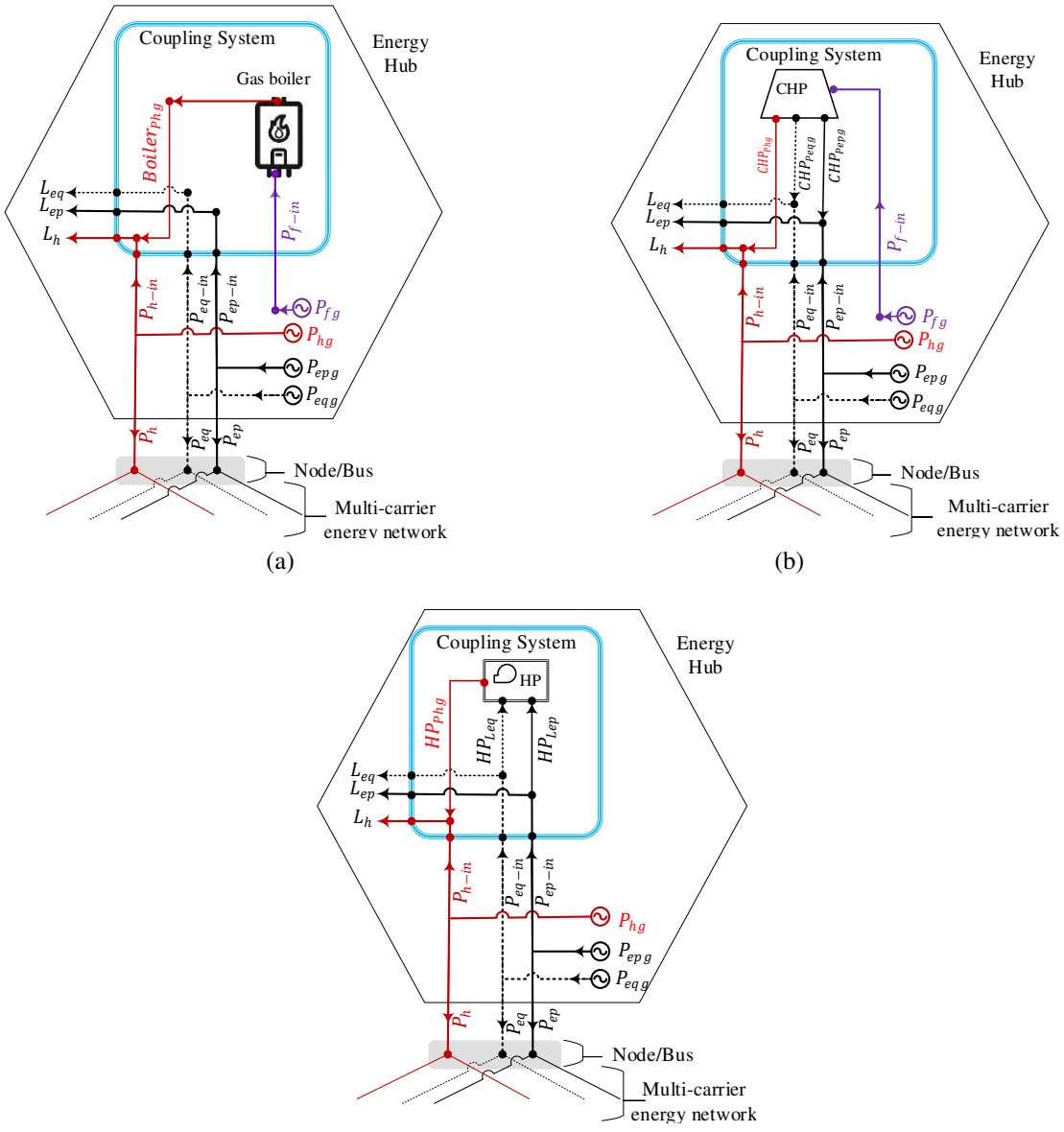

Fig. 5-1. Examples of energy hubs and their EEH representations showing the interactions between heat, electricity and fuel energy carriers. (a) a hub with a HOB, (b) a hub with a CHP, (c) a hub with a HP. In the figure, P_{fg}, P_{hg}, P_{epg} and P_{eqg} terms indicate the local generations of fuel, heat, active and reactive powers, respectively. The terms P_h, P_{ep} and P_{eq} represent the heat, active and reactive power injections into the network, respectively. P_{h-in}, P_{f-in}, P_{ep-in} and P_{eq-in} are the heat, fuel, active and reactive power inputs into the coupling system, respectively. L_h, L_{ep}, and L_{eq} denote the heat, active and reactive power demands. $Boiler_{Phg}$, HP_{Phg} and CHP_{Phg} represent the heat power outputs of the gas boiler, the HP and the CHP, respectively. The terms HP_{Lep} and HP_{Leq} represent the active and reactive electric power consumptions of the HP while CHP_{Pepg} and CHP_{Peqg} designate the active and reactive power generations from the CHP, respectively.

$$\begin{bmatrix} L_{ep} \\ L_{eq} \\ L_h \end{bmatrix} = \begin{bmatrix} 1 & 0 & 0 & 0 \\ 0 & 1 & 0 & 0 \\ 0 & 0 & 1 & \eta_b \end{bmatrix} \begin{bmatrix} P_{epg} - P_{ep} \\ P_{eqg} - P_{eq} \\ P_{hg} - P_h \\ P_{fg} \end{bmatrix} \tag{5-1}$$

$$\begin{bmatrix} L_{ep} \\ L_{eq} \\ L_h \end{bmatrix} = \begin{bmatrix} 1 & 0 & 0 & \eta_{el} \\ 0 & 1 & 0 & -\eta_{el} \dfrac{\sqrt{1 - pf_{CHP}{}^2}}{pf_{CHP}} \\ 0 & 0 & 1 & \eta_{th} \end{bmatrix} \begin{bmatrix} P_{epg} - P_{ep} \\ P_{eqg} - P_{eq} \\ P_{hg} - P_h \\ P_{fg} \end{bmatrix} \tag{5-2}$$

$$\begin{bmatrix} L_{ep} + HP_{Lep} \\ L_{eq} + HP_{Lep} \dfrac{\sqrt{1 - pf_{HP}{}^2}}{pf_{HP}} \\ L_h - HP_{Lep} * COP \end{bmatrix} = \begin{bmatrix} 1 & 0 & 0 \\ 0 & 1 & 0 \\ 0 & 0 & 1 \end{bmatrix} \begin{bmatrix} P_{epg} - P_{ep} \\ P_{eqg} - P_{eq} \\ P_{hg} - P_h \end{bmatrix} \tag{5-3}$$

$$\begin{bmatrix} L_{ep} \\ L_{eq} \\ L_h \end{bmatrix} = \begin{bmatrix} 1 & 0 & 0 \\ 0 & 1 & 0 \\ 0 & 0 & 1 \end{bmatrix} \begin{bmatrix} P_{epg} - P_{ep} \\ P_{eqg} - P_{eq} \\ P_{hg} - P_h \end{bmatrix} \tag{5-4}$$

where η_{el} and η_{th} are the electrical and thermal efficiencies of the CHP plant, respectively, while pf_{CHP} refers to its power factor; COP is the coefficient of performance of the HP while pf_{HP} is its power factor; η_b is the thermal efficiency of the HOB. The power factors of the HP and the CHP are taken to be positive if they are lagging and negative if they are leading.

5.3. Single-hour integrated load flow case studies

5.3.1. Description of the case studies

Four case studies (Cases 5-A to 5-D) with different topologies and different hub numbers are considered in this section to investigate the validity and flexibility of the proposed model. The topologies are shown in Fig. 5-2.

Each hexagon represents an energy hub consisting of demands, local generations and coupling devices. The black lines represent the electricity network while the red solid lines and the dotted blue lines with arrows represent the supply and return pipes of the heating network, respectively. V_i represents the voltage at bus i (indicated by light grey circles) of the electricity network while $\dot{m}_k$ denotes the mass flow rate injected into the network from hub k. On the other hand, $\dot{m}_{i-j}$ represents the mass flow rate in a pipe connecting nodes i and j on the supply side of the DHN. There is equal and opposite mass flow in the corresponding return pipes. The directions of the mass flows indicated in Fig. 5-2 are initial assumptions. If any flow becomes negative after solving the load flow problem, then that flow direction is meant to be opposite to what has been assumed initially. The P_k terms represent power injections from hub k into the network.

Case 5-A (Fig. 5-2(a)) is used for validation and comparison with a recent research work. The data for the heating and electricity networks are extracted from [95]. The simulation is first run with a constant heat transfer coefficient for all the pipes as it is assumed in [95]. The simulation is then repeated using standard pipe parameters with a standard insulation.

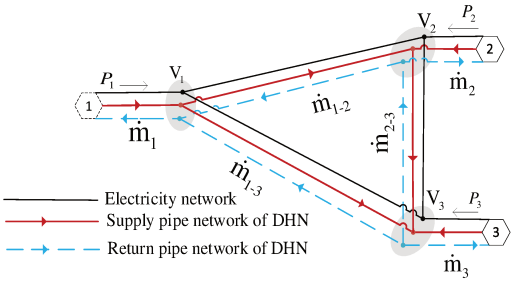

(a) Case 5-A for comparison with [95]

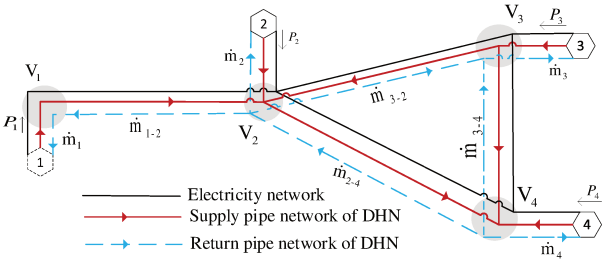

(b) Case 5-B

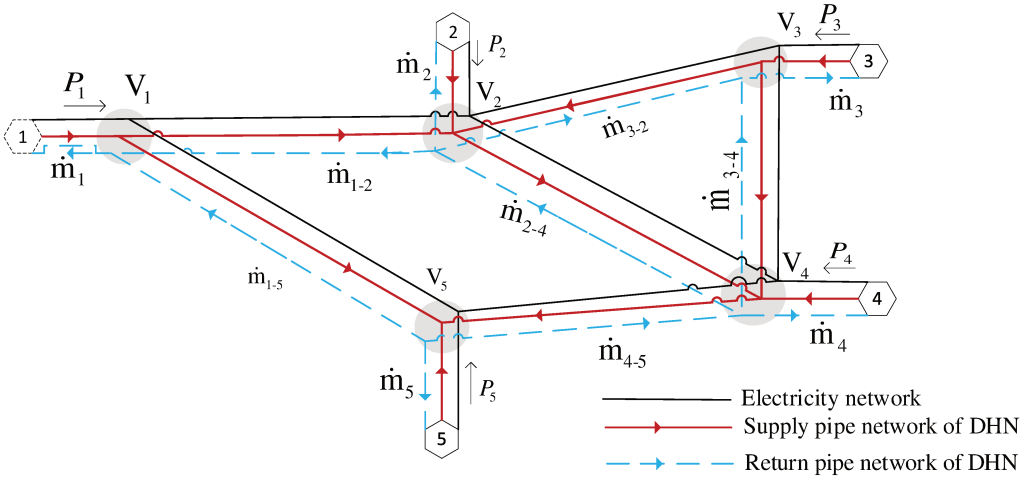

(c) Case 5-C

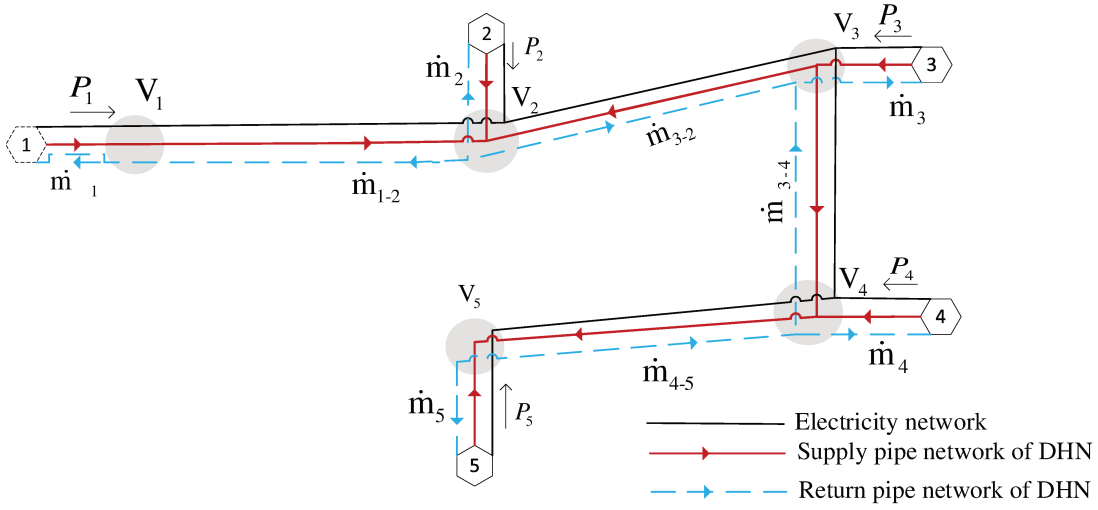

(d) Case 5-D

Fig. 5-2. Network configuration of case studies 5-A to 5-D

Cases 5-B to 5-D (Figs 5-2(b) – 5-2(d)) are additional case studies selected to illustrate the flexibility of the proposed tool. For these three cases, ACSR Ostrich type three phase transmission lines and typical transformers (of rating 4.16 kV, 1 MVA) are considered and their parameters are taken from [102]. Similarly, standard parameters of district heating pipes (DN-50 with type II insulation) are taken from isoplus® [118]. The outdoor temperature for all cases is assumed 10 °C, and equation (4-16) is used to determine the thermal resistance between the water in each pipe and the surface of the earth. The details of the hub data and the network parameters are included in Table C-1 and Table C-2 of Appendix C.

All hubs have CHP plants. Each CHP plant can be of any type as far as the fuel-to-active power, fuel-to-reactive power and fuel-to-heat power efficiencies are known. In addition to the outputs of the CHP plants, there are also electric and heat powers generated independently at each hub. These generations can be in the form of distributed generations such as wind, solar PV, solar thermal and so on. The data with regard to the amount of generations and demands together with the coupling matrices for each hub are given in Table C-3 and equation (C-1), in Appendix C.

In all cases, hub 1 is considered as a slack hub (indicated by dotted hexagon). In Case 5-C and Case 5-D, hub 3 is assumed to be *PV* and *temp_supply* type while the remaining hubs are treated as *PQ* and *temp_return* hubs (see Table C-3). Exception is made for Case 5-B to see the flexibility of the proposed model: hub 3 is assumed as *PV* and *temp_return* type while hub 4 and hub 2 are both considered as *PQ* and *temp_supply* type.

5.3.2. Results and discussions

5.3.2.1. Comparison with previous study – Case 5-A

The simulation for Case 5-A converged in 0.4 s taking 5 iterations within a tolerance of 10^{-6} pu. Table 5-1 – Table 5-4 show the results presented in [95] and the new results found using the proposed model. As it can be seen from Table 5-1 and Table 5-2, there is no difference in the values of the electrical parameters, which can be taken as a cross-validation for electrical network part. There are differences in the heating network parameters, however, as it can be seen in Table 5-3 and Table 5-4. The deviations could be due to the difference in the algorithms implemented to compute the thermo-hydraulic model. As it was discussed in *Section 4.2*, the node-loop equations are used in [93, 95] to model the hydraulic part of the heating network. A rather hybrid hydraulic model that consists of hydraulic heads and pipe flows is used in this dissertation, which is more flexible.

Table 5-1: Comparison of hub parameters for electricity network – Case 5-A.

Hub	**Voltage**				**Electricity generation and consumption (kW + jkvar)**			
	[95]		***Proposed***		**[95]**		***Proposed***	
i	$\|V\|$ *(pu)*	θ (°)	$\|V\|$ *(pu)*	θ (°)	$L_{ep} + j\,L_{eq}$	$P_{epg} + jP_{egg}$	$L_{ep} + j\,L_{eq}$	$P_{epg} + jP_{egg}$
1	1.060	0	1.060	0	145.1 +j0	50866.2+j27363	145.1 +j0	50866+j27363
2	0.98	-7.0219	0.98005	-7.0219	30000+j15000	0+j0	30000+j15000	0 + j0
3	1.000	-6.1156	1.000	-6.1156	30136+j15000	10173+j10218.1	30136+j15000	10173+j10218

Table 5-2: Comparison of line flows in the electricity network – Case 5-A.

Line	Electricity flow (kW + jkvar)			
	[95]		*Proposed*	
i-j	$(P_{ep} + jP_{eq})_{ij}$	*Losses*	$(P_{ep} + jP_{eq})_{ij}$	*Losses*
1 - 2	26980.6+j15810.6	0.4352+j4351.8	26981+j15811	0.4352+j4351.8
1 - 3	27740.5+j11552.4	0310.2+j3101.9	23740+j11552	0310.2+j3101.9
2 - 3	-3454.6-j3541.2	12.7+j0127.4	-3454.6-j3541.2	12.7+j0127.4

Table 5-3 : Comparison of hub parameters for heating network – Case 5-A.

Hub	Nodal hydraulic head		Heat generation and consumption (kW)				Temperature (°C)			
	Proposed		[95]		*Proposed*		[95]		*Proposed*	
i	H_s *(m)*	H_r *(m)*	L_h	P_{hg}	L_h	P_{hg}	T_s	T_r	T_s	T_r
1	5517	10	0	28676.8	0	28647	120	48.6805	120	48.536
2	10.666	5516.3	35000	0	35000	0	119.04	50	117.09	50
3	4383.8	1143.2	20000	29000	20000	29000	123.541	49.534	123.54	49.04

Table 5-4: Comparison of branch parameters in the heating network – Case 5-A.

Branch	Heating network					
	[95]			*Proposed*		
$i-j$	$\dot{m}_{ij}$ *(kg/s)*	Ph_{ij} *(kW)*	*Loss (kW)*	$\dot{m}_{ij}$ *(kg/s)*	Ph_{ij} *(kW*	*Loss (kW)*
1 - 2	64.6943	19175.967	890.1	65.962	19547	890.28
1 - 3	31.4533	9500.8	877	29.893	9100.2	873.09
2 - 3	-56.5335	-1674.1	909.7	-58.778	-16343	883.88

Further inspecting the results (by computing the inlet and outlet water temperature for each pipe), it is found that the conservation of energy at node 3 is not obeyed in [95]. At node 3, on the supply pipe network, it is observed that there is a mixing of water coming from node 1 and water coming from the source connected at node 3. The two incoming water temperatures are different. Consequently, the outgoing water temperature at node 3 (i.e. the inlet temperature of water in pipe 3-2) is expected to be different from the water temperature of the source connected to node 3 (i.e. 123.54 °C), unlike to what it is assumed in [95].

The accuracy of the two approaches can be further compared by considering the net heat power injection into the network at node 3. The given heat generation and heat demands at node 3 indicates that there is 9 MW of net heat power injection into the network (see Table 5-3). This should be reflected on the nodal mass flow rate injected into the network and its temperatures on the supply and return sides. In [95], the nodal mass flow rate (calculated from conservation of mass) is 25.08 kg/s while the temperature difference between supply and return sides is 74.01 °C. Computing the heat power injection using these values gives 7.76 MW, which contradicts with the given data of 9 MW. On the other hand, the corresponding nodal mass flow rate and the temperature difference found using the proposed methodology are 28.89 kg/s and 74.51 °C, respectively. The heat power injected into the network calculated by these values gives 9.0 MW which exactly matches with the given data. Hence the proposed model gives more accurate results than the one presented in [95].

Table 5-5 summarizes the network parameters and line flow results found using heat transfer coefficients calculated by applying equation (4-16) on the corresponding standard parameters

of the pipes used (i.e. DN-150 pipes) with a standard insulation (data taken from [118]), instead of assuming constant heat transfer coefficient for all heating network pipes (which is the case in [95]). The simulation took 6 iterations which is one iteration more than the one with a constant heat transfer coefficient. This can be associated with the variation of the convective coefficient of water with the changes in the mass flow rate at each iteration. As it can be seen in Table 5-5, the heat losses by assuming standard pipe parameters are higher (96.8% more) than the one found by assuming a constant heat transfer coefficient. The mass flow rates, the supply and return temperatures and the heat power generation from the slack hub are changed as a result. However, the electricity network parameters remain unaffected.

Table 5-5: Hub parameters and line flows in the heating network using standard pipe parameters with standard insulation layer – Case 5-A.

Hub	**Nodal hydraulic head**		**Heat demand and generation (kW)**		**Temperature (°C)**		**Line $i-j$**	**Line flows in the heating network**		
	H_s *(m)*	H_r *(m)*	L_h	P_{hg}	T_s	T_r		$\dot{m}_{ij}$ *(kg/s)*	Ph_{ij} *(kW)*	*Loss (kW)*
1	5517	10	0	31212	120	47.284	***1-2***	69.733	20886	1772.3
2	1196	4331	35000	0	113.79	50	***1-3***	32.905	10326	1710.9
3	4553	974.05	20000	29000	123.54	48.166	***2-3***	-61.456	-15886	1728.6

5.3.2.2. Results and discussions on Cases 5-B to 5-D

The load flow simulation took 10 iterations for Case 5-B with a convergence tolerance of $8.88*10^{-06}$ pu, while it took 10 and 11 iterations for Cases 5-C and 5-D with a tolerance of $3.05*10^{-06}$ pu and $3.66*10^{-06}$ pu, respectively. Each of the simulations took less than a second on Intel CORE i5 processors (HP® desktop with MATLAB® R2016a and Toshiba® laptop with MATLAB® R2017a).

The contribution of each hub in the overall generation and consumption of different energy carriers is shown in Fig. 5-3. The figure illustrates the sole generations of heat and electricity (referred as local generation) separately from the heat and electricity power produced using the CHP plants. The segments of the bars in all cases indicate the share of different hubs. The details* of CHPs' contributions are also tabulated in Table 5-6 while the nodal and branch operating parameters are summarised in Table 5-7 and Table 5-8.

It can be seen from Fig. 5-3 that the total active power demand for each network is greater than the corresponding total active power locally generated. The same is true for the reactive power and heat power (except for Case 5-C, which is associated with a relatively high heat loss). The deficits between the demand and generations together with the losses in the network are compensated by the contributions from the CHP plants.

Conservation of energy can be checked by comparing the distribution losses computed from the power balance, on one hand, and those losses calculated from the branch operating parameters, on the other hand.

* All conservation of energy and mass are crosschecked in higher resolution than those tabulated in Tables 5-6, 5-7 and 5-8.

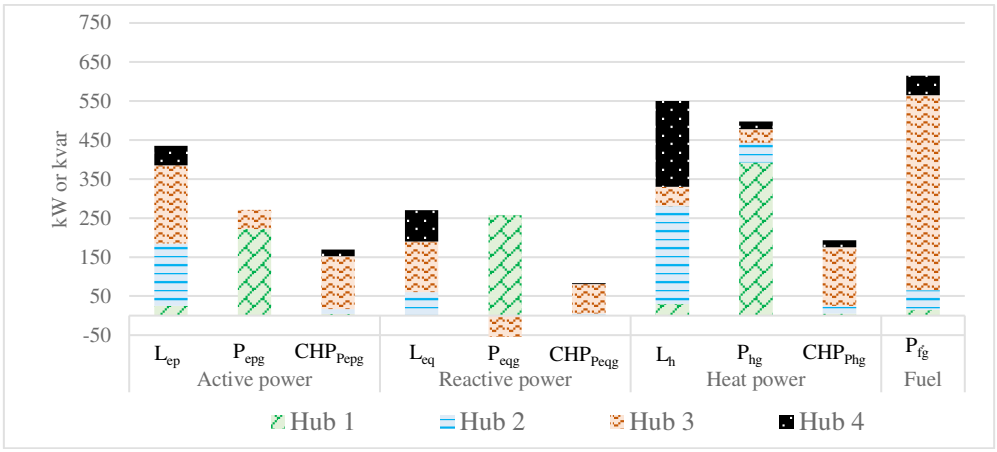

(a) Case 5-B

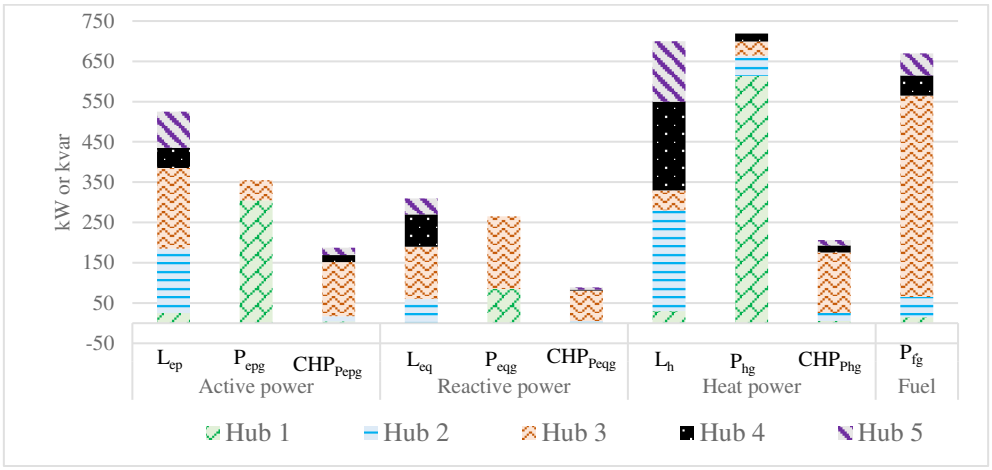

(b) Case 5-C

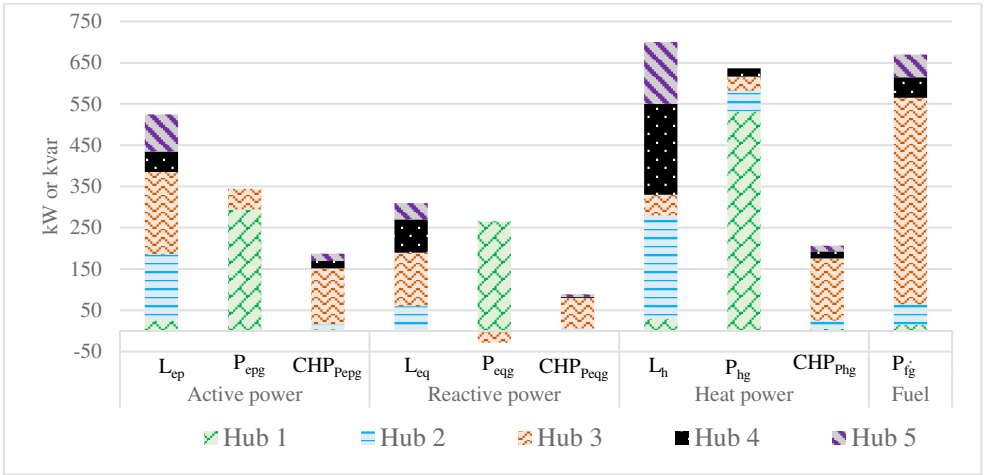

(c) Case 5-D

Fig. 5-3. Hubs' contribution in the generation and consumption of electricity, heat and fuel – Cases 5-B to 5-D. In the legends, L_{ep}, P_{epg} and CHP_{Pepg} represent the active power demand, sole generation and production from the CHP plants, respectively. Similarly, L_{eq}, P_{eqg} and CHP_{Peqg} denote the reactive power demand, sole generation and production from the CHPs while L_h, P_{hg} and CHP_{Phg} stand for the heat power demand, sole production and contribution from the CHPs, respectively. P_{fg} represents the fuel power used by the CHP plants that are installed at different hubs.

Table 5-6: Input and outputs of the CHP plants at different hubs – Cases 5-B to 5-D.

	CHP at hub	Fuel inputs (kW)	Active Power		Reactive Power		Heat Power	
			$C_{ep(f)}$	(kW)	$C_{eq(f)}$	(kvar)	$C_{h(f)}$	(kW)
Case 5-B	1	14.882889	0.3	4.465	0.1	1.488	0.36	5.358
	2	50	0.25	12.5	0.08	4	0.4	20
	3	500	0.27	135	0.15	75	0.3	150
	4	50	0.35	17.5	0.05	2.5	0.35	17.5
	Total	*614.8829*	-	*169.465*	-	*82.988*	-	*192.858*
Case 5-C	1	14.883	0.3	4.465	0.1	1.488	0.36	5.358
	2	50	0.25	12.5	0.08	4	0.4	20
	3	500	0.27	135	0.15	75	0.3	150
	4	50	0.35	17.5	0.05	2.5	0.35	17.5
	5	55	0.33	18.15	0.1	5.5	0.25	13.75
	Total	*669.883*	-	*187.615*	-	*88.488*	-	*206.608*
Case 5-D	1	14.883	0.3	4.465	0.1	1.488	0.36	5.358
	2	50	0.25	12.5	0.08	4	0.4	20
	3	500	0.27	135	0.15	75	0.3	150
	4	50	0.35	17.5	0.05	2.5	0.35	17.5
	5	55	0.33	18.15	0.1	5.5	0.25	13.75
	Total	*669.883*	-	*187.615*	-	*88.48829*	-	*206.608*

For example, the contributions from all the CHP plants in Case 5-B is 169.465 kW of active, 82.988 kvar of reactive and 192.85 kW of heat powers (see Table 5-6). Adding these powers to the locally produced active, reactive and heat powers and subtracting the corresponding loads (refer Table C-3 and Table 5-7(a)) gives the respective distribution losses (5.938 kW, 13.71 kvar and 140.68 kW respectively). These values are exactly the same as the sum of the corresponding power losses calculated by the model on branch basis for each pipe and transmission lines as indicated in Table 5-8(a). The losses account for 1.36%, 5.07% and 25.57% of the respective demands.

It can be noted that hub 2 in Case 5-B was initially set as *temp_supply* type (see Table C-3 in Appendix C) assuming it could have an excess of heat power to be injected into the network. On the contrary, hub 3 was set as *temp_return* type assuming it could have a deficit of heat power. But, the results show that there is a deficit of heat power at hub 2 and excess of heat at hub 3 (see the mass flow injections at each hubs in Table 5-7(a)). Hence, the return temperature at hub 2 is fixed to the maximum possible value and the supply temperature is solved. At hub 3, on the other hand, the supply temperature is fixed to the maximum possible value and the return temperature is solved in the load flow. This shows the model's capability to detect if a given hub is acting as a source or a consumer and configure the load flow equations accordingly.

Cases 5-C and 5-D are extensions of Case 5-B with the addition of hub 5, which has no heat and electricity sole generations, but a CHP that takes 55 kW of fuel and produces both heat and electricity. The outputs of the CHP plant are 18.15 kW of active power, 5.5 kvar of reactive power and 13.75 kW of heat power (see Table 5-6) which are insufficient to supply the demands (90 kW, 40 kvar and 150 kW respectively) of the hub. The deficits and the additional losses in the connecting branches led to more generations at the slack hubs of Case 5-C and Case 5-D, as compared to Case 5-B.

Table 5-7: Hub-level operating parameters of the electricity and heating networks.

(a) Case 5-B

Hub	***Electricity***						***DHN and Fuel***							
	$\|V\|$ $(pu)^*$	θ $(^o)$	P_{epg} (kW)	P_{eqg} $(kvar)$	L_{ep} (kW)	L_{eq} $(kvar)$	P_{hg} (kW)	L_h (kW)	P_{fg} (kW)	$\dot{m}$ (kg/s)	T_s (^oC)	T_r (^oC)	H_s (m)	H_r (m)
1	1.000	0.000	221.473	258.178	25.000	0.000	392.829	30.000	14.883	1.799	80.000	31.096	135.000	1.000
2	0.979	-0.083	0.000	0.000	160.000	60.000	50.000	250.000	50.000	-1.092	74.397	35.000	91.694	44.306
3	1.050	-0.074	50.000	-57.453	200.000	130.000	35.000	50.000	500.000	0.676	80.000	32.304	91.650	44.350
4	0.982	-0.150	0.000	0.000	50.000	80.000	20.000	220.000	50.000	-1.384	66.518	35.000	86.618	49.382
		Total	***271.473***	***200.725***	***435.000***	***270.000***	***497.8287***	***550.0000***	***614.8829***	***0.0000***				

(b) Case 5-C

Hub	***Electricity***						***DHN and Fuel***							
	$\|V\|$ $(pu)^*$	θ $(^o)$	P_{epg} (kW)	P_{eqg} $(kvar)$	L_{ep} (kW)	L_{eq} $(kvar)$	P_{hg} (kW)	L_h (kW)	P_{fg} (kW)	$\dot{m}$ (kg/s)	T_s (^oC)	T_r (^oC)	H_s (m)	H_r (m)
1	1.0000	0.0000	305.0825	84.9088	25.0000	0.0000	613.7802	30.0000	14.8829	2.7642	80.0000	29.0733	135.0000	1.0000
2	0.9706	-0.2654	0.0000	0.0000	160.0000	60.0000	50.0000	250.0000	50.0000	-1.0069	72.7157	30.0000	105.8792	30.1208
3	1.0500	-0.4229	50.0000	180.1220	200.0000	130.0000	35.0000	50.0000	500.0000	0.5464	90.0000	30.9628	105.8825	30.1175
4	0.9626	-0.3032	0.0000	0.0000	50.0000	80.0000	20.0000	220.0000	50.0000	-1.4012	66.1215	35.0000	103.1225	32.8775
5	1.0334	-0.4653	0.0000	0.0000	90.0000	40.0000	0.0000	150.0000	55.0000	-0.9025	71.0735	35.0000	104.9399	31.0601
		Total	***355.082***	***265.031***	***525.000***	***310.000***	***718.7802***	***700.0000***	***669.8829***	***0.0000***				

(c) Case 5-D

Hub	***Electricity***						***DHN and Fuel***							
	$\|V\|$ $(pu)^*$	θ $(^o)$	P_{epg} (kW)	P_{eqg} $(kvar)$	L_{ep} (kW)	L_{eq} $(kvar)$	P_{hg} (kW)	L_h (kW)	P_{fg} (kW)	$\dot{m}$ (kg/s)	T_s (^oC)	T_r (^oC)	H_s (m)	H_r (m)
1	1.0000	0.0000	294.7118	265.5685	25.0000	0.0000	531.5600	30.0000	14.8829	2.4205	80.0000	29.9575	135.0000	1.0000
2	0.9763	-0.2938	0.0000	0.0000	160.0000	60.0000	50.0000	250.0000	50.0000	-0.9393	75.7910	30.0000	58.8439	77.1562
3	1.0500	-0.7092	50.0000	-28.0289	200.0000	130.0000	35.0000	50.0000	500.0000	0.5654	90.0000	32.9424	45.5164	90.4836
4	0.9819	-1.3041	0.0000	0.0000	50.0000	80.0000	20.0000	220.0000	50.0000	-1.0887	75.0560	35.0000	10.4388	125.5612
5	1.0855	-1.6464	0.0000	0.0000	90.0000	40.0000	0.0000	150.0000	55.0000	-0.9579	68.9882	35.0000	1.3375	134.6625
		Total	***344.712***	***237.540***	***525.000***	***310.000***	***636.5600***	***700.0000***	***669.8829***	***0.0000***				

* A line-to-line voltage base value of 4.16 kV is considered in the simulation.

Table 5-8: Selected branch-level operating parameters in the electricity and heating networks.

(a) Case 5-B

Hubs		***Electricity***				***DHN***						
*From (**i**)*	*To (j)*	*Current (pu)*[*]	*Apparent Power flow (kVA)*	*Active power lost (kW)*	*Reactive power lost (kvar)*	*Pipe flow (kg/s)*[†]	$T_{s(i)}$ (^oC)	$T_{s(j)}$ (^oC)	$T_{r(i)}$ (^oC)	$T_{r(j)}$ (^oC)	*Heat Power flow (kW)*	*Heat power lost (kW)*
1	*2*	0.402-0.519i	200.937+259.666i	3.8087	5.3629	1.7989843	80	74.396825	31.095865	32.931418	368.18698	56.00432
2	*4*	-0.015+0.107i	-7.452-52.574i	0.0805	-0.1239	0.6438246	74.396825	63.67863	30.839005	35	117.36245	40.09058
3	*2*	-0.105+0.466i	-55.605-244.698i	1.4760	6.1788	-0.0634283	34.729812	74.396825	32.304497	18.565422	-0.6437935	14.176504
3	*4*	0.077-0.252i	40.6045+132.245i	0.5724	2.2951	0.7397617	76.118466	68.989565	32.304497	35	135.64379	30.415402
			Total	***5.9376***	***13.7129***						***Total***	***140.687***

(b) Case 5-C

Hubs		***Electricity***				***DHN***						
*From (**i**)*	*To (j)*	*Current (pu)*[*]	*Apparent Power flow (kVA)*	*Active power lost (kW)*	*Reactive power lost (kvar)*	*Pipe flow (kg/s)*[†]	$T_{s(i)}$ (^oC)	$T_{s(j)}$ (^oC)	$T_{r(i)}$ (^oC)	$T_{r(j)}$ (^oC)	*Heat Power flow (kW)*	*Heat power lost (kW)*
1	*2*	0.6349-0.6922i	317.4537+346.0956i	7.7903	11.3056	1.4578	80.0000	73.1522	27.8706	29.8084	318.0467	53.6016
2	*4*	0.2009-0.2559i	98.0559+123.7299i	0.7284	0.8496	0.4611	72.7157	58.6422	29.3900	35.0000	83.6105	37.9854
3	*2*	-0.1187+0.2913i	-63.468-152.4611i	0.6391	2.5991	0.0102	90.0000	10.2280	10.0565	29.8084	3.4072	4.2417
3	*4*	0.0884-0.5294i	48.4684+277.5839i	2.3733	10.1150	0.5362	90.0000	78.3515	31.3598	35.0000	131.5928	34.3089
1	*5*	-0.0658+0.5194i	-32.906-259.6985i	3.2753	7.9798	1.3064	80.0000	71.0735	30.4153	33.3992	271.0919	65.1173
4	*5*	0.2270-0.6512i	110.9226+312.8485i	2.8910	10.6702	-0.4039	58.4237	71.0735	35.0000	29.8219	-39.5914	30.1332
			Total	***17.6973***	***43.5192***						***Total***	***225.388***

(c) Case 5-D

Hubs		***Electricity***				***DHN***						
*From (**i**)*	*To (j)*	*Current (pu)*[*]	*Apparent Power flow (kVA)*	*Active power lost (kW)*	*Reactive power lost (kvar)*	*Pipe flow (kg/s)*[†]	$T_{s(i)}$ (^oC)	$T_{s(j)}$ (^oC)	$T_{r(i)}$ (^oC)	$T_{r(j)}$ (^oC)	*Heat Power flow (kW)*	*Heat power lost (kW)*
1	*2*	0.548-0.534i	274.177+267.057i	5.1746	7.4016	2.4205	80.0000	75.7910	29.9576	31.2344	506.9166	55.5703
3	*2*	-0.224+0.381i	-120.241-198.394i	1.2615	5.2615	-1.4812	73.1378	75.7910	32.9424	32.0172	-249.1643	22.1821
3	*4*	0.198-0.222i	105.241+115.365i	0.7290	2.9748	2.0466	77.7959	75.0560	32.9424	33.9086	384.1645	31.7432
4	*5*	0.145-0.074i	72.012+34.890i	0.1615	0.3900	0.9579	75.0560	68.9882	32.6683	35.0000	169.9212	33.6713
			Total	***7.3267***	***16.0279***						***Total***	***143.1669***

[*] The current per unit values are based on 4.16 kV line-to-line voltage and 500 kVA apparent power base values.

[†] The mass flows through the pipe connecting hubs *i* and *j* as observed on the supply pipe network of the DHN.

The active, reactive and heat power losses for Case 5-C (3.37%, 14.04% and 32.2%, respectively) are higher than the losses in Case 5-D (1.39%, 5.17% and 20.45% respectively). One reason for this is the higher number of transmission lines and pipes used in Case 5-C as compared to Case 5-D. The reactive power loss on a transmission line can be negative when the reactive power supplied by shunt capacitive part of the line becomes greater than what is consumed by the inductive part of the transmission line as it is the case for line 2-4 in Case 5-B (see Table 5-8(a)).

As it can be seen from Table 5-8, mass flows through pipe 3-2 in Case 5-B, pipe 4-5 in Case 5-C and pipe 3-2 in Case 5-D are negative implying that the directions of flow in these pipes are opposite to what are assumed in Fig 5-2. Similarly, mass flow rates from each hub into the network are assumed positive if the hub is acting as a heat source and negative otherwise, as shown in Fig. 5-2. The results show that hubs 2, 4 and 5 are acting as a heat sink and hubs 1 and 3 are acting as a heat source (see Table 5-7). It can also be observed that the sum of all mass flows from each hub into the DHN (indicated by $\dot{m}$) are zero for all cases which shows the conservation of mass is holding true.

Although Case 5-C and Case 5-D have the same load profiles for all hubs, there is a very significant difference on their hydraulic head profiles (see Fig. 5-4 and Table 5-7). The hydraulic head, which is the sum of pressure head and altitude, may not need to be exactly equal to the values indicated in Table 5-7. However, the same relative hydraulic head difference between different hubs should be maintained to guarantee the required pipe mass flows in the network. All hydraulic heads on the supply pipe network or all hydraulic heads on the return pipe networks can be increased/decreased by the same amount as far as they remain in the acceptable hydraulic head ranges. These minimum and maximum acceptable hydraulic head limits depend on the altitude and atmospheric pressures of the site where the pipes are buried. Such limits should be guaranteed to avoid boiling of water inside a pipe (minimum limit) and damage of pipes (maximum limit) [119].

The highest and the lowest hydraulic heads on the supply network side of the DHN in Case 5-C are 135 m and 103.123 m while in Case 5-D they are 135 m and 1.34 m, respectively (see Table 5-7 and Fig. 5-4). It means that the DHN in Case 5-C needs a lower pumping energy than Case 5-D. This could be associated with the topological differences. Due to more parallel paths in Case 5-C, there are lower mass flow rates in each path with a lower pressure difference between the connected hubs as compared to a single radial path in Case 5-D.

The temperature profiles of the heating network, as it can be seen from Fig. 5-4, shows that all the supply temperatures are less than or equal to the maximum of the values specified at *temp_supply* hubs (i.e. 90 $^{\circ}$C at hub 3, Table C-3). Similarly, all the return temperatures are less than or equal to the maximum of the values specified at *temp_return* hubs (i.e. 35 $^{\circ}$C at hubs 4 and 5, Table C-3)[*]. It can also be observed that all the temperatures are above the

[*] Most of currently operating DHNs (categorized as 3rd generations) supply heat using pressurised water in the range of 70 - 100 $^{\circ}$C while the future 4th generation are expected to use supply temperatures as low as 50 - 60 $^{\circ}$C [24]. The corresponding return temperatures are lower than 45 $^{\circ}$C and 25 $^{\circ}$C, respectively. In this thesis, temperatures in the ranges of both 3rd and 4th generation DHNs are considered.

temperature of earth's surface (assumed 10 °C). The inlet and outlet temperatures of each pipe in both the supply and return pipe networks can be referred from Table 5-8.

The results show that for the same dimension of pipe, the drop in temperature and the heat loss (in percentage of the amount transported) increase as the mass flow rate decreases. Accordingly, the largest temperature drop is observed on pipe 3-2 of Case 5-C (both on supply and return network). It also shows that the heat loss across this pipe is higher than what is actually transported. In this case, it may be economical to isolate the pipe (more discussion can be found in *Chapter 6*). On the other hand, less pipe mass flow implies less friction and, as a result, less pumping energy required to keep the mass flows.

The voltage profiles for all hubs are depicted in Fig. 5-5. It shows that, although Case 5-C and Case 5-D have the same load and generation profiles, except at the slack hub, they experience different voltage profiles due to their topological differences. In all cases, the slack hub and hub 3 (which is *PV* hub) have a voltage magnitude of 1.0 pu and 1.05 pu, respectively, which is in agreement with their definition in Table C-3.

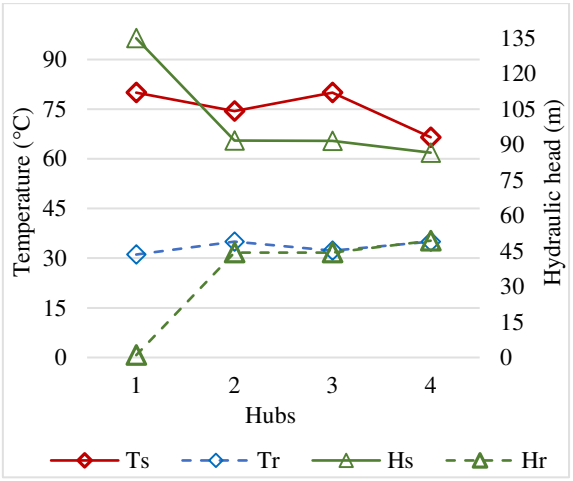

(a) Case 5-B

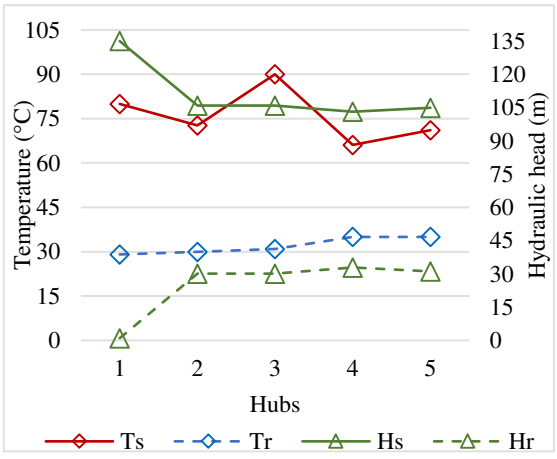

(b) Case 5-C

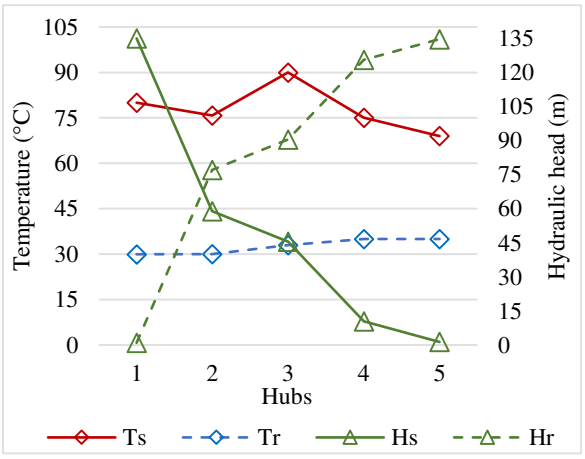

(c) Case 5-D

Fig. 5-4. Temperature and hydraulic head profiles after load flow solution – Cases 5.B to5-D.

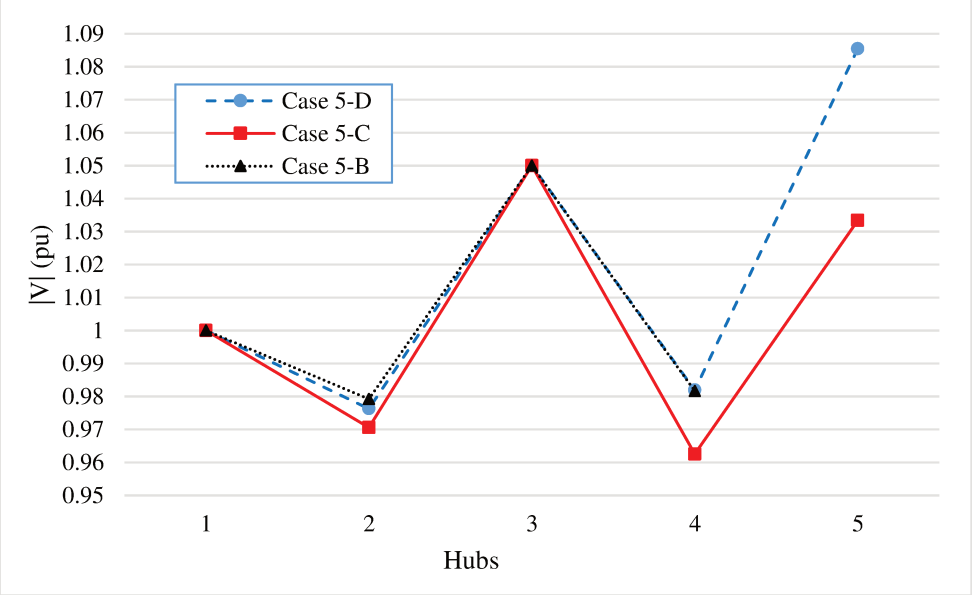

Fig. 5-5. Voltage profiles of electricity network for Cases 5-B to 5-D.

In order to keep the voltage magnitudes constant at the *PV* hubs (e.g. hub 3), a reactive power generation or consumption takes place. As it can be referred from Fig. 5-3 and Table 5-7, there is consumption of reactive power at hub 3 in Cases 5-B and 5-D and reactive power generation in Case 5-C to keep hub 3 at its specified value of 1.05 pu (this value is an arbitrarily selected value for illustration, Table C-3).

5.4. Pseudo-dynamic simulation of coupled electricity and heating networks

In the previous section, the steady state operating parameters of coupled electricity and heat distribution networks are studied for a single time step. The variation of operational parameters over a longer time period can be studied using a pseudo-dynamic simulation. A given time period is decomposed into appropriate simulation time steps. Each time step should be short enough to assume the change in the input parameters are negligible. The time step should also be long enough in order for all the operational parameters reach their steady state values.

In a MES consisting of electricity and heating networks, the later takes longer time to reach steady state [120]. K. Sartor and P. Dewalef [121] used experimental setup to validate their heat transport model of a DHN. It is concluded that the temperature transient may take up to few minutes for small to medium sized DHN and up to hours for large DHN. It means that if an hour is selected as a simulation time interval for a medium scale DHN, both of the electricity and heating networks are able to reach their steady state.

In that context, a pseudo-dynamic simulation is conducted on coupled electricity and heating networks consisting of a CHP, HOB, HPs and solar PV. The simulation helps to investigate the annual variation of the following operational parameters: nodal voltage, nodal mass flow

rate, pipe flow rate, supply and return temperatures from the energy hubs, inlet and outlet temperatures of water in the supply and return pipes, power losses on both networks, fuel consumption, and the amount of imported and exported energy.

5.4.1. Description of the case study and operation scenarios

A six-hub case study (Case 5-E as shown in Fig. 5-6) is considered for the pseudo-dynamic simulation. For simplicity, each of the electricity and heat distribution networks are represented using single line. The electricity network consists of ACSR Ostrich type three phase lines operating at 4.16 kV (parameters taken from [102]). The pipes in the heating network are DN-50 with series-II insulation layer (parameters taken from isoplus® [118]). The details for both networks are summarised in Table 5-9.

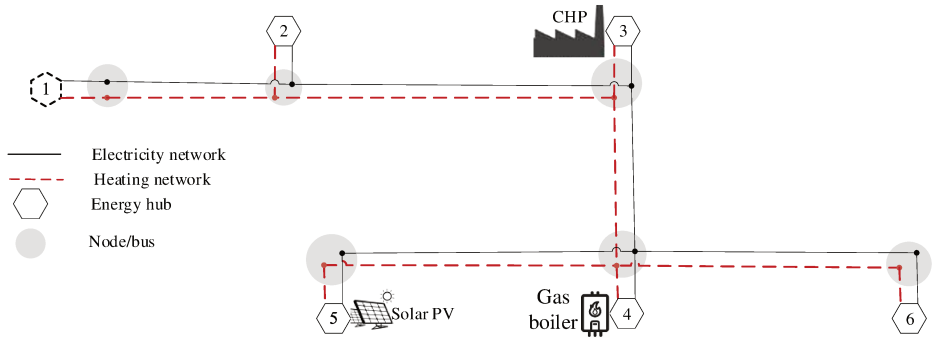

Fig. 5-6. The layout of the heating and electricity network considered for Case 5-E.

Table 5-9: Pipe and transmission line parameters for Case 5-E.

Hubs		**Carrier pipe parameters**					**Insulation**		**Outer jacket**		**Transmission lines**			
from	*to*	*L (km)*	R_1 *(mm)*	R_2 *(mm)*	k_2 *(W/mK)*	*e (mm)*	R_3 *(mm)*	k_3 *(W/mK)*	R_4 *(mm)*	k_4 *(W/mK)*	*L (mi)*	*R (mΩ/mi)*	*X (mΩ/mi)*	*B (μS/mi)*
1	2	1	26.95	30.15	40	0.05	67	0.027	70	0.40	0.6	307	458	9.46
2	4	1	26.95	30.15	40	0.05	67	0.027	70	0.40	0.6	307	458	9.46
3	2	1	26.95	30.15	40	0.05	67	0.027	70	0.40	0.6	307	458	9.46
3	4	1	26.95	30.15	40	0.05	67	0.027	70	0.40	0.6	307	458	9.46
4	5	1	26.95	30.15	40	0.05	67	0.027	70	0.40	0.6	307	458	9.46
3	6	1	26.95	30.15	40	0.05	67	0.027	70	0.40	0.6	307	458	9.46
4	6	1	26.95	30.15	40	0.05	67	0.027	70	0.40	0.6	307	458	9.46

The yearly pattern is approximated by taking 2 days from each season (February 6, March 23, May 6, Jun 23, August 7, September 23, November 7 and December 23) giving a total of 192 simulation hours. These hours and the corresponding profiles are taken only to demonstrate the capacity of the tool in handling pseudo-dynamic simulation of a highly coupled MES. Depending on the accuracy and level of details required, the number of simulation hours can be increased for better representation of the year, but with the cost of longer computational time.

The demand profiles of residential and commercial buildings located in Idaho, USA (which has more or less the same weather condition as Nantes, France) are extracted from Open

Energy Information database [122]. All the heating demands, including domestic hot water, are assumed to be supplied through the DHN. The DHN pipes are assumed to be buried at 0.5 m depth from the surface. The soil temperature at this depth for the 192 hours is taken from AgriMet online weather database [123]. A uniform temperature profile is assumed around all the DHN pipes. Accordingly, equation (4-18) is used to calculate the thermal resistance of each pipe in the thermo-hydraulic model.

Table 5-10 summarizes the location, type, lowest and peak values of the electricity and heat demands. Solar PV, waste incineration CHP, gas fired HOB and HPs are considered to supply the energy demands. These technologies are dispatched in a merit order based on their operating cost.

Table 5-10: Summary of the demand profile considered in Case 5-E.

Hubs	Electricity demand				Heat demand		Load type
	Active		Reactive		lowest (kW)	Peak (kW)	
	lowest (kW)	Peak (kW)	Lowest (kvar)	Peak (kvar)			
2	8.68	67.10	5.38	41.6	2.61	77.09	Residential
4	17.36	134.21	5.73	44.29	5.22	154.19	Residential
6	50.68	199.50	24.33	95.76	2.00	54.64	Small hotel

A 200 kW peak solar PV generation plant is connected at hub 5. The electricity production from the solar PV is forecasted for a year using HOMER® [33]. The generation profiles for the selected eight days are then extracted and considered as active electric power production at hub 5. All the available PV generation is assumed to be fed into the electricity distribution network.

The waste incineration CHP plant is connected at hub 3 (also referred to as CHP3). The peak rating of the CHP is 70 kW_e and 80 kW_{th} with the corresponding efficiencies of 35% and 40%. It runs at a lagging power factor of 0.86. The CHP is assumed to have two equal units. Considering annual inspection and maintenance periods, the units are scheduled as follows:

- both units run at full capacity during winter days.
- only one unit runs during autumn and spring days.
- both units are turned off during summer days.

The gas boiler is installed at hub 4 with 45 kW_{th} capacity at 90% efficiency. It is scheduled to supply part of the local heat demand at hub 4 exceeding 100 kW_{th}.

The three HPs, 20 kW_e capacity each with a COP of 4.0 running at 0.9 lagging power factor, are considered. Two scenarios are defined based on their location. In Scenario I, the HPs are installed at hubs 2, 4 and 6 with designation HP2, HP4 and HP6, respectively. They are scheduled to supply the local heat demand at the corresponding hub with a maximum limit of 80 kW_{th}. In Scenario II, on the other hand, HP2, HP4 and HP6 are altogether installed at hub 3, represented as HP3. The heat produced by HP3 at each hour is equal to the heat that could have been produced by HP2, HP4 and HP6 collectively in Scenario I. The scheduling of the CHP at hub 3, the gas boiler at hub 4 and the solar PV at hub 5 is the same in both scenarios. Table 5-11 summarizes the technologies considered in the two scenarios.

Table 5-11: Summary of the technologies considered in the two scenarios – Case 5-E.

	Technologies connected					
	Hub 1	Hub 2	Hub 3	Hub 4	Hub 5	Hub 6
Scenario I	Slack hub	HP2	CHP3	Boiler4, HP4	Solar PV	HP6
Scenario II	Slack hub	---	CHP3, HP3(=HP2+HP4+HP6)	Boiler4	Solar PV	---

Fig. 5-7 to Fig. 5-9 show the duration curves of the total consumption of each energy carrier. The numbers in the legends indicate the corresponding hubs. Fig. 5-7(a) shows the duration curve of heat demand while Fig. 5-7(b) depicts the fuel consumption pattern for the gas boiler and the CHP plant. Both of them are plotted using the total heat demand as a reference. The fuel consumption of the gas boiler follows the heat demand of hub 4 (indicated as load4) exceeding the 100 kW threshold, but the CHP scheduling is not strictly following the hourly total heat demand profile as it is scheduled on seasonal bases. The duration curves shown in Fig. 5-8 and Fig. 5-9 consist of the active and reactive power consumptions of the coupling technologies, in addition to the residential and commercial electrical loads. It should be noted that the total active and reactive power demands are the same in both scenarios. The only difference is the location of the HPs.

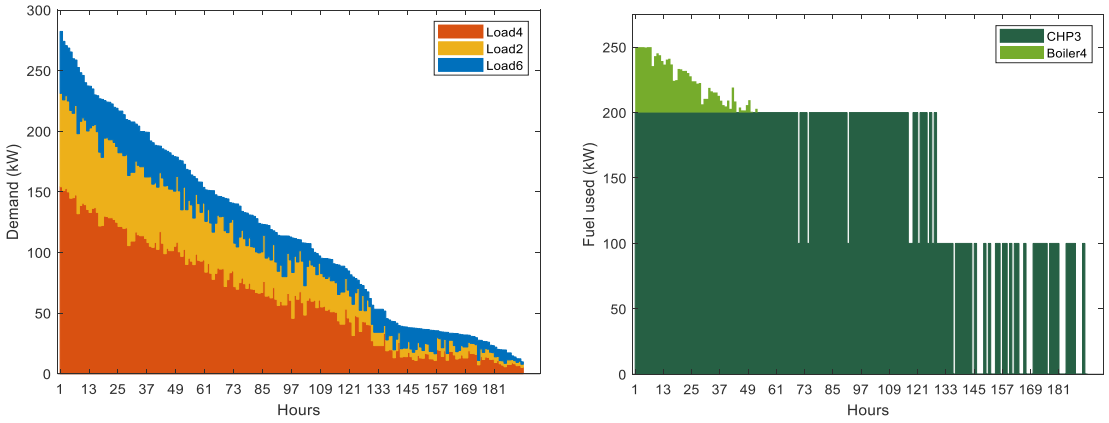

(a) (b)

Fig. 5-7. Duration curves of (a) the heat demand and (b) fuel consumption – Case 5-E.

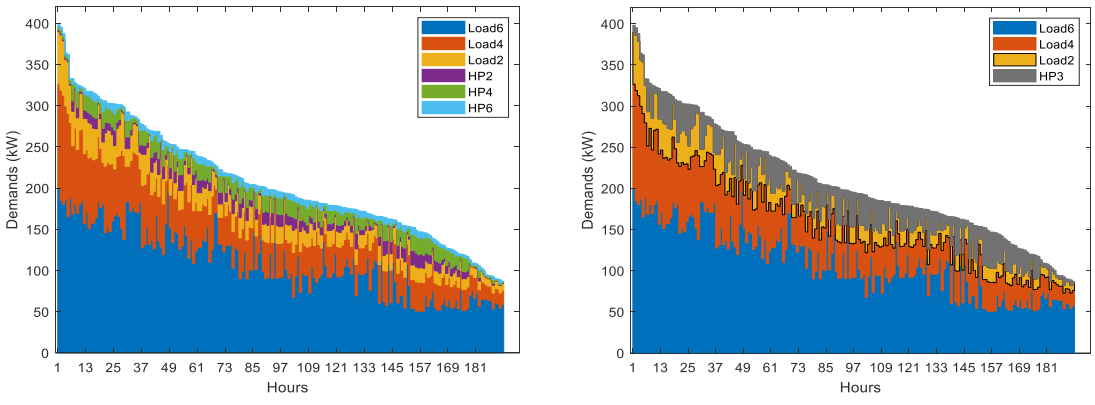

(a) (b)

Fig. 5-8. Duration curves for active power demand: (a) Scenario I and (b) Scenario II – Case 5-E

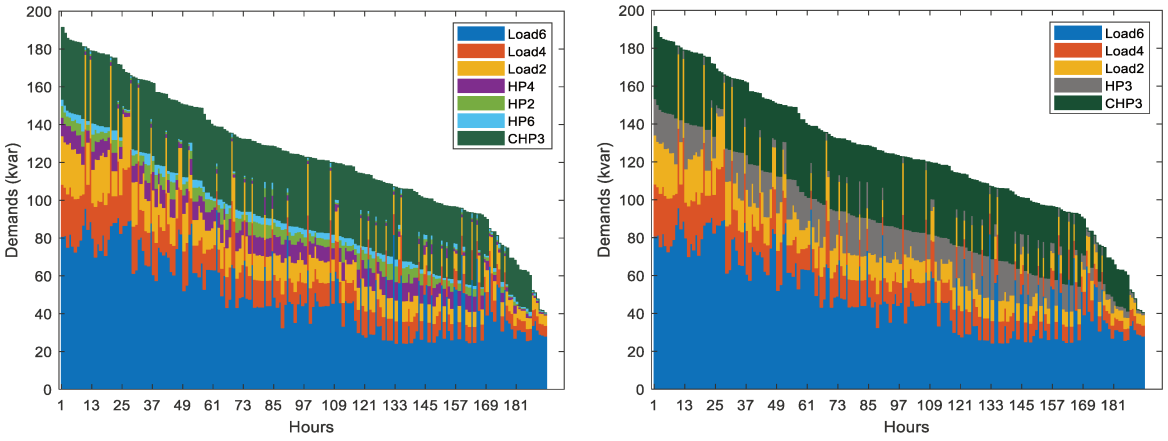

(a) (b)

Fig. 5-9. Duration curves for reactive electric power demand: (a) Scenario I and (b) Scenario II – Case 5-E.

5.4.2. Additional coupling equations

In addition to the coupling configurations discussed in *Section 5.2*, two new interactions are visible in Table 5-11. The first is between a HOB and a HP at hub 4 in Scenario I while the second is between a CHP and a HP at hub 3 in Scenario II. The EEH representations of these two interactions are shown in Fig. 5-10. The corresponding coupling equations are derived as shown in equations (5-5) and (5-6).

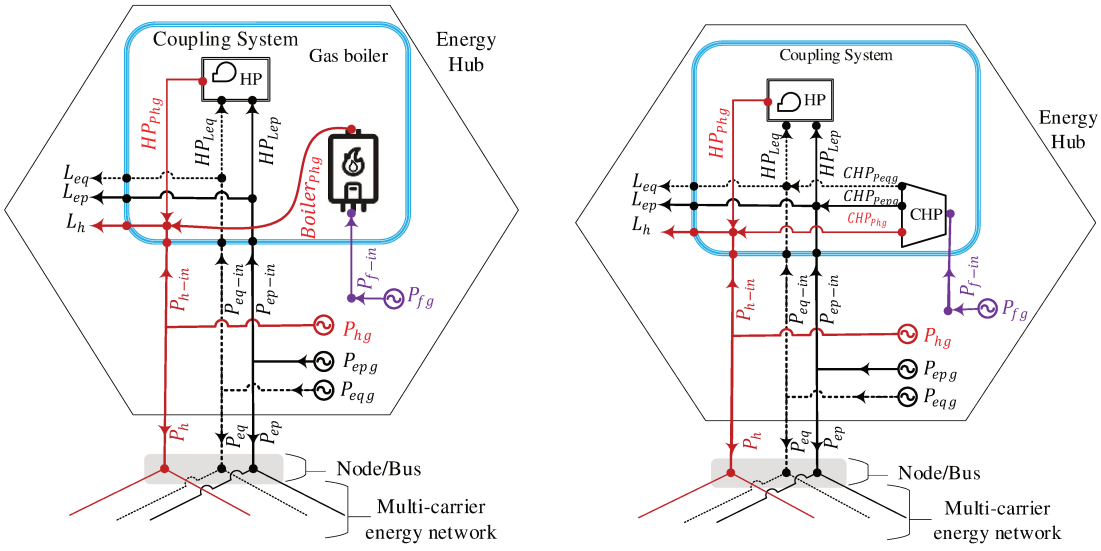

(a) (b)

Fig. 5-10. EEH representations showing the interactions between heat, electricity and fuel energy carriers: (a) a hub with a HOB and a HP, (b) a hub with a CHP and HP.

$$\begin{bmatrix} L_{ep} + P_{ep-HP} \\ L_{eq} + P_{ep-HP}\dfrac{\sqrt{1-pf_{HP}{}^2}}{pf_{HP}} \\ L_h - P_{ep-HP} * COP \end{bmatrix} = \begin{bmatrix} 1 & 0 & 0 & 0 \\ 0 & 1 & 0 & 0 \\ 0 & 0 & 1 & \eta_b \end{bmatrix} \begin{bmatrix} P_{epg} - P_{ep} \\ P_{eqg} - P_{eq} \\ P_{hg} - P_h \\ P_{fg} \end{bmatrix} \tag{5-5}$$

$$\begin{bmatrix} L_{ep} + P_{ep-HP} \\ L_{eq} + P_{ep-HP}\dfrac{\sqrt{1-pf_{HP}{}^2}}{pf_{HP}} \\ L_h - P_{ep-HP} * COP \end{bmatrix} = \begin{bmatrix} 1 & 0 & 0 & \eta_{el} \\ 0 & 1 & 0 & -\eta_{el}\dfrac{\sqrt{1-pf_{CHP}{}^2}}{pf_{CHP}} \\ 0 & 0 & 1 & \eta_{th} \end{bmatrix} \begin{bmatrix} P_{epg} - P_{ep} \\ P_{eqg} - P_{eq} \\ P_{hg} - P_h \\ P_{fg} \end{bmatrix} \tag{5-6}$$

5.4.3. Results and discussions

In solving the load flow problem, the supply temperatures of all the heat-exporting hubs are assumed to be 85 °C while the return temperatures of all hubs that import heat from the network are taken to be 35 °C. The only exception to this assumption is the slack hub where the neighbourhood heat grid (it could be also underground thermal storage) is assumed to be capable of extracting all the available heat whenever the network is exporting. Accordingly, the slack hub return temperature is assumed to be equal to the soil temperature when the network is exporting heat. On the other hand, the slack hub is assumed to be capable of supplying heat to the network at a supply temperature of 85 °C whenever the network is importing heat. A slack hub with a thermal storage is covered in *Chapter 7*.

5.4.3.1. Analysis for the overall network

The heat power generated from different technologies are plotted in Fig. 5-11. The total heat demand in both scenarios, for 192 hours, is about 22.403 MWh. The heat generations from the CHP and the gas boiler are 11.52 MWh and 1.109 MWh, respectively. The sum of the heat produced from the three heat pumps (HP2, HP4 and HP6) in scenario I is 20.074 MWh. The same amount of heat is generated from HP3 in Scenario II. In both scenarios, the total heat generated from the technologies is 32.703 MWh, which is much higher than the total demand. However, as the generation technologies are located at different places, the heat loss in the network is different for the two scenarios. The total heat lost in Scenario I is about 5.453 MWh while it is about 11.095 MWh in Scenario II. The reason for the lower heat loss in Scenario I (less by 51%) than Scenario II is because of the installation of HPs near to the heat demands. There is more heat transportation and, hence, more heat loss in Scenario II than Scenario I.

The total exported and imported heat powers in Scenario I are 4.899 MWh and 61.361 kWh, respectively. This implies that there is a net export of 4.838 MWh of heat in Scenario I. In the case of Scenario II, the system has exported 1.012 MWh and imported 1.815 MWh of heat resulting in a net import of 0.803 MWh of heat. Thus, Scenario I is more efficient than Scenario II from the DHN point of view.

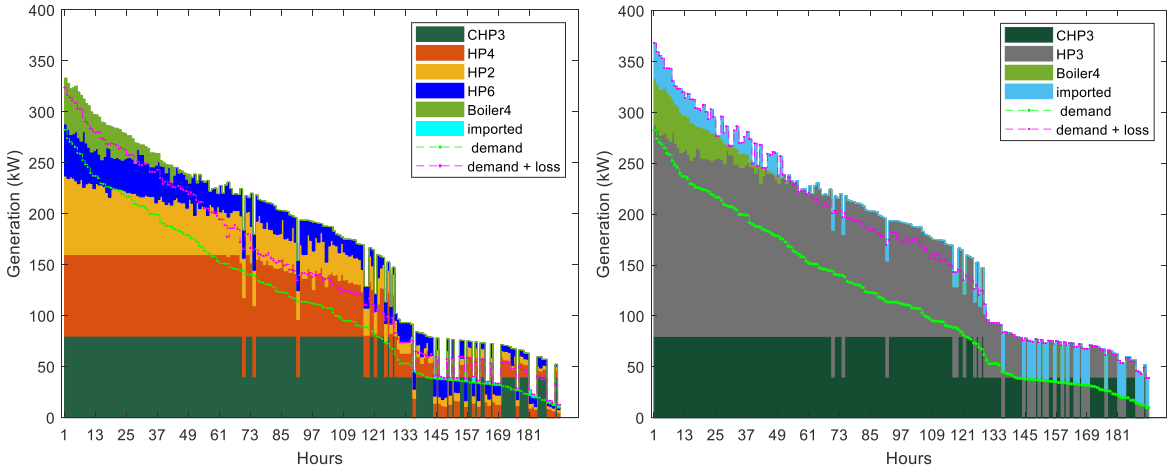

(a) (b)

Fig. 5-11. Duration curves of heat power generated: (a) Scenario I and (b) Scenario II – Case 5-E.

The duration curves for active power generation, as shown in Fig. 5-12, are quite similar in the two scenarios. The main reason is the voltage level (4.16 kV) which is high relative to the electricity demand, the size of the HPs and the length of distribution networks. Further investigation considering lower (0.4 kV) distribution networks is presented in *Chapter 6*.

The active electricity generated in 192 hours from the CHP and solar PV is about 10.08 MWh and 6.142 MWh, respectively. The total active power demand for the connected loads at Hubs 2, 4 and 6 is 34.959 MWh. In addition, 5.018 MWh of active power is consumed by the HPs. It shows that the generations from the CHP and the solar PV cover only 32.2% of the total demand. The active power losses in the network is 257.052 kWh in Scenario I and 245.32 kWh in Scenario II, which accounts only 0.643% and 0.614% of the total active electricity demand. The slight difference between the two scenarios is due to the HPs in Scenario I being located far from hub 3 where there is active electricity source. The very low distribution loss also manifests the advantage of high voltage level relative to the installed electricity demands.

Although the network is importing active electricity most of the time in both scenarios, it also exports occasionally as indicated by the circles in Fig. 5-12. During these hours, the sum of the electricity generated from the CHP and the solar PV is higher than the total demand plus the loss at the corresponding hour. The total imported and exported active electricity in Scenario I is 24.416 MWh and 403.976 kWh, respectively. In other words, the energy system in Scenario I is importing a net of 24.012 MWh active electricity in 192 hours. Similarly, the energy system in Scenario II is importing 24.405 MWh and exporting 404.201 kWh of active electricity with a net import of 24.001 MWh.

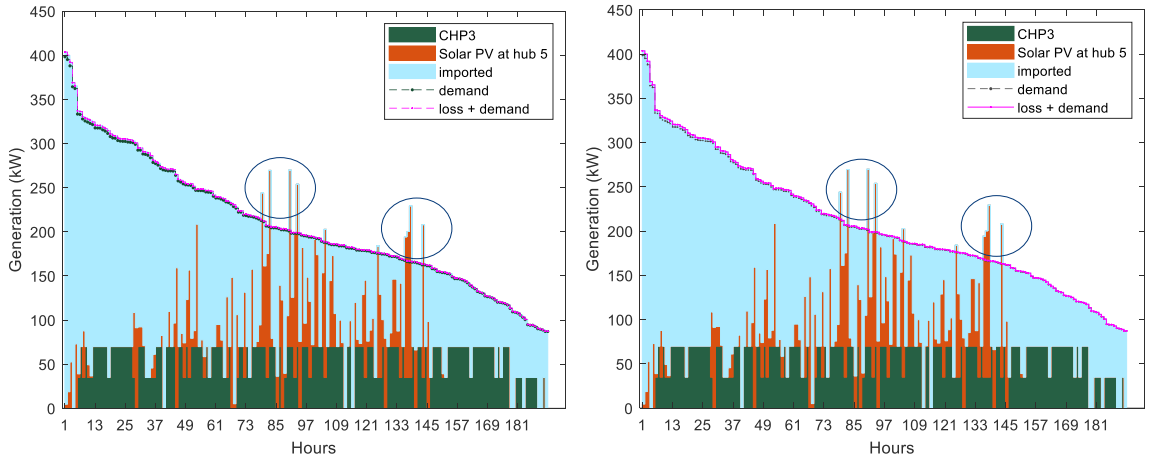

Fig. 5-12. Duration curves of active electricity generation: (a) Scenario I and (b) Scenario II – Case 5-E.

Like the active electricity, the duration curves of reactive power generation for the two scenarios, as shown in Fig. 5-13, are quite the same. As there is no local reactive electricity generation, all the reactive power demands of the connected electric loads, the HPs and the CHP are covered by importing from the neighbourhood. The total reactive power demand of connected electric loads in both scenarios is 16.507 Mvarh. The reactive power consumption by the HPs is 2.431 Mvarh while the consumption by the CHP is 5.472 Mvarh. The reactive power lost in the network is about 290.394 kvarh in Scenario I and 272.877 kvarh in Scenario II. Thus, Scenario II is marginally more efficient than Scenario I from the electricity network point of view.

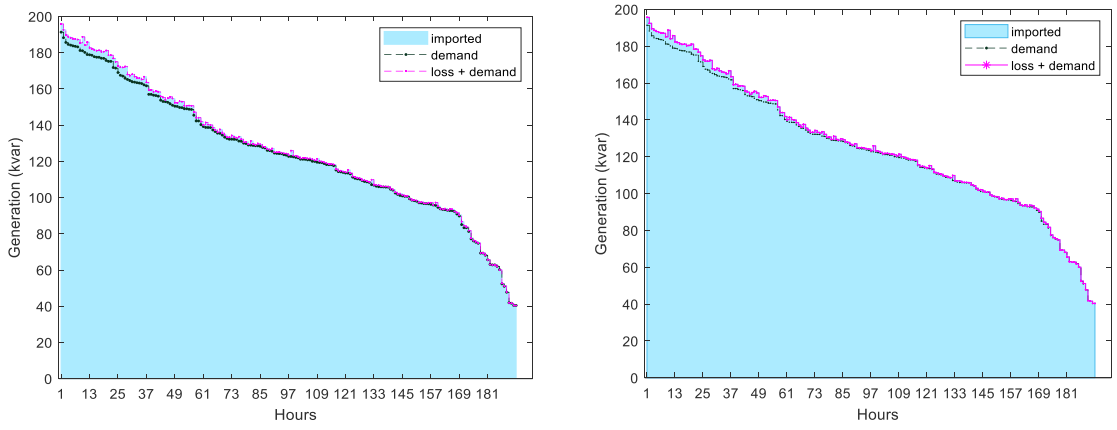

Fig. 5-13. Duration curves of reactive electricity generation: (a) Scenario I and (b) Scenario II – Case 5-E.

To compare the two scenarios in terms of operating cost, the following price data are considered. The waste incineration CHP plant and the solar PV are assumed to have zero operational cost. Energy prices of 0.2 €/kWh of active electricity, 0.1 €/kWh of heat from the neighbourhood and 0.113 €/kWh of gas for the boiler are assumed. The pumping cost to overcome the pressure drops across the pipes is also taken into account. In addition, a selling price while exporting is assumed to be equal to 60% of the buying price.

The hourly operating cost of the two scenarios are plotted in Fig. 5-14. Negative costs in Fig. 5-14 imply a net earning from exporting energy. Although the cost of electricity used for circulation pumps are insignificant (the right axes in Fig. 5-14), the values in Scenario II are higher due to the need for transportation of heat. The total operating cost for the 192 hours is 4,686.4 € for Scenario I and 5,093.6 € for Scenario II (8.7% higher). The corresponding costs of electricity consumed by the circulation pumps are only 0.078 € and 1.101 €, respectively. It shows that installing the HPs near to the heat demand, i.e. Scenario I, is more economical for the given load profiles and energy prices.

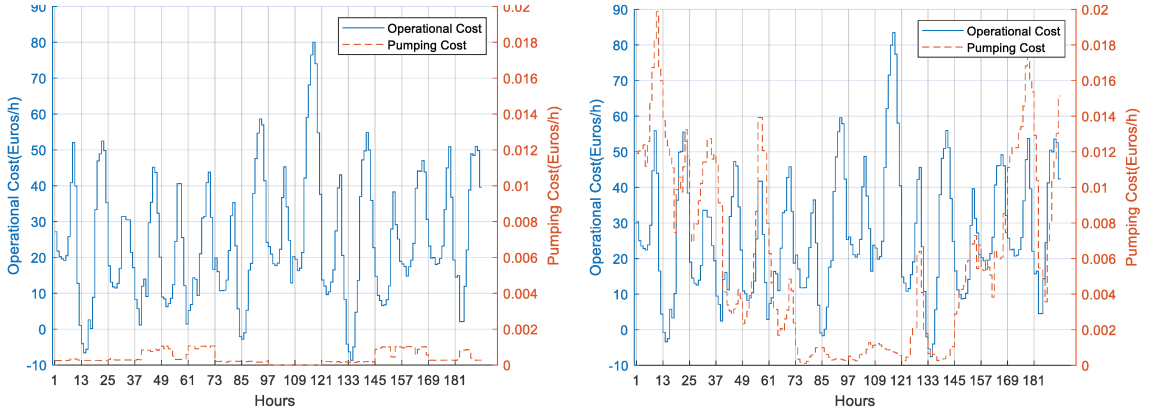

Fig. 5-14. Comparision in terms of pumping cost and total operating cost: (a) Scenario I and (b) Scenario II – Case 5-E.

5.4.3.2. Analysis at hub level

Fig. 5-15 shows the variation of supply temperature, return temperature and mass flow rate at hub 1 for the two scenarios. It can be observed that the supply temperature always remains above or equal to the return temperature. Scenario I is always exporting heat, as indicated by negative nodal mass flows, except for the interval between hours 97 – 120 during which the CHP is shut down. Scenario II, on the other hand, imports heat more often as it is indicated by the positive nodal mass flows. When the network is importing heat, the supply temperature of hub 1 is set to 85 °C (by assumption) while its return temperature is determined by the network. On the other hand, when the network is exporting heat, the supply temperature of hub 1 is determined by the network while its return temperature becomes equal to the soil temperature (by assumption).

Hub-based analysis can also be done for electrical parameters such as voltage magnitude and voltage angle. Fig. 5-16 shows these parameters at hubs 5 and 6 for the two scenarios. The voltage profiles of both scenarios are quite similar, which implies that the electricity distribution network's operational parameters are less affected by the location the HPs when compared to the DHN's operational parameters. This can be again associated with the distribution voltage level.

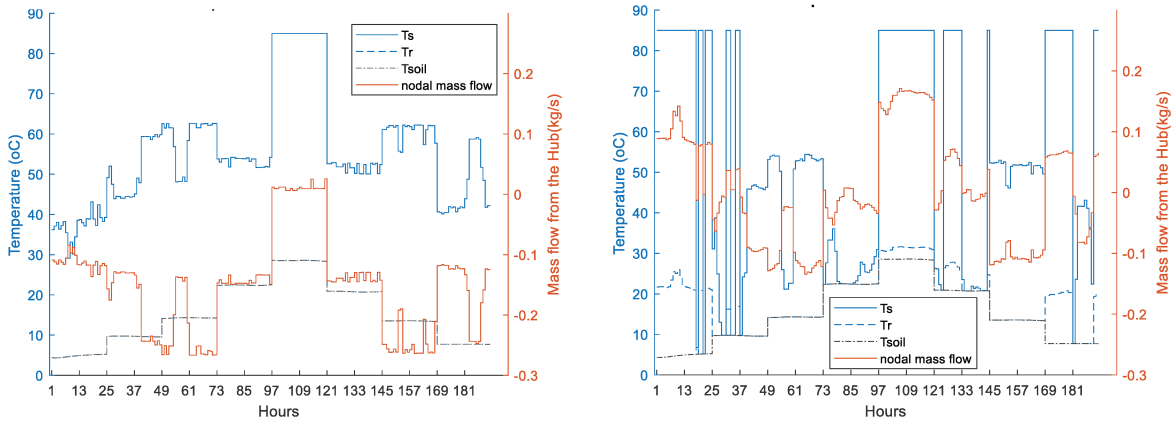

Fig. 5-15. Temperature and mass flow profiles at hub 1: (a) Scenario I and (b) Scenario II – Case 5-E.

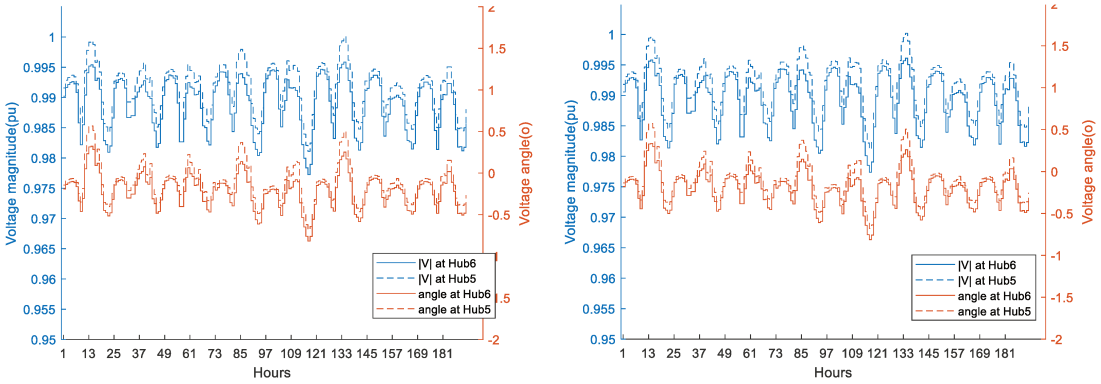

Fig. 5-16. Voltage magnitude and angle at hubs 5 and 6: (a) Scenario I and (b) Scenario II – Case 5-E.

5.4.3.3. Analysis at branch level

Branch-level parameters, such as mass flow rate, inlet and outlet temperature of each pipe, branch power flows, power losses, pressure drops and voltage drops can be studied using the proposed model. As an example, the variation of inlet and outlet water temperatures on the supply and return side of pipe 2-3, is shown in Fig. 5-17.

As the temperature drop is a function of the temperature difference between the water and the soil, there is less temperature drop in the return pipe as compared to the supply pipe. When the mass flow rate is positive, the supply temperature at the end of the pipe near to hub 2 (*Ts-start*) is greater than the other end (*Ts-end*). Whenever the mass flow rate becomes negative, the supply temperature at the end located near to hub 3 (*Ts-end*)) becomes greater than the end point located near to hub 2 (*Ts-start*). The same is true for the return pipe, but opposite of the supply pipe as the water flows in the opposite direction.

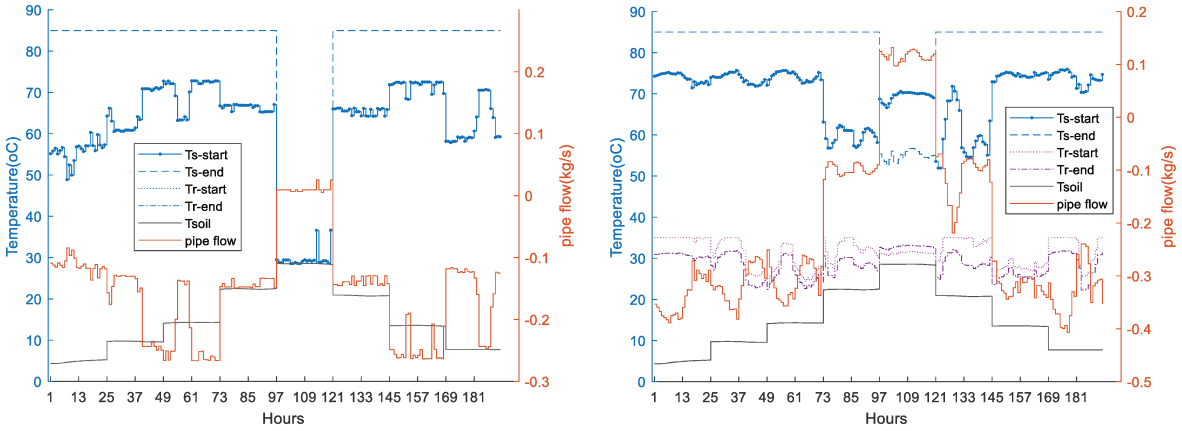

Fig. 5-17. End point water temperatures of pipe 2-3: (a) Scenario I and (b) Scenario II – Case 5-E.

The return temperatures at both ends of the pipe 2-3 are overlapped with the soil temperature in Scenario I (Fig. 5-17(a)). This is due to the way HP2 is scheduled. HP2 is always producing heat that is sufficient only to supply the heat demand in hub 2. As a result, there is a nearly zero mass flow between hub 2 and the network. It means that all the mass flow on the return side of pipe 2-3 is coming from the slack hub return flow, which is at a temperature equal to the soil temperature. This can also be confirmed from the similarity of the flows shown in Fig. 5-15(a) and Fig. 5-17(a). This is not the case in Scenario II as the heat demand at hub 2 is supplied through the network. Hence, the return flow in pipe 2-3 is a combination of the return flow from hub 2 and the return flow from the slack hub (during exporting).

During the hours 97 – 120, the CHP is turned off. During this period, the pipe flow in Scenario I is nearly zero. As a result, the end water temperatures on both supply and return sides of the pipe get closer to the soil temperature. The pipe flow in Scenario II, on the other hand, is above 0.1 kg/s. As a result, the inlet and outlet water temperatures are higher than the soil temperature but lower than the pre-set limits, 85 °C for supply and 35 °C for return, as shown in Fig. 5-17(b).

5.5. Summary

This chapter demonstrated the flexibility of the integrated load flow model developed in the previous chapter. The model is tested with meshed and radial topologies of highly coupled electricity and heating networks consisting of CHPs, solar PV, HOB and HPs. The results found are consistent with the theory. It is also shown that the proposed model is more accurate and realistic in comparison with a methodology followed in [95]. The capacity of the model in capturing all the important operating parameters of both heating and electricity distribution networks is demonstrated.

Any possible changes of mass flow direction are automatically handled in the algorithm. Its scalability in integrating various distributed generations is also illustrated. Varieties of coupling technologies can also be integrated into the model through the coupling matrices.

A comparison between radial and meshed networks revealed the possibility of higher distribution losses in the latter case. On the other hand, the pseudo-dynamic simulation case study shows that sizing the generation capacities of coupling technologies based on one type of demand profile could lead to undersized or oversized generation for the other network. The results also showed that the distribution losses and the total operating cost vary depending on the location of heat pumps.

The following chapter illustrates how an optimisation routine can be combined with the integrated load flow model to determine optimal placement of coupling technologies and their economic dispatch.

6. Optimal Placement of Coupling Technologies

The load flow case studies presented in the previous chapter merely determine the operating parameters of the distribution networks for a set of demand and generation profiles. Neither an economic dispatch of the energy technologies nor any nodal and branch constraints are considered. For the distribution networks to function properly, their operating parameters should be within their permissible range. This chapter presents how economic dispatch of generation plants including coupling technologies can be achieved without violating the constraints in the heating and electricity distribution networks. Such analysis is referred to as an integrated optimal power flow.

In the next sections, optimal placement of coupling technologies is discussed first. As the governing equations are dependent on the location of the coupling technologies, flexible load flow model is required which can automatically configure itself while searching for the best location of the coupling technologies. The novel contribution of the proposed methodology in overcoming that challenge is illustrated. It is then followed by integrated optimal power flow application in reducing meshed topology and finding optimal temperature profiles of a heating network.

6.1. Metaheuristic algorithms for optimising MESs

As the load flow model of a multi-carrier distribution network is very complex and highly nonlinear, it is cumbersome to optimise it using conventional deterministic approaches. Heuristic/metaheuristic optimisation techniques are more suitable to handle such highly nonlinear objective functions and constraints. They are also getting wider applications due to the advancements in computers. Genetic Algorithm [124–127], Teaching Learning Based Algorithms [128, 129], Honey Bee Mating Algorithms [130] and Particle Swarm Optimisation (PSO) [131, 132] are some of them which are commonly used in the energy fields. Finding the best place for distributed generations (DGs) is one area where such algorithms can be applied. Both the size and location of the DG influence the power loss and operational parameters of the distribution network. Optimal placement of a DG, usually near to the load centre, helps to decrease distribution losses [126].

As analytical methods may not be appropriate to optimally place multiple DGs, Kansal et al. [131] proposed a hybrid of PSO and analytical algorithms. The PSO is used to find the optimal location of DGs, which is followed by the analytical method to determine their optimal sizes. Yammani et al. [126], on the other hand, used a variety of genetic algorithm to optimally place and size DGs in the electricity network. Pazouki et al. [127] also used genetic algorithm to find out the optimal place and size of a CHP plant in a MES consisting of gas, heat and electricity energy carriers. Heat demands are assumed to be supplied locally

either from a CHP or from a gas boiler. In all of the papers, minimization of losses in the electricity network is considered as a main objective function even for DGs that produce both heat and electricity.

Unlike the DGs in the electricity network, the optimal placement of DGs in the heating network is not studied very well. Marguerite et al. [133] used linear programming to study the optimal dispatch of multi-source DHN while Vesterlund et al. [134] used an evolutionary mixed integer linear programing for thermo-economical optimisation of a multi-source DHN. Neither the optimal placement nor the coupling with the electricity network are considered in their study.

A HP can be taken as a DG for the heating network while it is a distributed load in the electricity network. Thus, the HP will be economical if it is installed near to the electricity generation and near to the thermal load at the same time. However, the electricity generation and the thermal load centre are usually far apart. In that case, both of the electricity and the heating networks should be duly considered to find the optimal placement of the HP. A PSO-based algorithm is developed to handle such applications by taking the flexibility and modularity advantages of the integrated load flow model discussed in the previous chapters.

PSO is first proposed in [135], and is a widely used metaheuristic optimisation algorithm which applies the intelligence of stochastic population of particles to arrive at a global best value [136]. It tries to find the global best value in analogy to the way a flock of birds scatter and regroup. The whole group is referred to as a population (swarm) and its individual members are called particles. For a problem with M decision variables, the position of each particle is defined by a vector with M-dimensions, as shown in equation (6-1). The new direction and speed of the particle (v_{i-new}) is calculated using equation (6-2) which is then applied in equation (6-3) to find the new position of the particle (x_{i-new}).

$$x_i = (x_{i1}, x_{i2}, \dots, x_{iM}) \tag{6-1}$$

$$v_{i-new} = \omega v_{io} + c_1 r_1 (x_{i-best} - x_i) + c_2 r_2 \left(x_{g-best} - x_i\right) \tag{6-2}$$

$$x_{i-new} = x_i + v_{i-new} \tag{6-3}$$

where ω is the inertia/damping factor; v_{io} is the current velocity of particle i; c_1 is a self-accelerating (exploration) factor; c_2 is a global accelerating (exploitation) factor; x_i is the current position of particle i; x_{i-best} is the best position of the particle in the past; x_{g-best} is the global best position achieved so far; r_1 and r_2 are random numbers between 0 and 1.

The maximum iteration and number of particles in a PSO algorithm depend on the nature of the problem, the number of decision variables and the parameters of the PSO itself. Ullmann et al. [137] suggested fixed values of personal and global acceleration factors ($c_1 = c_2 = 1.494$) while Aote et al. [138] argued that better results can be found using a step-by-step variation in the following order: $c_1$decreasing from 2.5 to 0.5 and c_2 increasing from 0.5 to 2.5. The logic behind such variations is to explore locally in the first iterations and then fine-tune the global best towards the last iterations. Both approaches are tested for the problem at

hand and the latter is found to give faster convergence. The value of ω is also made to vary from 0.9 to 0.4 [138]. To allow each particle explore its region progressively, the velocity vector is kept within ± 20% of its maximum range.

6.2. Objective function and constraints

The general objective function of the integrated optimal power flow is minimization of the total operating cost of the MES. It can be expressed using equation (6-4). The operating cost is the sum of all costs of local generations and imports in both networks including fuels consumed by the coupling devices. It also includes the consumption of circulation pumps.

$$\begin{aligned} \mathcal{F} &= min(Operating\ cost) \\ &= min\left(\sum_{hubs} C_{Phg} + \sum_{hubs} C_{Pelg} + \sum_{hubs} C_{Pfg} \pm C_{Ph(1)} \pm C_{Pel(1)}\right) \end{aligned} \tag{6-4}$$

where C_{Phg} and C_{Pelg} are the costs of heat and electricity locally generated while C_{Pfg} is the cost of fuel consumed at each hub. The terms, $\pm C_{Ph(1)}$ and $\pm C_{Pel(1)}$ refers to the cost of heat and electricity imported (positive) or exported (negative) at the slack hub, respectively.

Generally, the total electricity consumption of the circulation pumps is very small when compared to the total electrical demand in the system. Hence, their impact on the operational parameters of the electricity network is neglected. However, in a thermo-economic optimisation, when supply temperatures are reduced to minimize the heat distribution loss, the mass flow rate circulating in the network rises. Correspondingly, the electricity consumed by the circulation pumps increases and its cost may become competing factor in the thermo-economic optimisation (especially if there are very cheap heat sources relative to the electricity). Hence, it is important to consider the pumping cost as part of the imported electricity at the slack hub.

The circulation pumps serve two purposes. The first is to overcome the frictional and local pressure losses in the heating network while the second is to guarantee the minimum pressure difference required between the supply and the return pipes on the primary side of a remote consumer substation. The corresponding electricity consumptions are calculated using equation (6-5) (first and second terms on the right hand side, respectively).

$$\begin{aligned} P_{el(pumping)} = (1 + C_{loc}) * & \sum_{p \in all\ pipes} \frac{g * \left|\Delta H_p * \dot{m}_p\right|}{\eta} \\ + & \sum_{c \in consumers} \left(\frac{g * \Delta H_c}{\eta} |\dot{m}_c|\right) \end{aligned} \tag{6-5}$$

where $P_{el(pumping)}$ is active electric power consumed by circulation pumps; g is gravitational acceleration; ΔH_p is the frictional head loss on the pipe p (assuming straight pipe); $\left|\dot{m}_p\right|$ is the magnitude of the mass flowrate in the pipe; η is efficiency of the circulation pump (it is

assumed to be 80%); C_{loc} is a fraction to take the local pressure losses due to valves and junctions into account; ΔH_c is the hydraulic head difference at the consumer substation in meter while $|\dot{m}_c|$ is the magnitude of mass flow rate on the primary side of the substation. In this and the next chapters, the values of C_{loc} and ΔH_c are assumed to be 0.3 and 5.1 m ($\approx 50\ kPa$), respectively [139].

There are both equality and inequality constraints that should not be violated while achieving the objective function. The integrated load flow model discussed in *Section 4.5* defines the equality constraints. The inequality constraints, on the other hand, include the voltage limit at each bus (equation (6-6)), the limit on line current (equation (6-7)), maximum allowed mass flow in each pipe (equation (6-8)), the limit on the supply temperature of heat source hubs (equation (6-9)) and the limit on the return temperature at heat consuming hubs (equation (6-10)). The temperature limits depend on the characteristics of heat sources, the temperature levels required at the secondary side of heat consumers and the regulations of the municipality, such as Legeionellosis issues [119].

$$V_{min} \leq |V_k| \leq V_{max} \tag{6-6}$$

$$0 \leq \left|I_{ij(rms)}\right| \leq I_{max} \tag{6-7}$$

$$0 \leq \left|\dot{m}_{ij}\right| \leq \dot{m}_{max} \tag{6-8}$$

$$T_{s(min)} \leq T_{s(k)} \leq T_{s(max)}, \textit{ for net-heat-source hubs} \tag{6-9}$$

$$T_{r(min)} \leq T_{r(k)} \leq T_{r(max)}, \textit{ for net-heat-consuming hubs} \tag{6-10}$$

6.3. Optimal placement and sizing of coupling technologies – Cases 6-A and 6-B

6.3.1. Nested PSO

A two layer nested PSO is implemented to determine optimal location and sizes of the coupling technologies. Multiple HPs and a HOB are considered in a coupled electricity and heating networks for illustration. The outer PSO is dedicated for optimal placement while the inner PSO determines the economical dispatch (optimal power flow) for the given location of the energy technologies.

The flow chart of the nested PSO is shown in Fig. 6-1, and it is described below.

i. The network topology, together with the details of pipe and transmission line parameters, is used as input. In addition, data about the demand, generation and coupling technologies together with their generation price and capacity constraints are also fed into the model.

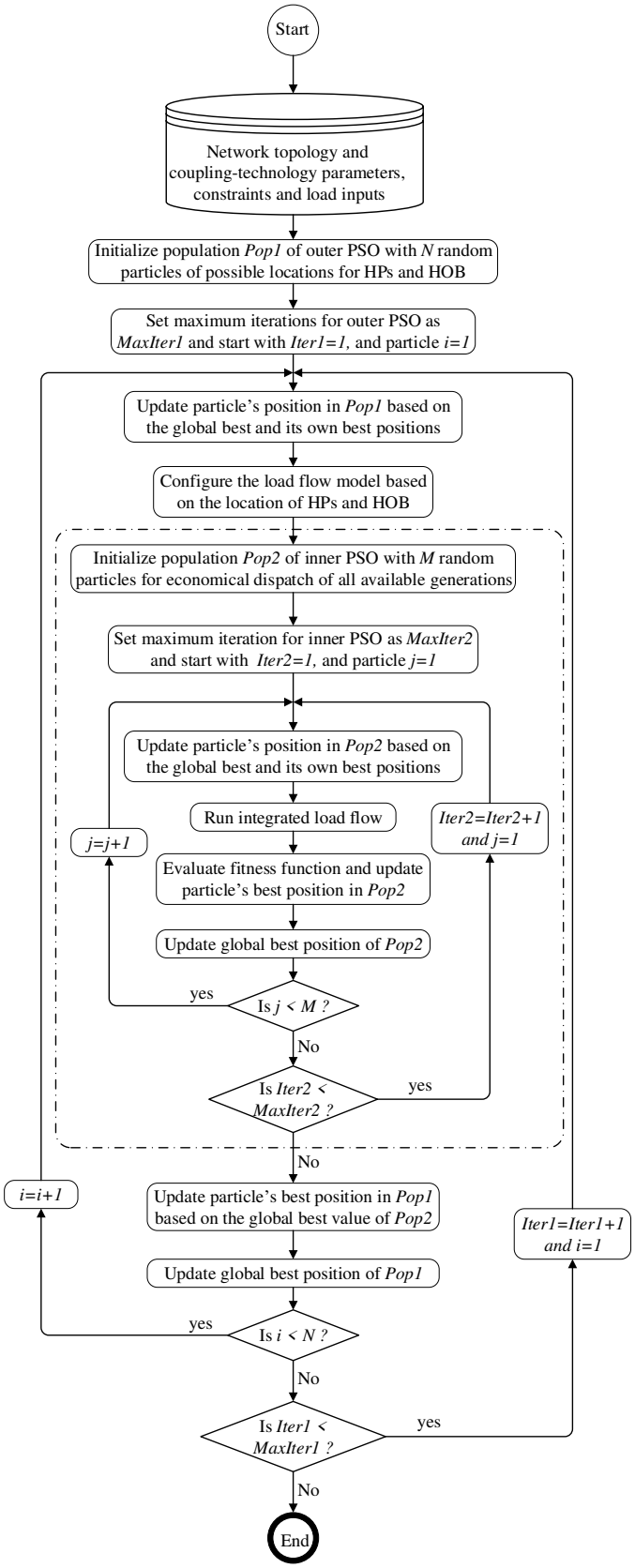

Fig. 6-1. Flow chart of the nested PSO applied for optimal placement and sizing of HPs and a HOB – Cases 6-A and 6-B.

ii. Random population of *N* particles is generated in the outer PSO each of them containing whole numbers corresponding to the hubs where the HPs and HOB are located. Placement of multiple units at the same hub is possible.

iii. The position of each particle in the outer PSO is updated according to equation (6-3).

iv. The equations of the integrated load flow model are configured according to the location of the HPs and the HOB.

v. The inner PSO, shown within the broken rectangle in Fig. 6-1, is used to evaluate the fitness of each particle from the outer PSO loop. A random population of *M* particles is generated in the inner PSO to find out the best operational sizes of the HPs and HOB together with other generations that have fixed locations (i.e. integrated optimal power flow).

vi. The position of each particle in the inner PSO are updated according to equation (6-3).

vii. Integrated load flow is then computed for each particle in the inner PSO loop which is followed by fitness evaluation using equation (6-4).

viii. The fitness values are compared with the particle's best fitness and the global best fitness values in the inner PSO. Accordingly, the particle's best position and the global best position are updated.

ix. Steps (vi)-(viii) are computed for each of the *M* particles in the inner PSO.

x. If the pre-set maximum iteration of the inner PSO (*MaxIter2*) is not reached, step (ix) is repeated.

xi. The global best fitness value returned from the inner PSO loop is used as the particle's fitness value in the outer PSO loop.

xii. This value is used to update the particle's best and the global best positions in the outer PSO.

xiii. Steps (iii)-(xii) are computed for each of the *N* particles in the outer PSO.

xiv. If the pre-set maximum iteration of the outer PSO (*MaxIter1*) is not reached, step (xiii) is repeated.

xv. The best location of the HPs and HOB is contained in the global best position of the outer PSO while their economical dispatch is contained in the corresponding global best position of the inner PSO.

In both of the PSO loops, the global best value is updated after evaluating each particle's fitness and the latest global best value is used to update the position of the next particle. However, if parallel computing is used, the global best value need to be updated after the fitness of all particles are evaluated.

6.3.2. Description of case studies and common input data

Two case studies (Case 6-A and Case 6-B) are considered for demonstration. A waste to energy CHP and HPs couple the electricity and heating networks. In addition, solar PV and wind power plants are considered as DGs. HOB is also considered as a competitive technology. The optimal placement of the HPs depends on the availability of the electricity and the location of the thermal load. In order to make the optimisation problem more challenging, the sources of electricity are assumed to be installed at hubs where there is no thermal demand. In addition, the following single-hour assumptions are made for both case studies.

- The installation of solar PV panels, wind turbines and waste to energy CHP plants are site specific and it is difficult to relocate them. Their locations are assumed to be fixed at certain hubs.

- Hub 1 is considered as a slack hub at which any import/export from/to the neighbourhood network takes place. The prices of electricity and heat coming from the neighbourhood are assumed to be 0.2 €/kWh and 0.1 €/kWh, respectively. A power purchase agreement of 0.12 €/kWh for active electric power is considered. As such practical agreement is not yet fully developed for heating networks, it is neglected (i.e. 0.0 €/kWh).

- A reactive power penalty of 0.02 €/kvarh is considered for the imported reactive electric power at the slack hub in excess of 48.5% (corresponding to a 0.9 lagging power factor) of the imported active electric power.

- The price of gas used in the HOB is taken to be 0.113 €/kWh. The HOB thermal efficiency is 90%.

- The operating cost of solar PV and wind power plant are assumed to be negligible.

- A typical municipal solid waste has a lower heating value of 11 MJ/kg [114]. Profitability of waste-to-energy plants highly depends on the gate fee, which varies from country to country between 10 $/ton to 100 $/ton [140]. A waste-to-energy CHP plant (with an internal combustion engine) that has an electrical efficiency of 31% and thermal efficiency of 57% is assumed [114] at a 0.9 lagging power factor. Operating cost of the waste-to-energy CHP plant is assumed to be -0.016 €/kWh which corresponds to a gate fee of 50 €/ton of waste with an average heating value of 11 MJ/kg.

- All the HPs are assumed to run at a COP of 4.0 and a lagging power factor of 0.9.
- The electricity network is assumed to be balanced three phase system. All transmission lines are assumed to be three phase ACSR Waxwing type with resistance, reactance, susceptance and ampacity of 0.262 Ω/km, 0.386 Ω/km, 4.31 μS/km and 480 A, respectively [141]. Double conductors are used between hubs 1 and 2. The limit on nodal voltages is set to be within the range 0.9 – 1.1 pu.
- All pipes in the DHN are of DN-100 type with standard insulation layer. The parameters (carrier pipe thickness and outer diameter of 3.6 mm and 114.3 mm, and outer jacket thickness and outer diameter of 3.2 mm and of 200 mm, respectively) are taken from isoplus® [118]. The maximum allowed flow rate for all pipes is 9.3 kg/s. Thermal conductivity of the carrier pipe, outer jacket and insulation material are 40 W/mK, 0.4 W/mK and 0.027 W/mK, respectively. Surface roughness of the carrier pipe is assumed to be 0.05 mm.
- Temperature optimisation is not considered in these two case studies. Hence, all heat-source hubs have supply temperatures of 70 ℃ and all hubs acting as heat consumers have return temperatures of 50 ℃ (on the network side). A uniform soil temperature of 4.36 ℃ is assumed around the supply and return pipes of the DHN.
- Both residential and commercial demands are considered. Peak demand of one/two residential buildings and a small hotel located in Idaho, USA are taken as a reference from an Open Energy Information database [122]. An electrical power factor of 0.95 and 0.9 lagging is assumed for residential and commercial demands, respectively.

The first case study deals with a small part of a distribution network in a densely populated area while the second case study deals with a sparsely populated area connected with a relatively larger network size.

6.3.3. Scenarios

Two scenarios are considered for both case studies. In the first scenario, the optimisation is conducted only from the heating network point of view. Hence, the costs due to the electricity distribution loss and any constraints in that network are neglected. The second scenario, on the other hand, considers both networks in the integrated optimisation. Accordingly the objective function defined in equation (6-4) is modified as shown in equation (6-11) with $\alpha=1$ for Scenario I and $\alpha=0$ for Scenario II).

$$\mathcal{F} = min\{(Operating\ Cost) - \alpha(Cost\ of\ electricity\ distribution\ loss)\} \quad (6\text{-}11)$$

6.3.4. Specific inputs, results and discussions on Case 6-A

6.3.4.1. Specific input data for Case 6-A

Fig. 6-2 describes the single line diagram of the first case. The CHP with a maximum of 200 kW waste intake capacity is installed at hub 3. A solar PV with 50 kW output is connected at hub 5. The electricity distribution network is at 0.4 kV. Two heat pumps, each of which are rated at 25 kWe, and a HOB that can take up to 30 kW of gas are considered in the optimisation. A swarm of 5 particles with 15 iterations is considered in the outer PSO while a swarm with 10 particles and 70 iterations is used in the inner PSO. The load distributions for this case study are summarized in Table 6-1.

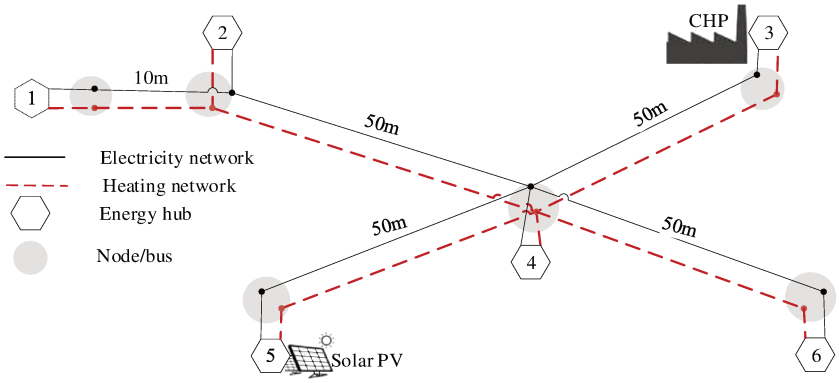

Fig. 6-2. One-line diagram of the heating and electricity network considered in Case 6-A.

Table 6-1: Load distribution for Case 6-A.

	Hub 1	Hub 2	Hub 3	Hub 4	Hub 5	Hub 6	Total
Active electric power demand (kW)	0	67.1	0	134.21	0	199.5	400.81
Reactive electric power demand (kvar)	0	22.08	0	44.16	0	96.56	162.8
Heat demand (kW)	0	77.09	0	154.19	0	54.64	285.92

6.3.4.2. Results and discussions on Case 6-A

The optimal locations and sizes of the two HPs and the HOB together with the resulting distribution losses and power imports are summarized in Table 6-2. The optimal location of the HPs in Scenario I are found to be at hubs 2 and 6. Although the highest heat demand is at hub 4 (see Table 6-1), HPs are not placed at this hub as it gets cheap heat from CHP3, which has no connection other than hub 4. As a result, the HPs are placed closer to the other heat loads. In scenario II, on the other hand, both HPs are placed at hub 2. Neither hub 3 nor hub 5 are selected, though thy have cheap electricity sources. This is associated with the fact that hub 2, which has heat demand, is located near to the slack hub through which the larger proportion of the active power is imported (see Table 6-2). In both scenarios, the CHP and solar PV are dispatched at their maximum output while no HOB is selected. Importing heat is also found to be expensive relative to the heat from HPs.

Table 6-2: Optimal location and dispatches of the HPs and the HOB for Case 6-A.

Scenarios	Energy carrier	HPs		HOB	CHP	PV	Imported	Loss
I	Location (hub numbers)	2	6	4	3	5	1	total
	Active electricity (kW)	19.45	24.67	0.00	62.00	50.00	350.38	17.45
	Reactive electricity (kvar)	-9.42	-11.95	0.00	-30.03	0.00	239.90	25.71
	Heat (kW)	77.80	98.68	0.00	114.00	0.00	0.00	4.58
II	Location (hub numbers)	2	2	6	3	5	1	total
	Active electricity (kW)	25.00	19.33	0.00	62.00	50.00	347.52	14.37
	Reactive electricity (kvar)	-12.11	-9.36	0.00	-30.03	0.00	235.47	21.17
	Heat (kW)	100.00	77.32	0.00	114.00	0.00	0.00	5.38

The results for both scenarios shows that the optimal placement of HPs is not aligned with the active electricity generation (hubs 1, 3 and 5). They are placed rather at some of the hubs where there is heat demand. In scenario I, 54.6% of the 290.5 kW heat produced and 100 % of the 462.38 kW active power generated are transported in their corresponding distribution networks. In the case of scenario II, however, 73.55% of the 291.3 kW heat and 100% of 459.52 kW active power are delivered through the distribution networks. As a result, scenario I has lower heat loss (1.6% of the heat demand) than Scenario II (1.9% of the heat demand). The active electric power loss, on the other hand, is higher (3.9% of the demand including HPs' consumption) for Scenario I than Scenario II (3.2% of the demand including HPs' consumption).

The pumping power required for circulation in Scenarios I and II are 0.12 kW and 0.16 kW respectively, which are negligible relative to the total electricity demand. It is also found that only 0.05% and 0.07% of this pumping energy is used to overcome the friction and local pressure losses in the network, respectively, while the remaining is used to keep the pressure difference at the consumer substations. The costs of pumping energy for Scenarios I and II are 0.024 €/h and 0.032 €/h, which are less significant relative to the corresponding cost of heat loss (0.46 €/h and 0.54 €/h respectively). This is in agreement with the findings of [134] but in disagreement with the findings of [139]. The possible reasons could be the difference in the pipe parameters (diameter, length etc.) and operational strategies. The operating cost of the whole network is 68.3 €/h in Scenario I. This value is reduced to 67.68 €/h in Scenario II which shows nearly 1% saving.

Fig. 6-3 depicts the temperature and mass flow profiles at different hubs. A positive mass flow implies that the hub is acting as a source of heat. Hub 6, for example, is acting as a source in Scenario I and as a consumer in Scenario II. When the mass flow from the hub is closer to zero, the water gets more time to lose its heat and, as a results, its temperature gets closer to the soil temperature (for example the return temperature at hub 2 in Scenario I). If the mass flow is zero, as it is the case for hub 5 in both scenarios, the steady state temperature of water on both of the return and supply pipes becomes equal to the soil temperature.

The pipe mass flows on the supply pipe network of the DHN are shown in Fig. 6-4. All the flows are within the acceptable range of 9.3 kg/s defined in *Section 6.3.2*. Negative flow for Pipe 4-6 implies that the flow is opposite to the positive flow direction initially assumed (which was from hub 4 to hub 6).

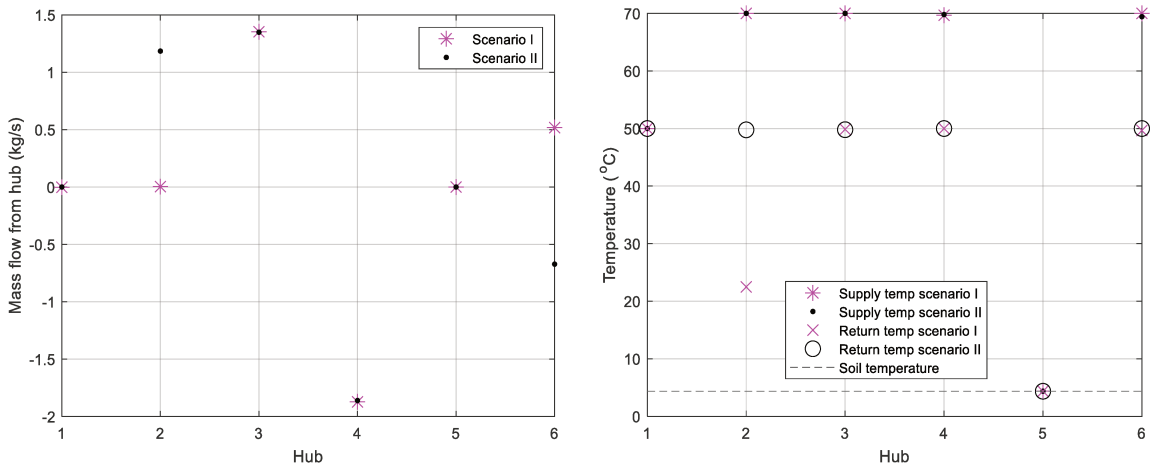

(a) (b)

Fig. 6-3. (a) The mass flow injected into the network from each hub and (b) the corresponding supply and return temperatures for the two scenarios of Case 6-A.

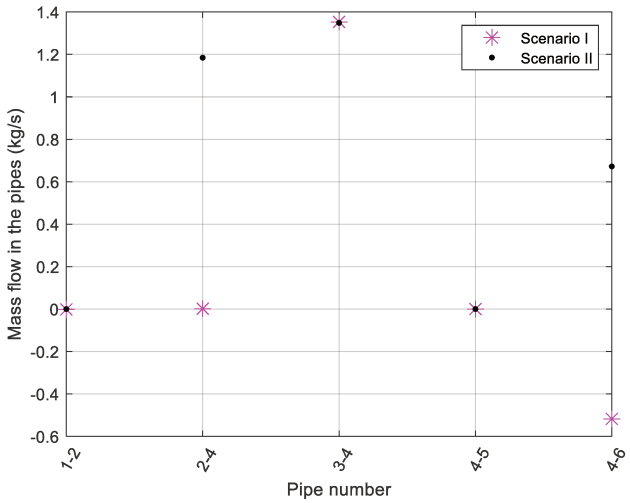

Fig. 6-4. Mass flow in the pipes for two scenarios of Case 6-A.

The voltage magnitude profiles, as shown in Fig. 6-5(a), are within the limits defined in *Section 6.3.2*. Scenario II has a relatively better voltage profile. The root mean square current through each transmission line are illustrated in Fig. 6-5(b). It looks that the current in Line1-2 is above the acceptable limit of 480 A. But, since double conductors are assumed for each phase, the current in each conductor is still in the acceptable range. It also shows that the current in Line 2-4 in Scenario I is 484.5 A which is slightly higher than the acceptable limit. It means that optimising HPs without the consideration of electricity network constraints (as is the case for Scenario I) could lead to overloading of the electrical distribution network. The current through line 2-4 in Scenario II is not far from the limit of 480A (ACSR Waxwing type). For better security and reliability of the system, the voltage level of the distribution grid needs to be upgraded or any reinforcement mechanism should be applied.

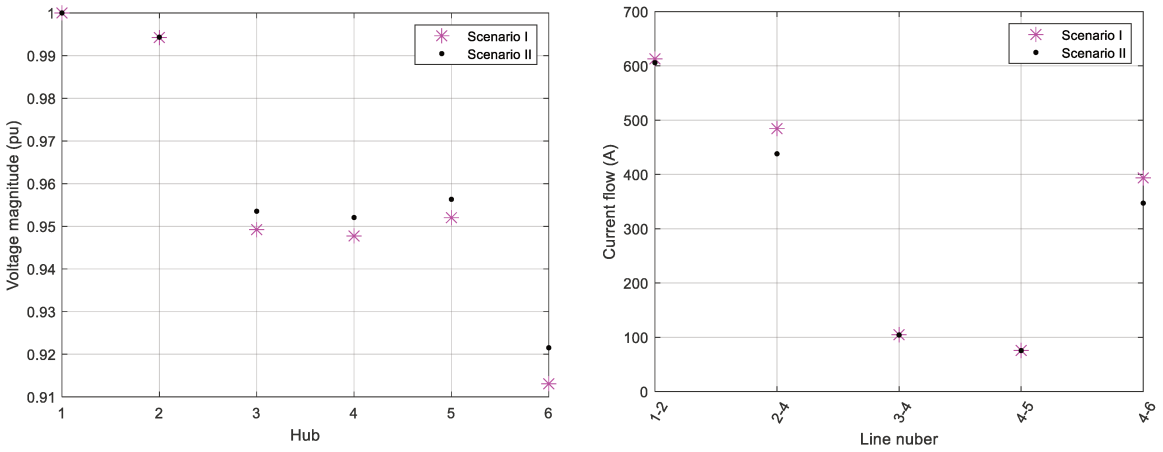

(a) (b)

Fig. 6-5. (a) Voltage magnitudes at different hubs and (b) phase currents through the transmission lines for the two scenarios of Case 6-A.

6.3.5. Specific inputs, results and discussions on Case 6-B

6.3.5.1. Specific input data for Case 6-B

A one-line diagram describing the layout of the second case study is shown in Fig. 6-6. The load distributions are summarized in Table 6-3. A CHP is installed at hub 2 and its maximum waste intake capacity is 3 MW. A wind power plant with 1 MW active electrical output is connected at hub 26.

The electricity distribution network is at 4.16 kV except for part of the network after buses 7, 19 and 27, which is at 0.4 kV. Step down transformers (4.16 kV/0.4 kV) with 0.9 – 1.1 pu tap setting are installed near to the buses 7, 19 and 27, as shown in Fig. 6-6. The tap settings are set to 0.9 to improve the voltage profile in the 0.4 kV distribution network.

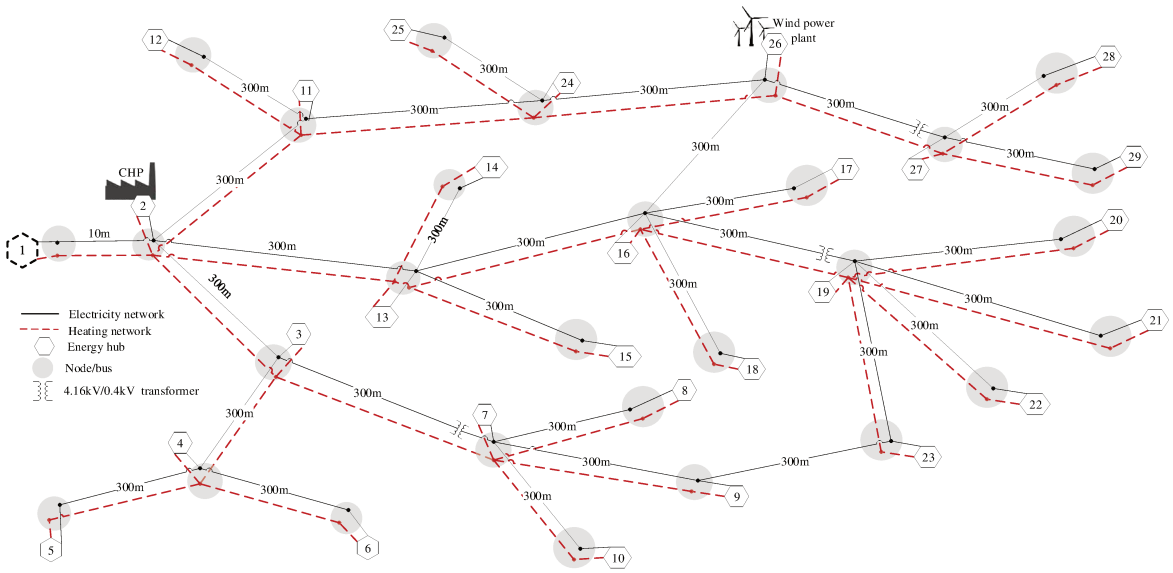

Fig. 6-6. One-line diagram of a 29 hub coupled heating and electricity network considered for Case 6-B.

Table 6-3: Load distribution for Case 6-B.

	Hub 1	Hub 2	Hub 3	Hub 4	Hub 5	Hub 6	Hub 7	Hub 8	Hub 9	Hub 10
Active electric power demand (kW)	0	0	134.21	134.21	134.21	134.21	0	134.21	134.21	134.21
Reactive electric power demand (kvar)	0	0	44.16	44.16	44.16	44.16	0	44.16	44.16	44.16
Heat demand (kW)	0	0	154.18	154.18	154.18	154.18	0	154.18	154.18	154.18
	Hub 11	Hub 12	Hub 13	Hub 14	Hub 15	Hub 16	Hub 17	Hub 18	Hub 19	Hub 20
Active electric power demand (kW)	134.21	134.21	0	199.5	199.5	199.5	199.5	199.5	0	134.21
Reactive electric power demand (kvar)	44.16	44.16	0	96.56	96.56	96.56	96.56	96.56	0	44.16
Heat demand (kW)	154.18	154.18	0	54.64	54.64	54.64	54.64	54.64	0	154.18
	Hub 21	Hub 22	Hub 23	Hub 24	Hub 25	Hub 26	Hub 27	Hub 28	Hub 29	Total
Active electric power demand (kW)	134.21	134.21	134.21	134.21	134.21	0	199.5	134.21	134.21	**3478.6**
Reactive electric power demand (kvar)	44.16	44.16	44.16	44.16	44.16	0	96.56	44.16	44.16	**1330.1**
Heat demand (kW)	154.18	154.18	154.18	154.18	154.18	0	54.64	154.18	154.18	**2948.9**

Four HPs, each of which are rated at 100 kW_e, and a HOB that can take up to 100 kW of gas are considered in the optimisation. A swarm of 10 particles with 30 iterations is considered in the outer PSO, while a swarm with 15 particles and 70 iterations is used in the inner PSO.

6.3.5.2. Results and discussions on Case 6-B

Table 6-4 presents the optimal location and operational sizes of the HPs and the HOB for the two scenarios. It also shows that the full capacity of the CHP and the wind power plants are selected in both scenarios. The remaining electricity is imported from the neighborhood grid while the heat deficit is covered using HPs. Similar to Case 6-A, the HOB and the neighborhood DHN are avoided. In addition, the hubs with electricity generation (hubs 1, 2 and 26) are not selected for optimal placement of the HPs. This is again due to the absence of thermal loads at those hubs. In Scenario I, 53.03% of the total 3.22 MW heat and 100% of the 4.06 MW active power is transported in the electricity network. In the case of Scenario II, however, 93.55% of the total 3.23 MW heat and 100% of the total 3.98 MW active power are distributed in the corresponding networks.

Table 6-4: Optimal location and dispatches of the HP and the HOB for Case 6-B.

Scenarios	Energy carrier	HPs				HOB	CHP	Wind	Imported	Loss
I	Location (hub numbers)	8	23	25	29	14	2	26	1	total
	Active electricity (kW)	91.28	94.55	94.77	97.74	0.00	930.0	1000	2134.7	207.83
	Reactive electricity (kvar)	-44.2	-45.79	-45.90	-47.34	0.00	-450.42	0.00	2275.4	311.7
	Heat (kW)	365.1	378.2	379.1	390.96	0.00	1710.0	0.00	-0.06	275.8
II	Location (hub numbers)	7	7	11	16	23	2	26	1	total
	Active electricity (kW)	100.0	100.0	87.10	94.04	0.00	930.00	1000	2052.2	122.49
	Reactive electricity (kvar)	-48.4	-48.43	-42.18	-45.55	0.00	-450.42	0.00	2052.8	184.54
	Heat (kW)	400.0	400.0	348.4	376.2	0.00	1710.0	0.00	0.0	285.62

The heat loss in the distribution network for Scenarios I and II are 9.35% and 9.69% of the heat demand, while the active electricity losses are 5.39% and 3.17% of the electricity consumption, respectively. Compared with Case 6-A, the losses are higher which is partly due to longer branches and larger percentage of power flows in the networks.

Table 6-4 also shows that, although the increase in the heat loss from scenario I to II is not significant, the reduction in the electricity loss is tremendous, which is 41.2%. This can be explained by considering the way HPs are installed. In Scenario I, the HPs are placed at the farthest nodes relative to the CHP plant. Nodes 8, 23 and 29 belong to the 0.4 kV distribution network while node 25 belongs to the 4.16 kV distribution network. On the other hand, all of the four HPs are installed inside or very close to the 4.16 kV network in Scenario II. The current drown by the HPs at each of the 0.4 kV nodes is equal to the amount of current they could draw at 4.16 kV multiplied by the transformer ratio (10.4 times in this case). The higher the current flowing, the more the losses it causes in the distribution networks for the same transmission line parameters.

The pumping power required for circulation in Scenarios I and II are 3.79 kW and 5.3 kW respectively, which are again negligible relative to the total electricity demand. Unlike to Case 6-A, about 50.73% and 59.06% of this pumping energy are used to overcome the friction and local pressure losses in the network, respectively, both of which are significant. However, the costs of the pumping energy are still insignificant when they are compared to the cost of heat lost (2.74% and 3.71% considering the importing prices of heat and electricity). The system operating cost is 404.5 €/h for Scenario I while it is 384.65 €/h for Scenario II which shows a reduction of about 5%. It means that a relatively larger saving can be achieved for larger networks by applying an integrated optimisation rather than considering the heating network alone.

It is important to note that nodes 9 and 10 are as optimal as node 8 to place a HP due to the symmetry in the network dimensions and the connected loads at these nodes (see Table 6-3 and Fig. 6-6). This applies to other symmetrical nodes too. The more asymmetry in the network, the faster the PSO gets to the global optimum.

Fig. 6-7 shows the nodal mass injection from each hub and the corresponding temperature profiles on the supply and return pipes. The nodal mass flows for both Scenarios lookalike for all nodes except where the HPs are installed (hubs 7, 8, 11, 16, 23, 25 and 29 in Fig. 6-7(a)).

Hubs with no heat consumption and production, for example 13, 19 and 26, can be treated as either sources or consumer in the numerical computation depending on the direction of mass flow obtained from the load flow solution. The nodal mass flow is always zero at these hubs. However, the temperature can vary depending on the assumption. In any case, the heat power injected into the network is zero. The mass and temperature balances at the mixing nodes are also guaranteed. Hubs 13 and 26, for instance, are acting as heat sources in Scenario I, and their supply temperatures are fixed at 70 °C. Their return temperatures are then determined by the network, and are equal to the outgoing return temperatures of the corresponding nodes.

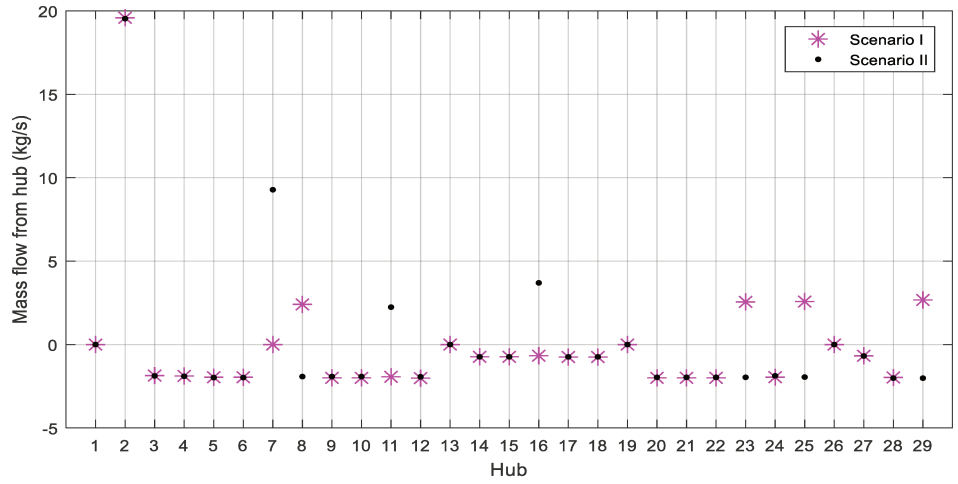

(a)

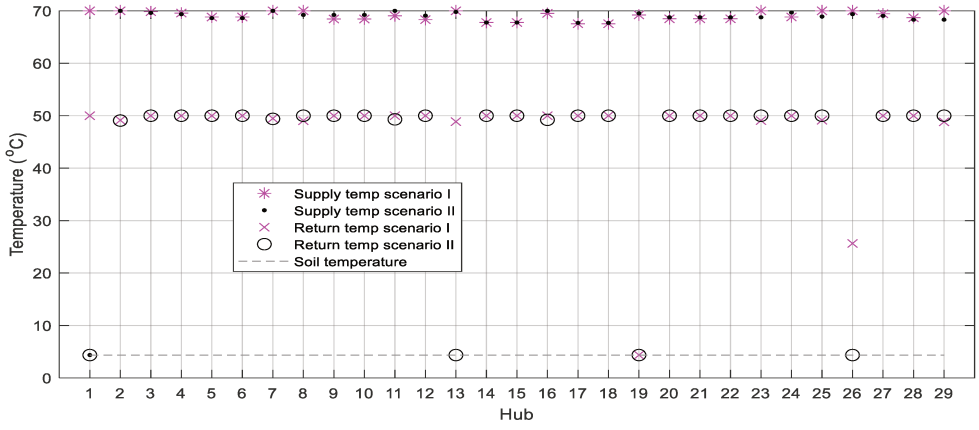

(b)

Fig. 6-7. (a) The mass flow injected into the network from each hub and (b) the corresponding supply and return temperatures for the two scenarios of Case 6-B.

In scenario II, however, hubs 13 and 26 are, treated as heat consumers and their return temperatures are equal to the soil temperature because of zero nodal mass flow. The supply temperatures then become equal to the outgoing supply temperature of the mixing at the respective nodes. Hub 19, on the other hand, is treated as a heat consumer in both scenarios.

Further comparison of the two scenarios can be made in terms of pipe flows, line currents and nodal voltages. The pipe flows on the supply pipe networks of the DHN are depicted in Fig. 6-8. The magnitude of all pipe flows are below the acceptable range of 9.3 kg/s. The current flows through each transmission line, as shown in Fig. 6-9, are also below the limit of 480 A. However, the voltage magnitudes at hubs 8 and 29 in Scenario I are below the acceptable limit of 0.9 pu (see Fig. 6-10). These nodes belong to the 0.4 kV distribution network. Although the nearby transformers are set at the lowest possible tap setting of 0.9, they are not enough to keep the voltage above 0.9 pu. The voltage profiles in Scenario II, however, are within the acceptable range of 0.9 – 1.1 pu.

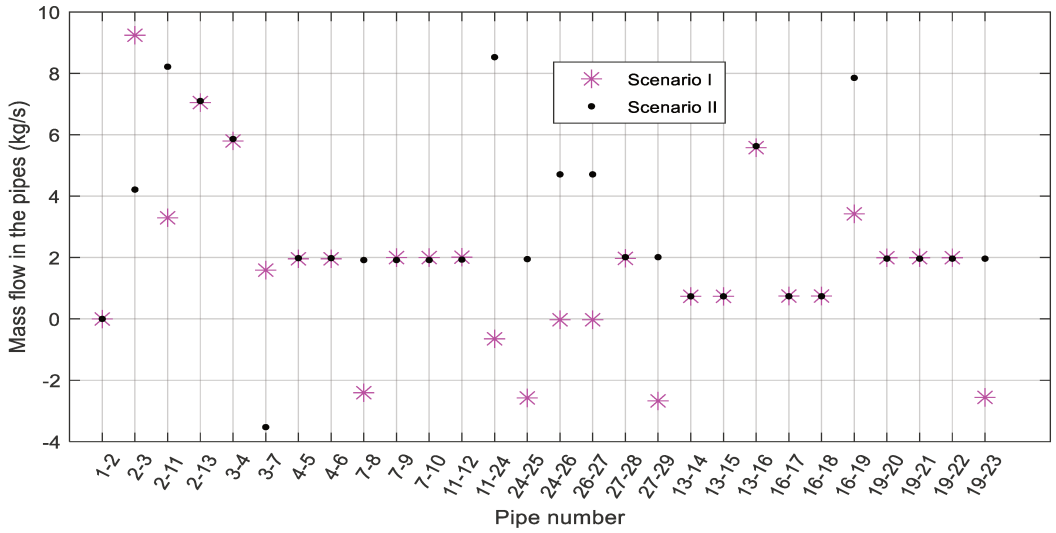

Fig. 6-8. Mass flow in the pipes for the two scenarios of Case 6-B.

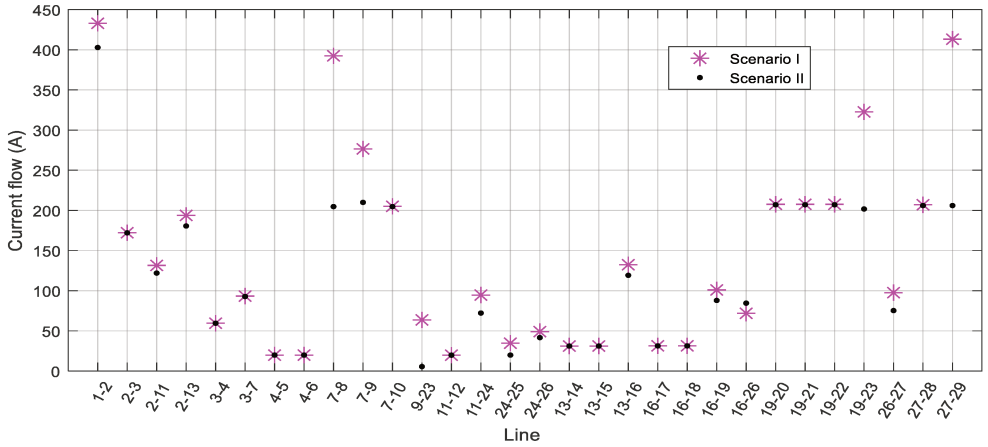

Fig. 6-9. Phase currents through the transmission lines for the two scenarios of Case 6-B.

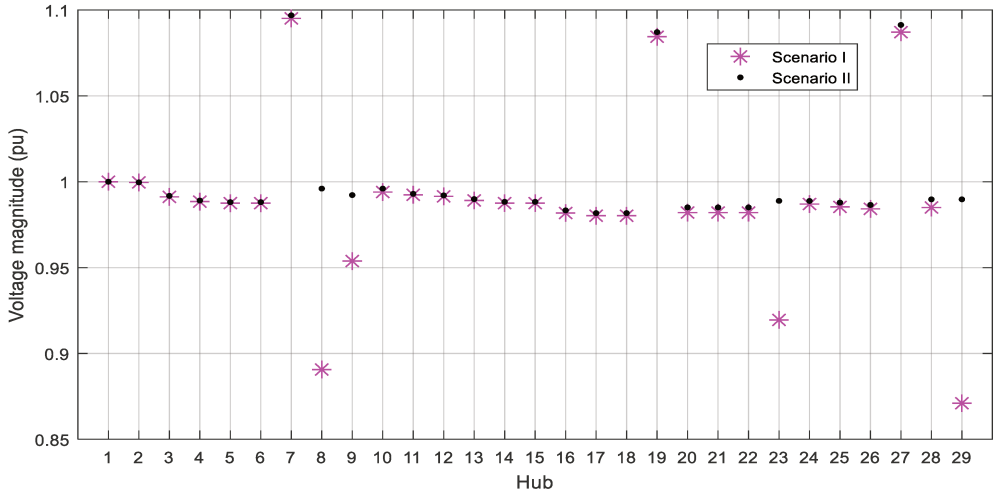

Fig. 6-10. Voltage magnitudes at different hubs for the Case 6-B.

6.4. Thermo-economic optimisation of an electrified DHN

The focus of the optimal power flow in Cases 6-A and 6-B was on finding the optimal placement of coupling devices. Supply temperatures of heat sources and return temperatures of heat consumer hubs were fixed to constant values. They are, however, important control variables in the operation of DHN. This case study considers a thermo-economic optimisation of a DHN that is electrified using HPs and a CHP plant.

Furthermore, a step-by-step approach is followed, as shown in Fig. 6-11, to identify and isolate lossy branches from a meshed DHN topology. It starts by formulating the integrated load flow model (step 1 in Fig. 6-11). An integrated optimal power flow is run in order to determine the economical dispatch of the energy technologies without violating network constraints such as branch capacities (step 2). As DHNs are designed and installed by taking a margin for reliability and future expansions, it is not uncommon to find meshed DHN topologies with pipes running below their capacity. In that case, isolating non-critical branches could reduce distribution losses steps (3 and 4). Once all of the non-critical lossy branches are isolated, further improvement on the operation of the DHN is made by optimally placing and sizing movable heat sources, such as HPs (step 5). This is followed by a thermo-economic optimisation, in which the supply temperature profile of heat sources and the return temperature of substations (on the primary side) are considered, to further reduce the operating cost of the DHN (steps 6 and 7). The objective function in this case study is the same as the one defined by equation (6-4) subject to the constraints discussed in *Section 6.2*.

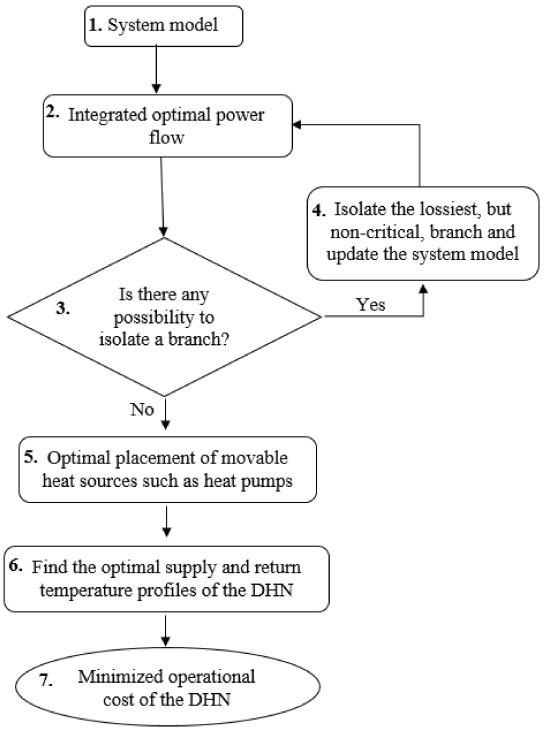

Fig. 6-11. A step-by-step approach followed in thermo-economic optimisation.

6.4.1. Description of the case study – Case 6-C

The layout of the case study is shown in Fig. 6-12. As the focus is on the heating network, the radial electrical distribution network is considered only for the purpose of delivering the electricity required by the DHN.

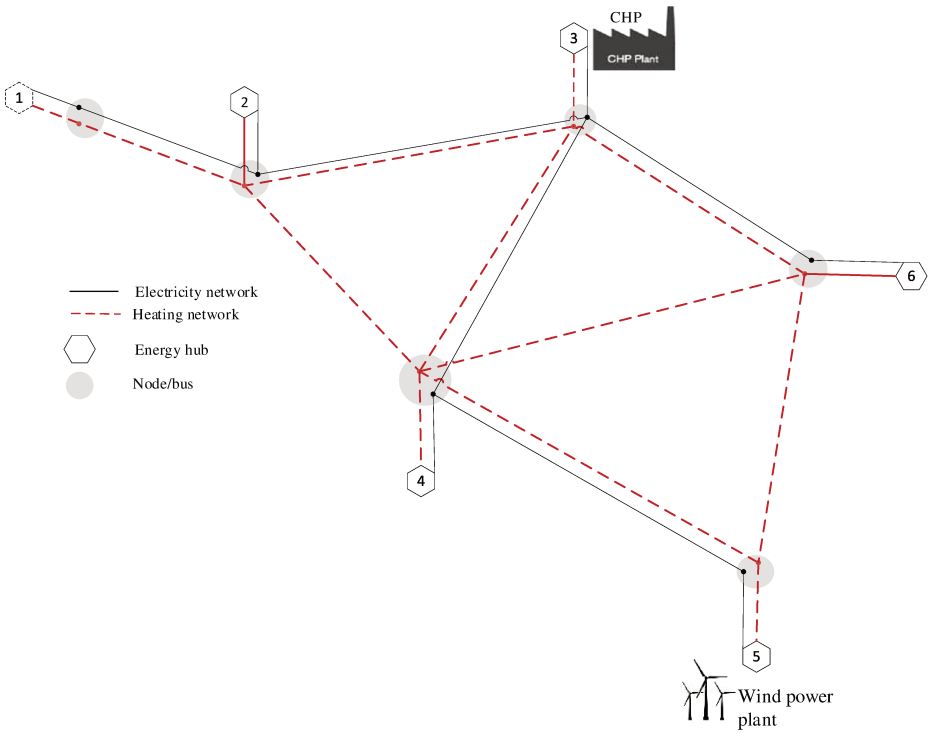

Fig. 6-12. A hypothetical electrified DHN considered for Case 6-C.

All the DHN pipes are assumed to be DN-50 type with standard insulation (parameters are taken from [118]). The soil temperature around the pipe is -5 °C. The electricity network is assumed to be balanced 4.16 kV three phase system with maximum allowed line current of 480 A [102]. The details of the pipe and insulation parameters together with the resistance and reactance of the electrical transmission lines are presented in Table D-1, in Appendix D.

No electrical load is considered at each hub, except for the consumption of HPs. By doing so, the electricity lost in the network (merely for electrifying the DHN) can be computed and taken into account in the cost optimisation. The heat demands at each hub are summarised in Table 6-5. To supply these demands, a gas fired CHP plant and a wind power plant are assumed to be permanently connected at hubs 3 and 5, respectively. In addition, two HPs are available as a means of electrifying the DHN.

Table 6-5: Heat demand at different hubs – Case 6-C.

	Hub 1	**Hub 2**	**Hub 3**	**Hub 4**	**Hub 5**	**Hub 6**
Heat demand (kW)	0	500	200	1000	200	500

The CHP plant has 1000 kW of gas intake capacity with typical thermal and electrical efficiency of 47% and 38%, respectively [142]. For the given simulation hour, the wind power plant is assumed to have a maximum of 125 kW power output. The two HPs have 125 kW and 380 kW electrical ratings both running at a COP of 4.0 and unity power factor. Their locations vary depending on the scenarios that are to be discussed in *Section 6.4.2*.

The average price of electricity and natural gas for household consumptions at EU level in 2019 are taken as references for this case study [143, 144]. Accordingly, the price of imported electricity is assumed to be 0.22 €/kWh and the price of gas used in the CHP plant is 0.07 €/kWh. The price of imported heat from the neighbourhood is taken to be.0.1 €/kWh (taking the Swedish household market as a reference). Selling prices of 0.132 €/kWh of electricity and zero for heat are assumed when exporting to the neighbourhood. Operational cost of the wind power plant is assumed to be negligible. All the prices are rough approximations and vary from place to place. The optimisation results also vary accordingly. Here, they are taken only for illustration purpose.

6.4.2. Scenarios

A stepwise procedure is followed to arrive at the best operational strategy of the system. For comparison purpose, the procedures are categorised into four scenarios. The electricity distribution network topology remains the same in all the scenarios.

6.4.2.1. Scenario I - Base case

This scenario corresponds to step 2 in Fig. 6-11. The network topology shown in Fig. 6-12 is considered. The 125 kW_e and 380 kW_e HPs are placed at hubs 5 and 3, respectively. All sources' supply temperatures are assumed to be at 85 $^{\circ}C$ while all the return temperatures from the consumers are set at 40 $^{\circ}C$. Optimal power flow is run using a single PSO (population size of 20 and a maximum iteration of 100) algorithm.

6.4.2.2. Scenario II - Reduced topology

In this scenario, the effect of isolating lossy branches is demonstrated using a simple greedy algorithm. The algorithm identifies and isolates one lossiest branch at a time in order to arrive at an optimal topology step by step. The process is repeated until all non-critical branches are isolated (steps 2, 3 and 4 in Fig. 6-11). A maximum of three branches can be isolated from the three loops shown in Fig. 6-12. The HPs are kept at the same hubs as they were in the base case scenario, and the optimal power flow is run under the same conditions. Based on the results of the optimal power flow, the 1st lossiest branch is identified and isolated. The optimal power flow is then repeated to isolate the second and then the third lossiest branches, at the end, giving a reduced topology of the DHN. Lastly, the optimal power flow is computed on the reduced topology. The reduced network topology is further used in the consecutive scenarios.

6.4.2.3. Scenario III - Optimal placement of HPs

This scenario corresponds to step 5 in Fig. 6-11. A nested PSO algorithm is used to find out the optimal placement of the two HPs. In a nested PSO algorithm, the details of which is covered in *Section 6.3.1*, the outer PSO is dedicated to find the best location of the HPs while the inner PSO solves the optimal power flow based on the location of the HPs dictated by the outer PSO loop. The outer PSO loop has a population size of 5 and maximum iteration of 10 while the internal PSO has a population size of 20 and a maximum iteration of 100. A reduced network topology is used in this scenario while keeping the same other conditions as the previous scenarios.

6.4.2.4. Scenario IV - Thermo-economic optimisation

This scenario deals with the thermo-economic optimisation of the reduced network topology after the HPs are placed at their optimal location (steps 6 and 7 in Fig. 6-11). The supply temperature range is taken between 60 °C and 95 °C while a return temperature range is assumed between 30 °C and 55 °C (equations (6-9) and (6-10)). A single PSO (population size of 30 and a maximum iteration of 100) is applied to determine not only the economic dispatch, but also the optimal supply and return temperatures of the hubs.

6.4.3. Results and discussions on Case 6-C

6.4.3.1. Base case (Scenario I)

The hub level load flow results of Scenario I are presented in Table 6-6. The table shows the sole electricity generation (P_{epg}), consumption of HPs (HP_{Lep}), heat generated by the HPs (HP_{Phg}), the electricity and heat produced by the CHP (CHP_{Pepg} and CHP_{Phg}), the locally generated heat (P_{hg}), the heat demand (L_h), the nodal mass flow rate ($\dot{m}$) and the nodal temperatures on the supply and return sides (T_s and T_r) of the DHN.

The total amount of heat demand is 2400 kW. Although the total heat produced by the CHP and the HP is 90 kW more than the total heat demand, it is not enough to compensate the losses in the network. Hence, additional 46.19 kW of heat is imported from the neighbourhood. On the other hand, the wind and the CHP plants produced 125 kW and 380 kW of electricity, respectively. The electricity lost in the distribution network is zero because all the generated electricity is consumed locally by the HPs.

Table 6-6: Hub-level results of the optimal power flow (base case) – Case 6-C.

Hub	P_{epg} *(kW)*	HP_{Lep} *(kW)*	HP_{Phg} *(kW)*	CHP_{Pepg} *(kW)*	CHP_{Phg} *(kW)*	P_{hg} *(kW)*	L_h *(kW)*	$\dot{m}$ *(kg/s)*	T_s *(°C)*	T_r *(°C)*
1	0.00	0.00	0.00	0.00	0.00	46.19	0.0	2.98	43.40	39.69
2	0.00	0.00	0.00	0.00	0.00	0.00	500.0	-5.01	63.84	40.00
3	0.00	380.0	1520.0	380.0	470.0	0.00	200.0	9.35	85.00	39.26
4	0.00	0.00	0.00	0.00	0.00	0.00	1000.0	-6.08	79.32	40.00
5	125.0	125.0	500.00	0.00	0.00	0.00	200.0	1.52	85.00	37.81
6	0.00	0.00	0.00	0.00	0.00	0.00	500.0	-2.76	83.26	40.00

Table 6-7, on the other hand, shows the branch-level load flow results. It shows the pipe mass flow rate and the inlet and outlet temperatures both on the supply and return pipes. It can be seen that the highest temperature drops both on the supply and return pipes occurred on the branch connecting hubs 5 and 6. This is associated to the lowest mass flow in the branch resulting in a higher residence time and, as a result, causing higher temperature drop.

Table 6-7 also shows the net heat delivered through each branch, the corresponding pumping energy, the losses and their energy efficiency. The total heat loss can be calculated by subtracting the total demand from the total heat injected into the network by referring Table 6-6, or by adding the branch heat losses shown in Table 6-7. The total heat loss in this network is about 136.19 kW (5.67%).

Table 6-7: Branch-level results of the optimal power flow (base case) – Case 6-C.

Hubs		**Supply pipe network of the DHN**			**Return pipe network of the DHN**		**Branch i to j**			
i	***j***	Flow (kg/s)	$T_{s(i)}(^{\circ}C)$	$T_{s(j)}(^{\circ}C)$	$T_{r(i)}(^{\circ}C)$	$T_{r(j)}(^{\circ}C)$	$P_{el(pumping)}$ *(kW)*	*Net heat flow (kW)*	*Loss (kW)*	*Energy efficiency*
1	2	2.98	43.40	43.35	39.69	39.74	0.169	45.04	1.16	97.14%
2	3	-3.04	83.95	85.00	39.74	39.22	2.134	561.74	19.95	96.22%
2	4	1.00	63.84	61.44	38.43	40.00	0.087	90.13	16.65	84.34%
3	4	3.23	85.00	84.01	39.51	40.00	2.547	594.06	20.00	96.34%
3	6	3.09	85.00	83.97	39.05	39.56	2.248	574.32	19.93	96.28%
4	5	-1.01	81.88	85.00	40.00	38.44	0.088	176.66	19.75	89.90%
4	6	-0.84	79.60	83.26	40.00	38.13	0.052	139.14	19.42	87.72%
5	6	0.51	85.00	78.95	36.57	39.56	0.013	84.24	19.35	81.31%

6.4.3.2. Reduced topology (Scenario II)

The results in Table 6-7 show that the branch 5-6 is the lossiest (81.31% efficiency). The next lossiest branches are 2-4 and 4-6. However, the 2nd and the 3rd lossiest branches may be different as the optimal power flow results in a different solution once the 1st lossiest branch is isolated. Having this in mind, the branch 5-6 is first isolated and the optimal power flow is repeated with the new topology. The results are tabulated in Appendix D, Table D-2 and Table D-3. As it can be seen from Table D-2, branch 4-6 is the next lossiest branch , but not 2-4, which contradicts Table 6-7. This confirms the importance of a step-by-step approach. The optimal power flow is repeated again after removing the branch 4-6. The results are presented in Table D-4 and Table D-5. Table D-5 shows that the third lossiest branch is the one between hubs 1 and 2. However, this branch is mandatory to keep all hubs connected, and it cannot be isolated. So, the next lossiest branch, which is branch 2-4, is isolated. The remaining branches are critical to keep all nodes interconnected. Once all the branches 5-6, 4-6 and 2-4 are isolated from the base case topology (Fig. 6-12), the reduced (optimised) topology of the DHN looks like the one shown in Fig. 6-13. The topology can be said optimal for the given load and generation conditions.

An optimal power flow is then run to see how much saving is made in terms of both energy and money. The branch-level results are summarised in Table 6-8. The imported heat is zero and there is excess of electricity exported to the neighbourhood at hub 1.

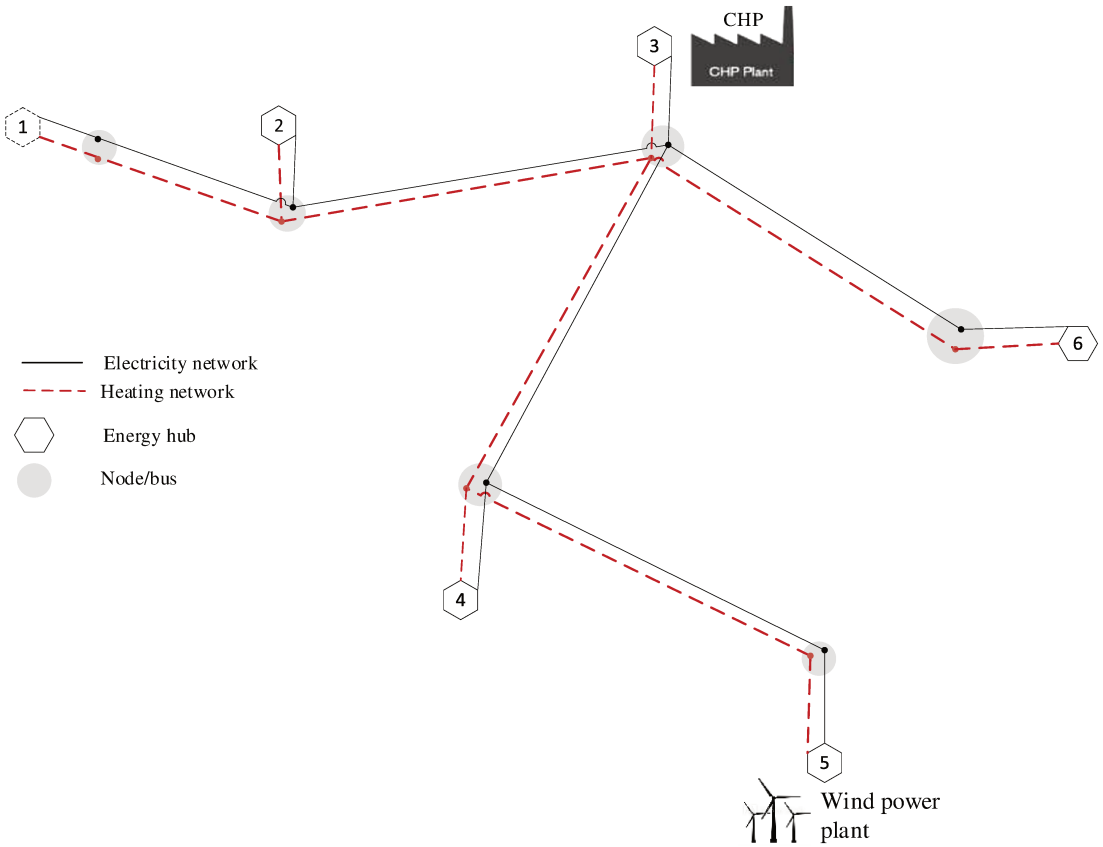

Fig. 6-13. The reduced network topology after isolating the lossy branches – Case 6-C.

Table 6-8: Hub-level results of the optimal power flow (reduced topology) – Case 6-C.

Hub	P_{epg} *(kW)*	HP_{Lep} *(kW)*	HP_{Phg} *(kW)*	CHP_{Pepg} *(kW)*	CHP_{Phg} *(kW)*	P_{hg} *(kW)*	L_h *(kW)*	$\dot{m}$ *(kg/s)*	T_s *(°C)*	T_r *(°C)*
1	-2.54	0.00	0.00	0.00	0.0	0.0	0.0	0.00	10.15	10.15
2	0.00	0.00	0.00	0.00	0.0	0.0	500.0	-2.73	83.83	40.00
3	0.00	377.46	1509.84	380.00	470.0	0.0	200.0	9.34	85.00	39.49
4	0.00	0.00	0.00	0.00	0.0	0.0	1000.0	-5.45	83.83	40.00
5	125.0	125.00	500.00	0.00	0.0	0.0	200.0	1.56	85.00	38.98
6	0.0	0.00	0.00	0.00	0.0	0.0	500.0	-2.73	83.83	40.00

Table 6-8 also shows that running the CHP at full rate is found to be economical than running the heat pumps at full rate. From the two HPs, the one installed at hub 5 is running at its full capacity (125 kW_e) due to the presence of 125 kW cheap local electricity generation from the wind plant. This also avoids the electricity loss that could be incurred while exporting the excess production from hub 5 to hub 1.

Table 6-9 summarises the branch power flows and their associated efficiencies. The total heat loss is reduced from 136.19 kW (Scenario I) to 79.86 kW which shows a 41.37% reduction. Though the cost of pumping energy increased slightly from 1.805 €/h to 1.88 €/h, the total operating cost has decreased from 76.42 €/h to 71.32 €/h. The loss in the electricity distribution network is again negligible compared to the demands of the HPs.

Table 6-9: Branch-level results of the optimal power flow (reduced topology) – Case 6-C

Hubs		Branch i to j			
i	j	$P_{el(pumping)}$ (kW)	Net heat flow (kW)	Loss (kW)	Energy efficiency
1	2	0.000	0.00	---	---
2	3	1.558	-500.00	19.98	96.16%
3	4	4.422	719.88	20.02	97.29%
3	6	1.558	500.00	19.98	96.16%
4	5	0.307	-280.12	19.88	93.37%

6.4.3.3. Optimal placement of HPs (Scenario III)

To further reduce the distribution loss, the optimal placement of HPs is determined using the nested PSO algorithm presented in *Section 6.3.1*. It is found that hubs 4 and 6 are the best places to install the 380 kW_e and the 125 kW_e HPs, respectively. The sizing of the HPs and operating parameters of the distribution network are summarised in Table 6-10 and Table 6-11. The total heat loss is now 64.11 kW which shows 19.72% and 52.93% reductions from Scenario II and Scenario I, respectively. In comparison to Scenario II (Table 6-8), the amount of electricity exported in Scenario III has increased by 3.09 kW. As the HPs are placed relatively farther from the electricity sources, there is a higher (about 0.85 kW) electricity distribution loss. On the other hand, the HPs are located relatively closer to the heat demands. As a result, the pumping cost has decreased from 1.88 €/h (Scenario II) to 0.5 €/h (Scenario III). The total operating cost becomes 69.56 €/h which shows 8.98% saving over Scenario I.

Table 6-10: Hub-level results after the optimal placement and sizing of the HPs – Case 6-C.

Hub	P_{epg} *(kW)*	HP_{Lep} *(kW)*	HP_{Phg} *(kW)*	CHP_{Pepg} *(kW)*	CHP_{Phg} *(kW)*	P_{hg} *(kW)*	L_h *(kW)*	$\dot{m}$ *(kg/s)*	T_s *(°C)*	T_r *(°C)*
1	-5.63	0.00	0.00	0.00	0.00	0.00	0.00	0.00	40.00	40.00
2	0.00	0.00	0.00	0.00	0.00	0.00	500.00	-2.79	82.75	40.00
3	0.00	0.00	0.00	380.00	470.00	0.00	200.00	1.41	85.00	39.23
4	0.00	373.52	1494.09	0.00	0.00	0.00	1000.0	2.53	85.00	38.34
5	125.00	0.00	0.00	0.00	0.00	0.00	200.00	-1.13	82.22	40.00
6	0.00	125.00	500.00	0.00	0.00	0.00	500.00	-0.01	1.00	1.00

Table 6-11: Branch-level results after optimal placement and sizing of the HPs – Case 6-C

Hubs		Branch i to j			
i	j	$P_{el(pumping)}$ (kW)	Net heat flow (kW)	Loss (kW)	Energy efficiency
1	2	0.000	0.00	---	---
2	3	1.676	-500.00	19.81	96.19%
3	4	0.225	-254.57	19.74	92.80%
3	6	0.000	0.00	---	---
4	5	0.123	200.00	19.79	91.00%

6.4.3.4. Thermo-economic optimisation (Scenario IV)

Unlike to a fixed supply and return temperatures in the previous scenarios, a thermo-economic optimisation is done in this scenario by relaxing the supply temperature range between 60 °C and 95 °C and the return temperature between 30 °C and 55 °C. The nodal and branch level optimisation results are presented in Tables 6-12 and 6-13.

Hubs 3 and 4 are sources of heat as they are indicated by positive nodal mass flows in Table 6-12 while hubs 2 and 5 are consumers. The return temperature of both hubs 2 and 5 are at 30 °C which is the lower limit. It implies that the lower the return temperature from the consumers the more economical the DHN will be.

The supply temperatures of hubs 3 and 4 are at 95 °C and 67.76 °C, respectively. Should the cost of pumping energy be not significant, both supply temperatures were expected to be equal to the minimum limit of 60 °C. However, both of them are higher than the lower limit and hub 3 is rather at the maximum limit. This shows that decreasing the sources temperatures further leads to not only a decrease in distribution loss, but also an increase in a mass flow rate, which in turn requires higher pumping energy. The optimisation found that the cost of the additional pumping energy is more expensive than the cost of heat loss that could be saved by decreasing the supply temperatures further than those values for this particular case study.

As it can be calculated from Table 6-12 or Table 6-13, the total distribution heat loss in Scenario IV has dropped further to 55.67 kW. This shows a 13.16% reduction from Scenario III and about 59.12% reduction from Scenario I.

In comparison to Scenario III, the cost of pumping decreased slightly from 0.5 €/h to 0.48 €/h. The electricity distribution losses also slightly dropped from 0.85 kW to 0.84 kW. The total operating cost this time becomes 69.26 €/h showing a 0.4% decrease from Scenario III and about 9.37% reduction from Scenario I.

Table 6-12: Hub-level results of the thermo-economic optimisation – Case 6-C.

Hub	P_{epg} *(kW)*	HP_{Lep} *(kW)*	HP_{Phg} *(kW)*	CHP_{Pepg} *(kW)*	CHP_{Phg} *(kW)*	P_{hg} *(kW)*	L_h *(kW)*	$\dot{m}$ *(kg/s)*	T_s *(°C)*	T_r *(°C)*
1	-7.74	0.00	0.00	0.00	0.00	0.00	0.00	0.00	10.00	10.00
2	0.00	0.00	0.00	0.00	0.00	0.00	500.00	-2.61	75.85	30.00
3	0.00	0.00	0.00	380.00	470.00	0.00	200.00	0.98	95.00	29.28
4	0.00	371.42	1485.67	0.00	0.00	0.00	1000.00	2.98	67.76	28.78
5	125.00	0.00	0.00	0.00	0.00	0.00	200.00	-1.33	65.84	30.00
6	0.00	125.00	500.00	0.00	0.00	0.00	500.00	0.00	10.00	10.00

Table 6-13: Branch-level results of the thermo-economic optimisation – Case 6-C.

Hubs		**Branch i to j**			
i	j	$P_{el(pumping)}$ (kW)	Net heat flow (kW)	Loss (kW)	Energy efficiency
1	2	0.000	0.00	0.00	---
2	3	1.365	-499.99	17.30	96.66%
3	4	0.359	-254.07	15.77	94.16%
3	6	0.000	0.00	0.00	---
4	5	0.196	200.00	15.83	92.66%

Fig. 6-14 presents the heat losses (left axis) and operating costs (right axis) under different scenarios. It shows how much the operating cost and the total heat loss are progressively decreased and how much of the total loss is shared by each of the branches.

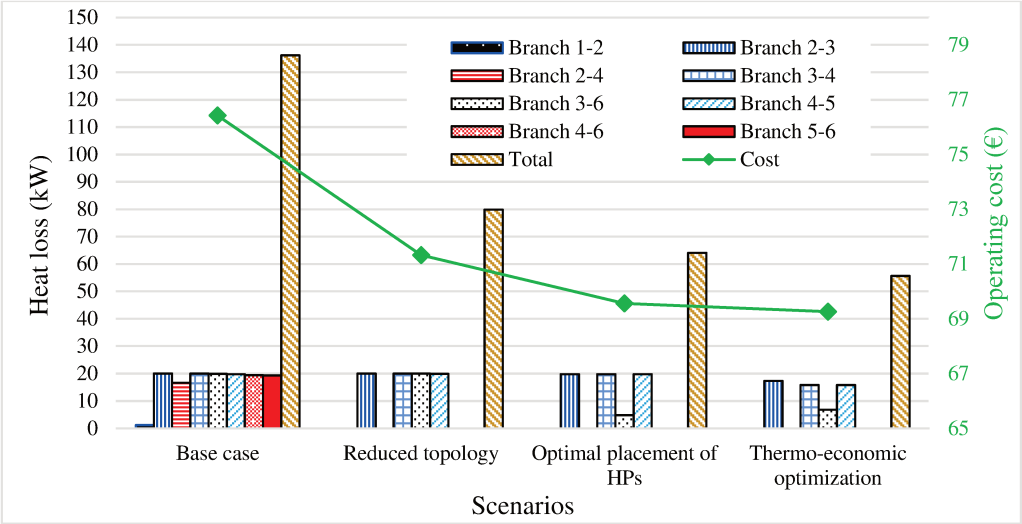

Fig. 6-14. Comparison of operating costs and heat losses at different operating scenarios – Case 6-C.

6.4.4. Computational efforts

All the simulations are done on MatlabR2017a platform on a Dell desktop computer with Intel Core i5-8400CPU processor running at 2.80 GHz and 2.81 GHz with a 64 bit Windows 10 operating system. Each of the simulations are repeated 10 times. Although the results were very close to each other, all the discussions are based on the best values obtained. The load flow simulations are completed in fractions of seconds. The optimal power flow simulations (Scenarios I and II) took between 95 – 187 seconds. The thermo-economic optimisation (Scenario IV) needed 137 – 275 seconds to finish due to larger population size used in the PSO. The optimal placement of HPs (Scenario III), on the other hand, took between 860 – 1040 seconds.

The simulation time step considered is one hour and all of the simulations were completed in a much shorter time. Furthermore, the optimal placement algorithm is supposed to be run only once before installing the HPs. In that regard, the time it takes can be ignored. However, these numbers are rough figures and vary with the network size and operating condition of the computer. They are meant only to give an idea how the simulations can be used in a real time application. It can be said that, the methodology proposed can be run on an ordinary desktop computer, and it is suitable for small to medium size district energy system simulations running on an hourly basis.

6.5. Summary

In this chapter, a PSO-based metaheuristic algorithm is developed and integrated with the load flow model. The algorithm is used to conduct an optimal power flow in a coupled heat and electricity distribution networks. It is also applied for optimal placement of coupling technologies, such as HPs. The chapter also discussed a step-by-step approach that can be used to isolate lossy branches in a meshed DHN.

The results show that placement and sizing of HPs only from the heating network point of view could overload and increase the loss in the electricity distribution network, especially when HPs are installed at low voltage distribution networks. It could also lead to unacceptable voltage profiles. Such issues are avoided using an integrated optimisation that considers the constraints and distribution losses in both networks. The integrated optimisation has also resulted in a lower operating cost for the overall system and a better voltage profile in the electricity distribution network.

The thermo-economic optimisation further revealed that the pumping cost may sometimes counter balance the advantages of lower supply temperatures. Hence, it is worthy to consider the total cost of pumping energy in thermo-economic optimisations. On the other hand, lowering the return temperature of the consumers (on the primary side) is found to be always economical.

In the following chapter, thermo-economic optimisation of coupled electricity and heating networks having both electrical and thermal load profiles will be presented. Time-series variation of load profiles and generation resources will also be taken into account.

7. Applications in the Presence of Intermittent Renewables and Variable Price Signals

Only case studies with a single hour (1 time-step) operating cost minimization are discussed in the previous chapter. This chapter expands the optimisation scope into a multiple-hours horizon. Thermo-economic optimisation of coupled electricity and heating networks involving both heat and electrical demands are studied. Furthermore, a thermal storage model is incorporated into the optimisation model. A model predictive control (MPC) algorithm is developed that can capture the synergy from the electricity and heating networks in the presence of intermittent renewables and variable electricity price signal. All the physical parameters and constraints of both networks together with the dynamics of the thermal storage are duly considered.

7.1. Thermal storage as a means of unlocking additional flexibility

The importance of thermal storages in unlocking additional flexibility and increasing the penetration of renewables into coupled electricity and heating sectors is reported in recent literature. Integration of thermal storage enables to decouple the production and consumption of heat in time (commonly referred to as peak shaving). Moreover, as electrical storage devices are more expensive (50 to 100 times) than thermal storage tanks [25, 26], any surplus of electricity can be converted and stored in the form of heat. Thermal storage and HPs can be used to couple the electricity and heating systems so that intermittent renewables, such as wind generations, can be effectively used [22, 27].

The level of flexibility that can be gained from the DHN inertia, building inertia and hot water thermal storages in the presence of electrical renewables are discussed in [28]. It is pointed out that the use of thermal storage may increase the total energy consumption due to the possibility of rising distribution losses during the charging and discharging process. However, its advantages weigh more because it reduces installation capacity (peak shaving potential), decreases the usage of expensive peak-load plants and increases the penetration level of intermittent renewable sources.

In order to have optimal overall system, both of the electricity and heat distribution networks need to be considered in the management of thermal storages. Such analyses are rare in literature. Use of heat distribution network and building thermal inertia as a storage in the presence of intermittent wind generation is discussed in [29, 30]. However, only the heating network is considered in these studies. Demand side management using buildings' inertia and additional hot water tank as thermal storages while taking the constraints in the electrical distribution grid is presented in [43]. A scenario based analysis shows how a demand side management can be used so that larger capacity of distributed HPs can be installed without

overloading the electricity distribution network. However, onsite heat supply for each building is assumed, and the heat distribution network is not considered. In addition, none of the three papers addressed the possibility of variable electricity tariff together with intermittent renewables availability for better management of thermal storages.

The flexibility that can be unlocked by combining variable electricity prices, demand side management and thermal storage in the presence of intermittent solar and wind power plants is studied in [145]. The results show that HPs and electric boilers together with the thermal storage can increase the capacity of renewables that can be installed in urban energy system. However, neglecting the impact of the management strategy on the distribution networks, as is the case in [145], might lead to non-optimal results due to high distribution losses, inadmissible voltage and/or temperature deviations. Moreover, an ideal thermal storage operating at constant return and supply temperatures is assumed, which is far from the reality.

The above short literature survey shows the importance of thermal storages in the coupled electricity and heating networks consisting of HPs, CHPs and renewable energy technologies. The thermal storage can serve for peak shaving, capturing intermittent renewables and also to take advantage of variable electricity price signals. These combined features, however, are not well studied in literature. The distribution networks' parameters together with the dynamics of the thermal storage are not considered either. In addressing these scientific gaps, the discussion in the following sections aims at the following two objectives:

- Demonstrate how a detailed model of a stratified thermal storage water tank can be incorporated with the EEH-based integrated optimal power flow model.
- Illustrate how a novel PSO-based MPC algorithm can be used to optimise the charging and discharging schedule of a thermal storage in the presence of grid electricity price signal, wind power generation, a HP, a CHP and a gas boiler.

7.2. Coupling equation that involves a thermal storage

In addition to the interactions among different energy technologies discussed in *Section 5.2*, an energy hub with a thermal storage will be considered in this chapter. Its EEH representation is shown in Fig. 7-1. The heat power flowing to/from the storage is indicated with $P_{h-storage}$. By referring the general coupling equation (3-3), the corresponding coupling equation for Fig. 7-1 can be derived as shown in equation (7-1).

$$\begin{bmatrix} L_{ep} \\ L_{eq} \\ L_h \end{bmatrix} = \begin{bmatrix} 1 & 0 & 0 & 0 \\ 0 & 1 & 0 & 0 \\ 0 & 0 & 1 & Z_{h(h)} \end{bmatrix} \begin{bmatrix} P_{epg} - P_{ep} \\ P_{eqg} - P_{eq} \\ P_{hg} - P_h \\ \dot{E}_h \end{bmatrix} \tag{7-1}$$

where $Z_{h(h)}$ refers to the charging/discharging efficiency of the thermal storage and $\dot{E}_h$ is the rate of change of stored heat, which is equal to the net charging power going into the thermal storage.

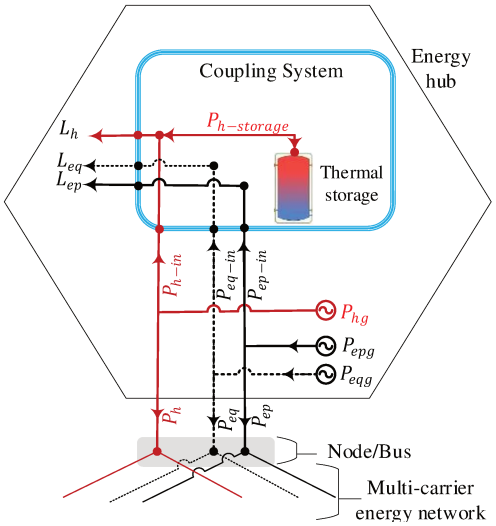

Fig. 7-1. The EEH representation of an energy hub with a thermal storage.

In equation (7-1), the thermal storage is represented by a constant charging/discharging efficiency and the rate of change of stored energy. This is convenient to represent electrical and gas storage technologies as the state of charge is the only factor that determines how much to charge and discharge for a given surplus/deficit of the corresponding energy carrier. In the case of thermal storages, however, the relative difference between the temperatures of the water inside the storage and the temperature of the incoming water determines how much of the surplus heat can be saved in the thermal storage. A surplus heat can only be stored if its temperature is higher than the temperature inside the storage. Hence, the use of equation (7-1) with a constant charging and discharging efficiency for a thermal storage could lead to unrealistic solutions. In order to overcome that drawback, detailed set of equations that govern the dynamics of the thermal storage are included.

7.3. Stratified thermal storage model

Comparison of capacity (fully mixed) and stratified (with a layer that separates the cold and hot water) storage water tanks are presented in [67, 146, 147]. It is indicated that the use of stratified model gives better accuracy. Stratified thermal storage has also additional advantage over the fully mixed storage. As the layers of a stratified storage tank are kept at different temperature levels, it is possible to discharge the storage at higher temperatures whenever required. This is not possible in the fully mixed storage.

The water flow during charging and discharging process in a three-layer model of a stratified thermal storage tank is shown in Fig. 7-2. The middle layer serves as a buffer between the hot (top layer) and cold (bottom layer) water in the tank. Discharging takes place always from the top (hot) layer, as depicted in Fig. 7-2(b). During the charging process (see Fig. 7-2(a)), the incoming water temperature is first compared with the average temperature of each layer to determine where it should be stored. Accordingly, even if the incoming water is colder than the water in the top layer, it will still have a chance to be stored either in the middle or bottom layer of the storage. Such features are not possible using a fully mixed storage.

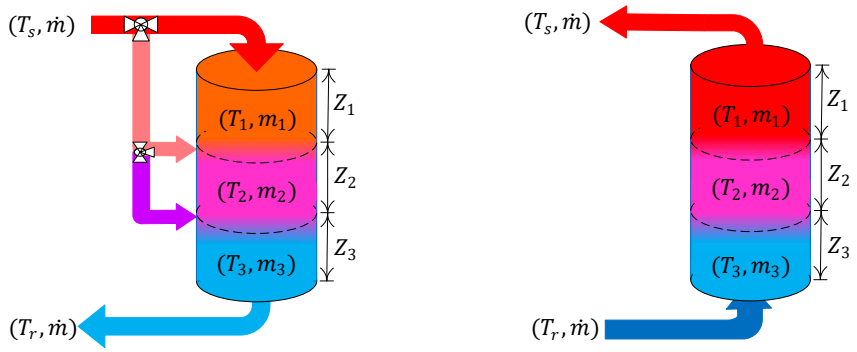

Fig. 7-2. Three layer stratified model of a thermal storage: (a) charging and (b) discharging.

The overall simulation is conducted on an hourly basis. Hence, the temperature of water leaving the storage is required not to vary during each hour. This constraint is handled by limiting the total hot (cold) water mass leaving the storage in each hour to be less or equal to the water mass in each layer. In addition, after following a natural stratified heat flow during each hour, the water in each layer is fully mixed at the end of each hour. The parameters that are used to model a three layer stratified thermal storage water tank are summarised in Table 7-1.

Table 7-1: Parameters describing a stratified thermal storage model

Symbols	***Definition***
K_s	Heat loss factor of the tank ($W.m^{-2}.K^{-1}$)
k_w	Thermal conductivity of water ($W.m^{-1}.K^{-1}$)
Z_1, Z_2 and Z_3	Heights of layer 1, layer 2 and layer 3 (m)
$R_{storage}$	Radius (m)
A_c	Cross-section area of the storage (m^2)
A_{s1}, A_{s2} and A_{s3}	Lateral surface areas of layer 1, layer 2 and layer 3 (m^2)
$V_{storage}$	Volume (m^3)
t	Current time (s)
Δt	Time step (s)
$T_{1(t-\Delta t)}, T_{2(t-\Delta t)}$ and $T_{3(t-\Delta t)}$	Temperatures (K) of water in layer 1, layer 2 and layer 3 at time $t - \Delta t$
$T_{1(t)}, T_{2(t)}$ and $T_{3(t)}$	Temperatures (K) of water in layer 1, layer 2 and layer 3 at time t
$T_{a(t)}$	Ambient (soil) temperature (K) at time t
m_1, m_2 and m_3	Mass (kg) of water in layer 1, layer 2 and layer 3
$\dot{m}$	Mass flow rate (kg/s) going into or leaving from the tank

Assuming an underground cylindrical water tank and a uniform soil temperature distribution around its surface, the optimal radius of a given storage volume ($V_{storage}$) that minimizes the surface heat loss can be calculated using equation (7-2).

$$R_{storage} = \sqrt[3]{V_{storage}/2\pi} \tag{7-2}$$

The state of charge of the thermal storage can be expressed in terms of the water temperature in the three layers. During the charging process, the flow inside the storage is downward from top to bottom (Fig. 7-2(a)). The 'new' hot water inflows at the top layer (if T_s is higher

than T_1) while the 'older' cold water leaves from the bottom layer. The water flowing from layer 2 to layer 3, for example, is 'new' for layer 3, but old (from previous time) for layer 2. It means that the temperature in layer 3 should be calculated before updating the temperature in layer 2.

The equations governing the thermal interaction between the layers and with the external environment are adapted from the TRNSYS® [148] model. The temperatures at the three layers during the charging phase are updated using equations (7-3) – (7-5).

$$T_{3(t)} = \frac{1}{C_p m_3}\left\{C_p \dot{m}\Delta t\left(T_{2(t-\Delta t)} - T_{3(t-\Delta t)}\right) + \frac{A_c k_w\left(T_{2(t-\Delta t)} - T_{3(t-\Delta t)}\right)\Delta t}{0.5(Z_2 + Z_3)} - A_{s3}K_s\left(T_{3(t-\Delta t)} - T_{a(t)}\right)\Delta t + C_p m_3 T_{3(t-\Delta t)}\right\} \tag{7-3}$$

$$T_{2(t)} = \frac{1}{C_p m_2}\left\{C_p \dot{m}\Delta t\left(T_{1(t-\Delta t)} - T_{2(t-\Delta t)}\right) + \frac{A_c k_w\left(T_{1(t-\Delta t)} - T_{2(t-\Delta t)}\right)\Delta t}{0.5(Z_1 + Z_2)} - \frac{A_c k_w\left(T_{2(t-\Delta t)} - T_{3(t-\Delta t)}\right)\Delta t}{0.5(Z_2 + Z_3)} - A_{s2}K_s\left(T_{2(t-\Delta t)} - T_{a(t)}\right)\Delta t + C_p m_2 T_{2(t-\Delta t)}\right\} \tag{7-4}$$

$$T_{1(t)} = \frac{1}{C_p m_1}\left\{C_p\, \dot{m}\Delta t\left(T_s - T_{1(t-\Delta t)}\right) - \frac{A_c k_w (T_{1(t-\Delta t)} - T_{2(t-\Delta t)})\Delta t}{0.5(Z_1 + Z_2)} - A_{s1}K_s(T_{1(t-\Delta t)} - T_{a(t)})\Delta t + C_p m_1 T_{1(t-\Delta t)}\right\} \tag{7-5}$$

For $T_2 < T_s \leq T_1$, the incoming flow bypasses layer 1 and flows directly into layer 2. In that case, the $\dot{m}$ term in equation (7-5) is replaced by zero and the term $C_p \dot{m}\Delta t\left(T_{1(t-\Delta t)} - T_{2(t-\Delta t)}\right)$ in the equation (7-4) becomes $C_p \dot{m}\Delta t\left(T_s - T_{2(t-\Delta t)}\right)$. Similarly if $T_3 < T_s \leq T_2$, the inflow will directly get into layer 3. Hence, the $\dot{m}$ terms in equations (7-4) and (7-5) are replaced with zeros and the term $C_p \dot{m}\Delta t\left(T_{2(t-\Delta t)} - T_{3(t-\Delta t)}\right)$ in equation (7-3) is changed into $C_p \dot{m}\Delta t\left(T_s - T_{3(t-\Delta t)}\right)$.

The temperatures at the three layers of the storage during the discharging phase are updated using equations (7-6) – (7-8).

$$T_{1(t)} = \frac{1}{C_p m_1}\left\{C_p \dot{m}\Delta t\left(T_{2(t-\Delta t)} - T_{1(t-\Delta t)}\right) - \frac{A_c k_w (T_{1(t-\Delta t)} - T_{2(t-\Delta t)})\Delta t}{0.5(Z_1 + Z_2)} - A_{s1}K_s(T_{1(t-\Delta t)} - T_{a(t)})\Delta t + C_p m_1 T_{1(t-\Delta t)}\right\} \tag{7-6}$$

$$T_{2(t)} = \frac{1}{C_p m_2}\left\{C_p \dot{m}\Delta t\left(T_{3(t-\Delta t)} - T_{2(t-\Delta t)}\right) + \frac{A_c k_w (T_{1(t-\Delta t)} - T_{2(t-\Delta t)})\Delta t}{0.5(Z_1 + Z_2)} - \frac{A_c k (T_{2(t-\Delta t)} - T_{3(t-\Delta t)})\Delta t}{0.5(Z_2 + Z_3)} - A_{s2}K_s\left(T_{2(t-\Delta t)} - T_{a(t)}\right)\Delta t + C_p m_2 T_{2(t-\Delta t)}\right\} \tag{7-7}$$

$$T_{3(t)} = \frac{1}{C_p m_3}\left\{C_p \dot{m}\Delta t\left(T_r - T_{3(t-\Delta t)}\right) + \frac{A_c k_w (T_{2(t-\Delta t)} - T_{3(t-\Delta t)})\Delta t}{0.5(Z_2 + Z_3)} - A_{s3} K_s \left(T_{3(t-\Delta t)} - T_{a(t)}\right)\Delta t + C_p m_3 T_{3(t-\Delta t)}\right\} \quad (7\text{-}8)$$

7.4. Model predictive control (MPC) for optimal thermal storage management

Thermal storages can be operated using either a rule-based or a model predictive control (MPC) strategy. The rule-based management is widely used in literature [32, 33, 43, 146, 149, 150] as it requires lower computational efforts. The rules are usually defined based on the conditions at a given instant of time. As a result, they are not able to capture any forthcoming opportunity. The opportunity can be due to variable tariffs and/or surplus production from renewables. In order to exploit such opportunities, the rules themselves need to be optimised considering a given time horizon. These kinds of problems are usually tackled using MPC algorithms [50, 58, 151–153]. The MPC will consider all future variables in a multi-time-step period (horizon) to determine the optimal strategy for the current time step. The time horizon should be short enough to reduce the computational cost, but also long enough to capture all possible opportunities.

Hot water thermal storages are usually designed for peak-shaving the heat demand and for capturing the cheap electricity prices, both of which follow similar daily patterns. In that regard, a time horizon of 24 hours is considered to demonstrate the proposed MPC algorithm.

7.4.1. Objective function and constraints

The objective function considered in the MPC is minimization of the total operating cost of the system for one day, as defined in equation (7-9). It takes the sum of hourly operating costs, previously defined in equation (6-4), over the 24-hours period. The objective function is subject to the equality and inequality constraints discussed in *Section 6.2*.

$$\mathcal{F} = min\left\{\sum_{hour=1}^{24} (Operating\ cost)_{hour}\right\} \quad (7\text{-}9)$$

7.4.2. MPC implementation using PSO

In order to understand how the MPC-based thermal storage management works, it is compared with a thermo-economic optimisation (in time series) without a storage, as shown in Fig. 7-3. The comparison also helps to highlight the flexibility advantages of the thermal storage.

Both algorithms start by taking data that describe the topology and parameters of the heating and electricity distribution networks, the location and coupling matrices of the energy

technologies (such as HP, CHP, gas boiler, wind turbine, thermal storage), time-series heat and electricity demands, electricity price signal, forecasts of renewable sources and the capacity constraints of the components in the system. Based on the input data, the integrated load flow problem is formulated and the decision variables are identified. This is followed by the definition of the PSO structures. The main difference between Fig. 7-3(a) and Fig. 7-3(b) lies on how the respective PSOs are implemented.

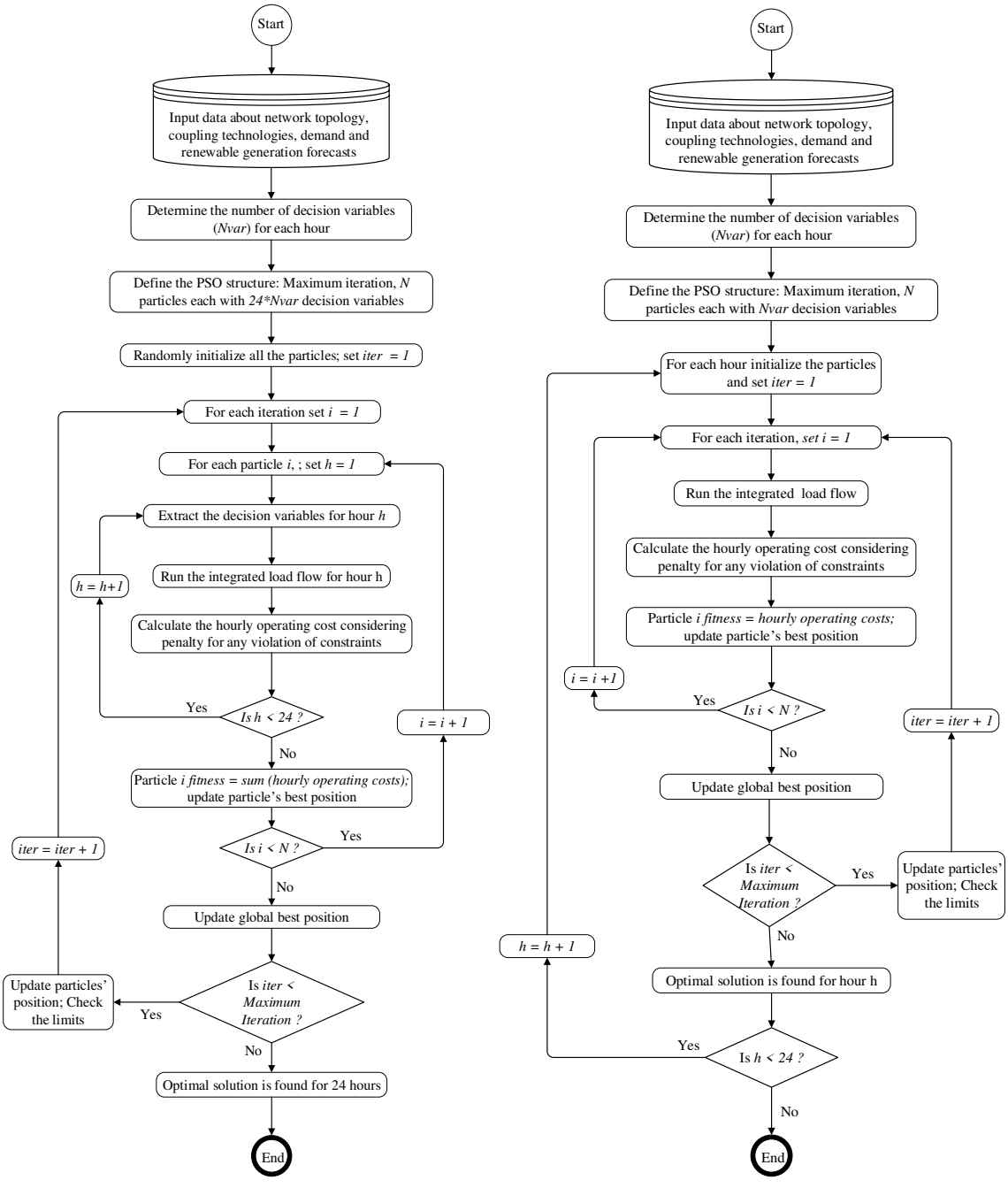

Fig. 7-3. Flow chart of thermo-economic optimisation: (a) with a thermal storage (MPC) and (b) without a thermal storage.

The MPC in Fig. 7-3(a) considers particles comprising of the decision variables of each hour cascaded over the 24-hours horizon. To evaluate the fitness of each particle, the values of the decision variables for each hour are extracted from the particle's position. Then, the integrated load flow model (discussed in *Section 4.5*) is evaluated on an hourly-basis. This includes simulation of the thermal storage. Hourly operating costs are calculated including penalties for any violation of the constraints. The total operating cost over the 24 hours gives the fitness of the particle. This is compared with the particle's best fitness in the past. The particle's best position is updated accordingly. Once all the particles have gone through similar steps, the global best position is updated by comparing the best fitness of all the particles with the previous global best fitness value. Equations (6-2) and (6-3) are then applied to determine the new position of all particles and the iteration of the PSO continues.

Unlike to the MPC algorithm, the case without a thermal storage (shown in Fig. 7-3(b)) does not need to have particles with cascaded hourly decision variables. The decision variables in a given hour have no relation with the corresponding variables in another hour. As a result, the optimisation can be decomposed into several sub-problems (one for each hour) with reduced dimensions. For each hour, the corresponding decision variables are randomly initialized. The integrated load flow model is then evaluated based on which the operating cost is calculated taking any penalty factor into account. The calculated operating cost will be the particle's fitness and is compared with particle's best fitness (in the past) in order to update its best position. Once all particles are evaluated that way, the global best position is updated by comparing the best fitness value of all particles with the global best fitness value achieved so far. The particles' and global best positions are then used to determine the new positions of each particle using equations (6-2) and (6-3). The PSO iteration continues until a satisfactory solution is achieved or a pre-set maximum iteration number is reached. Then, the optimisation moves to the next hour and the process repeats for all the 24 hours.

7.5. Description of the case study – Case 7-A

An energy system consisting of 13 hubs, as shown in Fig. 7-4, is considered to demonstrate the proposed methodology. A thermal storage is installed at hub 1, a HP at hub 2, a wind power plant at hub 5, a gas boiler at hub 6 and a CHP at hub 10. As it can be seen from Fig. 7-4, the hubs having the HP and the thermal storage are separated by a very short distance in order to make the case study closer to the common practice of putting them together. Treating them as separate hubs enables us to explore the thermal storage operating parameters. Hub 1 is also used as a slack hub.

7.5.1. Assumptions

All the heating network pipes are assumed to be DN-50 type with standard insulation, data taken from [118]. To avoid noise and wearing in the pipes, the water speed inside the pipes should not exceed 3.5 m/s [139, 154]. This implies an upper bound flowrate limit of 7.85 kg/s for all DN-50 pipes.

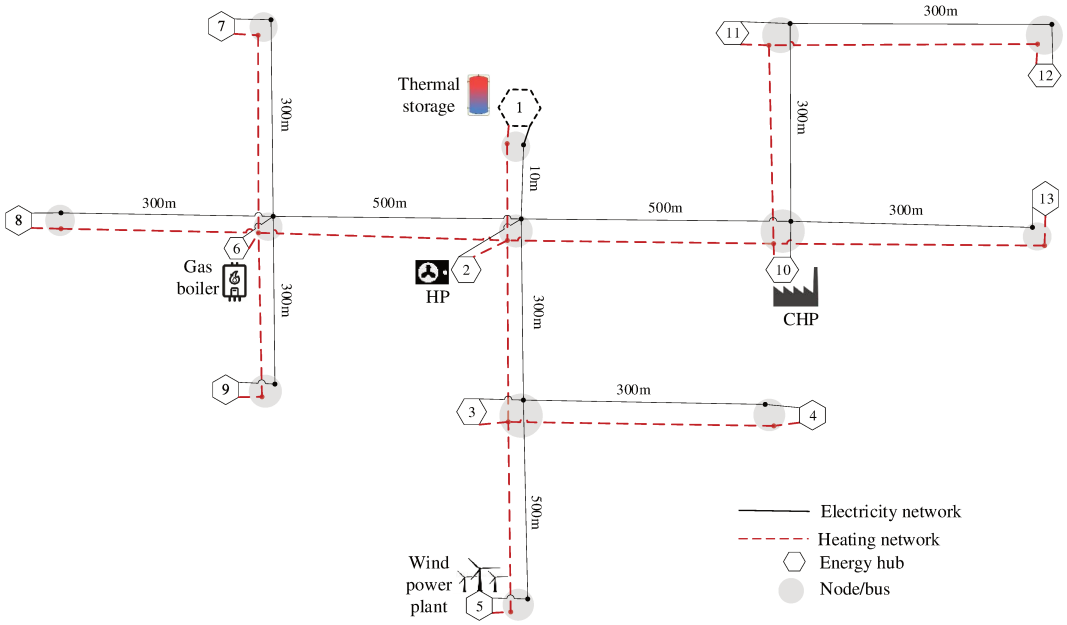

Fig. 7-4. Layout of a 13-hubs combined heating and electricity distribution network considered for Case 7-A.

The electricity network is balanced 4.16 kV three-phase system. All transmission lines are ACSR Waxwing type with resistance, reactance, susceptance and ampacity values of 0.262 Ω/km, 0.386 Ω/km, 4.31 μS/km and 480 A, respectively [141]. The allowed nodal voltage range is between 0.95 and 1.05 per unit.

The CHP plant has a gas intake capacity of 538 kW, and its thermal and electrical efficiencies are 49 % and 37 %, respectively [54]. It runs at unity power factor. The gas boiler can take a maximum of 300 kW of gas with a thermal efficiency of 90 %. The HP is rated at 200 kW_e and is assumed to run at constant COP of 4.0 with a 0.9 lagging power factor. A wind power plant of type Winflow (500 kW) running at unity power factor is considered. Its output is forecasted using HOMER [33]. The operating cost of the wind power plant is neglected.

The price of gas is 0.064 €/kWh. Two price levels are considered for grid electricity (for active power): 0.15 €/kWh during the cheap hours (23:00 – 06:00) and 0.2 €/kWh during the expensive hours (07:00 – 22:00), respectively. These prices are rough approximations of the French market for 2020.

In order to investigate the full capacity of the thermal storage, the heating network is assumed to be in islanded mode. As a result, there are no import and export possibilities in the heating network. The electrical network, on the other hand, can import from the external grid. But the incentives for feeding in excess production is assumed to be zero.

A supply temperature ranges of 65 – 95 °C is assumed for all hubs injecting heat into the network. In *Section 6.4*, it has been shown that the lowest possible value of the return temperature at heat consuming hubs is always selected in the optimisation. Hence, a fixed return temperature of 35 °C is assumed at all heat consuming hubs, except the slack hub where the storage is installed. The temperature at any place on the heating network is not allowed

to fall below 15 °C. A 40 m^3 thermal storage is considered with 1.1189 W/m^2K loss factor. Its initial temperature is assumed to be uniform and equal to 35 °C. Its dimensions are assumed to satisfy equation (7-2).

7.5.2. Input data

All, but hubs 1 and 5, have both electricity and heat demands. Fig. 7-5 shows the hourly heat and active electric power demands at different hubs for a typical winter day in February. The heat demand profiles are taken from Nantes DHN (the nodes are arbitrarily selected). Then, the electricity load profiles are generated using the correlation between the heat and electricity demands of residential buildings for similar weather, which are derived from online data available at Open Energy Information database [122]. All connected electrical loads are assumed to have a 0.95 lagging power factor. As it can be seen from Fig. 7-5, the highest peak demand for heat and electricity are recorded at hub 4 whereas hub 12 shows a relatively lowest demand.

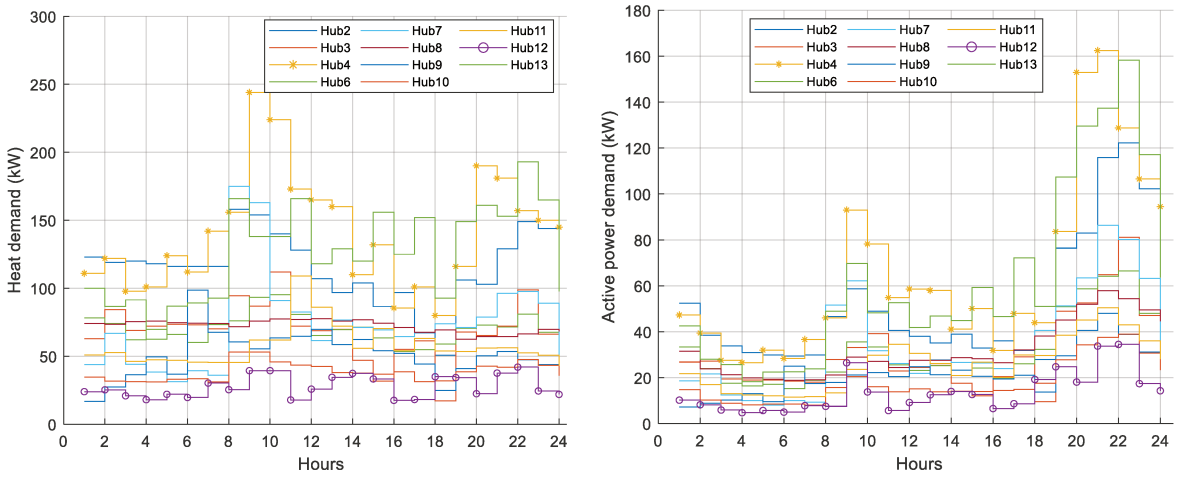

(a) (b)

Fig. 7-5. Demand profiles at different hubs: (a) heat power and (b) active electric power.

The forecasts of soil temperature, total demands and wind generation are plotted in Fig. 7-6 together with the price signal of grid electricity. The variation of soil temperature, taken at 1 m below the surface of earth (data taken from [123]), is not significant (i.e. between 4.3111 and 4.389 °C). This pattern is assumed around the outer surfaces of all heating network pipes and around the thermal storage.

It can be observed from Fig. 7-6 that the peak heat and electricity demands occur at different times. The heat demand peaks (1164.7 kW) at 9:00 while the active and reactive power demands reach their peaks (858.55 kW and 281.6 kvar, respectively) at 21:00. The daily residential demands of heat, active and reactive powers are about 20.228 MWh, 9.335 MWh and 3.062 Mvarh, respectively. The additional electricity demands due to the operation of the HP are discussed in *Section 7.6.2*.

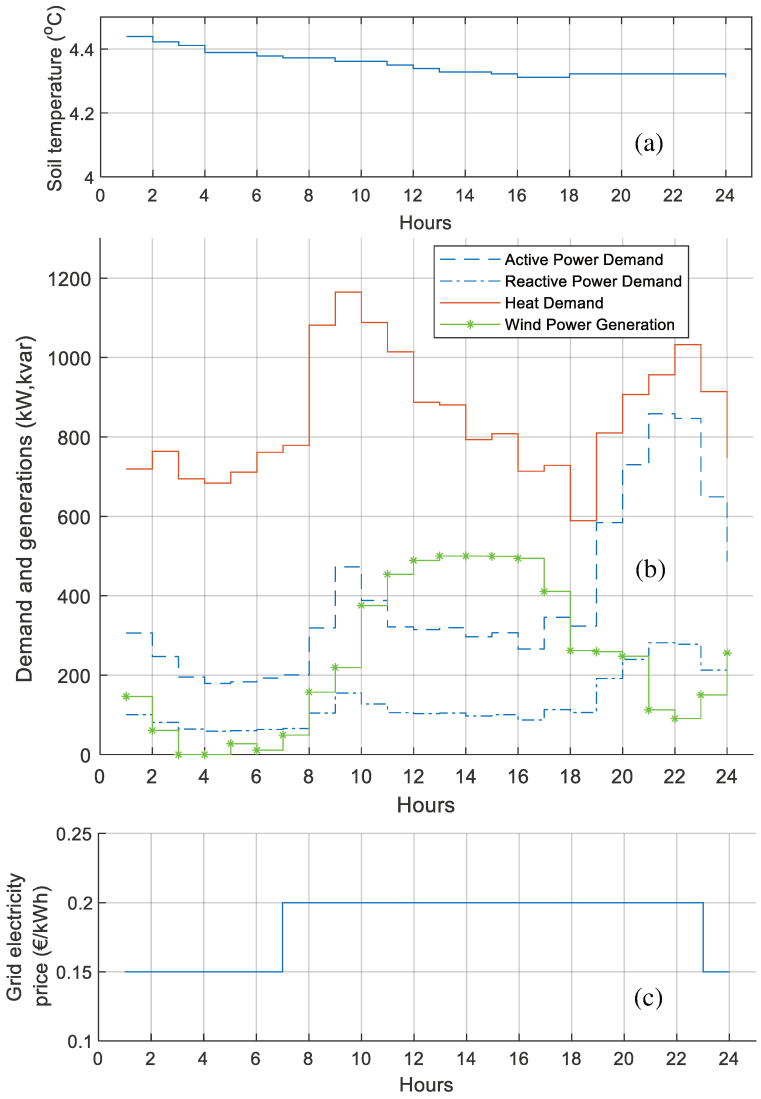

Fig. 7-6. Forecasts of (a) soil temperature, (b) total active, reactive and heat power demands, and wind turbine power generation, and (c) price of electricity from the grid for a typical winter day.

Fig. 7-6 also shows that the active power generated from the wind power plant, with zero cost, is higher than the active power demand during the hours 11:00 – 17:00. The surplus amounts 1.176 MWh, which accounts for 20.37% of the total production from the wind power plant (5.772 MWh). In addition, during the off-peak hours, the grid electricity price is relatively cheaper, as shown in Fig. 7-6(c). The integrated optimisation is conducted to exploit such opportunities by finding out the synergy of the heating and the electricity energy systems, which could be otherwise impossible.

7.5.3. Scenarios and PSO structures used

The values of six main decision variables for each hour are determined directly by the optimisation algorithm. Three of them are for the consumptions of the CHP, the HP and the gas boiler while the other three are for the supply temperatures at the corresponding hubs.

The supply temperature of a given hub is considered in the optimisation if and only if the hub is injecting heat into the network, i.e. acting as a source. In addition, there are about four decision variables that are evaluated indirectly from the other decision variables using the integrated load flow model. Two of them are the supply temperature and heat power going to/from the storage while the other two are the active and reactive power imports at the slack hub.

In order to quantify the synergy obtained from thermal storage integration, two scenarios are defined as follows:

I. In the first scenario, the system is run without a thermal storage. A PSO with 30 particles (each with 10 decision variables) and 100 iterations is used at each hour, which is implemented using the algorithm described in Fig. 7-3(b).

II. The thermal storage is considered in the second scenario. The optimal values of 240 decision variables, for a 24-hours horizon, are determined using the MPC algorithm (Fig. 7-3(a)). The PSO in this scenario is set with 300 particles and 500 maximum iteration.

7.6. Results and discussions on Case 7-A

The results and discussions are presented in three subsections. First, energy balance and selected operating parameters of the heating network are discussed in *Section 7.6.1* followed by a discussion on the energy balance and selected operating parameters of the electricity distribution network in *Section 7.6.2*. A summary of results at the system level is then presented in *Section 7.6.3*.

7.6.1. Energy balance and operating parameters of the heating network

The heat generated from the CHP, the HP and the gas boiler in the two scenarios are shown in Fig. 7-7. The CHP is running at full capacity during all hours except between 11:00 – 18:00 in Scenario I and between 11:00 –17:00 in Scenario II. The hours 11:00 – 17:00 correspond to the interval when the electricity generation from the wind turbine is higher than the active electricity demand while hour 18:00 is when the heat demand is at its lowest value (see Fig. 7-6(b)).

For the system without a thermal storage, as shown in Fig. 7-7(a), the CHP and the HP are used most of the time (between hours 1:00 – 7:00, 17:00 – 21:00, at 23:00 and at 24:00). Combinations of the gas boiler, the HP and the CHP are used between 8:00 – 13:00, at 15:00 and at 22:00. At hour 16:00, the HP is used alone while the HP and the gas boiler are used together at hour 14:00.

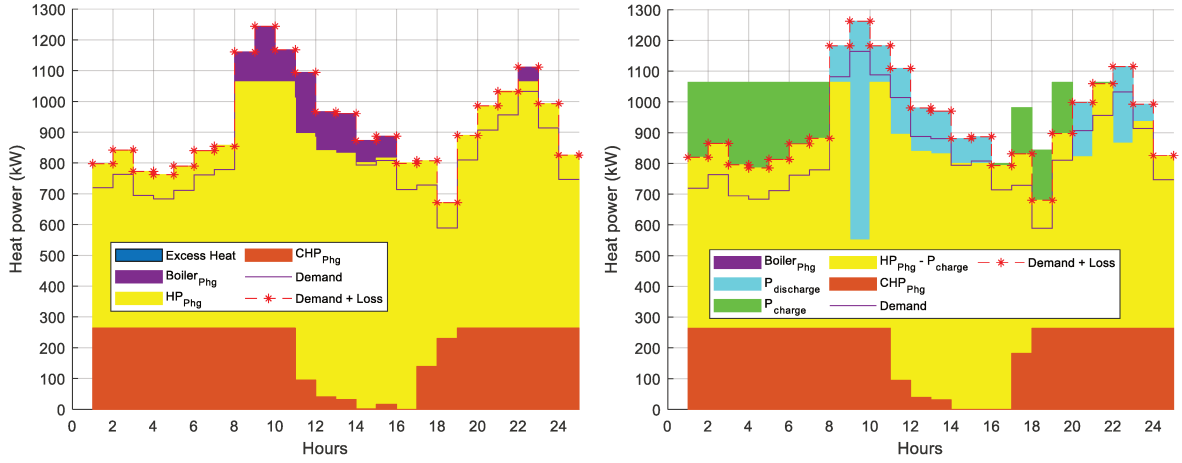

(a) (b)

Fig. 7-7. Heat generation and consumption for Case 7-A: (a) without a thermal storage and (b) with a thermal storage.

The HP runs at/near to its full capacity during hours 14:00 and 16:00 in Scenario I (Fig. 7-6(a)). This is due to the electricity generated from wind power plant which exceeds the demand (plus distribution loss) at these hours by 200.4 kW and 225.6 kW, respectively (see Fig. 7-6(b)). As a result, the HP runs at its maximum capacity taking 200 kW of the excess production. The left overs, 0.4 kW and 25.6 kW of active powers, are used by the circulation pumps (which require 1.9 kW and 1.04 kW respectively). Accordingly, there will be 24.56 kW of net surplus electricity at hour 16:00. The heat produced from the HP at hour 16:00 is sufficient to cover the demand and the loss. However, additional heat is required at 14:00 to compensate the distribution loss (nearly 100 kW). As the electricity demand is already met, the gas boiler is opted over the CHP for its higher thermal efficiency to cover the heat deficit. This implies that the economic dispatch of the technologies at a given hour highly depends on the heat and electricity demands, the price of the different energy carriers and their availability.

The terms 'P_{charge}' and '$P_{discharge}$' in Fig. 7-7(b) refer to the charging and discharging heat power flows to and from the storage, respectively. The figure shows that the gas boiler is completely avoided, and the peak-hour heat demands are effectively shifted to the hours when there is cheap electricity. It also shows that there is higher discharge from the thermal storage at hour 9:00. This hour corresponds to the peak heat demand, expensive grid electricity price and a wind generation lower than the active power demand (see Fig. 7-6(b)). Hence, the CHP generates heat and electricity at full capacity. Part of the electricity is used to supply the electricity demand and the remaining is used to run the HP. Any deficit is then covered by discharging the thermal storage.

The charging and discharging evolution of the thermal storage can be seen in Fig. 7-8. The left axis shows the stored energy (in blue) as a measure of the state of charge while the right axis shows the temperatures at different layers (in red). The stored energy is calculated by taking 35 $^{\circ}$C as a zero reference. It can also be observed that the thermal storage was fully discharged twice in the 24 hours. The negative values of stored energy, at some hours after

the storage is fully discharged, are caused by the temperature drops below 35 °C due to the heat loss to the surrounding soil. On the other hand, the temperature at the top layer is always below the maximum of 95 °C (maximum temperature in the system). This shows that the storage did not yet reach its full capacity.

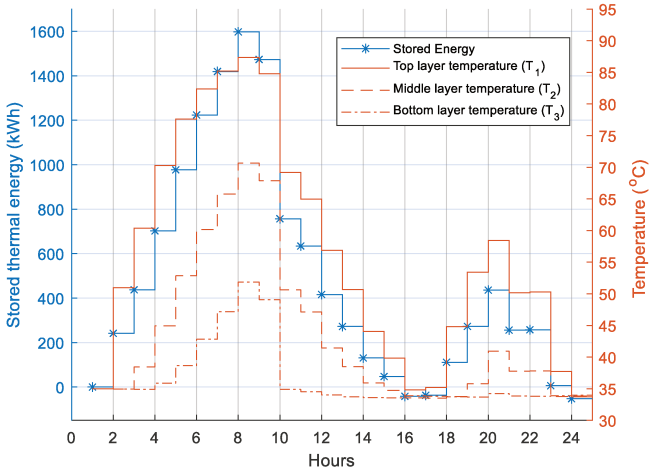

Fig. 7-8. The state of charge and temperature profiles at different layers of the thermal storage – Case 7-A.

The temperature profiles of selected hubs are shown in Fig. 7-9. Hubs 1, 2, 6 and 10 corresponds to the location of the thermal storage, HP, gas boiler and CHP, respectively. It can be seen from Fig. 7-9(a) that the supply temperatures are close to 65 °C most of the time. For some hours, the supply temperatures of hubs 6 and 10 drop slightly below 65 °C. These hours correspond to when the hubs are acting as a net heat consumer. This can be observed from their return temperatures being fixed at 35 °C at those hours. Fig. 7-9(b), on the other hand, shows that the source temperatures are near to 95 °C during the hours where the storage is charging (for example between 1:00 – 7:00). There is also a corresponding rise in the return temperature for hubs 1 and 2 above 35 °C.

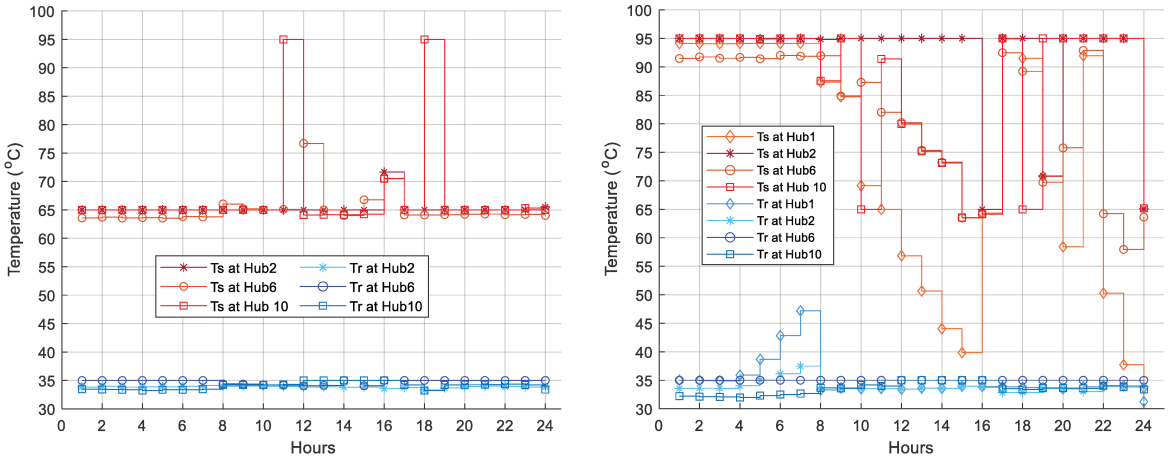

(a) (b)

Fig. 7-9. Supply and return temperature profile at selected hubs – Case 7-A: (a) without a thermal storage and (b) with a thermal storage.

The pipe flows for the two scenarios are shown in Fig. 7-10. All the pipe flows are below the acceptable limit of 7.85 kg/s. It can be seen that the flowrate in Pipe 3-5 is always zero in both scenarios. It is because of zero heat demand connected at Hub5. The flow in Pipe 2-10 changes between negative and positive in both scenarios, though at different magnitudes. The flow arte in Pipe 1-2 is almost zero all time in Scenario I indicating negligible heat flow (export) to the slack hub (see Fig. 7-10(a)). However, there is high flow rate (oscillating between negative and positive values) in the same pipe for scenario II corresponding to the charging and discharging of the thermal storage.

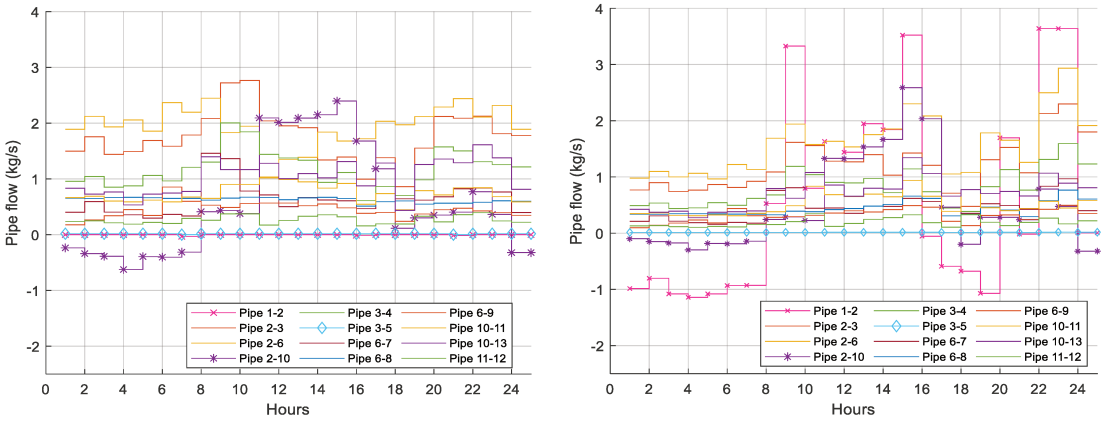

(a) (b)

Fig. 7-10. Pipe flows after thermo-economic optimisation on Case 7-A: (a) without a thermal storage and (b) with a storage 9.

7.6.2. Electricity network energy balance and operating parameters

The active and reactive power production and consumption for the two scenarios are shown in Fig. 7-11 and Fig. 7-12. The terms '$\text{Wind}_{\text{Pepg}}$' and '$\text{CHP}_{\text{Pepg}}$' refer to the active electricity produced from the wind and the CHP plants while 'HP_{Lep}' and 'HP_{Leq}' represent the active and reactive power consumptions of the HP, respectively. As discussed in the previous section, the surplus of electricity at hour 16:00 is because of the limit in the capacity of the HP. Comparing Fig. 7-11(a) and Fig. 7-11(b), it can be seen that the system with a thermal storage has imported more active electricity from the grid during the cheap hours 1:00 – 7:00. This additional electricity is converted into heat by the HP and is used to charge the thermal storage (see Fig. 7-7(b)). This is also reflected in the corresponding reactive power consumption of the HP shown in Fig. 7-12.

The active and reactive distribution losses are negligible in both scenarios. Having short transmission lines at a relatively high voltage level is the main contributing factor for such low distribution losses. This can be also observed from the voltage profiles shown in Fig. 7-13, which are very close to unity. Hub 1 is a reference hub and its voltage is fixed at 1 pu. The voltage magnitude at hub 5 follows the output pattern of the wind generation. As a result, it is the same in both cases. Slight differences, however, can be observed for hub 10 at hours 17:00 and 18:00 during which the CHPs in the two scenarios are dispatched at different levels (see Fig. 7-11).

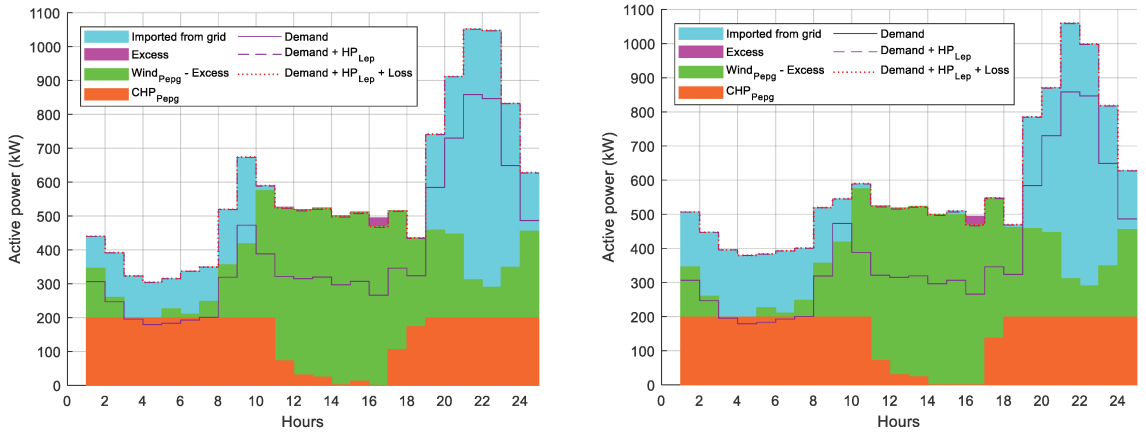

(a) (b)

Fig. 7-11. Active electricity generation and consumption for Case 7.1: (a) without a thermal storage and (b) with thermal storage.

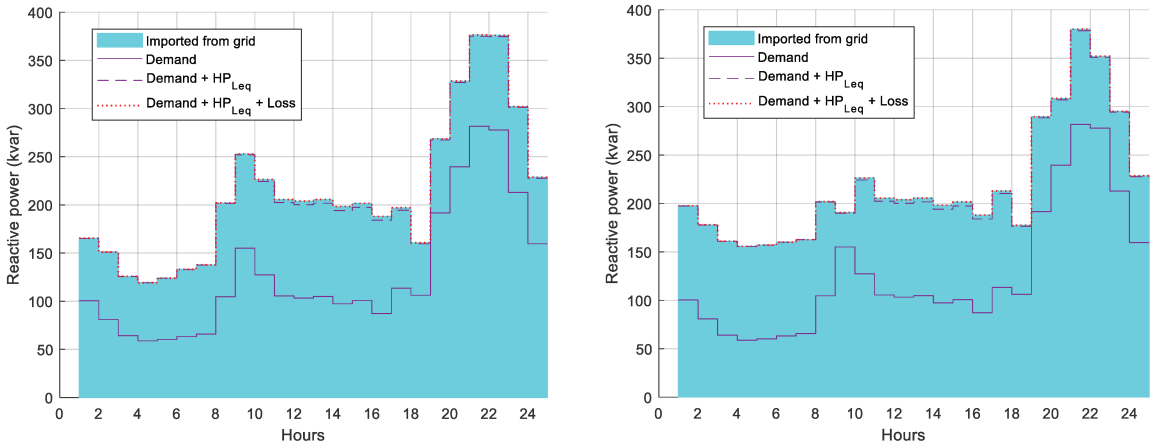

(a) (b)

Fig. 7-12. Reactive electricity generation and consumption for Case 7-A: (a) without a thermal storage and (b) with a thermal storage.

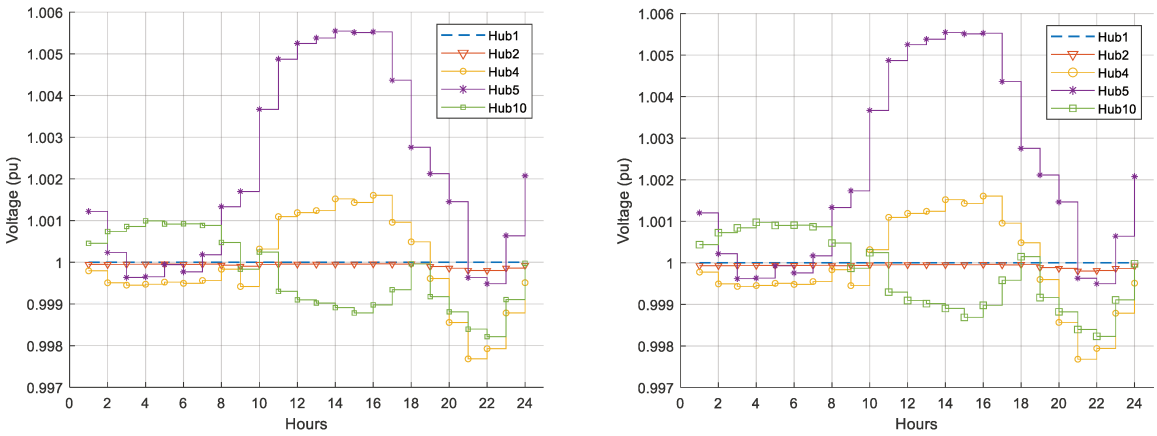

(a) (b)

Fig. 7-13. Voltage profile at different hubs in Case 7-A: (a) without a thermal storage and (b) with a thermal storage.

The root mean square value of current flowing through each transmission line is illustrated in Fig. 7-14. All line currents are far below the maximum limit of 480 A. The current profiles in the two scenarios look alike except for Line 1-2, through which the system interacts with the external electric grid. The difference corresponds to the time periods during which the thermal storage is charged and discharged which indirectly affects the dispatch of the HP.

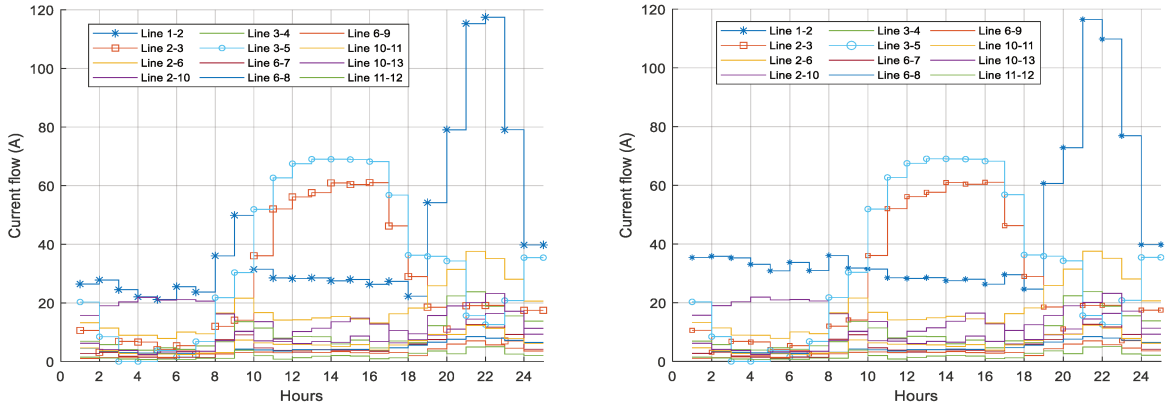

Fig. 7-14. Root mean square value of current flows through each transmission line for Case 7-A: (a) without a thermal storage and (b) with a thermal storage.

7.6.3. Overall system summary

Table 7-2 compares the system with and without a thermal storage using key parameters of the overall energy system. One of the results that shows the synergy of the heating and electricity networks is the amount of renewable-curtailment avoided. This is equivalently the amount of renewable generation effectively used in the system. Out of the 1.176 MWh surplus of electricity generated by the wind power plant (see *Section 7.5.3*), 97.90 % (with 7 kWh unused heat) is effectively used in the system without a thermal storage. Similarly, 97.96 % (with zero excess heat) of the curtailment is avoided in the system with a thermal storage. Only 24.66 kWh and 23.98 kWh of surplus wind generations are left unused, respectively (see Table 7-2).

Table 7-2: Summary of the optimisation results for the two scenarios in Case 7-A

	Without a thermal storage	**With a thermal storage (change)**
Total heat lost (kWh)	1900	2243 (18.1% ↑)
Electricity consumption of circulation pumps (kWh)	35.96	22.43 (38.1% ↓)
Total active electricity lost (kWh)	30.59	30.64
Total active electricity imported (kWh)	4109.9	4392.4 (6.9% ↑)
Surplus active electricity (kWh)	24.66	23.98
Reactive electricity imported (kvar)	5077.9	5238.4
Surplus heat (kWh)	7.03	2112.1 stored (10.4% of demand)
Heat imported (kWh)	0.0	2094.5 from storage
Gas used at the CHP and boiler (kWh)	9739.9 + 1140	9852.6 (9.5% CO_2 ↓)
Total operating cost (€)	1456.4	1426.8 (2.03% ↓)

Table 7-2 also shows that the system with a thermal storage totally avoided the gas boiler. As a result, the total gas consumption is reduced from 10877.5 kWh to 9852.6 kWh. This shows, roughly, a reduction of 9.45 % carbon emission. Furthermore, the thermal storage added flexibility by delivering 2094.5 kWh (about 10.4 % of the total heat demand). Its efficiency can be calculated by taking the ratio of discharged energy to the stored energy which gives 99.17 %.

It can also be seen from Table 7-2 that the system with a thermal storage exploited the cheap hours of the electricity price signal, as it is indicated by higher imported electricity (both active and reactive) from the grid.

In agreement with [28], the distribution loss in the heating network with a thermal storage is higher than the system without a storage (see Table 7-2). The reason is the requirement of higher temperature to charge the storage. The higher electricity consumption of circulation pumps in the system without a storage also indicates the presence of higher flow rate in the pipes caused by lower supply temperatures. However, there is no significant difference on the electricity distribution losses.

In terms of daily operating cost, the system with a thermal storage shows 2.03 % reduction. If it is taken alone, the economical saving for the particular day is not significant. However, considering the added flexibility in peak shaving together with the reduction in gas consumption, the thermal storage is still worthy to consider. Moreover, the results are only for a single day to illustrate the capacity of the tool. Annual optimisation should be combined with financial analysis of the whole system over its entire life span in order to determine the feasibility of thermal storage integration for the given case study, which is outside the scope of this thesis.

7.7. Summary

This chapter demonstrated the capacity of the EEH modelling approach, combined with PSO, in capturing the synergy between electricity and heat distribution networks in the presence of intermittent renewables and variable price signals. An energy system consisting of a CHP, HP, gas boiler, wind power plant and a thermal storage tank is investigated. A three layer stratified model of the thermal storage is incorporated into the integrated load flow model. Thermo-economic optimisation is then conducted using two scenarios. The first scenario used a simple PSO on hourly bases without the consideration of the thermal storage. An optimal management of the thermal storage is considered in the second scenario using a PSO-based MPC over a 24-hours horizon. The results show that significant amount of curtailment can be avoided in both scenarios. The scenario with a thermal storage has showed further advantages in terms of flexibility (peak shaving), reduction in emission and lower operating cost. It can be concluded that modelling and optimisation of MES based on the EEH approach is very effective in capturing the synergy from coupled electricity and heating networks and in quantifying the additional flexibility that can be obtained from thermal storage integration.

8. Closure

This chapter summarises the main findings and observations that are discussed in the previous chapters. It also highlights the potential users, the delimitations and possible ways that can be taken to complement and improve the tool developed in this thesis. In addition, both technical and market-oriented research paths that can be followed using the tool as a platform are identified.

8.1. Conclusions

This thesis presented a new approach in modelling, simulation and optimisation of multi-energy systems. The research questions listed in *Section 1.2* are addressed as follows.

1. *How can we capture the key operating parameters of the electricity and heat distribution networks consisting of meshed topologies with prosumers (nodes that act as producers and consumers alternatively)?*

A general framework of modelling the steady state load flow problem of multi-carrier distribution networks is formulated based on the extended energy hub concept. The modelling approach is then illustrated by developing a tool that can be used to conduct integrated load flow studies on highly coupled electricity and heating networks.

The algorithm, developed on MATLAB®, consists of more flexible hydraulic model and more realistic thermal model. Whenever it is required to simulate different network configurations, the user needs only to feed in the network data. The system of equations and the Jacobian matrix required for solving the integrated load flow problem are automatically configured, by which the tool overcomes the limitations of the models reported in literature. Comparative study also showed that the model proposed in this theses has better accuracy.

The capacity of the tool is also demonstrated in handling bidirectional power flows through the branches and between the hubs and the network. A given energy hub can operate alternatively either as a producer or as a consumer. Varieties of coupling technologies can also be integrated into the tool through the coupling matrices. CHPs, HPs, HOBs, wind power plants, solar photovoltaic and thermal storage are considered in different case studies with the full consideration of the operating parameters of both heating and electricity distribution networks.

The tool is tested with different network topologies consisting of highly coupled electricity and heating networks and the results found are consistent with the governing laws of Physics. The results of the integrated load flow study give the details of network operating parameters

such as voltage, mass flow rate, temperature, pressure, heat loss, electricity loss, slack hub generations and amount of power flow through each pipe and transmission line.

2. *Could the location of coupling technologies affect the performance of the overall energy system?*

Multiple-hours load flow studies are also conducted in the form of a pseudo-dynamic simulation on coupled electricity and heating networks consisting of a CHP, solar PV, gas boiler and HPs. It has been observed that the sizing of generation and coupling technologies based on only one type of demand profile could lead to undersized or oversized generation capacity for the other network. Comparative studies also showed that the HPs' location affects the distribution losses and operating parameters of both distribution networks.

3. *How can the optimal placement of the coupling technologies be determined? How can they be dispatched optimally without compromising the constituent distribution networks?*

For economical dispatch of generation units and coupling technologies, with the full consideration of the distribution networks' parameters, a metaheuristic optimisation algorithm is developed based on the PSO technique. It is applied to find the optimal location and sizes of distributed generation and coupling technologies. Two management strategies are compared: the first strategy takes only the heating network and neglects the electricity network while the second strategy considers both networks. The results show that optimising the location and sizes of HPs only from the heating network point of view could lower the heat loss. But, it is demonstrated that such management strategy may cause overloading and more losses in the electricity distribution network. It could also lead to unacceptable voltage profiles. The problem gets worse especially when large HPs are installed in a low voltage distribution network. On the other hand, an integrated optimisation that considers the constraints and distribution losses in both networks resulted in a lower operational cost for the overall system and a better voltage profile in the electricity distribution network.

The circulation pumps are used to overcome two types of pressure losses. The first corresponds to the frictional losses in the pipes while the second is related to the minimum pressure difference required at the substations (on primary side). Their relative magnitude depends on the size and operating strategy of the heating network. It is observed that the electricity consumption of circulation pumps is generally not significant compared to the total electricity demand. However, as the total cost of pumping energy can compete with the cost of heat loss in the network, especially if there are very cheap heat sources, the pumping cost should be taken into account in the thermo-economic optimisations.

A step-by-step approach of identifying and isolating lossy branches of a meshed DHN is demonstrated using an integrated optimal power flow. Such approach helps to operate the DHN efficiently during off-peak seasons (hours). The thermo-economic optimisation results further revealed that lowering the supply temperature does not necessarily result in a lower operational cost. The pumping cost may sometimes counter balance the advantages of lower

supply temperatures. However, lowering the return temperature of the consumers (on the primary side) is found to be always economical.

4. *What is the significance of a thermal storage in exploiting the synergies from electricity and heat distribution networks? How it can be optimally managed in the presence of intermittent renewables and variable price signals while considering all the technical constraints?*

The synergy from coupled heating and electricity networks can be further exploited using thermal storage tanks. Thermal storages can increase the flexibility in DHN by shaving the peak demands. They also increase the penetration of renewables in both electricity and heat distribution networks. An energy system consisting of a CHP, HP, gas boiler, wind power plant and thermal storage is investigated. Variable price signal for grid electricity is also considered. A PSO-based MPC is implemented to optimise the system over a 24-hours horizon. It is showed that significant amount of renewable curtailment can be avoided by coupling electricity and heating networks. Moreover, integrating thermal storage is found to have a 2.03% lower operating cost and 9.45% lower carbon emission than a system without a thermal storage. The thermal storage also made it possible to shift about 10.4% of the heat demand effectively from the peak hours toward the cheap electricity hours.

It is demonstrated (through case studies) that the EEH-based simulation and optimisation methodologies proposed in this thesis are scalable, flexible and very effective in capturing the important operating parameters and quantifying the synergy that can be obtained from the integrated electricity and heating networks.

8.2. Delimitations and recommendations for improvement

The case studies considered in this thesis are carefully selected to demonstrate the capacity of the tool and to pinpoint the scientific gaps that can be addressed by the proposed methodology. There are, however, some delimitations that could be further improved.

As the main focus of this thesis is on the multi-carrier energy distribution networks, neither the operational details of power plants nor the detail parameters of end users are considered. Instead, energy sources and coupling technologies are considered as energy conversion device and are represented in terms of their conversion efficiencies. The coupling matrices in all case studies are assumed to have constant conversion efficiencies. For example, the COP of each HP and efficiency of the CHP are assumed to be the same during partial loading and at different operating temperatures. Their operation is also assumed to be in the continuous range with no ramping up/down constraints. Efficiency curves of the corresponding technologies can be incorporated to get results that are very close to the reality. The ramping up/down parameters can also be handled by clearly defining them in the optimisation constraints. The way the stratified model of a thermal storage is incorporated into the load flow model can be taken as an example showing how the details of some technologies can be integrated.

Newton-Raphson numerical method is implemented in this thesis aiming to show the more comprehensive approach of solving the integrated load flow problem. Other numerical techniques, such as Gauss-Seidel and Quasi-Newton methods, can be tested so that the computational cost can be reduced while simulating larger network sizes. Algorithms that are specific to radial distribution networks can also be investigated using the Newton-Raphson method as a benchmark. Similarly, the simple greedy algorithm used for topology optimisation can be further tuned to reduce the likelihood of sub-optimal solutions. It can also be extended to larger case studies of meshed electricity and heat distribution networks.

Energy demands at the end users are assumed to be very accurate forecasts. In addition, intermittent renewable energy sources, such as solar PV and wind power generations are included in different case studies. The HOMER [33] simulation tool is used to estimate their generation outputs. The forecasting procedure, however, is not discussed in this thesis. These assumptions can be improved by considering uncertainties, which is another research area where the proposed tool can be used as a base. The tool can also be used to conduct sensitivity analysis on MES as a function of renewables' availability, variations in price signals and location of coupling technologies (e.g. HP vs CHP as a function of electricity and fuel price variations).

The other limitation is on the assumption that the control system in both heating and electricity distribution networks are capable of realizing the load flow and thermo-economic optimisation results. For example, the circulation pumps and pressure valves of the heating network are not explicitly included in the model. Also the control system on the secondary side of each heat substation is assumed to have the capacity to handle the temperature and mass flow rates considered in the primary side. Any deviations from the reality can be addressed by adjusting the constraints of the operating parameters of the distribution network, such as temperature and mass flow rates.

The distribution networks and the associated energy technologies considered in all case studies are assumed operational. As a result, the operating cost is considered as a main variable in the objective functions of the optimisation case studies. This can be complemented by considering the emission and investment cost of the network and coupling technologies which can be then used for planning future energy systems or expansion of existing ones.

Yet another limitation is with regard to the thermal inertia in the heat distribution networks. The model presented in this thesis considers hourly steady state operation of both heating and electricity networks. Though the electricity network reaches to steady state in fraction of seconds, the thermal networks may take from minutes up to hours to reach a steady state depending on their sizes. In this thesis, the case studies considered are small enough to assume hourly steady state operation and neglect the heating network inertia. For very large heating networks, however, consideration of thermal inertia gives more accurate results from operational control point of view. In that regard, the way the stead state models of the corresponding networks are integrated can be used as a base to integrate the dynamic models of the electricity and heat distribution networks. That opens a wider research area in the integration of smart grids and smart thermal networks.

The MPC implemented for optimal management of a thermal storage considers only a 24-hours horizon. It can be expanded for simulation horizons longer than 24 hours. Any possible uncertainty in the demand and generation forecast can be handled by incorporating a sliding window into the MPC algorithm. Other optimisation algorithms can also be compared with. The results can be further complemented by considering larger network sizes with more distributed generations. Comparative study can also be made by varying the location of the slack hub or by considering multiple slack hubs. Distributed thermal and electrical storage systems can be also considered.

All the algorithms in this thesis are developed on MATLAB. Hence, all the interactions with the user are made using MATLAB files and Microsoft Excel spreadsheets. This can be improved by developing a more user-friendly and object-based version of the tool.

In all case studies, as much as possible, all the boundary conditions and physical parameters are taken to be very close to the real systems. Validations are made analytically by making sure that all the governing principles (Physics laws) are obeyed. It is expensive to validate the model by establishing practical case study with all the required distributed sensors, as such systems are not yet available. The barrier on data communication between the electricity and heat distribution system operators is yet another challenge to apply and validate the tool in the existing systems. This could be overcome in the future when an integrated energy market is established.

8.3. Potential users and the future energy market

The frontline potential users of the tool, developed in this thesis, are distribution system operators (DSOs) in both the electricity and heating sectors. The tool helps to minimize distribution losses and lower operating cost of urban distribution networks that involve coupling technologies, such as HPs and CHPs. It can also be used to simulate distribution network operating parameters, such as voltage, current, temperature and mass flow rate. In addition, contingency analysis can also be performed.

The application scope ranges from distribution networks connecting couple of residential areas up to districts and cities where both networks co-exist. For very large networks, aggregation techniques can be applied to reduce the complexity and computational burdens. Aggregation is a bottom-up approach in which subnetworks of a larger distribution network are simulated first within the boundary condition of the larger network. Based on the results, each subnetwork is then represented by a node as a generation/load unit to simulate the next higher level subnetwork. For example, voltage and temperature levels (or pipe sizes) can be used to subdivide the electricity and heat distribution networks, respectively. The other option is to subdivide the distribution networks geographically. Such methodologies are subject to further studies.

The main challenge in fully implementing and realizing the optimal solutions that can be obtained using the developed tool is the barrier that arises from the way the electricity and heating markets are structured. The electricity market is increasingly liberalised from time to

time while the heating sector is still monopolised dominantly by municipalities or few companies. The level of data communication and transparency between the two markets is very limited. While integration of the energy sectors is given much emphasis, the market integration is not given equal attention. For instance, there are supports (e.g. EU directives) to install large HPs in the heating sector. However, this might necessitate upgrading the electricity distribution network from where the HPs get power. As there is no such binding regulation/framework to share the additional investment cost, such projects may get delayed. Absence of common platform is one of the contributing factors.

The developed tool can be used to setup the missing platform for stakeholders (such as DSOs, generation operators, municipalities, investors and policy makers) to come together and investigate the technical, environmental and financial aspects of an integrated energy systems. The platform also opens a market-oriented research area by serving as a decision support tool in the process of designing a suitable structure for the future energy market. The simulation and optimisation results can be used as input in developing business models for investors and in identifying incentives for policy makers. That way, the synergies can be realized faster, and the energy transition towards the carbon-neutral energy system can be accelerated.

References

[1] R. Joyeux and R. D. Ripple, 'Household energy consumption versus income and relative standard of living: A panel approach', Energy Policy, vol. 35, no. 1, pp. 50–60, Jan. 2007, doi: 10.1016/j.enpol.2005.10.012.

[2] U. Al-mulali, 'Exploring the bi-directional long run relationship between energy consumption and life quality', Renew. Sustain. Energy Rev., vol. 54, pp. 824–837, Feb. 2016, doi: 10.1016/j.rser.2015.10.125.

[3] R. Nadimi and K. Tokimatsu, 'Modeling of quality of life in terms of energy and electricity consumption', Appl. Energy, vol. 212, pp. 1282–1294, Feb. 2018, doi: 10.1016/j.apenergy.2018.01.006.

[4] 'IEA – International Energy Agency', IEA. https://www.iea.org (accessed Apr. 15, 2020).

[5] M. Mohammadi, Y. Noorollahi, B. Mohammadi-ivatloo, and H. Yousefi, 'Energy hub: From a model to a concept – A review', Renew. Sustain. Energy Rev., vol. 80, no. Supplement C, pp. 1512–1527, Dec. 2017, doi: 10.1016/j.rser.2017.07.030.

[6] International Renewable Energy Agency, 'Energy Transition'. https://www.irena.org/energytransition (accessed Jul. 10, 2019).

[7] '#Envision2030 Goal 7: Affordable and Clean Energy | United Nations Enable'. https://www.un.org/development/desa/disabilities/envision2030-goal7.html (accessed Apr. 21, 2020).

[8] European Commission, 'Paris Agreement', Climate Action - European Commission, Nov. 23, 2016. https://ec.europa.eu/clima/policies/international/negotiations/paris_en (accessed Sep. 15, 2019).

[9] European Commission, 'Clean energy for all Europeans package', Energy - European Commission, Oct. 20, 2017. https://ec.europa.eu/energy/en/topics/energy-strategy-and-energy-union/clean-energy-all-europeans (accessed Sep. 15, 2019).

[10] Eurostat, 'SHARES (Renewables) - Eurostat'. https://ec.europa.eu/eurostat/web/energy/data/shares (accessed Apr. 16, 2020).

[11] Directive 2012/27/EU of the European Parliament and of the Council of 25 October 2012 on energy efficiency, amending Directives 2009/125/EC and 2010/30/EU and repealing Directives 2004/8/EC and 2006/32/EC Text with EEA relevance, vol. OJ L. 2012.

[12] European Commission, 'Heating and cooling (facts and figuers)', Energy - European Commission, Jul. 10, 2015. https://ec.europa.eu/energy/topics/energy-efficiency/heating-and-cooling_en (accessed Apr. 16, 2020).

[13] 'District Energy in Sweden', Euroheat & Power, Nov. 15, 2019. https://www.euroheat.org/knowledge-hub/district-energy-sweden/ (accessed Apr. 16, 2020).

[14] 'District Energy in Latvia | Euroheat & Power'. https://www.euroheat.org/knowledge-hub/district-energy-latvia/ (accessed Apr. 16, 2020).

[15] 'District Energy in the Netherlands', Euroheat & Power, May 01, 2017. https://www.euroheat.org/knowledge-hub/district-energy-netherlands/ (accessed Apr. 16, 2020).
[16] 'Energy Policies of IEA Countries - Sweden 2019 Review', p. 166, 2019.
[17] 'Energy Policies of IEA Countries - France 2016 Review'. https://www.iea.org/countries/France/ (accessed Jul. 09, 2019).
[18] 'Statistics | France - Total Primary Energy Supply (TPES) by source (chart)'. https://www.iea.org/statistics/?country=FRANCE&year=2016&category=Energy%20supply&indicator=TPESbySource&mode=chart&dataTable=BALANCES (accessed Sep. 15, 2019).
[19] 'Statistics | Sweden - Total Primary Energy Supply (TPES) by source (chart)'. https://www.iea.org/statistics/?country=SWEDEN&year=2016&category=Energy%20supply&indicator=TPESbySource&mode=chart&dataTable=BALANCES (accessed Sep. 15, 2019).
[20] 'IEA, World Energy Balances 2019 preliminary edition'. https://www.iea.org/statistics (accessed Jul. 11, 2019).
[21] H. Farhangi, 'The path of the smart grid', IEEE Power Energy Mag., vol. 8, no. 1, pp. 18–28, Jan. 2010, doi: 10.1109/MPE.2009.934876.
[22] P. Crespo Del Granado, Z. Pang, and S. W. Wallace, 'Synergy of smart grids and hybrid distributed generation on the value of energy storage', Appl. Energy, vol. 170, pp. 476–488, May 2016, doi: 10.1016/j.apenergy.2016.01.095.
[23] J. Driesen and R. Belmans, 'Distributed generation: challenges and possible solutions', in 2006 IEEE Power Engineering Society General Meeting, 2006, p. 8 pp.-, doi: 10.1109/PES.2006.1709099.
[24] H. Lund et al., '4th Generation District Heating (4GDH): Integrating smart thermal grids into future sustainable energy systems', Energy, vol. 68, pp. 1–11, avril 2014, doi: 10.1016/j.energy.2014.02.089.
[25] H. Lund, P. A. Østergaard, D. Connolly, and B. V. Mathiesen, 'Smart energy and smart energy systems', Energy, vol. 137, pp. 556–565, Oct. 2017, doi: 10.1016/j.energy.2017.05.123.
[26] J. Hennessy, H. Li, F. Wallin, and E. Thorin, 'Flexibility in thermal grids: a review of short-term storage in district heating distribution networks', Energy Procedia, vol. 158, pp. 2430–2434, Feb. 2019, doi: 10.1016/j.egypro.2019.01.302.
[27] H. Lund, N. Duic, P. A. Østergaard, and B. V. Mathiesen, 'Future district heating systems and technologies: On the role of smart energy systems and 4th generation district heating', Energy, vol. 165, pp. 614–619, Dec. 2018, doi: 10.1016/j.energy.2018.09.115.
[28] A. Vandermeulen, B. van der Heijde, and L. Helsen, 'Controlling district heating and cooling networks to unlock flexibility: A review', Energy, vol. 151, pp. 103–115, May 2018, doi: 10.1016/j.energy.2018.03.034.

[29] W. Gu, J. Wang, S. Lu, Z. Luo, and C. Wu, 'Optimal operation for integrated energy system considering thermal inertia of district heating network and buildings', Appl. Energy, vol. 199, pp. 234–246, Aug. 2017, doi: 10.1016/j.apenergy.2017.05.004.

[30] J. Zheng, Z. Zhou, J. Zhao, and J. Wang, 'Integrated heat and power dispatch truly utilizing thermal inertia of district heating network for wind power integration', Appl. Energy, vol. 211, pp. 865–874, Feb. 2018, doi: 10.1016/j.apenergy.2017.11.080.

[31] 'EnergyPLAN', EnergyPLAN. https://www.energyplan.eu/ (accessed Nov. 22, 2019).

[32] Natural Resources Canada, 'RETScreen', Mar. 10, 2010. https://www.nrcan.gc.ca/energy/software-tools/7465 (accessed Nov. 05, 2018).

[33] HOMER Energy, 'HOMER - Hybrid Renewable and Distributed Generation System Design Software'. https://www.homerenergy.com/ (accessed Nov. 05, 2018).

[34] European Commission, 'Heating and cooling', Energy - European Commission, Jul. 10, 2015. https://ec.europa.eu/energy/en/topics/energy-efficiency/heating-and-cooling (accessed Nov. 20, 2019).

[35] 'EU to fight energy waste with the first Heating and Cooling Strategy', European Commission - European Commission. https://ec.europa.eu/commission/presscorner/detail/en/MEMO_16_311 (accessed Apr. 16, 2020).

[36] S. Werner, 'District heating and cooling in Sweden', Energy, vol. 126, pp. 419–429, May 2017, doi: 10.1016/j.energy.2017.03.052.

[37] F. Levihn, 'CHP and heat pumps to balance renewable power production: Lessons from the district heating network in Stockholm', Energy, Jan. 2017, doi: 10.1016/j.energy.2017.01.118.

[38] H. Shahrokni, F. Levihn, and N. Brandt, 'Big meter data analysis of the energy efficiency potential in Stockholm's building stock', Energy Build., vol. 78, pp. 153–164, Aug. 2014, doi: 10.1016/j.enbuild.2014.04.017.

[39] K. Kontu, S. Rinne, and S. Junnila, 'Introducing modern heat pumps to existing district heating systems – Global lessons from viable decarbonizing of district heating in Finland', Energy, vol. 166, pp. 862–870, Jan. 2019, doi: 10.1016/j.energy.2018.10.077.

[40] R. Lund and U. Persson, 'Mapping of potential heat sources for heat pumps for district heating in Denmark', Energy, vol. 110, pp. 129–138, Sep. 2016, doi: 10.1016/j.energy.2015.12.127.

[41] R. Lund, D. D. Ilic, and L. Trygg, 'Socioeconomic potential for introducing large-scale heat pumps in district heating in Denmark', J. Clean. Prod., vol. 139, pp. 219–229, décembre 2016, doi: 10.1016/j.jclepro.2016.07.135.

[42] T. Ma, J. Wu, L. Hao, W.-J. Lee, H. Yan, and D. Li, 'The optimal structure planning and energy management strategies of smart multi energy systems', Energy, vol. 160, pp. 122–141, Oct. 2018, doi: 10.1016/j.energy.2018.06.198.

[43] M. Arnaudo, M. Topel, and B. Laumert, 'Techno-economic analysis of demand side flexibility to enable the integration of distributed heat pumps within a Swedish neighborhood', Energy, vol. 195, p. 117012, Mar. 2020, doi: 10.1016/j.energy.2020.117012.

[44] E. Widl et al., 'Studying the potential of multi-carrier energy distribution grids: A holistic approach', Energy, vol. 153, pp. 519–529, Jun. 2018, doi: 10.1016/j.energy.2018.04.047.

[45] J. Allegrini, K. Orehounig, G. Mavromatidis, F. Ruesch, V. Dorer, and R. Evins, 'A review of modelling approaches and tools for the simulation of district-scale energy systems', Renew. Sustain. Energy Rev., vol. 52, pp. 1391–1404, décembre 2015, doi: 10.1016/j.rser.2015.07.123.

[46] J. Keirstead, M. Jennings, and A. Sivakumar, 'A review of urban energy system models: Approaches, challenges and opportunities', Renew. Sustain. Energy Rev., vol. 16, no. 6, pp. 3847–3866, Aug. 2012, doi: 10.1016/j.rser.2012.02.047.

[47] P. Mancarella, 'MES (multi-energy systems): An overview of concepts and evaluation models', Energy, vol. 65, pp. 1–17, février 2014, doi: 10.1016/j.energy.2013.10.041.

[48] M. Aghamohamadi, M. Samadi, and I. Rahmati, 'Energy generation cost in multi-energy systems; an application to a non-merchant energy hub in supplying price responsive loads', Energy, vol. 161, pp. 878–891, Oct. 2018, doi: 10.1016/j.energy.2018.07.144.

[49] I. van Beuzekom, M. Gibescu, and J. G. Slootweg, 'A review of multi-energy system planning and optimisation tools for sustainable urban development', in 2015 IEEE Eindhoven PowerTech, Jun. 2015, pp. 1–7, doi: 10.1109/PTC.2015.7232360.

[50] P. C. Blaud, P. Haurant, F. Claveau, B. Lacarrière, P. Chevrel, and A. Mouraud, 'Modelling and control of multi-energy systems through Multi-Prosumer Node and Economic Model Predictive Control', Int. J. Electr. Power Energy Syst., vol. 118, p. 105778, Jun. 2020, doi: 10.1016/j.ijepes.2019.105778.

[51] P. Gabrielli, M. Gazzani, E. Martelli, and M. Mazzotti, 'Optimal design of multi-energy systems with seasonal storage', Appl. Energy, vol. 219, pp. 408–424, Jun. 2018, doi: 10.1016/j.apenergy.2017.07.142.

[52] E. A. Martinez Cesena and P. Mancarella, 'Energy Systems Integration in Smart Districts: Robust optimisation of Multi-Energy Flows in Integrated Electricity, Heat and Gas Networks', IEEE Trans. Smart Grid, vol. 10, no. 1, pp. 1122–1131, Jan. 2019, doi: 10.1109/TSG.2018.2828146.

[53] J. Wu, J. Yan, H. Jia, N. Hatziargyriou, N. Djilali, and H. Sun, 'Integrated Energy Systems', Appl. Energy, vol. 167, pp. 155–157, Apr. 2016, doi: 10.1016/j.apenergy.2016.02.075.

[54] 'Centrale de cogénération | Vitobloc 200 Type EM-199/263', Viessmann, Jun. 25, 2018. https://www.viessmann.fr/fr/chauffage-collectif/cogeneration/centrale-cogeneration/vitobloc-200-em-199-263.html (accessed Mar. 17, 2020).

[55] B. Awad, M. Chaudry, J. Wu, and N. Jenkins, 'Integrated optimal power flow for electric power and heat in a MicroGrid', in CIRED 2009 - 20th International Conference and Exhibition on Electricity Distribution - Part 1, Jun. 2009, pp. 1–4.

[56] M. Arnaudo, M. Topel, P. Puerto, E. Widl, and B. Laumert, 'Heat demand peak shaving in urban integrated energy systems by demand side management - A techno-economic

and environmental approach', Energy, vol. 186, p. 115887, Nov. 2019, doi: 10.1016/j.energy.2019.115887.

[57] X. Liu and P. Mancarella, 'Modelling, assessment and Sankey diagrams of integrated electricity-heat-gas networks in multi-vector district energy systems', Appl. Energy, vol. 167, pp. 336–352, 2016.

[58] M. Arnold, R. R. Negenborn, G. Andersson, and B. D. Schutter, 'Model-based predictive control applied to multi-carrier energy systems', in 2009 IEEE Power Energy Society General Meeting, Jul. 2009, pp. 1–8, doi: 10.1109/PES.2009.5275230.

[59] M. Geidl, 'Integrated Modeling and Optimisation of Multi-Carrier Energy Systems', Doctoral Thesis, ETH Zurich, 2007.

[60] M. Geidl and G. Andersson, 'Optimal Power Flow of Multiple Energy Carriers', IEEE Trans. Power Syst., vol. 22, no. 1, pp. 145–155, Feb. 2007, doi: 10.1109/TPWRS.2006.888988.

[61] H. Khorsand and A. R. Seifi, 'Probabilistic energy flow for multi-carrier energy systems', Renew. Sustain. Energy Rev., vol. 94, pp. 989–997, Oct. 2018, doi: 10.1016/j.rser.2018.07.008.

[62] R. Niemi, J. Mikkola, and P. D. Lund, 'Urban energy systems with smart multi-carrier energy networks and renewable energy generation', Renew. Energy, vol. 48, pp. 524–536, décembre 2012, doi: 10.1016/j.renene.2012.05.017.

[63] A. Shabanpour-Haghighi and A. R. Seifi, 'Multi-Objective Operation Management of a Multi-Carrier Energy System', Energy, vol. 88, pp. 430–442, août 2015, doi: 10.1016/j.energy.2015.05.063.

[64] P. Mancarella, 'Smart Multi-Energy Grids: Concepts, benefits and challenges', in 2012 IEEE Power and Energy Society General Meeting, Jul. 2012, pp. 1–2, doi: 10.1109/PESGM.2012.6345120.

[65] 'Welcome | TRNSYS : Transient System Simulation Tool'. http://www.trnsys.com/index.html (accessed Apr. 30, 2020).

[66] H. Madani, J. Claesson, and P. Lundqvist, 'Capacity control in ground source heat pump systems: Part I: modeling and simulation', Int. J. Refrig., vol. 34, no. 6, pp. 1338–1347, Sep. 2011, doi: 10.1016/j.ijrefrig.2011.05.007.

[67] A. Campos Celador, M. Odriozola, and J. M. Sala, 'Implications of the modelling of stratified hot water storage tanks in the simulation of CHP plants', Energy Convers. Manag., vol. 52, no. 8, pp. 3018–3026, Aug. 2011, doi: 10.1016/j.enconman.2011.04.015.

[68] Z. Tian, B. Perers, S. Furbo, and J. Fan, 'Thermo-economic optimisation of a hybrid solar district heating plant with flat plate collectors and parabolic trough collectors in series', Energy Convers. Manag., vol. 165, pp. 92–101, Jun. 2018, doi: 10.1016/j.enconman.2018.03.034.

[69] B.-S. Park, M. Imran, I.-Y. Hoon, and M. Usman, 'Thermo-economic optimisation of secondary distribution network of low temperature district heating network under local conditions of South Korea', Appl. Therm. Eng., vol. 126, pp. 117–133, Nov. 2017, doi: 10.1016/j.applthermaleng.2017.07.080.

[70] H. Zhang, L. Zhou, X. Huang, and X. Zhang, 'Decarbonizing a large City's heating system using heat pumps: A case study of Beijing', Energy, vol. 186, p. 115820, Nov. 2019, doi: 10.1016/j.energy.2019.07.150.

[71] H. Lund and B. V. Mathiesen, 'Energy system analysis of 100% renewable energy systems—The case of Denmark in years 2030 and 2050', Energy, vol. 34, no. 5, pp. 524–531, May 2009, doi: 10.1016/j.energy.2008.04.003.

[72] 'energyPRO', EMD International, Aug. 13, 2018. https://www.emd.dk/energypro/ (accessed Apr. 30, 2020).

[73] 'energyPRO Project Examples', EMD International. https://www.emd.dk/energypro/support/project-examples/ (accessed Apr. 30, 2020).

[74] K.-H. Lee, D.-W. Lee, N.-C. Baek, H.-M. Kwon, and C.-J. Lee, 'Preliminary determination of optimal size for renewable energy resources in buildings using RETScreen', Energy, vol. 47, no. 1, pp. 83–96, Nov. 2012, doi: 10.1016/j.energy.2012.08.040.

[75] Y. Pan, L. Liu, T. Zhu, T. Zhang, and J. Zhang, 'Feasibility analysis on distributed energy system of Chongming County based on RETScreen software', Energy, vol. 130, pp. 298–306, Jul. 2017, doi: 10.1016/j.energy.2017.04.082.

[76] 'Evaluation of region-specific residential energy systems for GHG reductions: Case studies in Canadian cities', Energy Policy, vol. 37, no. 4, pp. 1257–1266, Apr. 2009, doi: 10.1016/j.enpol.2008.11.004.

[77] G. Bekele and G. Tadesse, 'Feasibility study of small Hydro/PV/Wind hybrid system for off-grid rural electrification in Ethiopia', Appl. Energy, vol. 97, pp. 5–15, Sep. 2012, doi: 10.1016/j.apenergy.2011.11.059.

[78] L. Montuori, M. Alcázar-Ortega, C. Álvarez-Bel, and A. Domijan, 'Integration of renewable energy in microgrids coordinated with demand response resources: Economic evaluation of a biomass gasification plant by Homer Simulator', Appl. Energy, vol. 132, pp. 15–22, Nov. 2014, doi: 10.1016/j.apenergy.2014.06.075.

[79] M. Wegener, A. Isalgué, A. Malmquist, and A. Martin, '3E-Analysis of a Bio-Solar CCHP System for the Andaman Islands, India—A Case Study', Energies, vol. 12, no. 6, p. 1113, Jan. 2019, doi: 10.3390/en12061113.

[80] 'Optimisation of hybrid renewable energy polygeneration system with membrane distillation for rural households in Bangladesh', Energy, vol. 93, pp. 1116–1127, Dec. 2015, doi: 10.1016/j.energy.2015.09.109.

[81] C. Waibel, R. Evins, and J. Carmeliet, 'Co-simulation and optimisation of building geometry and multi-energy systems: Interdependencies in energy supply, energy demand and solar potentials', Appl. Energy, vol. 242, pp. 1661–1682, May 2019, doi: 10.1016/j.apenergy.2019.03.177.

[82] R. Evins, 'Multi-level optimisation of building design, energy system sizing and operation', Energy, vol. 90, Part 2, pp. 1775–1789, Oct. 2015, doi: 10.1016/j.energy.2015.07.007.

[83] R. Wu, G. Mavromatidis, K. Orehounig, and J. Carmeliet, ‘Multiobjective optimisation of energy systems and building envelope retrofit in a residential community’, Appl. Energy, vol. 190, pp. 634–649, Mar. 2017, doi: 10.1016/j.apenergy.2016.12.161.

[84] E. Yao, H. Wang, L. Wang, G. Xi, and F. Maréchal, ‘Thermo-economic optimisation of a combined cooling, heating and power system based on small-scale compressed air energy storage’, Energy Convers. Manag., vol. 118, pp. 377–386, juin 2016, doi: 10.1016/j.enconman.2016.03.087.

[85] C. Rubio-Maya, J. Uche-Marcuello, A. Martínez-Gracia, and A. A. Bayod-Rújula, ‘Design optimisation of a polygeneration plant fuelled by natural gas and renewable energy sources’, Appl. Energy, vol. 88, no. 2, pp. 449–457, Feb. 2011, doi: 10.1016/j.apenergy.2010.07.009.

[86] I. G. Moghaddam, M. Saniei, and E. Mashhour, ‘A comprehensive model for self-scheduling an energy hub to supply cooling, heating and electrical demands of a building’, Energy, vol. 94, no. Supplement C, pp. 157–170, Jan. 2016, doi: 10.1016/j.energy.2015.10.137.

[87] M. C. Bozchalui, S. A. Hashmi, H. Hassen, C. A. Canizares, and K. Bhattacharya, ‘Optimal Operation of Residential Energy Hubs in Smart Grids’, IEEE Trans. Smart Grid, vol. 3, no. 4, pp. 1755–1766, décembre 2012, doi: 10.1109/TSG.2012.2212032.

[88] S. D. Beigvand, H. Abdi, and M. La Scala, ‘A general model for energy hub economic dispatch’, Appl. Energy, vol. 190, pp. 1090–1111, Mar. 2017, doi: 10.1016/j.apenergy.2016.12.126.

[89] J. Wasilewski, ‘Integrated modeling of microgrid for steady-state analysis using modified concept of multi-carrier energy hub’, Int. J. Electr. Power Energy Syst., vol. 73, pp. 891–898, décembre 2015, doi: 10.1016/j.ijepes.2015.06.022.

[90] B. Leitner, E. Widl, W. Gawlik, and R. Hofmann, ‘A method for technical assessment of power-to-heat use cases to couple local district heating and electrical distribution grids’, Energy, vol. 182, pp. 729–738, Sep. 2019, doi: 10.1016/j.energy.2019.06.016.

[91] S. Bracco, F. Delfino, F. Pampararo, M. Robba, and M. Rossi, ‘A dynamic optimisation-based architecture for polygeneration microgrids with tri-generation, renewables, storage systems and electrical vehicles’, Energy Convers. Manag., vol. 96, pp. 511–520, May 2015, doi: 10.1016/j.enconman.2015.03.013.

[92] J. Li, J. Fang, Q. Zeng, and Z. Chen, ‘Optimal operation of the integrated electrical and heating systems to accommodate the intermittent renewable sources’, Appl. Energy, vol. 167, pp. 244–254, Apr. 2016, doi: 10.1016/j.apenergy.2015.10.054.

[93] X. Liu, J. Wu, N. Jenkins, and A. Bagdanavicius, ‘Combined analysis of electricity and heat networks’, Appl. Energy, vol. 162, pp. 1238–1250, Jan. 2016, doi: 10.1016/j.apenergy.2015.01.102.

[94] P. F. Boulos, K. E. Lansey, and B. W. Karney, Comprehensive Water Distribution Systems Analysis Handbook for Engineers and Planners. American Water Works Assn, 2006.

[95] A. Shabanpour-Haghighi and A. R. Seifi, ‘An Integrated Steady-State Operation Assessment of Electrical, Natural Gas, and District Heating Networks’, IEEE Trans.

Power Syst., vol. 31, no. 5, pp. 3636–3647, Sep. 2016, doi: 10.1109/TPWRS.2015.2486819.

[96] M. Rees, J. Wu, and B. Awad, 'Steady state flow analysis for integrated urban heat and power distribution networks', in 2009 44th International Universities Power Engineering Conference (UPEC), Sep. 2009, pp. 1–5.

[97] M. Moeini-Aghtaie, A. Abbaspour, M. Fotuhi-Firuzabad, and E. Hajipour, 'A Decomposed Solution to Multiple-Energy Carriers Optimal Power Flow', IEEE Trans. Power Syst., vol. 29, no. 2, pp. 707–716, Mar. 2014, doi: 10.1109/TPWRS.2013.2283259.

[98] M. Batić, N. Tomašević, G. Beccuti, T. Demiray, and S. Vraneš, 'Combined energy hub optimisation and demand side management for buildings', Energy Build., vol. 127, pp. 229–241, Sep. 2016, doi: 10.1016/j.enbuild.2016.05.087.

[99] D. C. Walters and G. B. Sheble, 'Genetic algorithm solution of economic dispatch with valve point loading', IEEE Trans. Power Syst., vol. 8, no. 3, pp. 1325–1332, août 1993, doi: 10.1109/59.260861.

[100] H.-T. Yang, P.-C. Yang, and C.-L. Huang, 'Evolutionary programming based economic dispatch for units with non-smooth fuel cost functions', IEEE Trans. Power Syst., vol. 11, no. 1, pp. 112–118, février 1996, doi: 10.1109/59.485992.

[101] C. Rani and D. P. Kothari, 'Dynamic Economic Emission Dispatch problem with valve-point effect', in 2012 International Conference on Emerging Trends in Electrical Engineering and Energy Management (ICETEEEM), décembre 2012, pp. 109–114, doi: 10.1109/ICETEEEM.2012.6494514.

[102] J. D. Glover, M. S. Sarma, and T. Overbye, Power System Analysis & Design, SI Version. Cengage Learning, 2012.

[103] J. M. Cano, Md. R. R. Mojumdar, J. G. Norniella, and G. A. Orcajo, 'Phase shifting transformer model for direct approach power flow studies', Int. J. Electr. Power Energy Syst., vol. 91, no. Supplement C, pp. 71–79, Oct. 2017, doi: 10.1016/j.ijepes.2017.03.007.

[104] B. E. Larock, R. W. Jeppson, and G. Z. Watters, Hydraulics of Pipeline Systems. CRC Press, 1999.

[105] M. Pirouti, 'Modelling and analysis of a district heating network', PhD, Cardiff University, 2013.

[106] H. B. Nielsen, 'Methods for analyzing pipe networks', J. Hydraul. Eng., vol. 115, no. 2, pp. 139–157, 1989.

[107] M. Fedorov, 'Parallel implementation of a steady state thermal and hydraulic analysis of heat exchanger', Pomiary Autom. Kontrola, vol. R. 55, nr 10, pp. 815–819, 2009.

[108] H. K. Winning and T. Coole, 'Explicit Friction Factor Accuracy and Computational Efficiency for Turbulent Flow in Pipes', Flow Turbul. Combust., vol. 90, no. 1, pp. 1–27, Jan. 2013, doi: 10.1007/s10494-012-9419-7.

[109] I. Gabrielaitiene, B. Bøhm, and B. Sunden, 'Modelling temperature dynamics of a district heating system in Naestved, Denmark—A case study', Energy Convers. Manag., vol. 48, no. 1, pp. 78–86, Jan. 2007, doi: 10.1016/j.enconman.2006.05.011.

[110] P. Jie, Z. Tian, S. Yuan, and N. Zhu, ‘Modeling the dynamic characteristics of a district heating network’, Energy, vol. 39, no. 1, pp. 126–134, Mar. 2012, doi: 10.1016/j.energy.2012.01.055.

[111] J. Duquette, A. Rowe, and P. Wild, ‘Thermal performance of a steady state physical pipe model for simulating district heating grids with variable flow’, Appl. Energy, vol. 178, pp. 383–393, Sep. 2016, doi: 10.1016/j.apenergy.2016.06.092.

[112] T. L. Bergman, F. P. Incropera, D. P. DeWitt, and A. S. Lavine, Fundamentals of heat and mass transfer. John Wiley & Sons, 2011.

[113] ‘MATLAB - MathWorks’. https://www.mathworks.com/products/matlab.html (accessed May 14, 2020).

[114] C. Aracil, P. Haro, D. Fuentes-Cano, and A. Gómez-Barea, ‘Implementation of waste-to-energy options in landfill-dominated countries: Economic evaluation and GHG impact’, Waste Manag., vol. 76, pp. 443–456, Jun. 2018, doi: 10.1016/j.wasman.2018.03.039.

[115] P. A. Østergaard and A. N. Andersen, ‘Booster heat pumps and central heat pumps in district heating’, Appl. Energy, vol. 184, pp. 1374–1388, Dec. 2016, doi: 10.1016/j.apenergy.2016.02.144.

[116] B. Bach, J. Werling, T. Ommen, M. Münster, J. M. Morales, and B. Elmegaard, ‘Integration of large-scale heat pumps in the district heating systems of Greater Copenhagen’, Energy, vol. 107, pp. 321–334, juillet 2016, doi: 10.1016/j.energy.2016.04.029.

[117] H. Averfalk, P. Ingvarsson, U. Persson, M. Gong, and S. Werner, ‘Large heat pumps in Swedish district heating systems’, Renew. Sustain. Energy Rev., vol. 79, no. Supplement C, pp. 1275–1284, Nov. 2017, doi: 10.1016/j.rser.2017.05.135.

[118] Isoplus, ‘isoplus: Flexible and rigid pipes and pipeline systems: isoplus - isoplus Fernwärmetechnik’. http://www.isoplus-pipes.com/ (accessed Sep. 03, 2017).

[119] S. Frederiksen and S. Werner, District Heating and Cooling. Studentlitteratur AB, 2013.

[120] M.-H. Shariatkhah, M.-R. Haghifam, M. Parsa-Moghaddam, and P. Siano, ‘Modeling the reliability of multi-carrier energy systems considering dynamic behavior of thermal loads’, Energy Build., vol. 103, pp. 375–383, Sep. 2015, doi: 10.1016/j.enbuild.2015.06.001.

[121] K. Sartor and P. Dewalef, ‘Experimental validation of heat transport modelling in district heating networks’, Energy, vol. 137, pp. 961–968, Oct. 2017, doi: 10.1016/j.energy.2017.02.161.

[122] ‘Open Energy Information: Commercial and residential hourly load profile’. https://openei.org/datasets/files/961/pub/ (accessed Jan. 08, 2018).

[123] ‘AgriMet Pacific Northwest Region | Bureau of Reclamation’. https://www.usbr.gov/pn/agrimet/webagdayread.html (accessed Dec. 07, 2018).

[124] M. Nemati, M. Braun, and S. Tenbohlen, ‘Optimisation of unit commitment and economic dispatch in microgrids based on genetic algorithm and mixed integer linear

programming', Appl. Energy, vol. 210, pp. 944–963, Jan. 2018, doi: 10.1016/j.apenergy.2017.07.007.

[125] P. Subbaraj, R. Rengaraj, and S. Salivahanan, 'Enhancement of combined heat and power economic dispatch using self adaptive real-coded genetic algorithm', Appl. Energy, vol. 86, no. 6, pp. 915–921, Jun. 2009, doi: 10.1016/j.apenergy.2008.10.002.

[126] C. Yammani, S. Maheswarapu, and S. K. Matam, 'A Multi-objective Shuffled Bat algorithm for optimal placement and sizing of multi distributed generations with different load models', Int. J. Electr. Power Energy Syst., vol. 79, pp. 120–131, Jul. 2016, doi: 10.1016/j.ijepes.2016.01.003.

[127] S. Pazouki, A. Mohsenzadeh, S. Ardalan, and M. R. Haghifam, 'Optimal place, size, and operation of combined heat and power in multi carrier energy networks considering network reliability, power loss, and voltage profile', Transm. Distrib. IET Gener., vol. 10, no. 7, pp. 1615–1621, 2016, doi: 10.1049/iet-gtd.2015.0888.

[128] T. Niknam, R. Azizipanah-Abarghooee, and J. Aghaei, 'A new modified teaching-learning algorithm for reserve constrained dynamic economic dispatch', IEEE Trans. Power Syst., vol. 28, no. 2, pp. 749–763, mai 2013, doi: 10.1109/TPWRS.2012.2208273.

[129] A. Shabanpour-Haghighi, A. R. Seifi, and T. Niknam, 'A modified teaching–learning based optimisation for multi-objective optimal power flow problem', Energy Convers. Manag., vol. 77, pp. 597–607, Jan. 2014, doi: 10.1016/j.enconman.2013.09.028.

[130] T. Niknam, M. R. Narimani, J. Aghaei, S. Tabatabaei, and M. Nayeripour, 'Modified Honey Bee Mating optimisation to solve dynamic optimal power flow considering generator constraints', Transm. Distrib. IET Gener., vol. 5, no. 10, pp. 989–1002, Oct. 2011, doi: 10.1049/iet-gtd.2011.0055.

[131] S. Kansal, V. Kumar, and B. Tyagi, 'Hybrid approach for optimal placement of multiple DGs of multiple types in distribution networks', Int. J. Electr. Power Energy Syst., vol. 75, pp. 226–235, Feb. 2016, doi: 10.1016/j.ijepes.2015.09.002.

[132] J. Hazra and A. K. Sinha, 'A multi-objective optimal power flow using particle swarm optimisation', Eur. Trans. Electr. Power, vol. 21, no. 1, pp. 1028–1045, Jan. 2011, doi: 10.1002/etep.494.

[133] C. Marguerite, B. Bourges, and B. Lacarrière, 'Application of a District Heating Network (dhn) Model for an Ex-Ante Evaluation to Support a Multi-Sources Dh', presented at the 13th Conference of International Building Performance Simulation Association, August 26-28, Chambéry, France, Aug. 2013.

[134] M. Vesterlund, A. Toffolo, and J. Dahl, 'Optimisation of multi-source complex district heating network, a case study', Energy, vol. 126, pp. 53–63, May 2017, doi: 10.1016/j.energy.2017.03.018.

[135] J. Kennedy and R. Eberhart, 'Particle swarm optimisation', in Proceedings of ICNN'95 - International Conference on Neural Networks, Nov. 1995, vol. 4, pp. 1942–1948 vol.4, doi: 10.1109/ICNN.1995.488968.

[136] M. R. Bonyadi and Z. Michalewicz, ‘Particle Swarm Optimisation for Single Objective Continuous Space Problems: A Review’, Evol. Comput., vol. 25, no. 1, pp. 1–54, Mar. 2016, doi: 10.1162/EVCO_r_00180.

[137] M. R. D. Ullmann, K. F. Pimentel, L. A. de Melo, G. da Cruz, and C. Vinhal, ‘Comparison of PSO variants applied to large scale optimisation problems’, in 2017 IEEE Latin American Conference on Computational Intelligence (LA-CCI), Nov. 2017, pp. 1–6, doi: 10.1109/LA-CCI.2017.8285728.

[138] S. S. Aote, M. M. Raghuwanshi, and L. G. Malik, ‘Improved Particle Swarm Optimisation Based on Natural Flocking Behavior’, Arab. J. Sci. Eng., vol. 41, no. 3, pp. 1067–1076, Mar. 2016, doi: 10.1007/s13369-015-1990-5.

[139] H. Wang, L. Duanmu, X. Li, and R. Lahdelma, ‘Optimizing the District Heating Primary Network from the Perspective of Economic-Specific Pressure Loss’, Energies, vol. 10, no. 8, p. 1095, Aug. 2017, doi: 10.3390/en10081095.

[140] M. Rezaei, B. Ghobadian, S. H. Samadi, and S. Karimi, ‘Electric power generation from municipal solid waste: A techno-economical assessment under different scenarios in Iran’, Energy, vol. 152, pp. 46–56, Jun. 2018, doi: 10.1016/j.energy.2017.10.109.

[141] L. L. Grigsby, Electric Power Generation, Transmission, and Distribution. CRC Press, 2018.

[142] A. Campos Celador, A. Erkoreka, K. Martin Escudero, and J. M. Sala, ‘Feasibility of small-scale gas engine-based residential cogeneration in Spain’, Energy Policy, vol. 39, no. 6, pp. 3813–3821, Jun. 2011, doi: 10.1016/j.enpol.2011.04.011.

[143] Eurostat, ‘Electricity price statistics - Statistics Explained’. https://ec.europa.eu/eurostat/statistics-explained/index.php/Electricity_price_statistics (accessed Nov. 12, 2019).

[144] Eurostat, ‘Natural gas price statistics - Statistics Explained’. https://ec.europa.eu/eurostat/statistics-explained/index.php/Natural_gas_price_statistics (accessed Nov. 12, 2019).

[145] J. Salpakari, J. Mikkola, and P. D. Lund, ‘Improved flexibility with large-scale variable renewable power in cities through optimal demand side management and power-to-heat conversion’, Energy Convers. Manag., vol. 126, pp. 649–661, Oct. 2016, doi: 10.1016/j.enconman.2016.08.041.

[146] T. Schütz, R. Streblow, and D. Müller, ‘A comparison of thermal energy storage models for building energy system optimisation’, Energy Build., vol. 93, pp. 23–31, Apr. 2015, doi: 10.1016/j.enbuild.2015.02.031.

[147] M. A. Rosen, R. Tang, and I. Dincer, ‘Effect of stratification on energy and exergy capacities in thermal storage systems’, Int. J. Energy Res., vol. 28, no. 2, pp. 177–193, 2004, doi: 10.1002/er.960.

[148] ‘TRNSYS - Official Website’. https://sel.me.wisc.edu/trnsys/ (accessed Nov. 22, 2019).

[149] D. Olsthoorn, F. Haghighat, and P. A. Mirzaei, 'Integration of storage and renewable energy into district heating systems: A review of modelling and optimisation', Sol. Energy, vol. 136, pp. 49–64, Oct. 2016, doi: 10.1016/j.solener.2016.06.054.

[150] Y. Ruan, Q. Liu, Z. Li, and J. Wu, 'Optimisation and analysis of Building Combined Cooling, Heating and Power (BCHP) plants with chilled ice thermal storage system', Appl. Energy, vol. 179, pp. 738–754, Oct. 2016, doi: 10.1016/j.apenergy.2016.07.009.

[151] T. Fang and R. Lahdelma, 'Optimisation of combined heat and power production with heat storage based on sliding time window method', Appl. Energy, vol. 162, pp. 723–732, Jan. 2016, doi: 10.1016/j.apenergy.2015.10.135.

[152] F. Verrilli et al., 'Model Predictive Control-Based Optimal Operations of District Heating System with Thermal Energy Storage and Flexible Loads', IEEE Trans. Autom. Sci. Eng., vol. 14, no. 2, pp. 547–557, Apr. 2017, doi: 10.1109/TASE.2016.2618948.

[153] J. H. Lee, 'Model Predictive Control and Dynamic Programming', in 2011 11th International Conference on Control, Automation and Systems, Oct. 2011, pp. 1807–1809.

[154] J. Zeng, J. Han, and G. Zhang, 'Diameter optimisation of district heating and cooling piping network based on hourly load', Appl. Therm. Eng., vol. 107, pp. 750–757, Aug. 2016, doi: 10.1016/j.applthermaleng.2016.07.037.

Appendices

Appendix A. Derivation of admittance matrix and electrical power injection equations

In per unit system (the same equation for single phase and three phase system), the apparent power injected at bus i ($S_{e(i)}$) in complex number notation is defined by equation (A-1) [102].

$$S_{e(i)} = V_i * I_i^* \tag{A-1}$$

where V_i is the voltage at bus i while I_i^* is the conjugate of the current injected at bus i. According to Kirchhoff's current law, the current injected at bus i is the sum of all outgoing current flows from the same bus. Each outgoing current flow is then expressed in terms of Ohm's law as a function of line admittance (y_{ij}) and voltage difference at the two ends of the line ($V_i - V_j$) as shown in equation (A-2).

$$I_i = \sum_{j=1, j\neq i}^{N} I_{ij} = y_{ii}V_i + \sum_{j=1, j\neq i}^{N} y_{ij}(V_i - V_j) \tag{A-2}$$

The term y_{ii} in equation (A-2) refers to half of the susceptance of the line aggregated at the two ends of the line (usually designated by $b/2$), and N is the total number of buses in the network. Equation (A-2) can be further rearranged as shown in equations (A-3).

$$I_i = \sum_{j=1}^{N} y_{ij}V_i - \sum_{j=1, j\neq i}^{N} y_{ij}V_j = V_i \sum_{j=1}^{N} y_{ij} + \sum_{j=1, j\neq i}^{N} -y_{ij}V_j \tag{A-3}$$

Equivalently,

$$I_i \equiv Y_{ii}V_i + \sum_{j=1, j\neq i}^{N} Y_{ij}V_j \tag{A-4}$$

where $Y_{ii} = \sum_{j=1}^{N} y_{ij}$ and $Y_{ij} = -y_{ij}$

In a more compact form, the current injection described in equation (A-4) can be rewritten as shown in equation (A-5) where $\boldsymbol{I}$, $\boldsymbol{Y}$ and $\boldsymbol{V}$ are matrices representing current injections at all buses, network admittance matrix and voltages at all buses.

$$I_i = \sum_{j=1}^{N} Y_{ij}V_j \quad \equiv \quad \boldsymbol{I} = \boldsymbol{YV} \tag{A-5}$$

The elements of network admittance matrix can be represented in rectangular form ($Y_{ij} = G_{ij} + jB_{ij}$) while the voltages are represented in polar form ($V_i = |V_i|\angle\theta_i$). Hence, the per-

unit apparent/complex power can be formulated by substituting equation (A-5) into (A-1). $P_{ep(i)}$ and $P_{eq(i)}$ are the active and reactive components of injected power at bus i.

$$S_{e(i)} = P_{ep(i)} + jP_{eq(i)} = V_i * I_i^* = V_i \sum_{j=1}^{N} (Y_{ij}V_j)^* \tag{A-6}$$

After substitution for V and Y and separating real and imaginary parts, the active power and reactive power injections at bus i are given by equations (A-7) and (A-8), respectively.

$$P_{ep(i)} = \sum_{j=1}^{N} |V_i|\,|V_j|\left(G_{ij}cos\theta_{ij} + B_{ij}sin\theta_{ij}\right) \tag{A-7}$$

$$P_{eq(i)} = \sum_{j=1}^{N} |V_i|\,|V_j|\left(G_{ij}sin\theta_{ij} - B_{ij}cos\theta_{ij}\right) \tag{A-8}$$

θ_{ij} is the voltage angle difference between nodes i and j ($\theta_i - \theta_j$).

For a transmission line with a tap changing transformer, the admittance matrix needs to be updated by considering the pi-equivalent of the transformer. Figure A-1 shows a tap changing transformer and its pi-equivalent model adapted from [103]. The term y_{ij} represents the sum of the transformer leakage and the line admittances while a refers to the pu tap setting. By referring Fig. A-1 (b) and equation (A-4), the elements of the network admittance matrix associated with buses i and j are updated using equations (A-9) – (A-11).

$$Y_{ij} = -\frac{y_{ij}}{a} \tag{A-9}$$

$$Y_{ii} = y_{ii} + \sum_{j=1, j\neq i}^{N} \frac{y_{ij}}{a^2} \tag{A-10}$$

$$Y_{jj} = y_{jj} + \sum_{i=1, j\neq i}^{N} y_{ij} \tag{A-11}$$

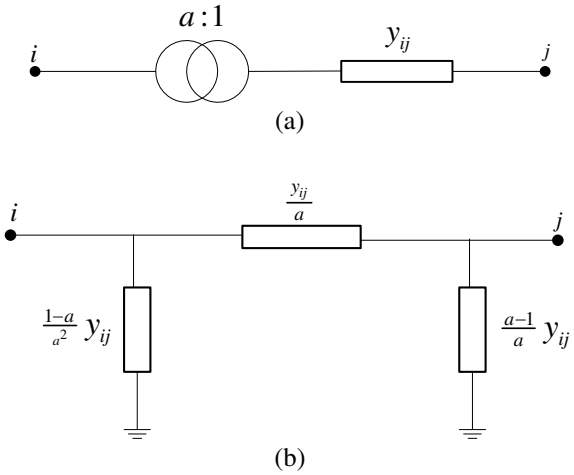

Fig. A-1. A transmission line with a tap changing transformer: (a) one-line diagram and (b) pi-equivalent model.

Appendix B. Equations for calculating elements of the Jacobian matrix

From the electrical and thermo-hydraulic models, expressed in per-unit, the following equations are derived. The superscript (subscripts) i and j refers to hub numbers and their corresponding points of interconnections (i.e. nodes/busses) while the subscripts m and n indicate the number of those pipes in their respective order (based on the layout of the network, they are automatically extracted). Equations (B-1) to (B-8) hold true for the electrical model.

$$\frac{\partial P_{ep}^{i}}{\partial \theta_j} = |V_i||V_j|\left(G_{ij}sin\theta_{ij} - B_{ij}cos\theta_{ij}\right), \qquad for\ all\ j \neq i \tag{B-1}$$

$$\frac{\partial P_{ep}^{i}}{\partial \theta_i} = \sum_{j=1, j\neq i}^{N} |V_i|\,|V_j|\left(-G_{ij}sin\theta_{ij} + B_{ij}cos\theta_{ij}\right) = -P_{eq_i}^{i} - B_{ii}|V_i|^2 \tag{B-2}$$

$$\frac{\partial P_{ep}^{i}}{\partial |V_j|} = |V_i|\left(G_{ij}cos\theta_{ij} + B_{ij}sin\theta_{ij}\right), \qquad for\ all\ j \neq i \tag{B-3}$$

$$\frac{\partial P_{ep}^{i}}{\partial |V_i|} = \sum_{j=1, j\neq i}^{N} |V_j|\left(G_{ij}cos\theta_{ij} + B_{ij}sin\theta_{ij}\right) + 2|V_i|G_{ii} = \frac{P_{ep}^{i}}{|V_i|} + G_{ii}|V_i| \tag{B-4}$$

$$\frac{\partial P_{eq}^{i}}{\partial \theta_j} = -|V_i||V_j|\left(G_{ij}cos\theta_{ij} + B_{ij}sin\theta_{ij}\right), \qquad for\ all\ j \neq i \tag{B-5}$$

$$\frac{\partial P_{eq}^{i}}{\partial \theta_i} = \sum_{j=1, j\neq i}^{N} |V_i|\,|V_j|\left(G_{ij}cos\theta_{ij} + B_{ij}sin\theta_{ij}\right) = P_{ep}^{i} - G_{ii}|V_i|^2 \tag{B-6}$$

$$\frac{\partial P_{eq}^{i}}{\partial |V_j|} = |V_i|\left(G_{ij}sin\theta_{ij} - B_{ij}cos\theta_{ij}\right), \qquad for\ all\ j \neq i \tag{B-7}$$

$$\frac{\partial P_{eq}^{i}}{\partial |V_i|} = \sum_{j=1, j\neq i}^{N} |V_j|\left(G_{ij}sin\theta_{ij} - B_{ij}cos\theta_{ij}\right) - 2|V_i|B_{ii} = \frac{P_{eq}^{i}}{|V_i|} - B_{ii}|V_i|^2 \tag{B-8}$$

Let's define a nodal mass flow rate injected from hub i into the network be $\dot{m}_i$. Then, equations (B-9) to (B-13) hold true for the thermo-hydraulic model.

$$\frac{\partial P_{h}^{i}}{\partial T_{s(j)}} = 0\ for\ i \neq j \tag{B-9}$$

$$\frac{\partial P_{h}^{i}}{\partial T_{s(i)}} = -\dot{m}_i \tag{B-10}$$

$$\frac{\partial P_h^i}{\partial T_{r(j)}} = 0 \; for \; i \neq j \tag{B-11}$$

$$\frac{\partial P_h^i}{\partial T_{r(i)}} = \dot{m}_i \tag{B-12}$$

$$\frac{\partial P_h^i}{\partial \dot{m}_{pipe(m)}} = \begin{cases} +\left(T_{s(i)} - T_{r(i)}\right) & if \; the \; pipe \; flow \; is \; leaving \; node \; i \\ -\left(T_{s(i)} - T_{r(i)}\right) & if \; the \; pipe \; flow \; is \; going \; into \; node \; i \\ 0 & otherwise \end{cases} \tag{B-13}$$

Consider the Jacobina matrix in equation (B-14). The first three rows refer to the coupled mismatch equations while the last three refer to the uncoupled mismatch equations discussed in *Section 4.5.1*. Accordingly, the elements of the Jacobian matrix can be calculated using equations (B-15) to (B-50).

$$-\begin{bmatrix} \Delta \boldsymbol{P_{ep}} \\ \Delta \boldsymbol{P_{eq}} \\ \Delta \boldsymbol{P_h} \\ \Delta \boldsymbol{H_{pipe}} \\ \Delta \boldsymbol{E_s} \\ \Delta \boldsymbol{E_r} \end{bmatrix} = \begin{bmatrix} \frac{\partial(\Delta \boldsymbol{P_{ep}})}{\partial \boldsymbol{\theta}} & \frac{\partial(\Delta \boldsymbol{P_{ep}})}{\partial |\boldsymbol{V}|} & \frac{\partial(\Delta \boldsymbol{P_{ep}})}{\partial \dot{\boldsymbol{m}}_{\boldsymbol{pipe}}} & \frac{\partial(\Delta \boldsymbol{P_{ep}})}{\partial \boldsymbol{H}} & \frac{\partial(\Delta \boldsymbol{P_{ep}})}{\partial \boldsymbol{T_s}} & \frac{\partial(\Delta \boldsymbol{P_{ep}})}{\partial \boldsymbol{T_r}} \\ \frac{\partial(\Delta \boldsymbol{P_{eq}})}{\partial \boldsymbol{\theta}} & \frac{\partial(\Delta \boldsymbol{P_{eq}})}{\partial |\boldsymbol{V}|} & \frac{\partial(\Delta \boldsymbol{P_{eq}})}{\partial \dot{\boldsymbol{m}}_{\boldsymbol{pipe}}} & \frac{\partial(\Delta \boldsymbol{P_{eq}})}{\partial \boldsymbol{H}} & \frac{\partial(\Delta \boldsymbol{P_{eq}})}{\partial \boldsymbol{T_s}} & \frac{\partial(\Delta \boldsymbol{P_{eq}})}{\partial \boldsymbol{T_r}} \\ \frac{\partial(\Delta \boldsymbol{P_h})}{\partial \boldsymbol{\theta}} & \frac{\partial(\Delta \boldsymbol{P_h})}{\partial |\boldsymbol{V}|} & \frac{\partial(\Delta \boldsymbol{P_h})}{\partial \dot{\boldsymbol{m}}_{\boldsymbol{pipe}}} & \frac{\partial(\Delta \boldsymbol{P_h})}{\partial \boldsymbol{H}} & \frac{\partial(\Delta \boldsymbol{P_h})}{\partial \boldsymbol{T_s}} & \frac{\partial(\Delta \boldsymbol{P_h})}{\partial \boldsymbol{T_r}} \\ \frac{\partial(\Delta \boldsymbol{H_{pipe}})}{\partial \boldsymbol{\theta}} & \frac{\partial(\Delta \boldsymbol{H_{pipe}})}{\partial |\boldsymbol{V}|} & \frac{\partial(\Delta \boldsymbol{H_{pipe}})}{\partial \dot{\boldsymbol{m}}_{\boldsymbol{pipe}}} & \frac{\partial(\Delta \boldsymbol{H_{pipe}})}{\partial \boldsymbol{H}} & \frac{\partial(\Delta \boldsymbol{H_{pipe}})}{\partial \boldsymbol{T_s}} & \frac{\partial(\Delta \boldsymbol{H_{pipe}})}{\partial \boldsymbol{T_r}} \\ \frac{\partial(\Delta \boldsymbol{E_s})}{\partial \boldsymbol{\theta}} & \frac{\partial(\Delta \boldsymbol{E_s})}{\partial |\boldsymbol{V}|} & \frac{\partial(\Delta \boldsymbol{E_s})}{\partial \dot{\boldsymbol{m}}_{\boldsymbol{pipe}}} & \frac{\partial(\Delta \boldsymbol{E_s})}{\partial \boldsymbol{H}} & \frac{\partial(\Delta \boldsymbol{E_s})}{\partial \boldsymbol{T_s}} & \frac{\partial(\Delta \boldsymbol{E_s})}{\partial \boldsymbol{T_r}} \\ \frac{\partial(\Delta \boldsymbol{E_r})}{\partial \boldsymbol{\theta}} & \frac{\partial(\Delta \boldsymbol{E_r})}{\partial |\boldsymbol{V}|} & \frac{\partial(\Delta \boldsymbol{E_r})}{\partial \dot{\boldsymbol{m}}_{\boldsymbol{pipe}}} & \frac{\partial(\Delta \boldsymbol{E_r})}{\partial \boldsymbol{H}} & \frac{\partial(\Delta \boldsymbol{E_r})}{\partial \boldsymbol{T_s}} & \frac{\partial(\Delta \boldsymbol{E_r})}{\partial \boldsymbol{T_r}} \end{bmatrix} \begin{bmatrix} \Delta \boldsymbol{\theta} \\ \Delta |\boldsymbol{V}| \\ \Delta \dot{\boldsymbol{m}}_{\boldsymbol{pipe}} \\ \Delta \boldsymbol{H} \\ \Delta \boldsymbol{T_s} \\ \Delta \boldsymbol{T_r} \end{bmatrix} \tag{B-14}$$

B.1: Equations for the first row of the Jacobian matrix:

$$\frac{\partial\left(\Delta P_{ep}\right)_i}{\partial \theta_j} = C^i_{ep(ep)} \frac{\partial P^i_{ep}}{\partial \theta_j} + C^i_{ep(eq)} \frac{\partial P^i_{eq}}{\partial \theta_j} \tag{B-15}$$

$$\frac{\partial\left(\Delta P_{ep}\right)_i}{\partial |V|_j} = C^i_{ep(ep)} \frac{\partial P^i_{ep}}{\partial |V|_j} + C^i_{ep(eq)} \frac{\partial P^i_{eq}}{\partial |V|_j} \tag{B-16}$$

$$\frac{\partial\left(\Delta P_{ep}\right)_i}{\partial \dot{m}_{pipe(m)}} = C^i_{ep(h)} \frac{\partial P^i_h}{\partial \dot{m}_{pipe(m)}} \tag{B-17}$$

$$\frac{\partial\left(\Delta P_{ep}\right)_i}{\partial H_j} = 0 \tag{B-18}$$

$$\frac{\partial\left(\Delta P_{ep}\right)_i}{\partial T_{s(j)}} = C^i_{ep(h)} \frac{\partial P^i_h}{\partial T_{s(j)}} \tag{B-19}$$

$$\frac{\partial\left(\Delta P_{ep}\right)_i}{\partial T_{r(j)}} = C^i_{ep(h)} \frac{\partial P^i_h}{\partial T_{r(j)}} \tag{B-20}$$

B.2: Equations for the second row of the Jacobian matrix:

$$\frac{\partial\left(\Delta P_{eq}\right)_i}{\partial \theta_j} = C^i_{eq(ep)} \frac{\partial P^i_{ep}}{\partial \theta_j} + C^i_{eq(eq)} \frac{\partial P^i_{eq}}{\partial \theta_j} \tag{B-21}$$

$$\frac{\partial\left(\Delta P_{eq}\right)_i}{\partial |V|_j} = C^i_{eq(ep)} \frac{\partial P^i_{ep}}{\partial |V|_j} + C^i_{eq(eq)} \frac{\partial P^i_{eq}}{\partial |V|_j} \tag{B-22}$$

$$\frac{\partial\left(\Delta P_{eq}\right)_i}{\partial \dot{m}_{pipe(m)}} = C^i_{eq(h)} \frac{\partial P^i_h}{\partial \dot{m}_{pipe(m)}} \tag{B-23}$$

$$\frac{\partial\left(\Delta P_{eq}\right)_i}{\partial H_j} = 0 \tag{B-23}$$

$$\frac{\partial\left(\Delta P_{eq}\right)_i}{\partial T_{s(j)}} = C^i_{eq(h)} \frac{\partial P^i_h}{\partial T_{s(j)}} \tag{B-25}$$

$$\frac{\partial\left(\Delta P_{eq}\right)_i}{\partial T_{r(j)}} = C^i_{eq(h)} \frac{\partial P^i_h}{\partial T_{r(j)}} \tag{B-26}$$

B.3: Equations for the third row of the Jacobian matrix:

$$\frac{\partial(\Delta P_h)_i}{\partial \theta_j} = C^i_{h(ep)} \frac{\partial P^i_{ep}}{\partial \theta_j} + C^i_{h(eq)} \frac{\partial P^i_{eq}}{\partial \theta_j} \tag{B-27}$$

$$\frac{\partial(\Delta P_h)_i}{\partial |V|_j} = C^i_{h(ep)} \frac{\partial P^i_{ep}}{\partial |V|_j} + C^i_{h(eq)} \frac{\partial P^i_{eq}}{\partial |V|_j} \tag{B-28}$$

$$\frac{\partial(\Delta P_h)_i}{\partial \dot{m}_{pipe(m)}} = C^i_{h(h)} \frac{\partial P^i_h}{\partial \dot{m}_{pipe(m)}} \tag{B-29}$$

$$\frac{\partial(\Delta P_h)_i}{\partial H_j} = 0 \tag{B-30}$$

$$\frac{\partial(\Delta P_h)_i}{\partial T_{s(j)}} = C^i_{h(h)} \frac{\partial P^i_h}{\partial T_{s(j)}} \tag{B-31}$$

$$\frac{\partial(\Delta P_h)_i}{\partial T_{r(j)}} = C^i_{h(h)} \frac{\partial P^i_h}{\partial T_{r(j)}} \tag{B-32}$$

B.4: Equations for the fourth row of the Jacobian matrix:

$$\frac{\partial(\Delta H)_m}{\partial \theta_j} = 0 \tag{B-33}$$

$$\frac{\partial(\Delta H)_m}{\partial |V|_j} = 0 \tag{B-34}$$

$$\frac{\partial(\Delta H)_m}{\partial \dot{m}_{pipe(n)}} = \begin{cases} -2k_m \dot{m}_{pipe(n)} & for\ m = n \\ 0 & otherwise \end{cases} \tag{B-35}$$

$$\frac{\partial(\Delta H)_m}{\partial H_j} = \begin{cases} +1 & if\ positive\ flow\ direction\ is\ leaving\ node\ j \\ -1 & if\ positive\ flow\ direction\ is\ into\ node\ j \\ 0 & otherwise \end{cases} \tag{B-36}$$

$$\frac{\partial(\Delta H)_m}{\partial T_{s(j)}} = 0 \tag{B-37}$$

$$\frac{\partial(\Delta H)_m}{\partial T_{r(j)}} = 0 \tag{B-38}$$

B.5: Equations for the fifth row of the Jacobian matrix:

$$\frac{\partial(\Delta E_s)_i}{\partial \theta_j} = 0 \tag{B-39}$$

$$\frac{\partial(\Delta E_s)_i}{\partial |V|_j} = 0 \tag{B-40}$$

In equations (B-41), if the flow in pipe n is positive and getting into node i equation (B-41a) is used. Instead, if the pipe flow is negative (opposite to the positive direction) and is still flowing into node i, then equation (B-41b) is used. Otherwise, equation (B-41c) is applied.

$$\frac{\partial(\Delta E_s)_i}{\partial \dot{m}_{pipe(n)}} = T_{s\_end(n)} - T_{s(i)} + \left(T_{s\_end(n)} - T_a\right) 2\pi U_{Rs(n)} R_{s(n)} \frac{L_{(n)}}{C_p \dot{m}_{pipe(n)}} \tag{B-41a}$$

$$\frac{\partial(\Delta E_s)_i}{\partial \dot{m}_{pipe(n)}} = T_{s\_start(n)} - T_{s(i)} + \left(T_{s\_start(n)} - T_a\right) 2\pi U_{Rs(n)} R_{s(n)} \frac{L_{(n)}}{C_p \dot{m}_{pipe(n)}} \tag{B-41b}$$

$$\frac{\partial(\Delta E_s)_i}{\partial \dot{m}_{pipe(n)}} = 0 \tag{B-41c}$$

$$\frac{\partial(\Delta E_s)_i}{\partial H_j} = 0 \tag{B-42}$$

$$\frac{\partial(\Delta E_s)_i}{\partial T_{s(j)}} = \left(\sum_{\substack{n \epsilon flowing \\ into\ node\ i}} \dot{m}_{pipe(n)} \right)_{supply\ side} \tag{B-43}$$

$$\frac{\partial(\Delta E_s)_i}{\partial T_{r(j)}} = 0 \tag{B-44}$$

B.6: Equations for the sixth row of the Jacobian matrix

$$\frac{\partial(\Delta E_r)_i}{\partial \theta_j} = 0 \tag{B-45}$$

$$\frac{\partial(\Delta E_r)_i}{\partial |V|_j} = 0 \tag{B-46}$$

In equations (B-47), if the flow in pipe n is positive and getting into node i equation (B-47a) is used. Instead, if the pipe flow is negative (opposite to the positive direction) and is still flowing into node i, then equation (B-47b) is used. Otherwise, equation (B-47c) is applied.

$$\frac{\partial(\Delta E_r)_i}{\partial \dot{m}_{pipe(n)}} = T_{r\_start(n)} - T_{r(i)} + \left(T_{r\_start(n)} - T_a\right) 2\pi U_{Rs(n)} R_{s(n)} \frac{L_{(n)}}{C_p \dot{m}_{pipe(n)}} \tag{B-47a}$$

$$\frac{\partial(\Delta E_r)_i}{\partial \dot{m}_{pipe(n)}} = T_{r\_end(n)} - T_{r(i)} + \left(T_{r\_end(n)} - T_a\right) 2\pi U_{Rs(n)} R_{s(n)} \frac{L_{(n)}}{C_p \dot{m}_{pipe(n)}} \tag{B-47b}$$

$$\frac{\partial(\Delta E_r)_i}{\partial \dot{m}_{pipe(n)}} = 0 \tag{B-47c}$$

$$\frac{\partial(\Delta E_r)_i}{\partial H_j} = 0 \tag{B-48}$$

$$\frac{\partial(\Delta E_r)_i}{\partial T_{s(j)}} = 0 \tag{B-49}$$

$$\frac{\partial(\Delta E_r)_i}{\partial T_{r(j)}} = \left(\sum_{\substack{n \epsilon flowing \\ into\ node\ i}} \dot{m}_{pipe(n)} \right)_{return\ side} \tag{B-50}$$

Appendix C. Input parameters for Cases 5-B to 5-D

Table C-1: Transmission line and transformer parameters for the electricity networks – Cases 5-B to 5-D

From hub	To hub	Transmission line parameters				Transformer parameters		
		R (Ω/mi)	X(Ω/mi)	B(S/mi)	L (mi)	Rs (pu)	Xs (pu)	Tap (pu)
1	2	0.307	0.458	9.46E-06	1.99	0	0	1
2	4	0.307	0.458	9.46E-06	1.55	0	0	1
3	2	0.307	0.458	9.46E-06	0.81	0.0035	0.035	1.1
3	4	0.307	0.458	9.46E-06	1.12	0.005	0.05	1.05
1	5	0.307	0.458	9.46E-06	2.36	0.003	0.03	1
4	5	0.307	0.458	9.46E-06	1.24	0.004	0.04	0.9

Table C-2: Carrier pipe, insulation and soil parameters for the heating networks – Cases 5-B to 5-D

Hubs			Carrier Pipe Parameters				*Insulation*		Outer Jacket		Soil		
from	*to*	*L (m)*	R_1 *(mm)*	R_2 *(mm)*	k_2 *(W/mK)*	*e (mm)*	R_3 *(mm)*	k_3 *(W/mK)*	R_4 *(mm)*	k_4 *(W/mK)*	*Z (m)*	k_s *(W/mK)*	*flow (kg/s)*
1	2	3200	26.95	30.15	40.5	0.05	67	0.027	70	0.40	0.5	1.15	10*
2	4	2500	26.95	30.15	35.6	0.06	67	0.027	70	0.40	0.5	1.15	10*
3	2	1300	26.95	30.15	45.1	0.09	67	0.027	70	0.40	0.5	1.15	10*
3	4	1800	26.95	30.15	42.0	0.10	67	0.027	70	0.40	0.5	1.15	10*
1	5	3800	26.95	30.15	38.0	0.08	67	0.027	70	0.40	0.5	1.15	10*
4	5	2000	26.95	30.15	40.0	0.10	67	0.027	70	0.40	0.5	1.15	10*

Table C-3: Generation and demands of electricity, heat and fuel power at different hubs – Cases 5-B to 5-D

Hub	***Electricity network hub data***							***District heating network hub data***							***Fuel***
	Type	*V (pu)*	θ (^{0})	P_{epg} *(kW)*	P_{eqg} *(kvar)*	L_{ep} *kW)*	L_{eq} *(kvar)*	*Type*	T_s (^{0}C)	T_r (^{0}C)	P_{hg} *(kW)*	L_h *(kW)*	H_s *(m)*	H_r *(m)*	P_{fg} *(kW)*
1	1	1	0	0*	0*	25	0	1	80	20*	0*	30	135	1	0*
2	3	1*	0*	0	0	160	60	3†	65*	30	50	250	50*	1*	50
3	2	1.05	0*	50	20*	200	130	2†	90	25*	35	50	50*	1*	500
4	3	1*	0*	0	0	50	80	3	70*	35	20	220	50*	1*	50
5	3	1*	0*	0	0	90	40	3	100*	35	0	150	50*	1*	55

NB: For electricity Type 1 is slack, 2 is PV and 3 is PQ while for DHN type 1 is slack, 2 is temp_supply and 3 is temp_return

Equation (C-1) represents the general format of the coupling matrix and specific coupling matrixes for each hub are given below.

$$C_{general} = \begin{bmatrix} C_{ep(ep)} & C_{ep(eq)} & C_{ep(h)} & C_{ep(f)} \\ C_{eq(ep)} & C_{eq(eq)} & C_{eq(h)} & C_{eq(f)} \\ C_{h(ep)} & C_{h(eq)} & C_{h(h)} & C_{h(f)} \end{bmatrix} \quad \text{(C-1)}$$

$$C_{hub1} = \begin{bmatrix} 1 & 0 & 0 & 0.3 \\ 0 & 1 & 0 & 0.1 \\ 0 & 0 & 1 & 0.36 \end{bmatrix}; C_{hub2} = \begin{bmatrix} 1 & 0 & 0 & 0.25 \\ 0 & 1 & 0 & 0.08 \\ 0 & 0 & 1 & 0.4 \end{bmatrix}; C_{hub3} = \begin{bmatrix} 1 & 0 & 0 & 0.27 \\ 0 & 1 & 0 & 0.15 \\ 0 & 0 & 1 & 0.3 \end{bmatrix};$$

* These values are initial assumptions for unknown variables which are then to be solved by load flow analysis.

† This is true only for Cases 5-C and 5-D. For Case 5-B, hub 2 is assumed to be a *temp_supply* while hub 3 is *temp_return* to see the effect of change of hub heat flow direction on the load flow solution.

$$C_{hub4} = \begin{bmatrix} 1 & 0 & 0 & 0.35 \\ 0 & 1 & 0 & 0.05 \\ 0 & 0 & 1 & 0.35 \end{bmatrix}; C_{hub5} = \begin{bmatrix} 1 & 0 & 0 & 0.33 \\ 0 & 1 & 0 & 0.1 \\ 0 & 0 & 1 & 0.25 \end{bmatrix}$$

Appendix D. Branch parameters and intermediate results for Case 6-C

Table D-1: Pipe and transmission line parameters for Case 6-C.

Hubs		**Carrier Pipe Parameters**					**Insulation**		**Outer Jacket**		**Transmission lines**			
from	to	L (m)	R_1 *(mm)*	R_2 *(mm)*	k_2 (W/mK)	e (mm)	R_3 *(mm)*	k_3 *(W/mK)*	R_4 *(mm)*	k_4 *(W/mK)*	L (km)	R (Ω/km)	X (Ω/km)	B (μS/km)
1	2	50	26.95	30.15	40	0.05	62.5	0.027	65.5	0.40	0.05	0.262	0.386	4.31
2	3	600	26.95	30.15	40	0.05	62.5	0.027	65.5	0.40	0.60	0.307	0.386	4.31
2	4	600	26.95	30.15	40	0.05	62.5	0.027	65.5	0.40	0.60	0.307	0.386	4.31
3	4	600	26.95	30.15	40	0.05	62.5	0.027	65.5	0.40	0.60	0.307	0.386	4.31
3	6	600	26.95	30.15	40	0.05	62.5	0.027	65.5	0.40	0.60	0.307	0.386	4.31
4	5	600	26.95	30.15	40	0.05	62.5	0.027	65.5	0.40	0.60	0.307	0.386	4.31
4	6	600	26.95	30.15	40	0.05	62.5	0.027	65.5	0.40	0.60	0.307	0.386	4.31
5	6	600	26.95	30.15	40	0.05	62.5	0.027	65.5	0.40	0.60	0.307	0.386	4.31

Table D-2: Hub-level results of the optimal power flow after isolating the 1st lossiest branch – Case 6-C.

Hub	P_{epg} *(kW)*	HP_{Lep} *(kW)*	HP_{Phg} *(kW)*	CHP_{Pepg} *(kW)*	CHP_{Phg} *(kW)*	P_{hg} *(kW)*	L_h *(kW)*	$\dot{m}$ *(kg/s)*	T_s (°C)	T_r (°C)
1	0.00	0.00	0.00	0.00	0.00	26.53	0.00	2.88	41.89	39.69
2	0.00	500.00	0.00	0.00	0.00	0.00	0.00	-5.09	63.48	40.00
3	0.00	200.00	1520.00	380.0	470.0	0.00	380.00	9.35	85.00	39.24
4	0.00	1000.00	0.00	0.00	0.00	0.00	0.00	-5.98	79.98	40.00
5	125.0	200.00	500.00	0.00	0.00	0.00	125.00	1.56	85.00	38.98
6	0.00	500.00	0.00	0.00	0.00	0.00	0.00	-2.72	83.98	40.00

Table D-3: Branch-level results of the optimal power flow after isolating the 1st lossiest branch – Case 6-C.

Hubs		**Branch i to j**			
i	*j*	$P_{el(pumping)}$ *(kW)*	*Net heat flow (kW)*	*Loss (kW)*	*Energy efficiency*
1	2	0.152	25.39	1.14	95.17%
2	3	2.141	-562.47	19.95	96.22%
2	4	0.050	71.33	16.54	81.13%
3	4	2.427	584.18	20.00	96.30%
3	6	2.344	583.48	19.92	96.32%
4	5	0.307	-280.12	19.88	93.28%
4	6	0.007	-64.36	19.11	77.10%

Table D-4: Hub-level results of the optimal power flow after isolating the 2nd lossiest branch – Case 6-C.

Hub	P_{epg} *(kW)*	HP_{Lep} *(kW)*	HP_{Phg} *(kW)*	CHP_{Pepg} *(kW)*	CHP_{Phg} *(kW)*	P_{hg} *(kW)*	L_h *(kW)*	$\dot{m}$ *(kg/s)*	T_s (°C)	T_r (°C)
1	0.0	0.00	0.0	0.00	0.00	7.57	0.0	2.80	40.34	39.69
2	0.0	0.00	0.0	0.00	0.00	0.00	500.0	-5.03	63.75	40.00
3	0.0	380.00	1520.0	380.0	470.0	0.00	200.0	9.38	85.00	39.40
4	0.0	0.00	0.0	0.00	0.00	0.00	1000.0	-5.98	79.97	40.00
5	125.0	125.00	500.0	0.00	0.00	0.00	200.0	1.56	85.00	38.98
6	0.0	0.00	0.0	0.00	0.00	0.00	500.00	-2.73	83.83	40.00

Table D-5: Branch-level results of the optimal power flow after isolating the 2nd lossy branch – Case 6-C

Hubs		**Branch i to j**			
i	*j*	$P_{el(pumping)}$ *(kW)*	*Net heat flow (kW)*	*Loss (kW)*	*Energy efficiency*
1	2	0.140	6.46	1.12	83.70%
2	3	2.576	-599.98	19.96	96.38%
2	4	0.087	89.79	16.64	84.30%
3	4	3.015	630.08	20.00	96.48%
3	6	1.558	500.00	19.98	95.87%
4	5	0.307	-280.12	19.88	93.28%

UNIVERSITE BRETAGNE SCIENCES LOIRE POUR L'INGENIEUR

IMT Atlantique
Bretagne-Pays de la Loire
École Mines-Télécom

KTH VETENSKAP OCH KONST

Exploitation des synergies des réseaux couplés de distribution d'électricité et de chaleur :
Modélisation, simulation et optimisation basées sur une approche étendue de hub énergétique

Mots clés : Hub énergétique étendu; Flux de charges; Flux de puissances intégrées optimaux; Réseaux énergétiques multi-vecteurs; Système multi-énergies; Placement optimal.

Résumé : La littérature récente montre qu'il existe un potentiel important de décarbonation et d'amélioration de l'efficacité des réseaux d'énergie, qui peut être exploité grâce à la synergie offerte par les systèmes multi-énergies (MES). Les technologies de couplages, telles que les centrales de cogénération, les pompes à chaleur et les stockages thermiques, sont largement recommandées pour une flexibilité accrue et un meilleur taux de pénétration des énergies renouvelables dans les secteurs du chauffage et de l'électricité. Sur la base de ce constat, la taille et le nombre de technologies de couplage dans les réseaux de distribution de chaleur, telles que les centrales de production combinée de chaleur et d'électricité (cogénération) et les pompes à chaleur (PAC), augmentent. Ces technologies étant exclusivement gérées par les gestionnaires de réseaux de chauffage urbain, leur fonctionnement devient parfois sous-optimal du point de vue du réseau électrique et elles peuvent entraîner une surcharge des réseaux de distribution d'électricité basse tension (en particulier pour les grandes puissances installées).

Des modèles de simulation et d'optimisation intégrés sont nécessaires pour exploiter efficacement les synergies sans compromettre les réseaux de distribution composants les MES. Ces modèles ne sont pas encore développés. Les outils classiques de simulation mono-vecteur d'énergie ne sont pas capables d'intégrer les paramètres de fonctionnement couplé clés des réseaux de distribution multi vecteurs.

Une nouvelle méthodologie de simulation et d'optimisation de MES est développée dans cette thèse, basée sur une approche d'Extended Energy Hub (EEH).

Une structure générale de modélisation est d'abord proposée sous forme modulaire, afin de pouvoir être facilement adaptée à tout type de réseaux énergétiques multi vecteurs. Celle-ci est ensuite utilisée pour développer les détails d'un modèle intégré de flux de charges régissant les réseaux couplés de chauffage et de distribution d'électricité. Plusieurs études de cas, traitant de topologies de réseaux radiales et maillées, sont considérées pour la démonstration et la validation numérique du modèle proposé.

Ce modèle de flux de charges est en outre combiné avec un algorithme d'optimisation afin de mener des études de flux de puissances intégrées optimaux. Le potentiel offert par cette démarche est illustré par l'étude du placement optimal des technologies de couplage, comme les pompes à chaleur (PAC), dans les réseaux couplés de chauffage et de distribution d'électricité. La capacité de l'outil développé est de plus illustrée par l'exploitation des synergies des réseaux couplés en présence d'énergies renouvelables intermittentes et d'un signal de prix de l'électricité variable.

Il est démontré que les méthodologies de simulation et d'optimisation basées sur l'EEH, proposées dans cette thèse sont très efficaces, flexibles et facilement évolutives pour intégrer les paramètres de fonctionnement clés des réseaux intégrés d'électricité et de chauffage urbain. Les modèles développés peuvent ainsi être utilisés comme plate-forme d'études de l'intégration des réseaux intelligents et des réseaux thermiques intelligents.

Exploiting the Synergies from Coupled Electricity and Heat Distribution Networks:
Modelling, simulation and optimization based on an extended energy hub approach

Keywords: Extended energy hub approach; Integrated load flow study; Integrated optimal power flow; Multi-carrier energy networks; Multi-energy system; Optimal placement.

Abstract: Recent literature shows that there is a significant potential of decarbonisation and efficiency improvement that can be achieved through the synergy from multi-energy systems (MESs). Coupling technologies, such as co-generation plants, heat pumps and thermal storages are widely recommended as means of unlocking additional flexibility and increasing the penetration of renewables in the heating and electricity sectors. In view of that, the size and number of coupling technologies, such as combined heat and power plants and heat pumps (HPs), being installed in the heat distribution networks are increasing. As these technologies are exclusively managed by the district heating network operators, their operation sometimes becomes suboptimal from the electricity network point of view, and they (in particular large HPs) may cause overloading of the low voltage electricity distribution networks.

Integrated simulation and optimisation models are required to exploit the synergies effectively without compromising the constituent distribution networks of MES. Such models are not yet well developed. The conventional single-energy-carrier simulation tools are not capable of capturing key operating parameters of the multi-carrier distribution networks either.

A novel methodology for simulation and optimisation of MES is developed in this thesis based on an Extended Energy Hub (EEH) approach.

The general framework is first developed in modular form so that it can be easily adapted for any type of multi-carrier energy networks. The framework is then used to develop the details of an integrated load flow model governing coupled heating and electricity distribution networks. Various load flow case studies with radial and meshed topologies are considered for demonstration and numerical validation of the proposed model.

The load flow model is further combined with a particle swarm optimisation algorithm in order to conduct integrated optimal power flow studies. Its contribution to the state of art is demonstrated by studying the optimal placement of coupling technologies, such as HPs and boilers in coupled heating and electricity distribution networks. The capacity of the model is further illustrated by exploiting the synergies using HPs together with thermal storage in the presence of intermittent renewables and variable electricity price signal.

It is shown that the EEH-based simulation and optimisation methodologies proposed in this thesis are very effective, flexible and easily scalable in capturing the key operating parameters of integrated electricity and district heating networks. The models can be used as a platform for further studies on integration of smart grids and smart thermal networks.

TRITA-ITM-AVL 2020:43
ISBN: 978-91-7873-679-9